Università degli Studi di Torino

Scuola di Dottorato in

Scienze della Natura e Tecnologie Innovative

Dottorato in

Scienze Farmaceutiche e Biomolecolari

(XXXII ciclo)

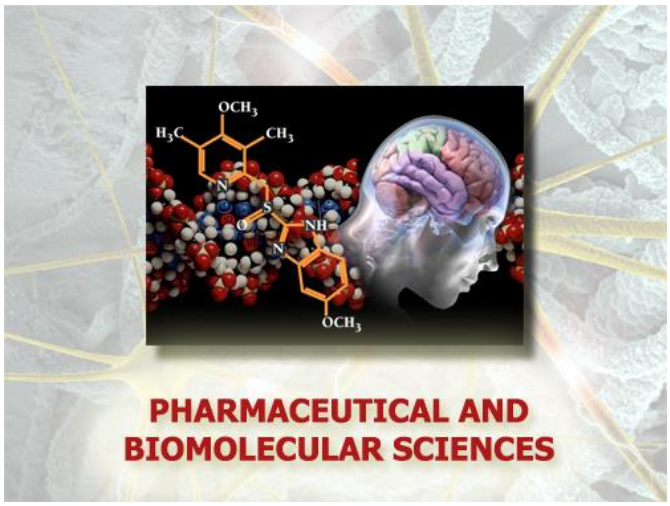

Improving the Diagnostic Efficacy in Pathological Models with Novel High Relaxivity Gadolinium Chelates.

Candidata:

Francesca La Cava

Tutors:

Enzo Terreno, Sonia Colombo Serra

Università degli Studi di Torino

Dottorato in

Scienze Farmaceutiche e Biomolecolari

Tesi svolta presso il

Dipartimento di Biotecnologie Molecolari e Scienze della Salute

CICLO: XXXII

TITOLO DELLA TESI: Improving the Diagnostic Efficacy in Pathological Models with Novel High Relaxivity Gadolinium Chelates.

TESI PRESENTATA DA: Francesca La Cava

TUTOR(S): Enzo Terreno, Sonia Colombo Serra

COORDINATORE DEL DOTTORATO: Gianmario Martra

ANNI ACCADEMICI: 2016/2019

SETTORE SCIENTIFICO-DISCIPLINARE DI AFFERENZA: Salute, Diagnostica, Ricerca Farmaceutica

Table of Contents

1.Introduction

Gadolinium based contrast agents (GBCAs) have been widely used since 1988 in clinic to enhance the quality of images acquired during Magnetic Resonance Imaging (MRI) acquisitions. Currently, GBCAs are used in 40% of MRI scans and 60% of neuro MRI scans. This corresponds to approximately 40 million administrations made worldwide every year.[1]

GBCAs have been successful since the first contrast agent hit the clinic. The reason for this success is that those agents are coupled with a technique such as MRI, which is minimally invasive, safe and it can improve an often-essential diagnostic information.

Administration of GBCAs during MRI causes a shortening of the longitudinal relaxation time (T_1) of the surrounding water protons, inducing an increase of signal in T_1-weighted images. The higher is the concentration of the CA in a certain anatomical region, the shorter is T_1 and the brighter is the image.
For example, GBCAs are used to detect a disruption of the Blood Brain Barrier. Since the passage of those molecules through an intact BBB is extremely limited, a signal increase in a certain region of the brain is often linked with the presence of a pathology, such as brain tumours, strokes, and neurodegenerative disorders. GBCAs can detect a change in vascular permeability outside the brain as well, as in the case of breast cancer detection, follow up and staging, detection of aneurysms or blood clot formation via angiographies, and reperfusion of the heart by exploiting the kinetics of contrast enhancement after injection.[2]

MRI contrast agents can be classified according to their bio distribution, and as a consequence may have different applications. Extracellular contrast agents (ECF) are low molecular weight chelates and distribute between the intravascular and cellular space. They are rapidly eliminated through the renal pathway and since they distribute into the extracellular space, they are used to identify leakage of the BBB, or altered tissue endothelium. “Blood pool” agents are instead high molecular weight chelates; since they are retained into the vascular space, they are used to image arteries or veins in the so-called Magnetic Resonance Angiography (MRA). Finally, there are “Organ specific contrast agents”, which are capable to target specific tissues or organs. For example, instead of being eliminated by the kidneys, those contrast agents prefer the hepatic elimination pathway, and thus can be used to detect liver malignancies.
Contrast agents can also be classified based on the molecular structure of the chelating ligand. They can be either acyclic (often said linear) or macrocyclic. The first are elongated structures, while the latter are cage-like structures that enclose the Gd (III) ion into a cavity.[3] Clinically approved GBCAs utilize an octadentate polyaminopolycarboxylato-based ligand, with a ninth coordination site available for water ligation. The coordinated water can be rapidly exchanged with bulk water molecules. GBCAs that have been approved for clinical use are illustrated below.

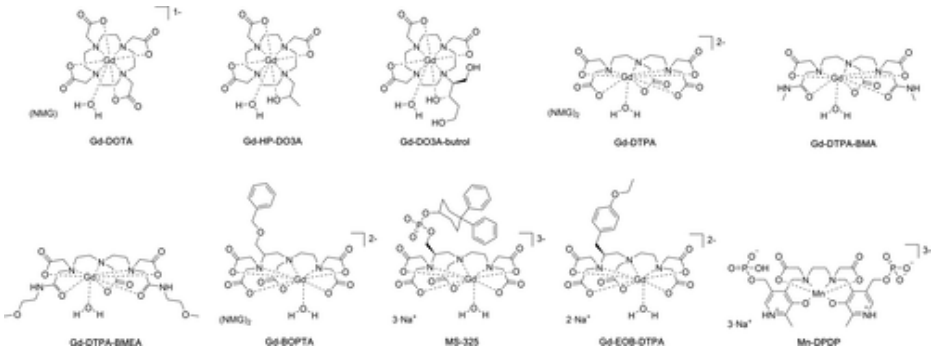

Figure 1 *Commercially approved T_1 contrast agents (NMG = meglumine). Taken from ref 2.*

Determinants of Relaxivity

GBCAs shorten both the observed longitudinal (T_1) and transverse (T_2) relaxation times of surrounding water protons. The rate constants are called relaxation rates and are defined by $1/T_1$ and $1/T_2$. The level by which a contrast agent can change the relaxation rate for unit of Gd concentration is called relaxivity (e.g. r_1 for longitudinal relaxation rate, r_2 for transversal relaxation rate). Even if the shortening effect involves both relaxation times, all the GBCAs commercially distributed are classified as T_1 agents and are used to increase signal in T_1-weighted images (rather than reduce signal in T_2-weighted sequences).

Relaxivity dependence of CA (contrast agent) concentration [mM] and relaxation rate is expressed by the following equation:

$$r1 = \frac{\Delta(\frac{1}{T1})}{[CA]}$$

The longitudinal relaxation times (T_1) of tissue and blood increase with increasing field.[4]

Relaxivity is not a constant but depends on different external parameters such as applied field and temperature, and on molecular parameters such as the hydration state of the molecule and the molecular size. Molecular parameters can be tuned and optimized to create contrast agents with much higher relaxivities than the ones on the market. The importance of an high-relaxivity contrast agent relies on the fact that a decrease of the injected dose can be performed, or else, they could be used to detect low-concentration targets in molecular imaging.

There are two main terms that contribute to paramagnetic relaxivity: dipole-dipole interactions between unpaired electron(s) and protons of water molecules that are directly coordinated to the paramagnetic center (inner-sphere, *is*) or protons of bulk water (outer-sphere, *os*). Contribution to the relaxivity by the inner sphere is mainly proportional by the hydration number *q*, which corresponds to the number of inner-sphere coordinated water molecules. Larger *q* values lead to an increase in relaxivity, which can be performed by increasing the coordination number of the paramagnetic center. However, an increase of the coordination number may lead to a decrease in stability of the contrast agent, which may lead to toxicity.

Relaxivity can also be increased by increasing values of the proton exchange rate, which is determined by the efficiency of the chemical exchange of water protons from the inner to the outer coordination sphere. This phenomena is the dominating contribution at physiological conditions, and it can occurs via exchange of the bound water molecule rot by the transfer of a water proton from the bound molecule to the bulk water. The rate and mechanism of the water exchange is related directly by the structure of the metal complex.
Inner-sphere relaxivity depends also by the rotational correlation time τ_R and electronic relaxation rates. An increase in τ_R leads to an increase in relaxivity. Rotational correlation time is strictly dependent by the conformation of the molecule: an increase in molecular weight, will lead to an increase in τ_R. Moreover, internal flexibility of the molecule also plays an important role: an increased rigidity of the structure of the contrast agent can lead to a slow isotropic overall motion, thus increasing τ_R and relaxivity. Electron spin relaxation influence is governed however by the decay of electron spin polarization (longitudinal relaxation).
Contribution to molar relaxivity can also be given by the interaction of the paramagnetic center with all the other water molecules, the outer-sphere contribution. [5]

Safety issues

For more than 15 years after clinical translation, the safety profile of GBCAs has been impressive: the incidence of adverse reactions with GBCAs was as low as 0.1%.[6] Since until late 1990s, GBCAs were considered less nephrotoxic than iodinated contrast media used in CT scanning.[7] The early results were so favourable that GBCAs were regarded as “safe” contrast agents and their use was deliberated.

However, a concatenation of studies in 2006 demonstrated GBCAs association with nephrogenic systemic fibrosis (NSF). This condition is characterized by progressive thickening of the skin and occasionally the trunk, with hyperpigmentation areas. The skin lesions often harden, and thus can be followed by flexure contractures, which result in impressive disability.[8] Since fibrotic changes usually develop in multiple different sites beside the skin such as the pleural tissue, the myocardium, the gastrointestinal tract, and the neural tissue, the disease has a rapid progression and is associated with increased mortality.[9]

Since ECF Contrast Agents are eliminated through kidneys, NSF develops exclusively in patients with impaired renal function that underwent serial GBCAs administrations. Even though GBCAs are often cleared with a half-life of 2 hours, in renal failure, half-life is prolonged by 30-120h, causing an increase in Gd retention and dissociation of the complex. Free Gd can form precipitates of salts with ion like phosphate and cause an initial infiltration of inflammatory cells due to accumulation in different tissues[5]. Since 2007, “*The Contrast Media Safety Committee of European Society of Urogenital Radiology*” established new guidelines to GBCAs administration, with a special caution to patients with chronic renal failure.[10]

Since 2013, there is mounting evidence that free Gd (III) is retained irreversibly into the Central Nervous System (CNS). Kanda *et al*.[11] were the first to establish a correlation with T_1 hyper intensities in MRI in the brain of patients with a history of repeated GBCA administration, independently on renal function. In particular, high signal intensities were identified in the dentate nucleus and globus pallidus of 381 patients with a history of neoplastic disease, which used MRI and GBCA to evaluate tumor size, metastasis detection and follow up. Subsequently, Kanda et al, 2014, observed in a retrospective study that CNS T_1 enhancement in MRI correlated with the number of GBCAs administrations.[12] All patients included in this study had received linear agents for MRIs as standard care, which were gadopentate dimeglumine or gadodiamide. In 2015, a *post mortem,* study was performed on the brain in 13 patients with normal renal function that underwent at least four GBCA intravenous injections for MRI monitoring[13]. The purpose of this study was to confirm the relationship between cumulative intravenous injections of GBCAs and deposition of the latter into the dentate nucleus and basal ganglia. Additionally, there were positive correlations between the number of GBCA administrations and the observed MRI signal intensity changes, confirming thus that gadolinium deposits are present in the brain after GBCA-enhanced MRI scans, and that these areas can be seen as hyperintensity areas in non-enhanced MRI scans.

Therefore, it was demonstrated extensively by numerous research groups that there is an increase of T_1 signal intensity within the brain of patients who have been administered several doses of linear or macrocyclic GBCAs[14 15 16].

In 2008, experiments of stability were performed on both macrocyclic and linear agents. GBCAs were incubated with human serum at 37°C, pH=7.4 and concentrations of 1 $mmol^{-1}$ for 15 days. While the macrocyclic agents remained stable, linear GBCAs released free Gd^{3+}.[17 18] The percentage of gadolinium dissociated was 2% for the ionic linear GBCAs (gadopentate dimeglumine, gadobenate dimeglumine, gadoxetate and gadofosveset) and 20% for the non-ionic linear GBCAs (gadodiamide and gadoversetamide), confirming the low dechelation rate of the macrocyclic agents, and the relative low stability of the non-ionic linear agents compared with the ionic ones. Since the non ionic and linear GBCAs showed significant level of dissociation, there is a potentially greater risk of Gadolinium deposition in the brain with these agents.

It is still not clear if the Gd (III) deposition into the brain has long-term effects, since no immediate toxic effects have been identified yet. None of the studies to date has determined if the deposits consist of free or chelated gadolinium, and there is no evidence if the latter would cause toxicity into the brain. If there were free Gd (III) ions deposited into the brain, blockade of the Ca^{2+} channels would be expected, since different studies with animal models utilizing free Gd^{3+} demonstrated that gadolinium competes with calcium to bind different receptors.[19]

Recently some groups tried to determine the characteristics of the gadolinium accumulated into the neural tissue by performing animal studies with linear and macrocyclic GBCAs. Frenzel *et al*. [20], in 2017 characterized GBCAs deposited into the brain of rats and discovered that linear agents exist into the brain in three forms: an insoluble fraction, a soluble fraction made of small intact GBCA molecules, and a soluble fraction bound to macromolecules of around 250-300 kDa. The quantities of the species found into the different fractions however were different in respect of the GBCA considered. In particular, gadobenate dimeglumine concentration was lower in respect to gadodiamide and gadopentate dimeglumine, both into the soluble and insoluble fractions, thus meaning that there is a divergence between linear agents. The soluble fraction bound to macromolecules would explain the high signal enhancement observed, because if Gd were bound to macromolecules, it would have a high signal intensity at lower concentrations. The macrocyclic agents however exists only into the intact form of the chelate. Another study by Gianolio *et al.*[21], confirmed that the gadodiamide deposited into the brain was into the form of insoluble species, while gadoteridol was into the form of intact chelate.

In 2017, following the studies on Gadolinium Brain deposition, the European Medicine Agency (EMA), decided to suspend the marketing authorization of three out of eight GBCAs that were currently used in clinic via intravenous administrations for MRI scans. The CAs which use was restricted were linear: gadopentate dimeglumine (Magnevist®), gadodiamide (Omniscan®), gadoversetamide (Optimark®). The use of gadobenate dimeglumine (Multihance®) was restricted only for liver scans.[22] The FDA (Food and Drug Administration) decided instead not to order any product withdrawals from the market but to add new warnings labels to advice prudence and care when ordering an MRI scan with GBCA administration.[23]

With such premises, it is important to search for new improved GBCAs with enhanced safety. The research and development areas have taken four main approaches:

1) Focusing on the development new GBCAs of higher relaxivity, in order to decrease the standard dose to be injected during the MRI scan, and consequently reducing the amount of gadolinium to be retained into tissues;

2) identify new gadolinium contrast agents, which are fairly more stable and inert to transmetalation;

3) Using molecular targeting associated with GBCAs, in order to reduce the dose.

4) Abandon Gd (III) as the metal of choice and move towards other contrast modalities.

It should be taken into consideration the fact that despite the safety concerns that were raised in this past few years, GBCAs have a good safety

profile. Especially, GBCAs associated fatalities are really rare, with a rate of 0.04 serious events per 1000 injections (40 per million). Over a 5 years reporting period, the total number of deaths associated with GBCAs was 41 deaths out of 51 million GBCA administrations (0.9 deaths per million administrations). [24] Naturally, new compounds will have to meet higher standards regarding safety and efficacy.

State of the Art

Current research is focusing on improving stability, safety and efficiency of new GBCAs. The design of a contrast agent which shares high relaxivity, low toxicity and good stability is a difficult challenge. In order to preserve the complex stability and limit the toxicity, it is hard to keep the efficiency high and surely it is not possible to reach levels of theoretical relaxivity.[25]

Currently, relaxivity of the contrast agents approved for clinical use is similar. At 1.5 T, the range in relaxivities is from 3.9 to 4.6 $s^{-1}mM^{-1}$, and at 3 T, from 3.4 to 4.5 in human whole blood.[26] Although small differences in degree of lesion enhancement have been shown between agents, for example, in brain imaging for Multihance as compared with Dotarem (two agents at the extremes of the range of relaxivities), no agent has ever been approved by either the FDA or EMA at half dose (0.05 mmol/kg) indication (excluding liver imaging), confirming the close clustering of relaxivities and, thus, enhancement effect of the approved agents. Robic *et al.* (2019), reported Gadopiclenol, a new extracellular and macrocyclic Gd chelate that exhibited high relaxivity, no protein binding, and high kinetic inertness, which is currently undergoing clinical trials (r_1 = 12.8 $mM^{-1}s^{-1}$ at 1.41 T and 11.6 $mM^{-1}s^{-1}$ at 3 T in human plasma).[27] Vagner *et al.* (2016), also reported improved AAZTA based ligands with a relaxivity almost double of the CAs currently approved in clinic.[28] Different approaches to increase relaxivity are currently being investigated, but to date, no new contrast agent has passed clinical trials. [29-30-31]

Contrast agents with a higher relaxivity than that in clinic need to be investigated, since they could provide a better tissue enhancement, improving the detection of small lesions that may be undetectable with the current clinical agents. Above all, it could provide the same contrast enhancement at a reduced dose compared with that of the existing compounds, thus reducing slightly the Gd introduced into the body, lowering the risk of the brain deposition, and Gd-related toxicity.

Animal models in preclinical development

Before going to clinic, a drug, and so a GBCA, has to pass three clinical trials, in addition to a first trial, being the preclinical phase. Into the preclinical phase, testing is performed on non-human species, and drugs are initially screened for toxicology, pharmacokinetics and efficacy.

Animal studies are conducted to test new drugs, proof of concept or mechanisms of action. Before going to clinic, preclinical studies acts as a bottleneck, in which only the drugs that prove to be safe and with a certain efficacy to treatment pass to the clinical trials, and hopefully, to the clinic.

Success rates for drugs during clinical development are low. Failure rates could be decreased by having more stringent success criteria during preclinical stages. Success during these stages is dependent heavily on the selected animal models, which allow assessment of target validity and predict clinical efficacy of the compound.

A model is defined as a simple representation of a complex system. Animal models are just simple representations of human diseases, and since human diseases are complex, an animal model attempts to represent one of the aspect of the disease needed to prove the efficacy of the drug of choice. This is why is of vital importance to identify and define the purpose for which an animal model is needed.

Animal models can contribute to our knowledge of biology and medicine, but only if designed and conducted adequately. Moreover, they are the bridge that links preclinical research to clinical research.

According to Denayer et al.[32], animal models can be validated according to a number of different criteria:

1. Face validity: This corresponds to the similarity in biology and symptoms between the animal model and the human disease. This criterion is however, often hampered by not knowing the biology that stands behind the disease symptoms.
2. Predictive validity: demonstration that clinically relevant interventions have the same effect on the animal model that should mimic the disease. This is often difficult to achieve because there is an incomplete correlation between the animal models and the human disease mechanism.
3. Target validity: the target under investigation, if present, should have a similar role in both the disease model and the clinic.

These hard to achieve criteria are often used to provide a general validation of a model. However, it is true that animal models can be used for different purposes, and often not all the criteria apply. It is important to list all the criteria the animal model should have for that general purpose, and try to fit all of them to render the model valid and efficient. Of course, not every criteria can be fit into a single model, so it is important to use different models to fit all the criteria, if applicable.

Improving the quality of the animal models is of essence to reduce the attrition rate that new drugs face when into clinical trials. Proper design and execution of the experiments into preclinical research, improvement of the way in which animal models are used in the decision making process and investment of the development of more sophisticated and clinical models could reduce the attrition rate, thus making animal models more valid and effective into drug development.

Animal models are also used to test the efficacy of new GBCAs. In particular, pathological models are a way to confirm whether the GBCA used reaches the zone of interest that has to be diagnosed, (*i.e*. tumor,

ischemia, multiple sclerosis, etc.) and if the contrast produced is high enough to differentiate between healthy and pathological tissue.

Following Denayer *et al.* criteria, a valid pathological animal model to test GBCAs MRI efficacy should satisfy the following conditions:

1. Have a clinical translatability. Contrast Enhanced-MRI is used to diagnose and follow up a variety of pathologies, but not everything. Animal models should be chosen accordingly.
2. High reproducibility. Every animal of the given model should be as standardized as possible to reduce group variability and ensure a high reproducibility. Therefore, animal models should be easy to induce and should be performed by the same operator.
3. High Vascularization of the tissue of interest. Non targeted GBCAs easily distribute into highly vascularized tissues. This is why usually, they are used for tumor diagnosis and other pathologies that are characterized by high vascularization.
4. Good MRI contrast after GBCA administration. Since the purpose of the animal model is to test GBCAs efficacy, it has to provide a high contrast after the administration of any GBCA. That means that the tissue of interest has to receive the contrast in order to compare different drugs.

Those criteria have to be used to look into literature and plan different pathological models that would satisfy the need for GBCAs efficacy studies.

Aim of the thesis

In this scenario, where the GBCAs are largely used in clinic, but at the same time new concerns are emerging, the research of new Gd-chelates with high relaxivity and high stability is undergoing to a new boost. This PhD thesis is inserted in this context, and specifically is aimed to test two novel high relaxivity GBCAs on healthy animals and on different pathological models, as a first step for translation to clinical trials.

In the first part of the thesis a linear, dimeric, albumin binder GBCA was fully characterized in vitro in terms of relaxometric properties and then its bio-distribution was evaluated on healthy animals and a pathological model of ischemia. In the second part, a dimeric macrocyclic GBCA, selected as possible candidate for clinical translation, was tested for its pharmacokinetics and its efficacy on a series of pathological models, properly selected: glioma, meningioma, cerebral ischemia and breast cancer.

2. Pathological Models setup and optimization

Introduction

This chapter will focus on the pathological models setup used in testing the efficacy of the two GBCA compounds object of this thesis.

Pathological models were designed by taking into consideration the purpose of the main study: GBCA efficacy studies. For this reason, as stated already in the introduction of this thesis, Denayer *et al.*[32] criteria were followed. A pathological model was considered to be ideal for GBCA efficacy studies if it was characterized by: 1) Easy Induction and High reproducibility 2) High success rate 3) Great clinical translation 4) Elevated vascularization 5) Good perfusion and retention of GBCA after injection.

Succeeding these pre-established criteria, five pathological models seemed to be fitting our purpose. Those were the following: C6 Rat Glioma; CH157MN Convexity Meningioma and CH157MN Skull Base Meningioma; Photoinduced Cerebral Rat Ischemia; BT-20, 4T1 and TS/A Breast Tumor.

Models were correctly induced with the aim to optimize the procedure, making it more feasible and reproducible, reducing the pain and stress associated to the animal and thus improving animal welfare in accordance to the 3Rs guidelines[33].

After induction, pathological models were followed by MRI acquisition of T_{2w} sequences to monitor the onset and development of the pathology. Assessment of vascularity and permeability was performed by Dynamic Contrast Enhanced MRI. Tumor and Ischemia identity were confirmed by histology.

C6 Rat Glioma: Introduction

Glioblastoma multiforme (GBM) is the most aggressive diffuse glioma of astrocytic lineage and is considered a grade IV glioma based on the WHO classification.[34] GBM is the most common malignant brain tumor: 54% of gliomas are GBM and it accounts for more than 17% of the population of all brain tumors.[35]

22,850 adults (12,630 men and 10,280 women) were diagnosed with brain and other nervous system cancer in 2015 in the US. GBM has an incidence of two to three per 100,000 adults per year, and accounts for 52 percent of all primary brain tumors. These tumors tend to occur in adults between the ages of 45 and 70. Between 2005 and 2009, the median age for death from cancer of the brain and other areas of the central nervous system was age 64.[36]

Medium survival with maximum safe resection, radiotherapy, and concurrent and adjuvant temozolomide, is 12-15 months.[37] Unfortunately, after initial treatment, GBM invariably recurs. Consequently, initial

diagnosis, prognosis, and targeted treatment of these tumors represent very active areas of investigation.

Imaging is fundamental in the diagnosis and follow-up of intracranial tumors. In particular, MRI, which slowly replaced CT, plays a central role in clinical diagnosis, surveillance, characterization and therapeutic follow up of gliomas.[38] Although a lesion can be observed in MRI just by acquiring a T_{2w} image, a hyper-intensity could reflect just an accumulation in water in the tissue, and Glioma diagnosis is confirmed in T_{1w} images after GBCA administration. In fact, pathological contrast enhancement following administration of intravenous gadolinium chelates reflects accumulation of paramagnetic compound in the interstitium, resulting from non-specifically increased blood–brain barrier permeability related to neovascularisation and necrosis.

Implantation of malignant cells into animal brain tissue closely resembles the actual mechanisms of tumor growth. Moreover, inflammatory and vascular reactions are included, mimicking the real event of spontaneous tumors.

Rat C6 glioma cell line was originally induced in random-bred Wistar-Furth rats by injection of N,N'-nitroso-methylurea[39] and subsequent cell culture propagation. C6 Glioma is morphologically similar to glioblastoma multiforme when injected into the brain of neonatal rats.[40] The tumor grows as a highly malignant astrocytoma invading brain, with zone of necrosis and pseudopalisading. Cells appear undifferentiated, with a high mitotic index, with a preferential zone of growth around blood vessels.

C6 Glioma microvasculature perfusion and degree of vascularization was thoroughly studied by Vajkoczy et al.[41] with a nude mouse model of C6 Glioma via intravital fluorescence microscopy. Microvasculature of the tumor is characterized by a homogeneous architecture full of microvessels. Following this studies, glioma microvasculation progression was divided in three stages: in Stage 1, the avascular stage (0 to 6 days post implantation) was characterized by a lag in tumor growth and by a start in the angiogenesis process within the host tissue. In stage 2 (6 to 14 days post implantation), a glioma microvasculature with a homogenous population of microvasculature was estabilished. This event concurred with the start of glioma proliferation; in stage 3 (14 to 22 days post implantation), microvasculature revealed a clear spatial division, and microvascular perfusion started to fail within the tumor center due to the presence of microvessels with either inactive or no blood flow. Moreover, it is important to notice that a high microvascular permeability was observed few days post tumor implantation, characterized by extravasation of low molecular molecules in the newly formed microvasculature.

The above mentioned features make the model an ideal candidate for GBCA efficacy studies validation. Therefore, a pilot study was established and C6 glioma cells were implanted into Wistar Rats. Tumor growth was followed by MRI for 4 weeks after induction, and contrast enhancement was evaluated by CE-MRI at least once a week.

Methods and Materials

Cell line culture and preparation: Rat glioma cells (C6) were supplied by Sigma Aldrich. An already available stock of C6 cells, given as kind gift from Bracco Research USA (BRU), was also used. Cells from Sigma were grown in Ham's F-12 medium supplemented with 5 % foetal bovine serum, 2 mM glutamine, 100 IU/mL penicillin and 100 µg/mL streptomycin. Cells from BRU were grown in DMEM medium supplemented with 5 % foetal bovine serum, 2 mM glutamine, 100 IU/mL penicillin and 100 µg/mL streptomycin. C6 cells were collected and washed two times with Ham's F-12 or DMEM. 10^5 or 10^6 C6 cells were re-suspended in 10 µL Ham's F-12 or DMEM and inoculated in animals with a Hamilton syringe.

Animal Studies: All the procedures involving the animals were conducted according to the national and international laws on experimental animal (L.D. 26/2014; Directive 2010/63/EU). No validated non-animal alternatives are known to meet the objectives of the study. 18 Wistar Rats between 5 and 6 weeks old were purchased from Charles River Laboratories, Calco (LC), Italy. Animals were kept in limited access, housed in groups of 3 in Makrolon® Tecniplast cages, type 4 (up to 5 animals/cage), air-conditioned facilities (20-24°C room temperature, 45-55% relative humidity, 15-20 air changes/h, 12-h light cycle). Food and water were available at libitum. Induction of tumor model was performed after a one week period of acclimation and observation.

Tumor model induction: Glioma tumor cells were implanted into the right striatum by using stereotaxic surgery. Rats were previously treated with carprofen (5mg/kg) one hour before surgery. Animals were induced with sevoflurane gas; surgery was performed with systemic anaesthesia, *i.e.* Xylazine 5 mg/kg (Rompun®) and Tiletamine Zolazepam (Zoletil®) 20 mg/kg. Rat's head was shaved and then the animal was mounted on the stereotaxic apparatus. Rat temperature was continuously monitored and maintained in the range 36.5-38.5°C. After cleaning the skin with a disinfectant (iodopovidone), a local anesthesia was administered (lidocaine) at a dose of 5 mg/kg. Bregma was then exposed and the induction sites identified using the following coordinates: (0.8 mm anterior, 3.2 mm lateral to Bregma and 4 (or 6) mm ventral to bone). A small hole was drilled into the skull at the site, and 10 µL of cell suspension, containing 10^5- 10^6 C6 cells was injected manually at a rate of approximately 1 µL/ min using a Hamilton syringe with 25G needle. Dura mater was destroyed during inoculation, where the needle path was built by using a needle with tip. The hole was closed using either bone wax or surgical glue after removing the needle, and the animal was removed from the stereotaxic apparatus. The wound was sutured with surgical glue or silk thread. Carprofen (5 mg/kg) was subcutaneously administered for 3 days after surgery.

Following tumor induction, animals were monitored daily for neurological and/or any other clinical signs onset. The Veterinary Officer administered

additional doses of analgesic (carprofen 5 mg/kg every 24 h) after the first observation of a tumor mass in MR images. Animals were daily monitored and a checklist of clinical signs was filled to evaluate body weight, general condition, spontaneous behavior, reaction to handling, breathing, suture condition, neurological abnormalities. Animals were sacrificed by overdose of anesthesia at the end of the study or when one of the following endpoints was reached:

- loss of weight > 20 %;
- tumor mass volume > 0.25 cm^3;
- severe or prolonged distress (according to checklist evaluation);
- within 30 days from the tumor induction

MRI studies: All animals showed only limited or none clinical sign one week after tumor induction and were imaged weekly (or two times a week for group 5 and 6, defined below) by an MRI scanner at 3 T (Bruker, Germany). Animals were anaesthetized with isoflurane or sevoflurane gas (about 1%) in O_2 and were placed on the MRI animal bed. In the case of administration of Gadovist®, *i.e.* if a tumor mass was clearly visible, an intravenous catheter was inserted in the tail vein of the animal under anesthesia, before positioning inside the MR scanner. During the experiment, anesthesia was maintained by adjustment of gas level in function of breath rate.^{1}H sequences (RARE T_2-weighted) on every anatomical section (axial, sagittal, and coronal) were acquired on the animal to obtain a proper anatomical reference. A series of 3D T_1-weighted FLASH and MSME scans were acquired before and after the intravenous administration of the gadolinium complex in order to follow the kinetic of the contrast agent in the diseased mass, having the following parameters:
FLASH: Matrix size = 192 x192x10, FOV = 3x3x1.8 cm, slice thickness 1.8 mm, TE = 2.7 ms, TR =75 ms, flip angle = 40°, acquisition time = 144 s;
MSME: Matrix size = 192 x128, FOV = 3x3cm, slice thickness 1.8 mm, number of echoes = 3, TE = 15.2 ms, TR = 388 ms, acquisition time = 50 s.
When required, Gadovist® was administered at a dose of 0.1 mmol/kg corresponding to an administration volume of 2 mL/kg of a 50 mM solution (obtained as dilution of the original formulation with saline), at an injection rate of 2 mL/min. The injection was performed manually with the help of a timer to check the injection rate. The kinetic of Gadovist® was followed up to 20 minutes post injection.
Data Analysis: Tumor volume was measured by selecting proper regions of interest (ROIs) over the tumor on both T_2 and T_1 weighted images. FLASH and MSME images analysis was also performed in terms of post contrast enhancement, by positioning the ROIs over brain tissue and tumor mass. ROIs positioning and signal quantification was performed by using a home developed plugin, running on ImageJ (imagej.nih.gov/ij/). Signal enhancement (enh) was calculated as follows:
$Enh = 100 (Signal_{postCA} - Signal_{preCA}) / Signal_{preCA}$,

where $Signal_{postCA}$ and $Signal_{preCA}$ indicate MR signal before and after CA administration, respectively.

Histology Studies: Histology was performed by using Hematoxylin and Eosin Staining on brains collected after animal euthanasia. Tissues were mounted and visualized on an optical microscope. Tumors were graded according to the WHO guidelines.[42]

Results

Eighteen animals underwent stereotaxic surgery to induce the development of C6 glioma in the right striatum. Different experimental conditions were tested to improve the outcome of the model and render it more reproducible. Moreover, different adjustments were made as a way to improve the animal welfare, reduce animal suffering and refine the current procedures.

Animals were divided in 6 experimental groups according to the conditions of cell inoculation and stereotactic coordinates, as summarized in Table A. Sixteen over eighteen animals survived the surgery procedure, while two animals did not survive the systemic anesthesia. All survived animals with the exception of animal 10 and 14 developed a tumor mass. After tumor induction, animals were imaged weekly (or closer) by MRI at 3 T with a surface coil, to monitor tumor onset and development, and administered with Gadovist® if a tumor mass was clearly visible, to evaluate tumor enhancement. After euthanasia, brains were excised, collected and stored in formalin to perform histology to identify the nature of the lesion.

Table A: Experimental Scheme

Group number	Animal number	Cell number	Stereotaxic coordinates
Group 1	1-3	10^{6*}	0.8 ant - 3.2 lat - 4 vent
Group 2	4-6	10^{5}	0.8 ant - 3.2 lat - 4 vent
Group 3	7-9	10^{6} insulin needle	0.8 ant - 3.2 lat - 4 vent
Group 4	10-12	10^{6} (from BRU, insulin needle)	0.8 ant - 3.2 lat - 4 vent
Group 5	13-15	10^{6} insulin needle, 15 minutes waiting after cell release	0.8 ant - 3.2 lat - 6 vent
Group 6	16-18	10^{6} insulin needle with the tip cut, 15 minutes waiting after cell release, surgical glue to seal the skull hole	0.8 ant - 3.2 lat - 6 vent

*Animal 3 was inoculated with $8x10^{5}$ cells due to an experimental error.

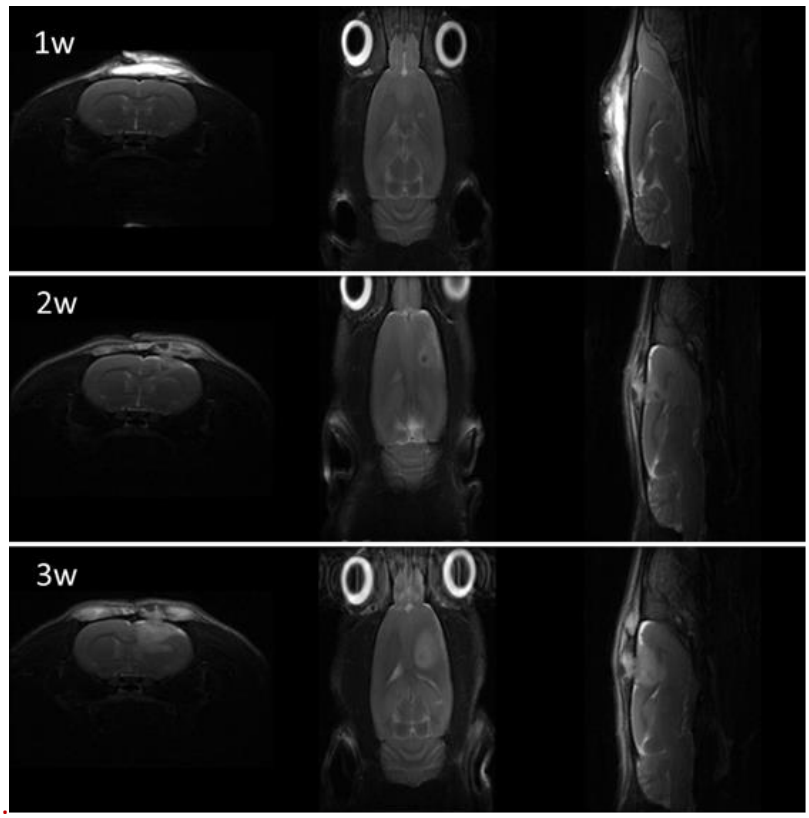

Figure 1 *Representative anatomical T_2-weighted of an animal belonging to group 1 at different weeks post tumor induction in all geometrical sections.*

A tumor mass was clearly visible from two weeks after surgical induction, as it is possible to see in Figure 1, which represents the anatomical T_{2w} images acquired in different geometrical sections and time points. In pre contrast T_{1w} images (MSME), brain tissue and tumor showed the same signal, and the first was not clearly discernible from the other. However, after contrast agent injection, there was an increase in enhancement in the lesion, rendering it more recognizable from the healthy tissue. This event is clearly visible in Figure 2, which represents a T_{1w} image pre and just after contrast agent injection.

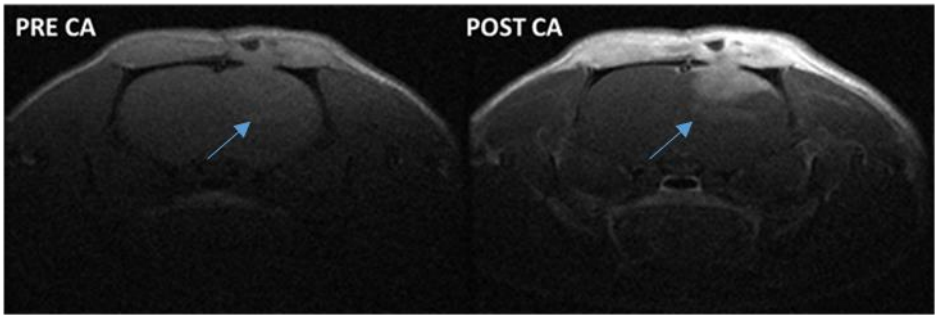

Figure 2 *Representative example of MSME images of an animal belonging to group 1 acquired before and just after administration of Gadovist®.*

Signal enhancement after contrast administration is reported in Figure 3. Observed enhancement of the tumor mass was assessed over time and no significant changes in enhancement were detected over the weeks of tumor growth.

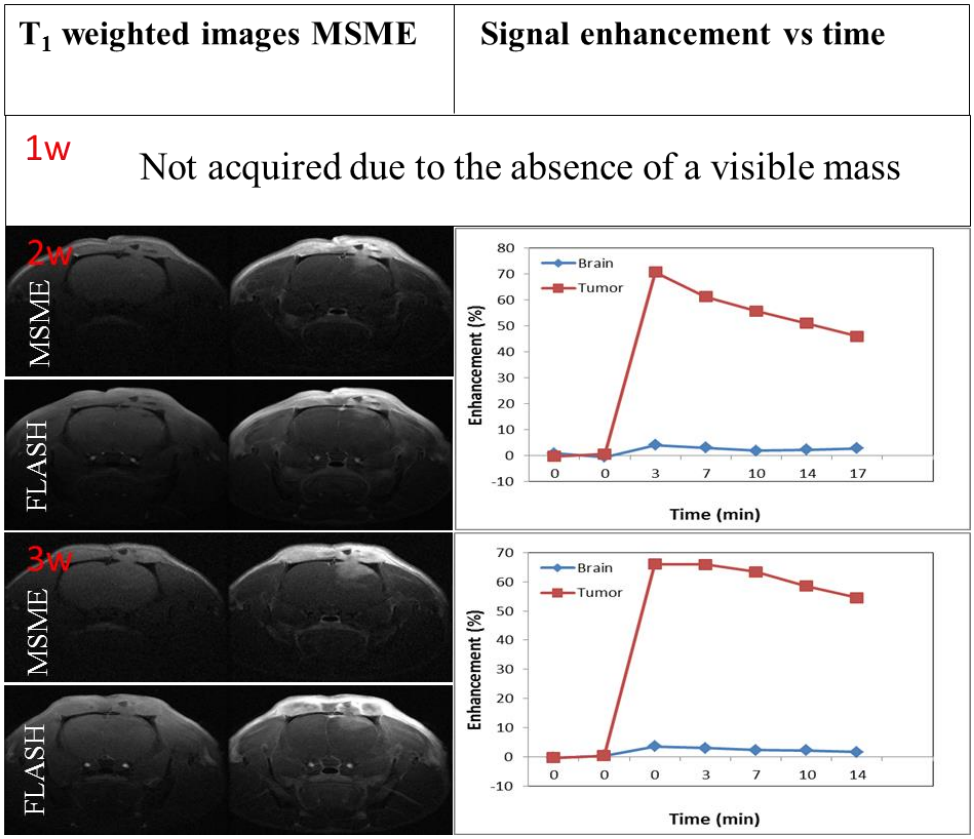

Figure 3 *Representative contrast enhanced T_1-weighted images and MSME signal enhancement as a function of time for brain tissue (blue) and tumor mass (red) at different weeks post tumor induction (Group 1).*

Experimental results in terms of mass dimensions and maximum enhancement value in FLASH and/or MSME images are reported in Table B. The first five groups show a similar tumor growth, with a mass usually visible in MRI after 2 weeks post induction, whereas group 6 shows a tumor development which is 2 or 3 days faster. This is probably due to the fact that induction procedure was improved, thus leading to a better evolution of the glioma.

Table B: Summary of experimental results.

Group	MRI 1w	MRI 2w		MRI 3w		MRI 4w		Mean Tumor volume at sacrifice (mm3)
	Anatomy	FLASH max enh (%)	MSME max enh (%)	FLASH max enh (%)	MSME max enh(%)	FLASH max enh (%)	MSME max enh (%)	
1	no tumor observed	x	x	80	78	70	80	212
2	no tumor observed	x	x	62	70	80	85	135
3	no tumor observed	55	x	65	65	x	x	45
4	no tumor observed	70	x	57	75	x	x	58
	8-9 days	**12days**						
5	no tumor observed	x	12	x	70	x	90	57
6	Large mass	x	80	x	70	x	70	63

The symbol x indicates that the experiment was not performed. The enhancement value refers to the highest value observed in the first 20 minutes post injection, averaged per group.

Tumor mass signal enhancement was always noticeable, ranging from 50 to 120% (with few exceptions at short times after induction). Enhancement was always superior in MSME images rather than in FLASH acquisitions, thus the latter were removed from the experimental protocol in groups 5 and 6.

Tumor development is fairly homogeneous between the groups. All groups, with the exception of Group 2, are characterized by the injection of the same number of cells. For this reason, Group 2 showed a slower development, consistent with the number of cells injected in the striatum. Group 1 and Group 3 differ only for the needle used for cells inoculation (G25 was used instead of G23), thus no differences can be observed. Group 4 was inoculated with a batch of C6 cells from different origin (kind gift of BRU), to see whether there was a difference from the commercial cells obtained from Sigma. As expected, the C6 glioma tumor growth is comparable between the two cell lines, both in terms of mass dimension and growth rate. The best experimental conditions in the first four groups were: use of G25 needle, Sigma cells, 10^6 cell number.

However, the first optimization of the model was not enough to assure reproducibility and to improve animal welfare. Tumor development was homogeneous but it had a major drawback, which was the presence of a large mass outside the skull rather than confined in the striatum. The mass seemed to start growing into the place of injection, but being the cells characterized by high malignancy, they tended to grow along the needle path, emerging from the skull. This discrepancy with expectation could be ascribed to a not enough deep ventral stereotaxic coordinate, or to a too fast removal of the needle, that caused cell dispersion. For these reasons, Group 5 was induced with an increased ventral coordinate up to 6 mm, and

cell release was followed by a 15 minutes waiting before needle removal, to avoid cell dissemination. Nevertheless, the obtained results did not differ significantly from the previous groups, since the occurrence of extra-cranial masses persisted. Consequently, in the last group the injection was performed by using a needle with the tip cut in order to facilitate diffusion of cells into the tissue. Moreover, the skull hole was sealed with surgical glue, which offers way more resistance that bone wax and thus should help with the containment of the mass.

Both Group 1 and Group 6 exhibited good results in term of growth and enhancement over time. However, Group 1 included animals with extra-cranial tumors and cerebral masses characterized by large area of edema that did not enhance after contrast. Conversely, the results obtained in Group 6 were satisfying, with two drawbacks, *i.e.* ventriculomegaly (enlargement of ventricles), and the onset of clinical signs observed by the Veterinary Officer 15 days post induction. In particular, all the animals showed clinical signs such as pink coloration of the mantle, nervousness to manipulation. Moreover, at 15 days post induction animals showed general discomfort and dehydration (n=3), loss of weight higher than 5% and loss of equilibrium (n=2), dyspnea, hypoesthesia and head tilt (n=1).

Ventriculomegaly was detected during MRI monitoring, and it was characterized by a mild enlargement of the third and lateral ventricles (Figure 4). Since no other ventricles or brain regions were interested in the pathology, and since no anomalous change in the skull appearance was reported by the Veterinary, Ventriculomegaly was considered mild and not linked with more important pathologies such as hydrocephalus. As reported in literature[43], mild ventriculomegaly is asymptomatic and thus was not considered a relevant drawback. The onset of the other clinical signs reported is however, considered important.

Since moderate to severe clinical signs were observed only after 15 days post tumor induction, the efficacy studies will be performed between 10 and 12 days post induction, in order to prevent the onset of clinical signs and improve the animal welfare.

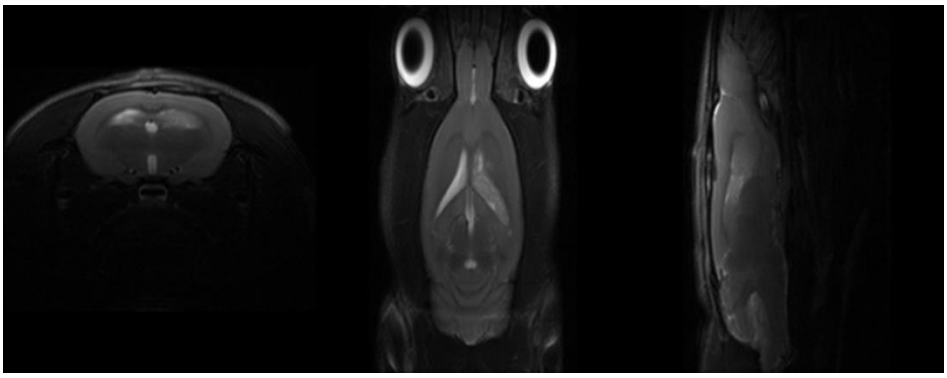

Figure 4 *Representative T_{2w} images of Rat 16, with enlargement of the 3rd and Lateral ventricles.*

Tumor identity was confirmed by histology. Gliomas were confirmed in all cases, and most tumors were characterized by infiltrative masses into the brain and small zones of hemorrages. (Figure 5)

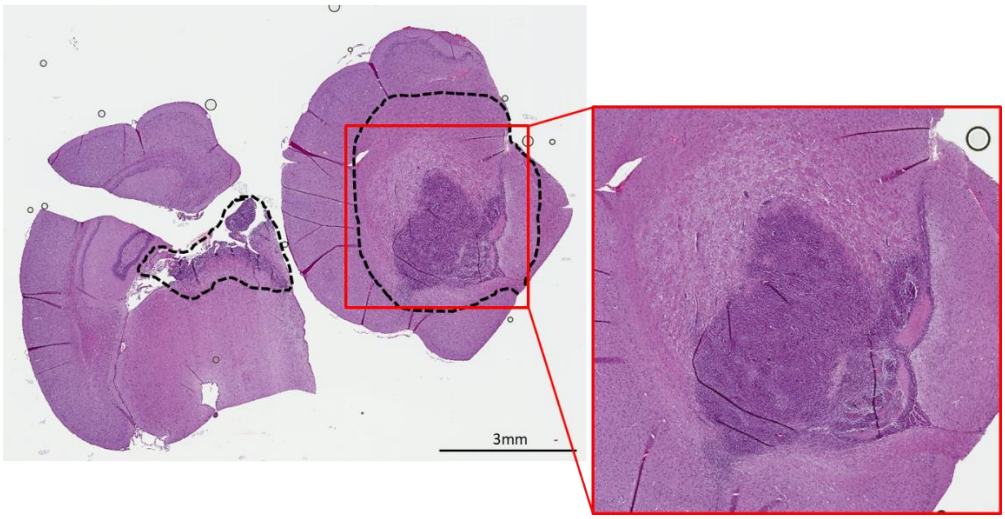

Figure 5 *Transversal section of a resected brain of a Rat with a C6 Glioma post 12 days induction.*

Conclusions

Glioblastoma Multiforme is the most common diagnosis in primary brain tumors in adults, often characterized by high morbidity and recurrence. Advances in neuroimaging and particularly MRI improved the characterization of the tumor in a noninvasive fashion, leading to a better diagnosis and prognosis.

Contrast Enhanced MRI can help diagnosis, staging, and characterization of cellularity or vascularization of gliomas with different techniques.[44] For these reasons, Rat C6 Glioma was chosen as a model for validation of novel GBCAs.

C6 Glioma tumor was correctly inoculated in 14/16 animals who survived the surgical procedure. Two animals did not survive the systemic anesthesia.

The animal model was characterized by means of MRI, in order to identify the time window by which there would be an identifiable mass, an high contrast enhancement after GBCA injection (>50%), and reduced clinical signs. As mentioned before, the deeper ventral coordinate together with the use of a blunt needle and dental cement to seal the hole, optimized the induction and phenotype of the tumor model. Moreover, the identification of a precise time window helped to reduce the severe clinical signs observed during the pilot study, and thus it was taken into consideration for the final efficacy studies.

CH157MN Meningioma: Introduction

Meningiomas are the most common primary tumors of the Central Nervous System (CNS), accounting for approximately the 33% of all primary

brain and spinal tumors. They arise from approximately any site of the dura mater, most commonly the skull vault, the skull base and the site of dural reflections (*i.e.* tentorium cerebelli, falx cerebri).

Generally, meningiomas are slow-growing tumours composed of neoplastic meningothelial cells. However, their localization in the brain can cause serious morbidity or mortality.[45] Meningiomas are classified according to the World Health Organization (WHO) criteria in three grades, the grade I being benign, while grades II and III being associated with a higher proliferation, increased mitotic activity, malignant cytology and a number of genetic alterations.[46] Tumor grading takes into account both the tumor subtypes known to have a high grade of recurrence, and specific histological features that determines biological aggression and response to therapy.

The incidence of meningioma increases progressively with age, where the average year of diagnosis is 65 years old. Women have an increased risk of developing this tumor: actually, the female to male ratio is of two/three to one.[47] This may mean that hormonal factors have a role in the development of this tumor: the incidence of meningioma in women is at its peak during reproductive years but it decreases with age and progesterone and androgen receptors are present in 66% of patients.[48-49]

Since meningiomas are mostly completely asymptomatic, 2-3% of the population may have developed a meningioma in their life without it being diagnosed: actually, incidental asymptomatic meningiomas were found in the 8% of patients post mortem, during autopsy. [50]

With the advent of CT and MRI, many meningiomas are discovered as incidental findings, during other disease investigations.[51] Meningiomas remain one of the most common incidental tumors, identified in 0.29% of MRIs.[52]

Neuroimaging is important in the diagnosis of meningiomas, especially in the case of incidental tumors.

On MRI, a typical meningioma is an extra-axial mass originating from the dura, which is isointense or hypointense to gray matter on T_{1w} images, and isointense or hyperintense on T_{2w} and proton density images. Usually, they display a strong enhancement after gadolinium administration due to high vascularization. Moreover, most meningiomas show a characteristic enhancement and thickening of the dura adjacent to the tumor, called “dural tail sign”. Even if it has been demonstrated that the dural tail sign is not a mark of tumor invasion but is predominantly a reactive process due to edema and vascular congestion, this characteristic is usually reported with WHO II atypical meningiomas, occurring in 35%-80% of the patients.[53]

The use of neuroimaging alone (MRI or CT) for the diagnosis of meningioma is difficult. However, sometimes it is not possible to do a

biopsy for the histological examination of the lesion, and these techniques can provide a tool for empiric treatment.

A malignant meningioma presents some features on MRI that can help differentiate it from a benign WHO grade I tumor, such as intratumoral cystic change, bone destruction, extension of the tumor through the skull base, peritumoral brain edema, low apparent diffusion coefficient (ADC) values and elevated cerebral blood volume.[54-55-56]

Overall, even though meningioma is mostly a benign pathology, is important to improve early detection and treatment of the tumor. This can be done involving different *in vitro* and *in vivo* studies on immortal cell lines as well as cells derived from operative specimens.[57-58]

The first animal model of the pathology involved the transplantation of meningioma human cells into guinea pig eyes in 1945.[59] Different xenograft animal models have been described since that time. The intracranial model of meningioma is the most biologically reproducible and desirable, but it is currently limited by the difficulty of tumor monitoring and by the impossibility to obtain a direct measurement of the mass. However, this problem can be overcome by introducing MRI as a way to characterize and monitor in real time the evolution of cerebral pathologies even in preclinical practice.

The first intracranial model of meningioma was reported by McCutcheon et al.[60], were different WHO grading meningiomas were placed into primary cell cultures, and then injected into the frontal white matter or subdural space of the brain of athymic nude mice. IOMM-Lee, an immortalized cell line, was also used. This study demonstrated for the first time the feasibility of growing intracranially a meningioma into mice, and that the tumors retain the histological characteristics and growth patterns of clinical meningiomas.

Ragel *et al*.,[61-62] established a model of intracranial meningioma with the stereotaxic injection of CH157MN and IOMM-Lee human immortal cells in the convexity and Skull Base. Both cells were transfected with Luciferase in order to monitor tumor growth and localization with Bioluminescence Imaging. Tumors that grew intracranially, showed histological, immunohistochemical and ultrastructural features consistent with clinical meningiomas, such as negative staining for GFAP, and positive staining for vimentin. Moreover, CH175MN meningiomas exhibited desmosomes and junctional complexes consistent with clinical meningioma.[63]

In this pilot study, CH157MN cell lines were used for the orthotopic induction of Skull Base of the Auditory Meatus and Convexity meningioma into mice.

CH157MN cell line was first isolated in 1977 from a meningioma resected from a 41 years old woman. Tsai *et al.*,[64] first characterized this cell line in

1995 for the vascular endothelial growth factor (VEGF) and vascular permeability factor (VPF), providing important information regarding tumor vascularity, permeability and angiogenesis.

47 nude female mice (23 athymic, 24 CD-1) were inoculated with CH157MN cells and imaged weekly on a 1T scanner, before and after administration of a commercial Gadolinium Based Contrast Agent (GBCA). The introduction of a non-invasive method as MRI, allowed a proper evaluation of tumor growth, vascularization and GBCA perfusion/permeability.

The optimization of both meningioma models, namely Convexity and Skull Base meningioma, together with the MRI characterization, was reported in the following technical report, published during my PhD: La Cava *et al*., AMEM 2019 (2) 58-63[65]

Methods and Materials

Cell line culture and preparation: CH157MN meningioma cells were obtained as kind gift of Dr. Yancey Gillespie, University of Alabama (USA). Cells were grown in cultured in DMEM F12 with with 7% foetal bovine serum (FBS), 2 mM glutamine, 100 IU/mL penicillin and 100 µg/mL streptomycin. CH157MN cells were collected and washed two times with DMEM F12. 5 x 10^4 - 5 x 10^5 (skull base) to 10^5-10^6 (convexity) CH157MN cells were re-suspended in 3-8 µL DMEM F-12 and inoculated in animals with a Hamilton syringe and stereotaxic device.

Animal Studies: All the procedures involving animals were conducted according to the national and international laws for the care and use of laboratory animals (L.D. 26/2014; Directive 2010/63/EU). This experimental protocol was approved by the Italian Ministry of Health with Authorization 724/2017 PR. No validated non-animal alternatives are known to meet the objectives of the study.

24 CD-1 female nude mice and 24 athymic female nude mice, between 4 and 5 weeks old were purchased from Charles River Laboratories, Calco (LC), Italy. Animals were kept in limited access, housed in groups of 6 in polysulfone Tecniplast Double Decker ventilated cages (up to 14 animals/cage), air-conditioned facilities (20-24°C room temperature, 45-55% relative humidity, 15-20 air changes/h, 12-h light cycle). Food and water were available at libitum. Induction of tumor model was performed after a one-week period of acclimation and observation.

Tumor model induction: Mice were subcutaneously administered with carprofen 5 mg/kg one hour before the surgery. Anesthesia was induced with sevoflurane gas and then systemically by injection of Rompun® 5 mg/kg and Zoletil® 40 mg/kg. After checking for absence of reflexes, the animal was positioned on the stereotaxic apparatus and its temperature was continuously monitored and maintained in the range of 36.5-38.5 °C.

After cleaning the skin with a disinfectant (iodopovidone), a local anesthesia was administered (lidocaine) at a dose of 3 mg/kg. Bregma was then exposed and the site of induction was identified by using the following coordinates: 3 mm anterior, 2 mm lateral to bregma and 2 mm under the frontal bone for the Convexity Meningioma and at the skull base (13-14 mm) for Skull Base Meningioma. A small hole was drilled manually, and a volume of 3-8 µL containing 5 x 10^4 - 5 x 10^5 (skull base) to 10^5-10^6 (convexity) CH157MN cells was released manually in approx. 1 µL/3 min by using a Hamilton syringe with 25G needle. The hole was closed after removing the needle, by using two different materials: bone wax or surgical glue, and the mouse removed from stereotaxic apparatus. The wound was sutured by using surgical glue or silk thread. Carprofen 5 mg/kg was subcutaneously administered for 3 days after surgery.

Following tumor induction, animals were monitored daily for neurological and/or any other clinical signs onset. The Veterinary Officer administered additional doses of analgesic (carprofen 5 mg/kg every 24 h) after the first observation of a tumor mass in MR images. Animals were daily monitored and a checklist of clinical signs was filled to evaluate body weight, general condition, spontaneous behavior, reaction to handling, breathing, suture condition, neurological abnormalities. Animals were sacrificed by overdose of anesthesia at the end of the study or when one of the following endpoints was reached:

- loss of weight > 20 %;
- tumor mass volume > 0.25 cm3;
- severe or prolonged distress (according to checklist evaluation);
- within 30 days from the tumor induction

MRI studies: All animals showed only limited or no clinical signs one week after tumor induction and were imaged weekly (or two times a week) by MRI (Icon, 1T, Bruker). Animals were anaesthetized with isoflurane or sevoflurane gas (about 1%) in O_2 and were placed on the MRI animal bed. In the case of administration of Gadovist®, i.e. if a tumor mass was clearly visible, an intravenous catheter was inserted in the tail vein of the animal under anesthesia, before positioning inside the MR scanner. During the experiment, anesthesia was maintained by adjustment of gas level in function of breath rate.

^{1}H sequences (RARE T_2-weighted) on each geometry were acquired on the animal to obtain a proper anatomical reference.

A series of 3D T_1-weighted FLASH and MSME scans were acquired before and after the intravenous administration of the gadolinium complex in order to follow the kinetic of the contrast agent in the diseased mass, having the following parameters:

FLASH: Matrix size = 192 x192x8, FOV = 1.7x1.7x0.96 cm, slice thickness 9.6 mm, TE = 5.4 ms, TR =60 ms, flip angle = 40°, acquisition time = 92 s, number of averages = 1;

MSME: Matrix size = 128 x128, FOV = 1.6x1.6 cm, slice thickness 1.2 mm, number of echoes = 1, TE = 9.2 ms, TR = 350 ms, acquisition time = 90 s, number of averages = 2.

When required, Gadovist® was administered at a dose of 0.1 mmol/kg corresponding to an administration volume of 2 mL/kg of a 50 mM solution (obtained as dilution of the original formulation with saline), at an injection rate of 2 mL/min. The injection was performed manually with the help of a timer to check the injection rate. The kinetic of Gadovist® was followed up to 20 minutes post injection.

Data Analysis: Tumor volume was measured by selecting proper regions of interest (ROIs) over the tumor on both T_2 and T_1 weighted images. FLASH and MSME images analysis was also performed in terms of post contrast enhancement, by positioning the ROIs over brain tissue and tumor mass. ROIs positioning and signal quantification was performed by using a home developed plugin, running on ImageJ (imagej.nih.gov/ij/). Signal enhancement (enh) was calculated as follows:

$$Enh = 100\ (Signal_{postCA} - Signal_{preCA}) / Signal_{preCA},$$

where $Signal_{postCA}$ and $Signal_{preCA}$ indicate MR signal before and after CA administration, respectively.

Histology Studies: Histology was performed by using Hematoxylin and Eosin Staining on brains collected after animal euthanasia. Tissues were mounted and visualized on an optical microscope. Tumors were graded according to the WHO guidelines.[66]

Results

CH157MN meningioma was induced on 47 nude mice, according to the experimental protocols summarized in Table A. The induction was successful in 35/47 animals, specifically in:

- 15/24 for Skull Base Meningioma (4 mice did not survive the systemic anesthesia and 1 showed clinical signs immediately after the surgery; 4 mice did not develop any tumor);(Group 1-4)
- 20/23 for Convexity Meningioma (1 mouse did not survive the systemic anesthesia; 2 mice did not develop any tumor). (Group 5-8)

Since no substantial difference or any fallouts in development of the tumor were observed within the two animal strains (*i.e.*, Athymic, CD-1), for simplicity the results presented here below will not consider anymore the strain as a variable.

Table A: Experimental Scheme and Results

Group	Cell Number/Suture Procedure	Stereotaxic Coordinates	Intraoperatory Mortality	Tumor Take Rate	Average Tumor	Avrg Max Enh (%)	Clinical Signs
1	$5{\cdot}10^4$/3 µL, surgical glue	Ant. 3 mm, Lat. 2 mm, Vent. 12-13 mm and needle with tip;	1/6	4/5	55	80	Neurological damage, unsteady gait, tumbling, apathy
2	$5{\cdot}10^5$/3 µL, surgical glue	Ant. 3 mm, Lat. 2 mm, Vent. at skull and needle without tip	1/6	3/5	85	70	No observations
3	$5{\cdot}10^4$/3 µL, silk thread (5.0)	Ant. 3 mm, Lat. 2 mm, Vent. at skull and needle without tip	1/6	2/5	45	70	Loss body weight <8%, dyspnea, isolation from the group, dehydration, closed eye lids, unsteady gait
4	$5{\cdot}10^5$/5 µL, silk thread (5.0)	Ant. 3 mm, Lat. 2 mm, Vent. at skull and needle without tip	2/6	4/4	50	55	Tachipnea, isolation from the group, immobility, closed lid eye, loss of coordination and equilibrium
5	10^5/3 µL, surgical glue	Ant. 3 mm, Lat. 2 mm, Vent. 2 mm and needle without tip	1/6	5/5	62	70	Domed head
6	10^6/8 µL, surgical glue	Ant. 3 mm, Lat. 2 mm, Vent. 2 mm and needle without tip	0/5	4/5	50	70	No observations
7	10^5/3 µL, bone wax+silk thread (5.0)	Ant. 3 mm, Lat. 2 mm, Vent. 2 mm and needle without tip	0/6	5/6	40	80	Domed head and retracted eyes
8	10^6/6 µL, bone wax+silk thread (5.0)	Ant. 3 mm, Lat. 2 mm, Vent. 2 mm and needle without tip	0/6	5/6	50	60	Domed head and retracted eyes

As detailed in Table A, once the inoculation site has been set, different experimental conditions were tested (*i.e.* the cell number and the method adopted to suture the surgical wound) to optimize the protocol.

The Convexity Meningioma generally showed a better outcome than the Skull Base model, in terms of success of the surgical procedure and in terms of animal welfare. Specifically, the intra-operative mortality was lower for 3 out of 4 groups inoculated superficially, indicating, as expected a minor surgery risk, since the needle stops at the surface rather than passing through the brain to reach the auditory meatus. Even after surgery, the occurrence of clinical signs was more severe for the Skull Base model, with the appearance of unsteady gait, domed head and loss of equilibrium. Loss of equilibrium was probably due to the specific location of the tumor in the auditory meatus. As a further advantage of the Convexity model, the tumor take rate was superior. Tumor volume, growth rate and maximum enhancement after GBCA administration were comparable between the two sites. All the different procedures to close the skull hole adopted for both the Skull Base and Convexity Meningioma were effective to avoid the appearance of any extra-cranial mass. Surgical glue rather than silk thread should be preferred to wound the suture to prevent the animal from opening it due to over-grooming.

A standard needle was used during cells inoculation only for three animals, while for all the other experimental groups the tip of the needle was cut. This choice was motivated by the fact that, only one animal over three inoculated using a standard needle developed an observable tumor mass; probably due to the fact that the presence of the tip caused surface tension, avoiding proper release of tumor cells.

Starting from one week after tumor induction, up to the end of the observation period (*i.e.* 30 days after tumor induction) or the occurrence of one of the end-points (*i.e.* tumor mass larger than 0.15 cm^3, weight loss ≥ 20%), animals without significant or prolonged clinical signs were imaged weekly (or closer) by MRI and administered with a GBCA in the presence of a clearly visible tumor mass. In the case of skull base meningioma, euthanasia after the occurrence of severe or prolonged clinical signs was required for 10 animals: 2 animals just after the surgical procedure, 1 animal one week post tumor induction and 7 animals two weeks post tumor induction. In the case of convexity meningioma, euthanasia was required for 4 animals: 2 animals one week post tumor induction and 2 animals two weeks post tumor induction.

A tumor mass was generally visible starting from 1 week/10 days from induction in both inoculation sites, as observable for representative animals in all geometrical sections of T_2-weighted images (Figure 6A-B). T_1-weighted images (pre and post contrast) together with signal enhancement *vs* time quantification are shown in panel A and B of Figure 7 for Skull Base

and Convexity meningioma, respectively. In pre contrast images, brain tissue and tumor mass showed the same signal, but after GBCA administration, the diseased tissue reached a higher enhancement and became clearly discernible from the contralateral region, *i.e.* auditory meatus for Skull Base Meningioma and healthy brain for Convexity Meningioma. The enhancement of the tumor mass was always noticeable, ranging from 50 to 120 % with two exceptions, immediately after induction and when the tumor mass was not well developed yet. Finally, meningioma identity and tissue vascularization were assessed by histological analysis. Both CH157MN orthotopic tumors exhibited histological analogies of human grade III meningioma tumor, such as nuclear polymorphism, large cells with eccentric nuclei and abundant cytoplasm and mitosis (Figure 8). The tumors displayed infiltrative growth, widespread vascularization and, often, the presence of hemorrhages.

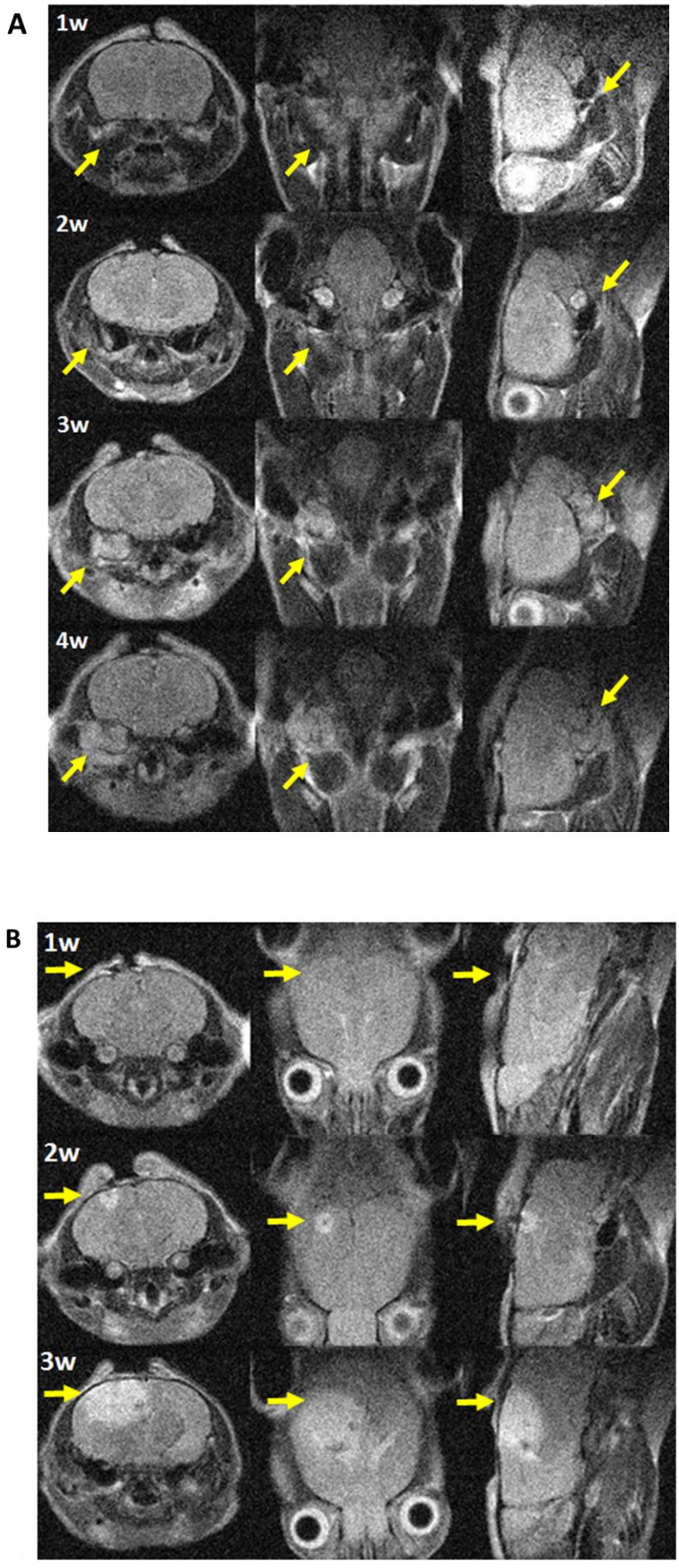

Figure 6. *Representative anatomical $T_{2\text{-weighted}}$ images at different weeks post tumor induction in all geometrical sections (from left to right axial, coronal and sagittal). A: Skull Base meningioma, Group 3. B: Convexity Meningioma, Group 8.*

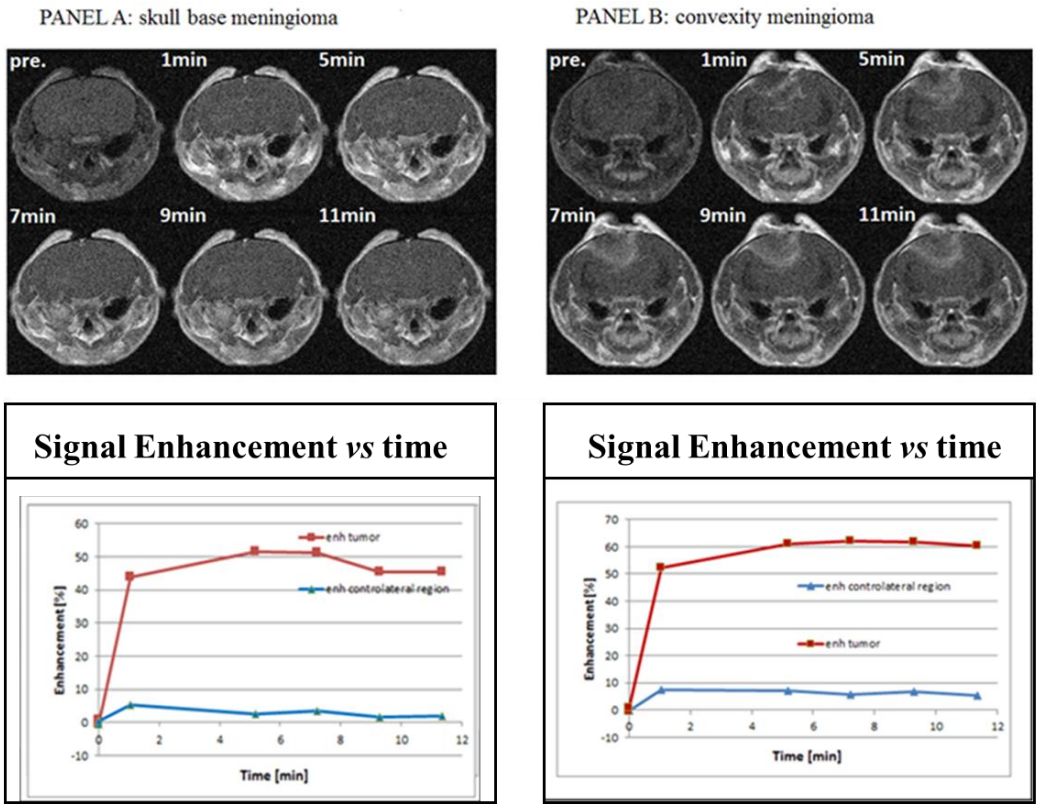

Figure 7 *Representative contrast enhanced T1-weighted images and MSME signal enhancement as a function of time for healthy contralateral tissue (blue) and tumor mass (red).*

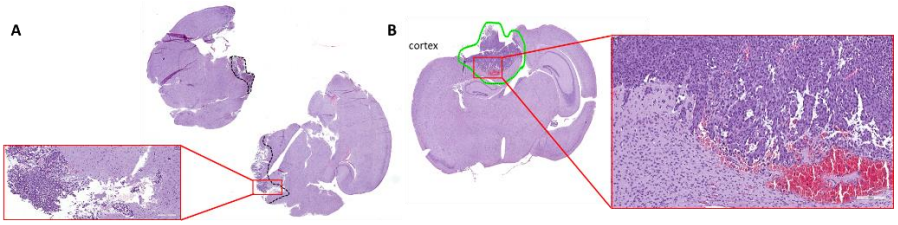

Figure 8 *Transversal section of CH157MN Skull Base (Panel A) and Convexity (Panel B) Meningioma.*

Conclusions

Two different models of orthotopic meningioma into mice were described and optimized.

In particular, Skull Base Meningioma was correctly induced into the auditory meatus of female nude mice. This model is really complicated to induce, and most stages are considered critical for both the correct induction of the model and the animal welfare. However, there are some steps that should really be taken into consideration when this model is induced:

1) Finding the correct ventral coordinate to the skull base. Ragel *et al.*, mentioned that the needle should stop at the base of the skull, but it is hard to identify the correct location of the meatus. Because of this reason, a series of different coordinates were identified with the aid of the mouse brain atlas. The best coordinate was identified based on the

fact that the needle encountered resistance when moved in the ventral position. However, is it important to notice that this coordinate stays true if the mouse used for this model has the same strain, sex and age described above.

2) The rate of cellular release into the auditory meatus. The volume needed to suspend the cells is fairly high for a mouse brain, so it is important that the release happens slowly and carefully, especially into the meatus. Else, an accumulation of edema into this site could cause massive clinical signs such as loss of equilibrium at the end of the procedure.

Convexity Meningioma was easier to induce and overall showed less clinical signs and troubleshooting. However, those steps should be performed with particular care for the correct induction of the model:

1. The Dura mater should not be damaged when drilling the skull. For this reason, the hole was drilled manually, with the use of magnifying glasses to help the operator. There will be a moment when the drill will encounter less resistance, and this is when the drilling has to stop. Else, the Dura mater will be broken and the cells will be inoculated into the brain.

2. Some tumors have a rapid development and tend to grow outside the skull. It is really important to close the hole correctly. For this reason, dental cement proved to be the more efficient choice to prevent the tumor from growing outside the skull.

Furthermore, for both models, a needle without tip should be used when cells are released, to prevent cellular dissemination and to actually deliver the cells into the inoculation site.

The feasibility and high reproducibility of both meningioma models proved them to be effective for GBCA validation MRI studies. Moreover, the *in vivo* models showed a marked perfusion by small size CA, probably due to enhanced vascularization and permeability. The precise locations as seen on MRI of the meningioma tumors proved to mimic the complex situations in human beings. [67]

However, Convexity meningioma was the model of choice for the following efficacy study with the lead compound. Overall, convexity meningioma was associated with better experimental outcomes, such as low mortality, no severe clinical signs, minor risk of cell dissemination through the brain tissue and overall, higher feasibility.

Photoinduced Rat Cerebral Ischemia: Introduction

Despite major technical advances in diagnosis, stroke remains a major health problem. Furthermore, its incidence is likely to increase in the future due to population aging and health transitions on going into

developing countries.[68] Particularly, stroke caused 4.85 million deaths and 91.4 million Disability-Adjusted Life Years (DALY) in developing countries in the last two decades (1990-2013), while 1.6 million deaths and 21.5 million DALYs in high-income countries.[69] It is essentially the second cause of death worldwide, and the first cause of acquired disability. Up to 87% of the total burden of stroke is attributed to ischemic stroke, which is a really complicated and heterogeneous disorder, with more than 100 pathologies implicated in its pathogenesis.[70] Ischemic strokes result from thromboembolic occlusion of a major cerebral artery or its branches. The occlusion results in deprivation of blood flow, which in turn, results in deprivation of energy and oxygen. This major event determines inhibition of electron changes, decrease of ATP, and most importantly, production of free radical species. Together with the glutamate release, accumulation of intracellular calcium and induction of the inflammatory processes, those events are part of the ischemic cascade, which leads to the production of irreversible tissue infarction due to cell death. The ischemic brain tissue surrounding its necrotic core is called “ischemic penumbra”.[71]

An ischemic stroke usually presents itself with neurological deficits, the like of them strictly depending on which area of the brain is affected. The symptoms usually evolve over hours, and may worsen or improve, depending on the severity of the ischemic penumbra.

Neuroimaging plays a key role in the outcome of the ischemic patient. Particularly, treatment of stroke, which consists of thrombolysis with recombinant tissue plasminogen activator (rt-PA) has to be administered within 4.5 hours of lesion onset to be affective. Currently, is available for only 5% of patients due to difficulty of ischemia diagnosis in the 4.5 hours of onset.[72]

In the last 30 years, many neuroimaging techniques have been proposed for penumbra detection and delineation. Even though non Contrast CT remains the gold standard for diagnosis and imaging of the acute stroke because is inexpensive, fast and easily available compared to other imaging techniques, its limited sensitivity in the acute setting required addition of MRI in clinical practice.

Magnetic Resonance Imaging is particularly useful in the first hours after onset of stroke, for hemorrhage detection and for penumbra identification, because of its higher sensitivity and specificity. In particular, Diffusion Weighted Imaging (DWI) is valuable already in few minutes after arterial occlusion, even in small early infarcts. Together with perfusion MRI, is possible to detect the infarcted core and the penumbra, allowing the latter to be quantified and possibly, treated.[73]

Over the last 40 years, a branch of animal research has been focused on developing stroke animal models, with the aim to identify the complete mechanisms that underlie the onset of cerebral ischemia, and to validate

and develop new therapies. Stroke preclinical research usually involves small animals such as rabbits, mice and rats. The latter is particularly suitable for this study due to a great similarity in cerebral vasculature and physiology with humans.[74] Stroke models can reproduce transient ischemic attacks or permanent strokes.

The Middle Cerebral Artery Occlusion model (MCAo) is the most used way of causing stroke in preclinical research studies. This technique consist in the temporary occlusion of the Common Carotid Artery (CCA), introducing a suture in the Internal Carotid Artery (ICA) and thus occluding the blood flow in the MCA, causing a permanent damage. In a modified manner the suture can also be inserted in the External Carotid Artery (ECA) to reach the ICA, but it is usually more complicated and with worst outcomes. Even if this technique is highly reproducible and clearly reflects human physiology, it requires an increased expertise in microsurgery in order to increase the already low success rate. The MCA can also be occluded with electrocoagulation by directly exposing the Dura mater with a craniotomy. However, this technique may lead to injury of the underlying cortex, rupture of the vessel by drilling and furthermore, it has been demonstrated that it affects intracranial pressure and Blood Brain Barrier (BBB) functionality.[75]

The model of choice for efficacy studies validation was, however, the phototrombotic stroke model. This model relies on the injection of a photoactivable dye, Rose Bengal, with the simultaneous irradiation of the skull with a light beam at a specific wavelength. Illumination leads to activation of the Rose Bengal, resulting in formation of free radical formation, endothelial damage due to platelet activation and aggregation into pial and intraparenchymal vessels. The photothrombotic model was first introduced by Watson et al in 1985,[76] as a way to induce a focal cerebral stroke in the cortical vasculature of rats. If compared to the previously mentioned models, is simpler because it does not require actual surgery and manipulation of vessels. Furthermore, lesion size and location can be modulated by altering the irradiating intensity, duration of light exposure to the skull, ban position, and dye dose. Also, this technique does not impair long-term survival and is thus suitable for chronic stroke studies.[77]

Photochemically induced focal ischemia was previously used to verify efficacy and neurotolerability of GBCAs[78] and was characterized by MRI in multiple studies[79-80] For this reasons, ischemia was photoinduced on 24 Sprague Dawley Rats to better identify the induction conditions and to see whether this model is actually suitable for GBCA efficacy studies.

Methods and Materials

Animal Studies: All the procedures involving the animals were conducted according to the national and international laws on experimental animal (L.D. 26/2014; Directive 2010/63/EU). No validated non-animal alternatives are known to meet the objectives of the study. 24 Sprague Dawley Rats, 5 weeks old were purchased from Charles River Laboratories, Calco (LC), Italy. Animals were kept in limited access, housed in groups of 3 in Makrolon® Tecniplast cages, type 4 (up to 5 animals/cage), air-conditioned facilities (20-24°C room temperature, 45-55% relative humidity, 15-20 air changes/h, 12-h light cycle). Food and water were available at libitum. Induction of cerebral ischemia was performed after a one week period of acclimation and observation.

Ischemia photoinduction: Rats were previously treated with buprenorphine (0.05mg/kg) one hour before stereotaxic surgery. Animals were preliminary anesthetized with sevoflurane gas; surgery was performed at first with systemic anaesthesia, *i.e.* Xylazine 5 mg/kg (Rompun®) and Tiletamine Zolazepam (Zoletil®) 20 mg/kg, then it was decided to keep sevoflurane gas also for the surgery. Rat's head was shaved and then the animal was mounted on the stereotaxic apparatus. Rat temperature and breathing were continuously monitored and maintained in the range 36.5-38.5°C and 40-60 breaths/min, respectively. After cleaning the skin with a disinfectant (iodopovidone), a local anesthesia was administered (lidocaine) at a dose of 5 mg/kg. Bregma was then exposed and the induction site was identified using the following coordinates: 1 mm anterior, 3 mm lateral to Bregma. After removal of the periosteum, a green light beam (wavelength: 500 nm) was placed in the abovementioned coordinates, covering an area of 20 mm^2. Rose Bengal (Alfa Aesar, Thermo Fisher (Kandel) GmbH, Germany) was intravenously administered with a 1 mL syringe, at a rate of 0.1 mL/min, with a dose range of 8-40 mg/kg. During the Rose Bengal perfusion, the skull was irradiated for 20 minutes. The wound was sutured with surgical glue or silk thread. Buprenorphine (0.05 mg/kg) was subcutaneously administered for 3 days after surgery. Following ischemia induction, animals were monitored daily for neurological and/or any other clinical signs onset. The Veterinary Officer administered additional doses of analgesic (buprenorphine 5 mg/kg every 24 h) if there was any onset of moderate to severe clinical signs. Animals were daily monitored and a checklist of clinical signs was filled to evaluate body weight, general condition, spontaneous behaviour, reaction to handling, breathing, suture condition, neurological abnormalities. Animals that showed only limited or none clinical sign was imaged by contrast enhanced MRI at 4-24 hours and 3-7-14 days after ischemia induction. Animals were sacrificed by overdose of anesthesia at the end of the study or when one of the following endpoints was reached:

- loss of weight > 20 %;

- severe or prolonged distress (according to checklist evaluation);
- within 30 days from cerebral ischemia induction.

MRI Experiments: From 4 hours up to 14 days after the photochemical induction, all the animals that showed only limited or none clinical sign directly referable to the cerebral ischemia were imaged weekly or closer by MRI (3 T Scanner equipped with a dedicated brain surface coil, Bruker). Animals were anaesthetized with isoflurane or sevoflurane gas (about 1%) in O_2 and were placed on the MRI animal bed. In the case of administration of Gadovist®, an intravenous catheter was inserted in the tail vein of the animal under anesthesia, before positioning it inside the MR scanner. During the experiment, anesthesia was maintained by adjustment of gas level in function of breath rate. ^{1}H sequences (RARE T_2-weighted) on each geometry were acquired on the animal to obtain a proper anatomical reference. A series of T_1-weighted MSME scans were acquired before and after the intravenous administration of the gadolinium complex in order to follow the kinetic of the contrast agent in the pathological lesion, having the following parameters: Matrix size = 192 x128, FOV = 3x3cm, slice thickness 1.8 mm, number of echoes = 3, TE = 15.2 ms, TR = 388 ms, acquisition time = 50 s. When required, Gadovist® was administered at a dose of 0.1 mmol/kg corresponding to an administration volume of 2 mL/kg of a 50 mM solution (obtained as dilution of the original formulation with saline), at an injection rate of 2 mL/min. The injection was performed manually with the help of a timer to check the injection rate. The kinetic of Gadovist® was followed up to 20 minutes post injection.

Data Analysis: The ischemic volume was measured by selecting proper regions of interest (ROIs) over the tumor on both T_2 and T_1 weighted images. MSME images analysis was also performed in terms of post contrast enhancement, by positioning the ROIs over brain tissue and tumor mass. ROIs positioning and signal quantification was performed by using a home developed plugin, running on ImageJ (imagej.nih.gov/ij/). Signal enhancement (enh) was calculated as follows:

$$Enh = 100\ (Signal_{postCA} - Signal_{preCA}) / Signal_{preCA},$$

where $Signal_{postCA}$ and $Signal_{preCA}$ indicate MR signal before and after CA administration, respectively.

Histology Studies: Histology was performed by using Hematoxylin and Eosin Staining on brains collected after animal euthanasia. Tissues were mounted and visualized on an optical microscope. Ischemia stage was determined according to Lee et al., work. [73]

Results

All animals underwent the surgical procedure in order to induce the permanent ischemia in the right cerebral cortex (M1, primary motor

cortex). As summarized in Table A, animals were divided in 4 experimental groups according to the photochemical induction conditions.

Table A: Experimental Scheme

Group number	**Rose Bengal dose [mg/kg]**	**Irradiation time [min]**	**MRI session**
Group 1	40*	20	4-24 h and 3-7-10-14 days post induction
Group 2	40*	20	4-24 h and 3-7-14 days post induction
Group 3	8* 20*	20	4-24 h and 3-5- 7-14 days post induction
Group 4	40**	20	4-24 h and 3-7-10-14 days post induction
The injection was performed: * with an automated perfusion pump (inj. rate = 0.1 mL/min) ** manually with the help of timer to check the injection rate (*i.e.* 0.1 mL/min)			

All 24 animals survived the surgery procedure and developed a detectable ischemic lesion with the only exception of four animals of the group 3. As already described, after ischemic induction, animals were imaged weekly (or closer) by MRI and administered with Gadovist® only when an ischemic lesion was clearly visible.

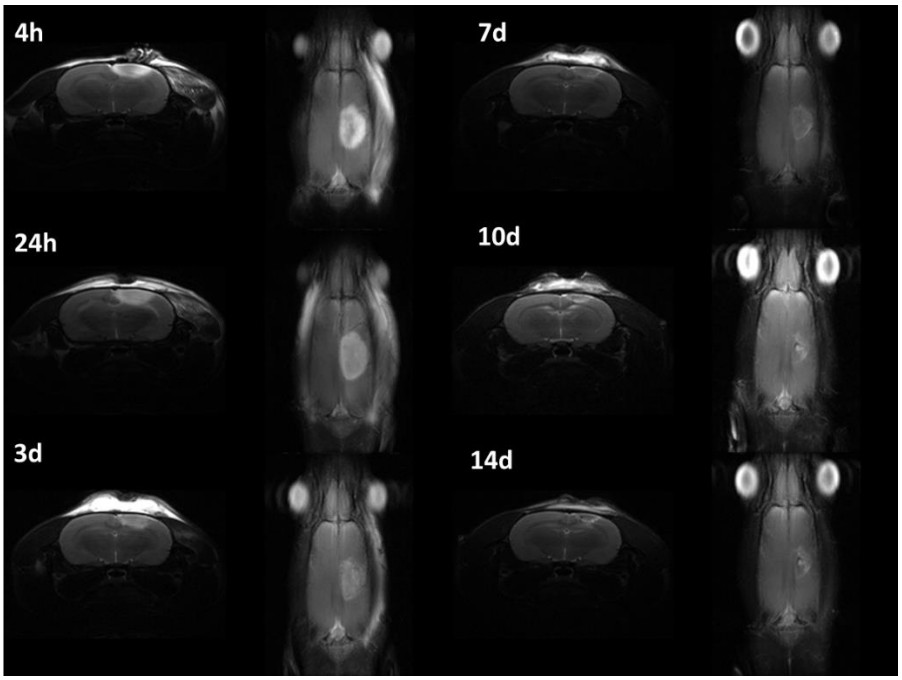

Figure 9 *Representative anatomical T_2-weighted at different days/weeks post ischemic induction in axial and coronal geometrical sections (Group 4).*

A representative example of T_2-weighted anatomical images, acquired at different times post ischemic induction is shown in Figure 9, while T_1-weighted images (pre and post contrast) together with signal enhancement *vs* time quantification are shown in Figure 10. For this representative animal, the ischemic lesion was clearly visible starting from 4 hours after the photochemical induction, as observable in axial and coronal geometrical section of T_2-weighted images. In pre contrast T_1-weighted images brain tissue and ischemic lesion showed quite the same signal (see the first column of Figure 10), but after CA administration the diseased tissue reached high enhancement and became clearly discernible from the healthy brain. An example of signal enhancement behavior as a function of time (for MSME images) is shown in Figure 11 and in the last column of Figure 10.

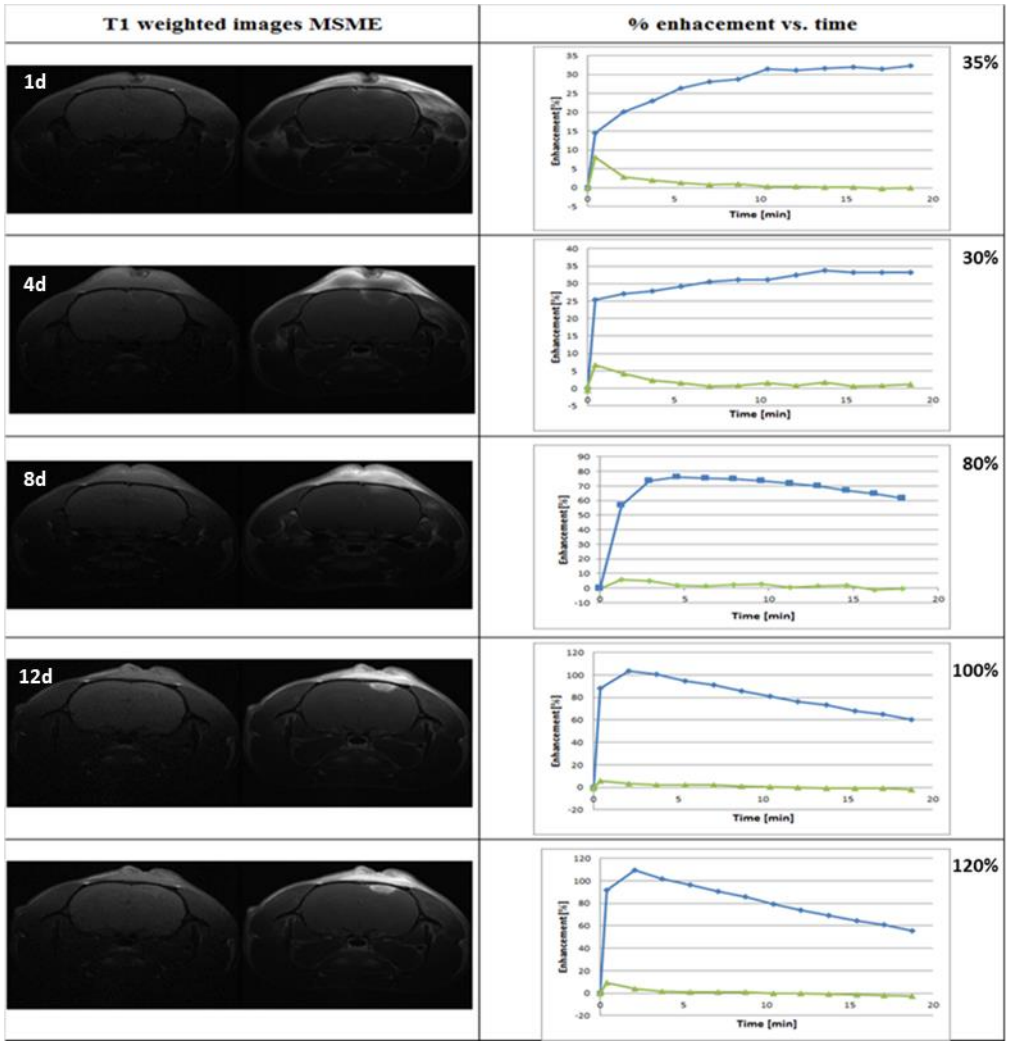

Figure 10. *Representative contrast enhanced T_1-weighted images and MSME signal enhancement as a function of time for healthy contralateral tissue (green) and ischemic lesion (blue) at different days/weeks post ischemic induction.*

A.

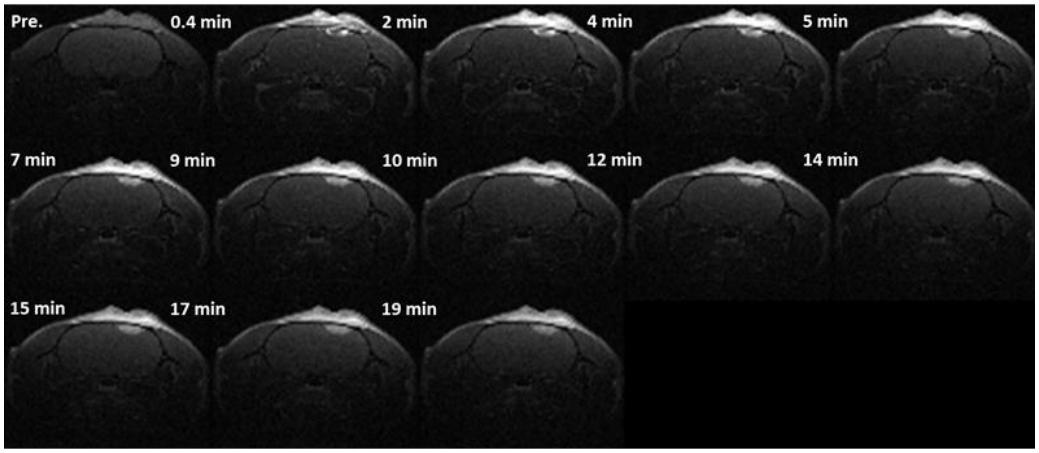

B.

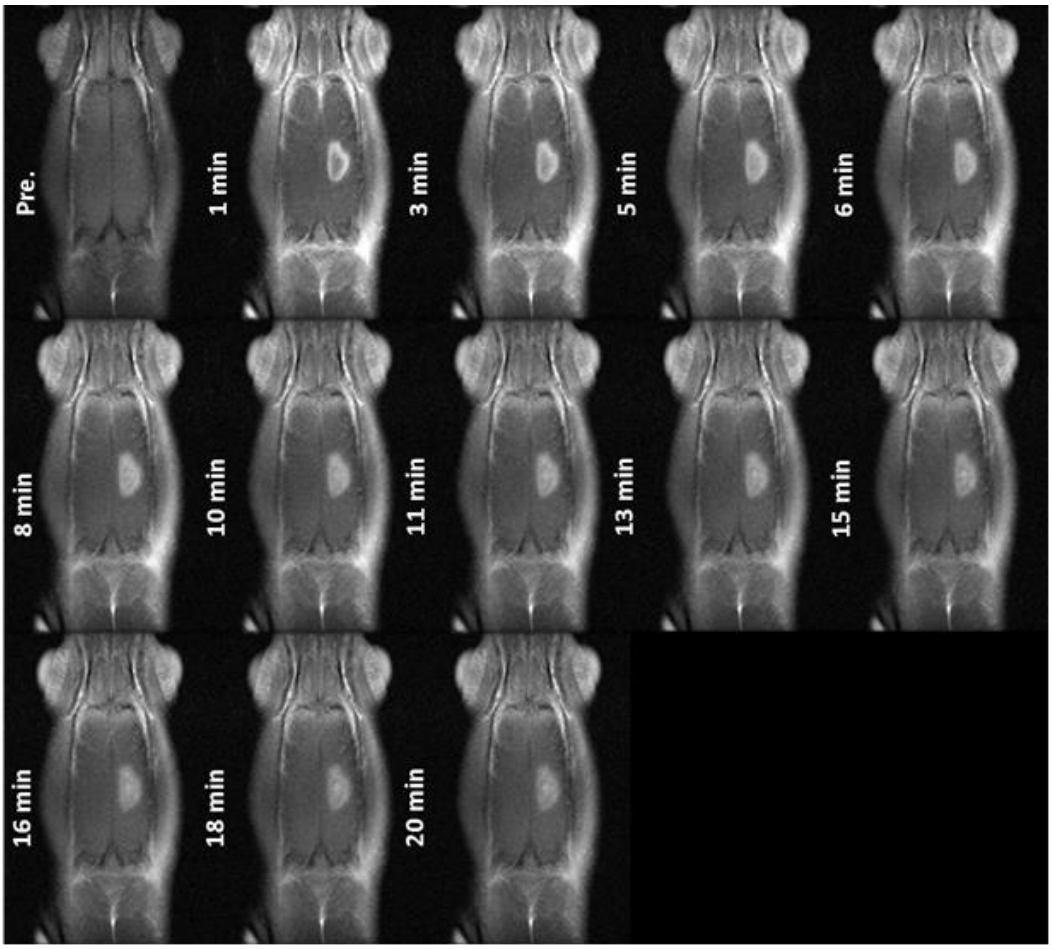

Figure 11 *Representative examples of MSME images acquired before and after administration of Gadovist®. Panel A: Axial section; Panel B: Sagittal Section.*

When present, the ischemic lesion was already visible on T_{2w} images as an area of high signal intensity, even after 4 hours of photochemical induction. The intensity got progressively higher with time, together with the ischemic volume after 24 hours. However, after 24 hours and especially after 3 days, the ischemic volume and the signal intensity were slightly

reduced on T_{2w} images. However, in gadolinium-enhanced T_{1w} images, the enhancement of the ischemic lesion was below 40 % up to 7 days after the induction, while at 7 days to 14 days post induction, the enhancement became always noticeable, ranging from 50 to 120% (Table B).

The observed enhancement increase after the seventh day post induction of the ischemic lesion is perfectly in line with what is reported in literature.[49]

Table B: Summary of Experimental Results

Group	MRI 4h		MRI 1d		MRI 3-5d		MRI 1w		MRI 10d		MRI 2w	
	Ischemic Volume, mm3	MSME max enh (%)	Ischemic Volume, mm3	MSME max enh (%)	Ischemic Volume, mm3	MSME max enh (%)	Ischemic Volume, mm3	MSME max enh (%)	Ischemic Volume, mm3	MSME max enh (%)	Ischemic Volume, mm3	MSME max enh (%)
1 (n=6)	50	x	40	30	48	26	25	57	24	60	15	105
2 (n=6)	33	26	45	x	17	30	17	50	x	x	x	x
3 (n=7)	x	x	14	x	x	x	x	x	x	x	-	-
4 (n=4)	x	x	x	x	x	x	x	x	x	x	-	-

The x symbol represents an experiment that was not performed.

Animals belonging to Group 1 and 2 received the same dose of Rose Bengal, i.e., 40 mg/kg, administered at a dose of 0.1 mL/min with a 20 min of irradiation with a green light beam. Bengal Rose was administered via an intravenous catheter in the tail vein, with the help of an automated infusion pump. The induction of the ischemic lesion was considered to be reproducible, seeing the consistency of the lesion in the two groups. However, two rats of the first induction groups showed acute tail phlebitis, as reported in Table B. The phlebitis became visible at the end of the Rose Bengal perfusion as a pink coloration of the tail, becoming acute phlebitis in the following days, thus evolving in complete necrosis of the tail.

Since the induction of ischemia in terms of reproducibility of the lesion in respect to the Rose Bengal was considered a success, the Group 2 of the experiment focused on eliminating the collateral effect that was the phlebitis. For this reason, the induction procedure was kept fixed (i.e., 40 mg/kg, 0.1 mL/min, infusion pump) and a series of adjustments were done, such as:

1) shielding of the tail from the room white light during and after the Rose Bengal perfusion;

2) size reduction of heparinized needle in the intravenous catheter to avoid an obstruction of the caudal vein;

3) application of a cortisone ointment on the tail at the end of the perfusion.

Despite these improvements, phlebitis became systematic. In particular, 5 out of 6 animals in Group 2 (animal ID 7, 8, 9, 10 and 11, as reported in the last column of Table B) showed tail necrosis as the evolution of acute post-perfusion phlebitis. Despite the necrosis, all the animals of Group 2 showed a good ischemic lesion comparable with the results obtained in Group 1. As reported in Table A, in Group 3 the administrated dose of Rose Bengal was reduced from 40 mg/kg to 8 mg/kg in the first three animals of the group (i.e. animal ID 13, 14 and 15) and to 20 mg/kg in the last four (i.e. animal ID 16, 17, 18 and 19). Reduction of the administrated dose of Rose Bengal was pursued in order to avoid the tail phlebitis systematically observed in the previous two groups.

With the dose reduction of Rose Bengal at 8 mg/kg, 3 out of 3 animals reported no sign of tail phlebitis but also no ischemic lesion detectable by MRI. This negative result in the ischemic induction led to the decision of increasing the Rose Bengal dose to an intermediate level, *i.e.* 20 mg/kg, in the last four animals of Group 3. As a result, a detectable ischemic lesion was observed (3 out of 4 animals showed an ischemia correctly induced). However, a case of tail necrosis was again detected, (1 out of 4 animals, see Table B).

The results obtained in Group 1, 2 and 3 clearly showed that cerebral ischemia can be correctly induced with the perfusion of Rose Bengal doses not less than 20 mg/kg but for such doses, there was observed tail phlebitis that evolved in necrosis within few days from the ischemic induction. In order to overcome this serious drawback, another attempt was performed in the last group, *i.e.* Group 4. As reported in Table A, all the animals of Group 4 underwent the same ischemic induction protocol previously applied in Group 1 and 2 but with a perfusion performed manually on the animal under gaseous anesthesia and not under the systemic one. These procedural changes allowed the establishment of tail hypoxia, hypoxemia and stiffness and at the same time to develop a good ischemic lesion. Since it is widely known that buprenorphine may cause respiratory depression even in humans [81], and that in some cases, Tiletamine-Zolazepam in combination with Xylazine (Zoletil,Rompun respectively) have caused cardiodepression,[82] the combination of the opioid and the systemic anesthesia could have caused a progressive reduction of oxygen levels, thus causing the tail phlebitis. Moreover, the utilization of an infusion pump made difficult to realize when there was a reduction of blood oxygenation and thus blood pressure, while with the manual infusion is easier to realize when it happens. Finally, the breathing rate can be easily controlled with the gaseous anesthesia (i.e. sevoflurane), thus avoiding hypoxia.

For these reasons, Group 4 showed the best results in term of ischemic lesion induction and animal welfare, and was chosen as the final procedure for the efficacy study.

Since the best enhancement observed in MRI was between 12 and 14 days post induction (see Figure 8), this time window was chosen as the best condition for the final efficacy study.

Histology confirmed the nature of ischemia, and it permitted the staging of the lesion in accordance to what was observed by Lee et al.[49]

As it is possible to see in Figure 12, ischemia lesion development and evolution can be divided in to three stages: Acute, SubAcute and Chronic, depending on the appearance of the lesion in histopathology. In the acute stage (4 hours-3 days), the lesion is characterized by a strong presence of edema, surrounded by an area of necrosis and presence of eosinophilic neurons and neutrophil infiltration. In the SubAcute stage (4 -12 days), the central necrosis expands, is surrounded by inflammatory cells and macrophages. This stage is usually characterized by a complete absence of the Blood Brain Barrier (BBB) in its lesion core, due to the fact that blood vessels are being replaced. In the chronic stage (12 to 14 days), the necrosis is completely resolved and the lesion is replaced by gliosis and fibrosis. Usually, astrocyte scar formation is complete after 2-4 weeks. During the end of the SubAcute and the Chronic stage, the edema is completely adsorbed and the presence of gliosis and fibrosis explains the higher enhancement observed in MRI.

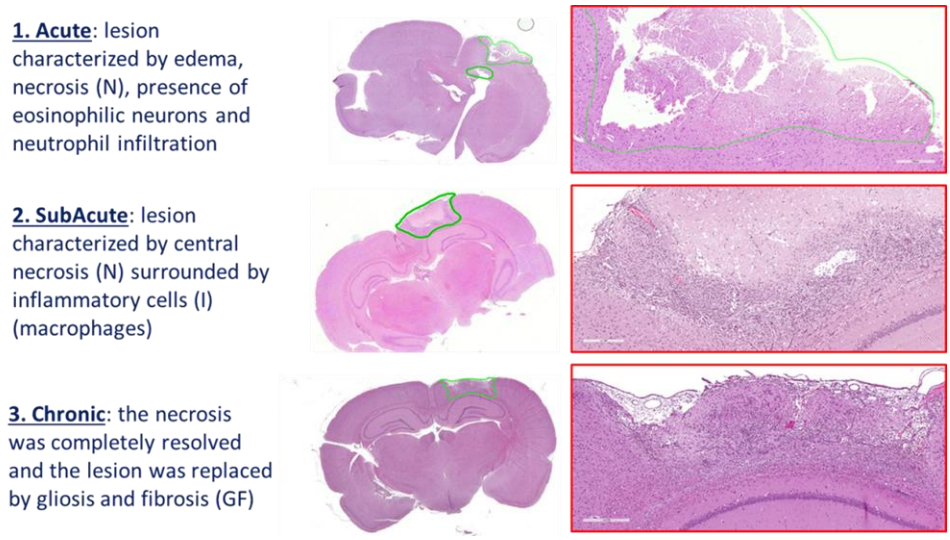

Figure 12 *Ischemia staging by histology of the brain excised at different days post ischemia induction.*

Conclusions

Cerebral ischemia was successfully induced on 20/24 rats. Four rats did not develop any detectable ischemic lesion.

The best experimental conditions for the photochemical induction of cerebral ischemia in the target region (*i.e.* right cortex) without the observation of tail necrosis are summed up here below:

Rose Bengal dose	40 mg/kg
irradiation time	20 min with a green light beam with wavelengths around 550 nm
green light beam position	1 mm anterior to Bregma, 3 mm lateral form the midline
perfusion modality	manual perfusion (i.e. at an injection rate of 0.1 mL/min with the help of a timer) of a total volume of 2 mL of Rose Bengal dissolved in sterile saline 0.9%
intravenous catheter	homemade MRI catheter (i.e. 23G and Polyethylene Tubing PE50)
anesthesia procedure	gaseous anesthesia after the administration of buprenorphine (0.05 mg/kg)

Those conditions proved to be the best in terms of experimental conditions, reproducibility and animal welfare, and thus were used to induce the model needed for the final efficacy study.

Breast Mouse Model: Introduction

Breast cancer is the most common and second most deadly cancer for women in the USA[83]. Although there are many factors that may increase an individual woman's breast cancer risk, women are generally considered high-risk if their lifetime risk of breast cancer is greater than or equal to 20%. [84] For those high-risk women, American Cancer Society and American Society of Radiology recommended supplemental screening together with the mammography.[85] Contrast Enhanced Magnetic Resonance Imaging (CE-MRI) is recommended in particular for those women that carry a mutation of BRCA, as well as women that are suspected to carry other high-risk mutations for breast cancer, and their first relatives.

Breast Cancer is defined as Triple Negative (TBNC) when there is a lack of immune-histochemical expression of the estrogen receptor (ER), progesterone receptor (PR), and human epidermal growth factor receptor 2 (HER2). TBNC accounts for approximately the 15% of all breast cancers worldwide.[86] Moreover, TBNC, together with basal like breast cancers, accounts for 75% of BRCA1 tumors derived mutation.

TBNC tends to grow more rapidly than positive breast cancers, and it is more aggressive. It is often associated with poor prognosis, including increased incidence of local recurrence and metastatic disease, especially into the lungs and brain[87]. As of today, there are no approved targeted treatments available, and local treatment or systemic chemotherapy are the primary choice for the treatment of TBNC.[88]

Several studies compared MRI features of TBNC with their histological appearance. [89-90-91] All the studies yielded the same evidence: TBNC tends to show more frequently a statistically significant MRI characteristic. Triple negative breast cancers exhibit a mass-type growth with smooth margins, intra-lesional necrosis, higher signal intensity on T_{2w} images, presence of edema and rim enhancement. Moreover, CE-MRI shows usually plateau-type dynamic curves.

Orthotopic models are usually the pathological model of choice when testing for new pharmaceuticals, especially because they are characterized by high translatability into clinic. Currently, breast cancer orthotopic mice models can be achieved with two main methods: orthotopic implantation of the cells under direct vision of the mammary fat pad (Orthotopic Direct Vision implant, ODV) or percutaneous blind injection in the nipple area to attempt the implantation of cells into the mfp (Orthotopic Percutaneous implant, OP). Even though the OP method is easier to perform and it requires minor skills and less time, it has been demonstrated to be less accurate and more confounding than ODV. ODV however, requires the direct display of the mfp and thus, it requires surgery, which is often stressful for the animal and is associated to a not negligible intraoperatory death. For this reason, in this part of the pilot studies I have introduced a new way of inducing orthotopic breast cancer, which consist into the direct injection of the cells into mfp by using Ultrasound to correctly identify the mfp and to guide the needle for tumor induction. This method was compared with both ODV and OP.

Among the different cell lines currently utilized in preclinical research, BT-20 human cell line was isolated in 1958 from an invasive ductal carcinoma from 74 years old woman. [92-93] Tumor derived from BT-20 cells show adequate malignancy and aggressiveness when injected into nude mice, forming grade II adenocarcinomas. However, the use of this cell line in the pilot study did not produce a positive result, and since they were considered unsuitable for MRI efficacy studies, two syngeneic cell lines were consequently utilized for the pilot study: 4T1 and TS/A.

The mouse derived mammary carcinoma 4T1 cell line was originally isolated by Dexter et al., in 1978 as a subpopulation derived from a spontaneous tumor originated in BALB/cfC3H mice.[94] 4T1 derived tumors are resistant to 6-thioguanine and they metastasize from the primary tumor into liver, lungs, brain and bone, making it the preferred model of human metastatic breast cancer. It is a triple negative cell line and is characterized by rapid growth and increased vascularization.

TS/A cell line was derived in 1983 from a spontaneous mammary adenocarcinoma in BALB/C mice. [95] They are widely used as a model of tumor immunogenicity because of their heterogeneity. TS/A cells express the estrogen receptor[96] and they form an adequately differentiated adenocarcinoma, with metastasis from the primary tumor into the lungs.

Following the induction of BT-20 into the mfp using the ODV, OP and US-guided injection and demonstrating the feasibility of the induction with the guidance of ultrasound; TS/A and 4T1 cells were injected into the mfp of BALB/C mice using only ultrasound guided injection as the method of choice.

All the models, despite their differences in induction, were characterized with MRI and intravenous injection of GBCA to prove their feasibility in a MRI based efficacy study.

Methods and Materials

Cell line culture and preparation: BT-20 cells were supplied by CLS (Cell Line Service). Cells were grown in DMEM F-12 medium supplemented with 10% foetal bovine serum, 2 mM glutamine, 100 IU/mL penicillin and 100 µg/mL streptomycin. For the induction, cells were collected and washed two times with DMEM F-12. Amounts of 10^6 to 10^7 BT-20 cells were re-suspended in 50-100 µL DMEM F-12 and inoculated in animals with a syringe (needle 29G).

Breast cancer cells 4T1 and TS/A were supplied by ATCC and University of Torino, respectively. Cells were grown in RPMI-1640 medium supplemented with 10% foetal bovine serum, 1% glutamine, 100 IU/mL penicillin and 100 µg/mL streptomycin. Mycoplasma free tested cells (EZ-PCR Mycoplasma Test Kit) were used to start propagation. Moreover, a further test was performed on cells used the day of inoculation and cells resulted free form mycoplasma contamination. 4T1 and TS/A cells were collected and washed two times with serum-free RPMI-1640 medium. Amounts ranging between $5x10^4$ to 10^6 cells were re-suspended in 50-100 µL serum-free medium and inoculated in animals with a syringe (needle 29G).

Animal Studies: All the procedures involving animals were conducted according to the national and international laws on experimental animal research (L.D. 26/2014; Directive 2010/63/EU). No validated non-animal alternatives are known to meet the objectives of the study. 23 *nu/nu* female mice, 4 weeks old, were purchased from Charles River Laboratories, Calco (LC), Italy. This strain was used for the inoculation of BT-20 cells via percutaneous injection, classic surgery, and US-guided injection. 26 BALB/C female mice, 4 weeks old, were purchased from Charles River Laboratories, Calco (LC), Italy. This strain was used for the injection of 4T1 and TS/A. Animals were kept in limited access, housed in groups of 6 in polysulfone Tecniplast Double Decker ventilated cages (up to 14 animals/cage), air-conditioned facilities (20-24°C room temperature, 45-55% relative humidity, 15-20 air changes/h, 12-h light cycle). Food and water were available at libitum. Induction of tumor model was performed after a one-week period of acclimation and observation.

Tumor induction: Different routes were used for the inoculation of BT-20 into the mammary fat pad. Those were the following: percutaneous injection, classic surgery, and US-guided injection. 4T1 and TS/A cell lines were injected with the help of Ultrasound.

1. *Percutaneous injection*: animals were weighted and administered with general gas anaesthesia (SevoFlo®). After checking for reflexes, a tweezer was used to pinch the fourth mammary fat pad, and a syringe was used for direct injection of the cells. Injection was defined as successful if a little bump was observed.
2. *Classic Surgery:* After recording their body weight, mice were subcutaneously administered with carprofen (5mg/kg) one hour before surgery. Anesthesia was induced with sevoflurane gas and then systemically by injection of Rompun® 5 mg/kg and Zoletil® 40 mg/kg. After checking for absence of reflexes, the animal was positioned on the heating pad and its temperature was continuously monitored and maintained in the range of 36.5-38.5 °C. After cleaning the abdomen with a disinfectant (iodopovidone), a local anesthesia was administered (lidocaine) at a dose of 3 mg/kg. A small incision between the fourth nipple and the midline with a scissor was performed, and the mammary fat pad was exposed with the use of a tweezer. A volume of 50 µL BT-20 was gently injected into the mfp with a syringe (29G needle). Injection was considered successful if a swelling was observed. The incision was sutured and then disinfected with iodopovidone. Animals were kept in a recovery cage until awakening.
3. *US guided injection:* After recording their body weight, mice were subcutaneously administered with carprofen (5mg/kg) one hour before procedure. Animals were weighted and administered with general gas anaesthesia (SevoFlo®). Mice were positioned on a heating pad and, after loading the cells with an insulin syringe, the syringe was mounted on the syringe guide. Injection into the mfp was made horizontally to the nipple area, and correct localization of the needle was checked with the use Vevo Lazr 2100 Ultrasound System with a MS550 Transducer (55 MHz). If the injection was successful, the mouse was removed from the heating pad and kept in a recovery cage until awakening.

After the orthotopical induction of the BT-20, 4T1 or TS/A breast tumor, animals were monitored daily and a checklist of clinical signs was filled to evaluate general condition, spontaneous behaviour, reaction to handling, breathing, hydration condition, etc. The body weight was recorded once a week or closer according to the Veterinary evaluation. Animals were checked for tumor growth one or two times by MRI, beginning on day 4 after tumor inoculation. At least 50% of animals with a visible tumor were imaged by contrast enhanced MRI once a week at 1-2-3 weeks post inoculation. Animals were sacrificed by overdose of anaesthesia and

cervical dislocation at the end of the study or when one of the following endpoints was reached:

- Loss of weight ≥ 20%;
- Severe or prolonged distress (according to checklist evaluation);
- Mass tumor volume ≥ 0.3 cm^3;
- Tumor ulceration;
- Within 40 days of tumor induction.
- Necrosis of the tail, according to Veterinary evaluation.

MRI Studies: Animals were anaesthetized with isoflurane or sevoflurane gas (about 1%) in O_2 and were placed on the MRI animal bed. In the case of administration of Gadovist®, an intravenous catheter was inserted in the tail vein of the animal under anesthesia, before positioning inside the MR scanner. During the experiment, anesthesia was maintained by adjustment of gas level in function of breath rate. ^1H sequences (RARE T_2-weighted) on each geometry was acquired at 1T (BT-20 animals) or 3T equipped with a surface coil (4T1 and TS/A) on the animal to obtain a proper anatomical reference. A series of 3D T_1-weighted MSME scans were acquired before and after the intravenous administration of the gadolinium complex in order to follow the kinetic of the contrast agent in the diseased mass, having the following parameters:
MSME: Matrix size = 128 x128, FOV = 2.5x2.5cm, slice thickness 1.5 mm, number of echoes = 3, TE = 18.47 ms, TR = 350 ms, acquisition time = 90 s.

When required, Gadovist® was administered at a dose of 0.1 mmol/kg corresponding to an administration volume of 2 mL/kg of a 50 mM solution (obtained as dilution of the original formulation with saline), at an injection rate of 2 mL/min. The injection was performed manually with the help of a timer to check the injection rate. The kinetic of Gadovist® was followed up to approx. half an hour post injection.

Data analysis: Tumor volume was measured by selecting proper regions of interest (ROIs) over the tumor on both T_2 and T_1 weighted images.
MSME images analysis was also performed in terms of post contrast enhancement, by positioning the ROIs over brain tissue and tumor mass. ROIs positioning and signal quantification was performed by using a home developed plugin, running on ImageJ (imagej.nih.gov/ij/). Signal enhancement (enh) was calculated as follows:

$$Enh = 100 (Signal_{postCA} - Signal_{preCA}) / Signal_{preCA},$$

where $Signal_{postCA}$ and $Signal_{preCA}$ indicate MR signal before and after CA administration, respectively.

Results

BT-20 Results

22 out of 23 animals underwent procedure for the induction of a BT-20 triple negative breast cancer into the left fourth mammary fat pad. Only one animal was not inoculated. As summarized in Table A, animals were divided into four experimental groups according to the different cell induction routes (*i.e.* surgical, external induction, US Guided).

Table A: Experimental Scheme of BT-20 cell injection.

Group number	Animal number	Inoculation Route	Cell number
Group 1	1-6	External injection into the MFP	10^7
Group 2	7-11	Injection into the MFP via surgery	10^7
Group 3	12-17	External injection into the MFP- US guided	10^6
Group 4	18-23	External injection into the MFP	$5\ 10^6$

All animals survived despite the difference in gravity of the two induction techniques. Unfortunately, tumour growth was not sufficient for DCE-MRI. Tumour did develop in some animals (9/22), but it reached a maximum volume of 10 mm^3, which proved to be really difficult to detect at a 1T MRI scanner (minimum expected volume was 50 mm^3). For this reason, tumour growth was monitored and assessed using a VEVO Lazr 2100 scanner, with a 50MHz transducer. If a mass was detected with Ultrasound Echography, mice were recruited for MRI acquisition and, if it was possible to detect a mass with MRI, animals were administered with Gadovist®.

Table B: Summary of Experimental Results

Group	MRI approx 2w		MRI approx 3w		MRI approx 4w		MRI approx 5w	
	Tumor Volume, mm^3	MSME avg max enh (%)	Tumor Volume,mm^3	MSME avg max enh (%)	Tumor Volume,mm^3	MSME avg max enh (%)	Tumor Volume,mm^3	MSME avg max enh (%)
1	<2	-	3	70	8	70	11	60
2	<2	-	3	40	10	40	10	50
3	3	80	6	50	3.5	80	3	-
4	3	30	7	30	5	80	10	80

Summary of the experimental results is reported in Table B. A representative example of T_2-weighted anatomical images acquired at different times post tumor induction is shown in Figure 13, T_1-weighted images (pre and post contrast) together with signal enhancement *vs* time quantification are shown in Figure 14. The tumor, when present, was visible in T_2-weighted anatomical images, where it appeared surrounded by the fat of the MFP, whereas it becomes darker and clearly more visible into T_1-weighted images. CA administration resulted in a 50%-80% signal enhancement. However, as already mentioned, the main limit of this model is the fact that the tumor is not palpable and thus not easily identifiable during MRI acquisitions.

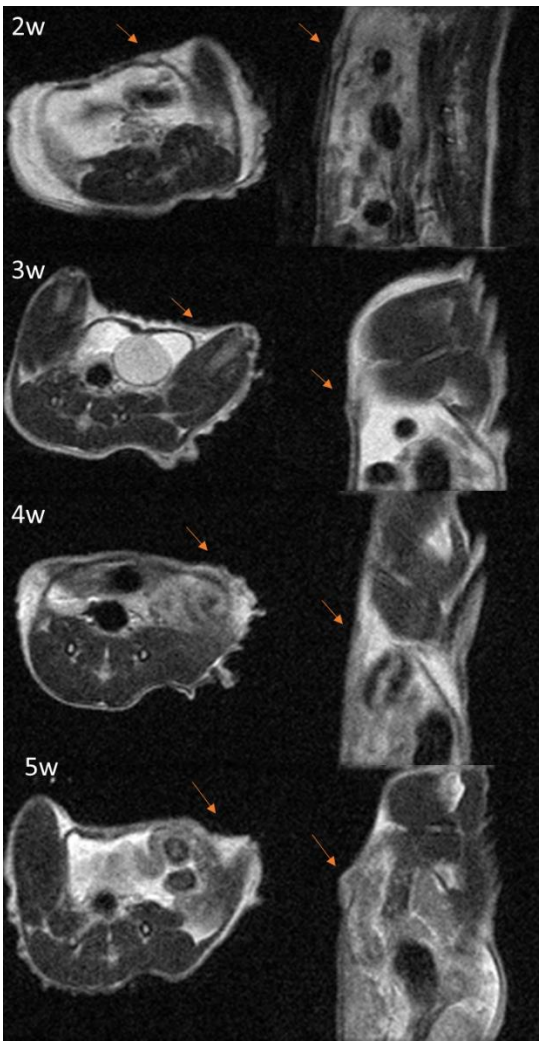

Figure 13 *Representative anatomical T_2-weighted at different weeks post tumor induction in axial and sagittal (Animal belongs to Group 1).*

This study served to identify the best route and experimental condition to induce a pathological model of triple negative breast cancer. As previously described, animals from Group 1 were injected with 10^7/70 µL BT-20 cells externally into the fourth left mfp with a G29 syringe. Volume suspension of the cells was too small and thus cells were not suspended correctly. However, tumour growth was observed in 3/5 animals. Tumour growth was correctly assessed with Ultrasound, and it proved to be correctly localized into the mammary fat pad. No subcutaneous growth was observed.

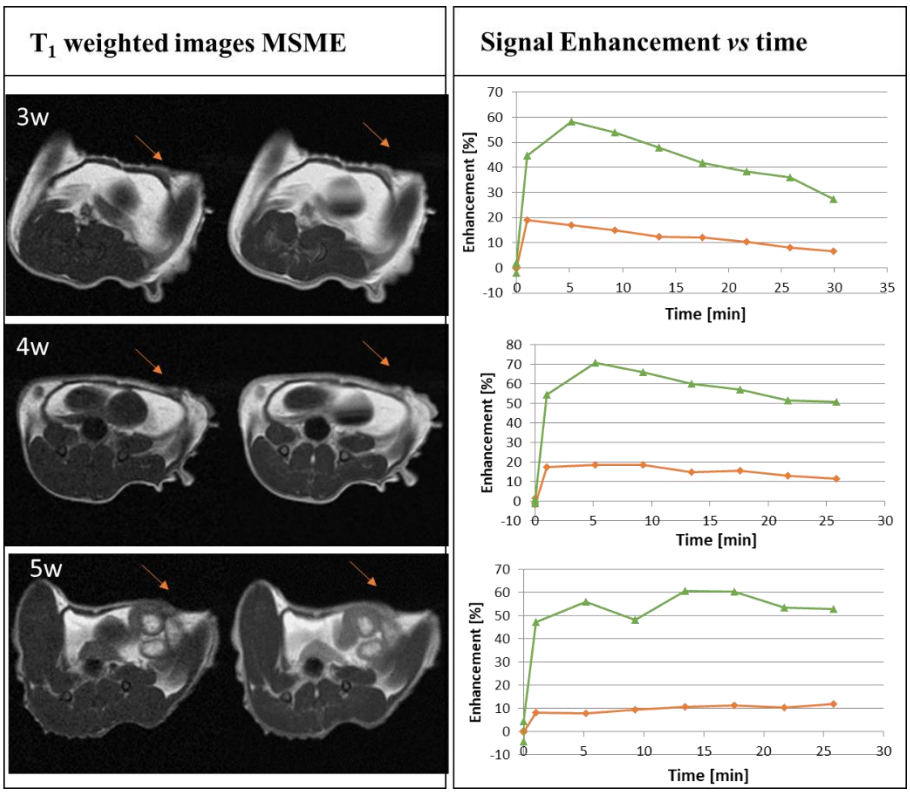

Figure 14 *Representative contrast enhanced T_1-weighted images and MSME signal enhancement as a function of time for healthy contralateral tissue (orange) and tumor mass (green) at different weeks post tumor induction.*

Animals from Group 2 underwent surgery, where the mammary fat pad is exposed after incision of the abdomen, and 10^7 cells were suspended correctly in 100 µl. Tumour growth was assessed as mentioned above, and when it was present (4/6 animals), it was correctly localized.

Since the two routes gave the same result, external injection was chosen as the best method of induction since it caused less distress to the animals (*i.e.* no incision, nor suture is needed for this procedure).

Lastly, Group 3 and 4 were induced by using the external injection route by guiding the needle with Echography, to improve and refine the method. Unfortunately, Group 3 did not reach a tumour volume of at least 10 mm^3 (max tumour volume observed was 4 mm^3 for 16); while an almost palpable tumour was reached in 2/6 animals of Group 4. This confirms the fact that a decrease in the number of cells injected will cause a minor tumour take rate and volume growth (see Table B).

Histology was performed to confirm the nature of the lesion and its localization into the mammary, when present. As expected, tumor was present in 7/16 tumors analysed, and it had a maximum volume of 2 mm^3. When present, the lesion was characterized by a differentiated adenocarcinoma into the mammary gland, under the muscle and subcutis (Figure 15).

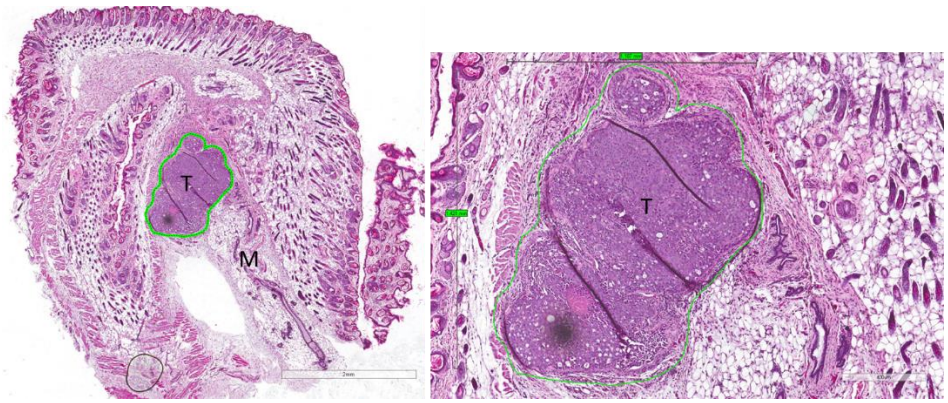

Figure 15 *Transversal section of a BT-20 induced tumor. T= Tumor; M= Mammary Gland.*

None of the Groups reached the minimum expected value of tumour volume (50 mm^3), therefore this pathological model results to be not suitable for the purpose of the study.

4T1 and TSA Results

All animals underwent the US guided procedure for the induction of orthotopic breast cancer. Animals were divided in 4 experimental groups, according to cell type and number, as reported in Table A.

Table A: Summary of Experimental Groups.

Group	Cell Type	Cell Number	MRI session
1	4T1	$5x10^5$	4-14 days after induction
2	4T1	10^6	4-14 days after induction
3	TS/A	$5x10^4$	7-24 days after induction
4	TS/A	$5x10^5$	5-19 days after induction

4T1 Tumor bearing mice: 11 out of 13 mice developed 4T1 tumor in the mammary fat pad, while the remaining two mice did not develop a discernable tumor mass. After tumor induction, animals were imaged weekly (or closer) by MRI and administered with Gadovist® if a tumor mass was clearly visible. A summary of results in terms of tumor volume and measured enhancement for each experiment is reported in Table B.

Table B Summary of results tumor volume mm^3 and average obtained enhancement in MSME images on 4T1 tumor bearing mice.

Group	MRI 4d post		MRI 8d post		MRI 10d post		MRI 14d post	
	Tumor volume (mm3)	avg enh (%)	Tumor volume (mm3)	avg enh (%)	Tumor volume (mm3)	avg enh (%)	Tumor volume (mm3)	avg enh (%)
1	37	110	56,5	110	98	93	217	56
2	30	120	70	75	146	85	218	60

A representative example of T_1-weighted anatomical images acquired at different times post tumor induction is shown in Figure 16, while T_1-weighted images (pre and post contrast) together with signal enhancement vs. time quantification are shown in Figure 17. A tumor mass was palpable and clearly visible starting after approx. four days after cell inoculation. The volume exponentially increased reaching the endpoint in about 15 days. No significant differences in tumor growth were observed between group 1 and 2, indicating that the two numbers of cell investigated are equivalent. Tumor growth curve for single groups and averaged over the two groups is reported in Figure 18.

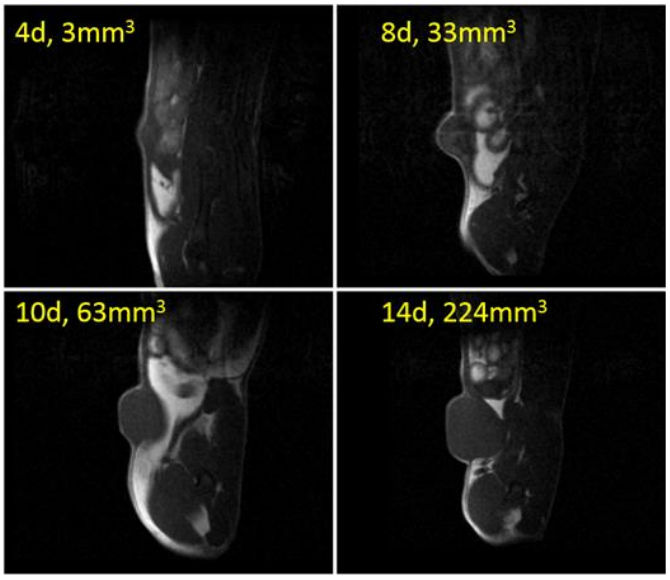

Figure 16 *Representative anatomical images of 4T1 tumor (group 1), at different stages of development*

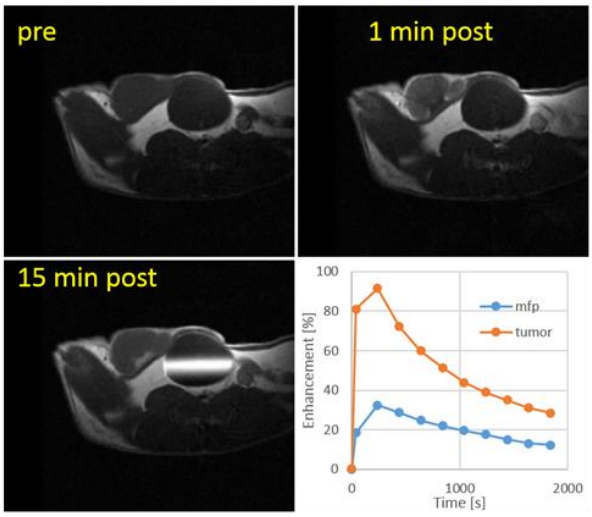

Figure 17 *Representative example of MSME pre and post contrast images, with the measured signal enhancement curve in mammary fat pad and tumor (an.ID: l01, 10 days post cell inoculation).*

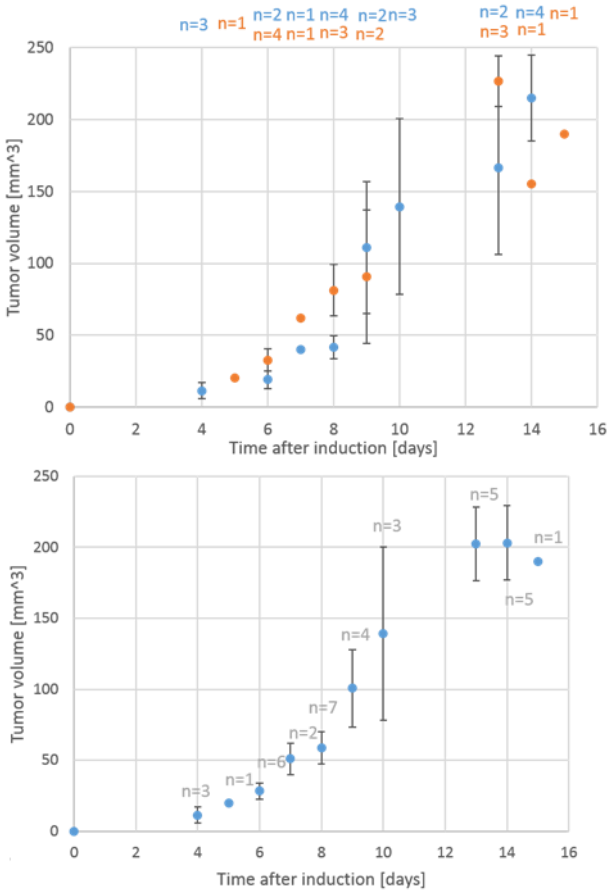

Figure 18 *4T1 tumor growth curve for single groups (group 1 blue dots, group 2 orange dots) up. Bottom: averaged data.*

In pre contrast T_1-weighted images (both spin and gradient echo) the mass and the mammary fat pad are well discernable, both in terms of structure and in terms of T_{1w} MR signal. In fact, the lipid composition of mammary fat pad causes a shortening of T_1 and appears extremely bright. Conversely, the diseased mass is much darker, see Figure 16. After CA administration

both selected tissues were characterized by a noticeable increment of signal. Immediately after the injection, the boundary of the tumor mass and shortly later the core became bright, reaching a maximum enhancement close to 100% or even higher. When the masses reached large volumes (i.e. 200 mm^3 or more) the observed maximum enhancement resulted lower (i.e. 50-70%).

TSA Tumor bearing mice: All mice*, i.e.* 13, developed TS/A tumor in the mammary fat pad. As already described, after tumor induction, animals were imaged weekly (or closer) by MRI and administered with Gadovist® if a tumor mass was clearly visible. A summary of results in terms of tumor volume and measured enhancement for each experiment is reported in Table C.

Table C: Summary of results tumor volume mm^3 and average obtained enhancement in MSME images on TS/A tumor bearing mice. (x= experiment not performed).

Group	MRI 4d post		MRI 8d post		MRI 10d post	
	Tumor volume (mm3)	avg enh (%)	Tumor volume (mm3)	avg enh (%)	Tumor volume (mm3)	avg enh (%)
1	13	x	20	88	21	x
2	27	100	36	x	x	x
Group	**MRI 14d post**		**MRI 20d post**		**MRI 24d post**	
	Tumor volume (mm3)	avg enh (%)	Tumor volume (mm3)	avg enh (%)	Tumor volume (mm3)	avg enh (%)
1	97.5	83	110	50	143	x
2	83	73	135	60	204	51

A representative example of T_1-weighted anatomical images acquired at different times post tumor induction is shown in Figure 19, while T_1-weighted images (pre and post contrast) together with signal enhancement *vs.* time quantification are shown in Figure 20 for MSME protocols, respectively. The tumor mass was palpable and clearly visible starting after 7-10 days after cell inoculation for group 3 and already after 6 days for group 4.

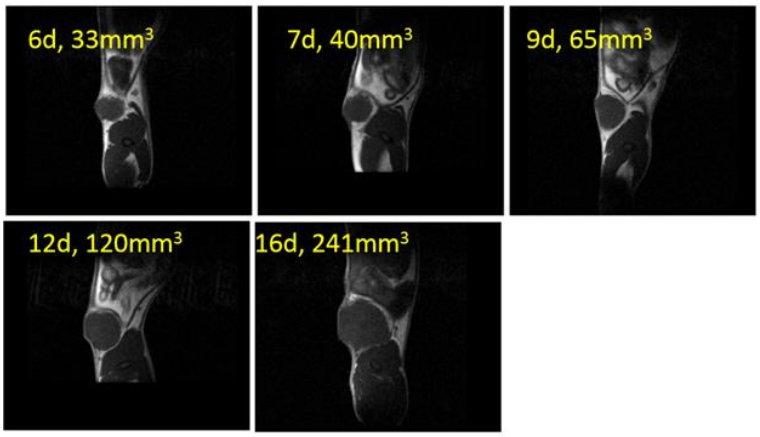

Figure 19 *Representative anatomical images of TS/A tumor, at different stages of development. (Group 3)*

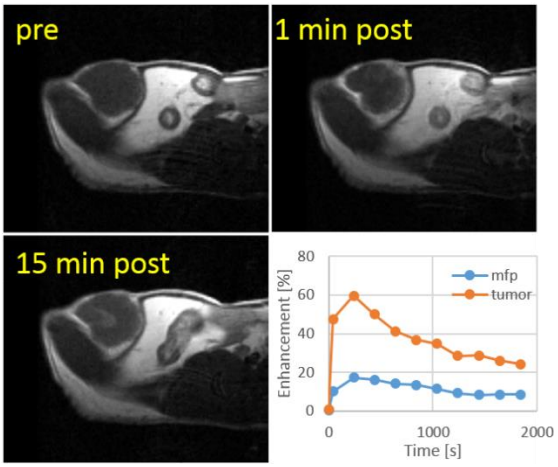

Figure 20 *Representative example of MSME pre and post contrast images, with the measured signal enhancement curve in mammary fat pad and tumor*

The volume exponentially increased with different power for group 3 and 4, reaching the end point after approx. 3 weeks for group 4 and keeping below 150 mm^3 after 25 days for group 3. Tumor growth curves for single groups are shown in Figure 21. Tumor growth monitoring was stopped at day 25 for group 3, even if far from the end-point due to both the slow development and the inhomogeneity among the group.

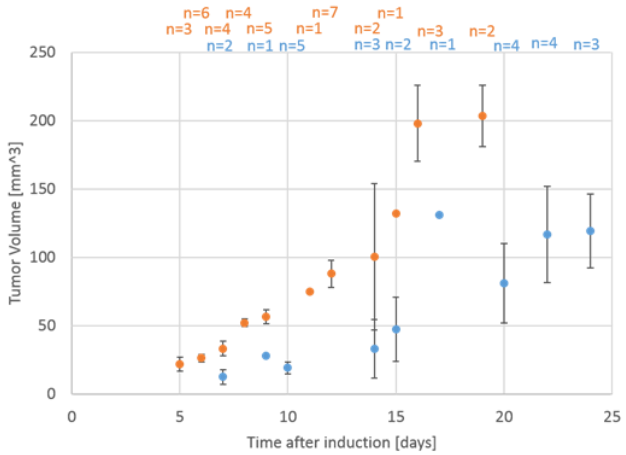

Figure 21 *TS/A tumor growth curve (group 3 blue dots, group 4 orange dots).*

As in the case of 4T1 model, in pre contrast T_1-weighted images the mass and the mammary fat pad are well discernible, both in terms of structure and in terms of T_{1w} MR signal. After CA administration both selected tissues were characterized by a noticeable increment of signal. Immediately after the injection, the boundary of the tumor mass and shortly later the core became bright, reaching a maximum enhancement around 70-80%. When the masses reached large volumes (*i.e.* 100 mm^3 or more) the observed maximum enhancement resulted lower (*i.e.* about 30-60%).

Histology confirmed in both cases the carcinogenic nature of the lesion. Both tumors (4T1 and TS/A) displayed features of poorly differentiated breast cancer, with the tumor correctly localized into the mammary gland. At larger volumes, both tumor exhibited area of necrosis, and this was more frequent especially for TS/A. (Figure 22)

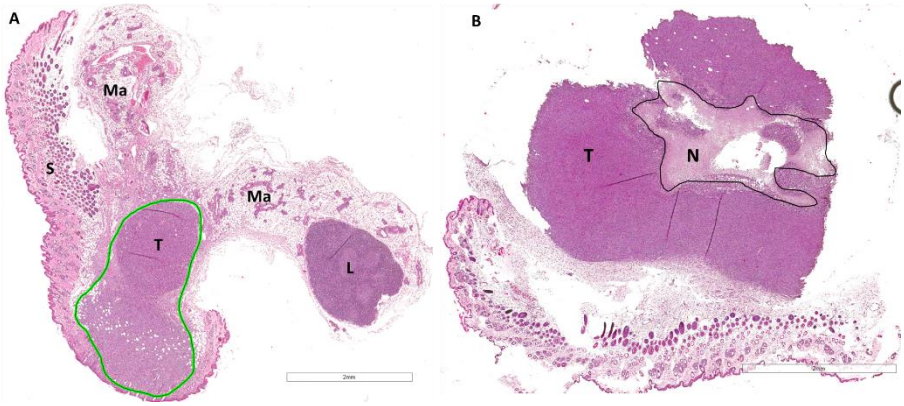

Figure 22 *Transversal Histological section of 4T1 (Panel A) and TS/A (Panel B) breast cancers. Ma= mammary gland; T= Tumor; S= Subcutis; L= lymph node*

Both tumors grew exponentially in less than 20 days to their end point. At the end of their observation period, ulceration of the nipple area was observed in both cell lines. However, there were some cases of early ulceration for the TS/A tumor model. Moreover, this model exhibited fairly less enhancement over time (Table C) in respect of 4T1 (Table B).

In addition, 4T1 cells are commercially available (while TS/A have been obtained as kind gift from the University of Turin) and the growth was more homogeneous, with substantially no outliers. For all these reasons 4T1 model will be selected as the model of choice for the definitive study, where the GBCA under development will be compared with commercial products. To optimize MRI enhancement and to limit as much as possible the impact of the tumor on the animal welfare, the definitive study will be carried out between 5 and 8 days after development, *i.e.* when the diseased mass volume will range between 20 and 60 mm^3.

Conclusions

BT-20 Breast tumor was correctly injected into 23/24 animals. Tumors did develop in almost all the animals, but only 9/23 were palpable. Nevertheless, the 9 animals that had a palpable tumor, reached a maximum volume of 10 mm^3 at the end of the observation period, falling into the limit of detection of MRI. BT-20 orthotopic tumor model is not considered suitable for the objectives of the study. Nonetheless, the first part of the study helped identify the best route of injection for the induction of an orthotopical model of breast cancer, causing a refinement of the method and an increase of animal welfare.

Since Breast cancer was needed for the last part of the efficacy studies of the Lead Compound, two other cell lines, 4T1 and TS/A, were tested using only the US guided injection as the method of choice for the induction of the model. In this case, murine mammary cancer was successfully induced on 24 out of 26 mice: 11 out of 13 for 4T1 model (2 mice did not develop any tumor) and 13 out of 13 for TS/A.

Both tumor models showed a fast growth (*i.e.* 2-3 weeks) and were well vascularized and perfused (*i.e.* observed enhancement around 80-100%). Nevertheless, the 4T1 model proved to be more suitable and homogenous for the objectives of the study than TS/A. No significant differences were observed between the two groups inoculated with different numbers of 4T1 cells.

In conclusion, the experimental conditions for the induction of murine breast cancer characterized by elevated enhancement after GBCA administration were identified in the present study and they will be adopted for the next steps of the project. Specifically $5 \cdot 10^5$ 4T1 will be inoculated in the mammary fat pad of BALB/c under US guide and MRI acquisition will be performed between 5 and 8 days after development, *i.e.* when the diseased mass will reach a volume ranging between 20 and 60 mm^3.

Final Conclusions

All the pathological models discussed in this chapter (C6 Rat Glioma, Ch157MN Meningioma, Photoinduced Rat Ischemia, Breast Mouse Tumor) were correctly induced, characterized and refined according to the 3Rs guidelines. By looking at the animal welfare, pathological models were correctly optimized in order to reduce severe suffering and, when a setup caused less clinical signs, it was preferred over others (*i.e.,* Convexity over Skull Base Meningioma). In all cases, MRI was used as a noninvasive method in order to help identify a specific time window of treatment that will be taken into consideration for the efficacy studies of the Lead Compound, that are going to be discussed in to the last chapter.

3. Improved GBCA for Blood Pool applications: $(Gd\text{-}DTPA)_2$-Chol

This chapter will focus on the *in vitro* and *in vivo* characterization of $(Gd\text{-}DTPA)_2$-Chol, the first of the two novel GBCAs explored in this first part of the thesis, in order to widen the current commercial portfolio for new improved MRI Contrast Agents.

The crucial property of a GBCA in term of efficacy is the longitudinal relaxivity (r_1), which is the concentration-normalized ability to reduce the longitudinal relaxation time (T_1) of surrounding protons. It is possible to increase r_1 in different ways, one of the most efficient being the reduction of the molecular rotational motion (τ_R), attainable through various routes such as the incorporation of the contrast agent into micelles, liposomes or nanoparticles,[97] the synthesis of polymers or dendrimers functionalized with gadolinium complexes,[98] or the promotion of non-covalent binding with plasma proteins.[99]

By establishing a supramolecular adduct, a relaxivity enhancement is observed. Moreover, the *in vivo* distribution of the complex changes. The fraction of paramagnetic complex bound to protein can hardly extravasate from the healthy vascular compartment, providing selective enhancement of vessels and leading to a preferential accumulation in tumor tissues, thanks to the hyper-permeability of cancer vasculature.[100]

A dinuclear gadolinium(III) chelate containing two moieties of diethylenetriaminepentaacetic acid (DTPA), covalently conjugated to an analogue of deoxycholic acid has been designed and synthesized (more information about the synthesis can be found in the article we published: F.La Cava *et al*., 2018[101]) exploiting both cited strategies at the same time to increase τ_R, *i.e.* the presence of multiple paramagnetic centers and the non-covalent binding to albumin. Indeed, similar dinuclear products have been already reported in literature,[102] but they were characterized by lower relaxivity and/or inferior (or not explored) blood pool properties.

A full relaxometric analysis and in vivo characterization on healthy rats and on a pathological model was carried out. In vitro analysis consisted of (i) the acquisition of nuclear magnetic resonance dispersion (NMRD) profiles in different media; (ii) the study of binding affinity to serum albumin; (iii) the measurement of ^{17}O transverse relaxation rate (R_{2p}) vs temperature and (iv) a transmetallation assay. Biodistribution MRI *in vivo* studies at 1T and blood pharmacokinetic were carried out in comparison with Gd-DTPA (Magnevist®, Bayer)[103] and gadocoletic acid trisodium salt (B22956/1, Bracco Imaging)[104], two well-known Gd-complexes both sharing the same chelating cage and the same deoxycholic residue of the investigated Gd-complex ($(GdDTPA)_2$-Chol). Finally, to complete the characterization,

$(GdDTPA)_2$-Chol was tested for its efficacy on a pathological model of cerebral ischemia in rats.

A good affinity to the plasma protein and, in particular, the availability of more than one binding site, allows the complex to reach a fairly high relaxivity value in plasma (approx. 20 mM-1s-1, 20 MHz, 310 K) as well as to show unexpectedly strongly enhanced properties of blood pooling, with an elimination half time in rats about 7 times longer than B22956/1. Moreover, MRI efficacy studies in pathological models demonstrated the complex ability into diagnosing and characterization of pathological lesions.

Further details are reported in the following sections.

Materials and Methods

Sample Preparation: In vitro experiments were carried out using $(Gd\text{-}DTPA)_2$-Chol diluted properly in the medium of interest to reach the desired gadolinium concentration. HSA was obtained by Sigma Aldrich (St. Louis, Missouri, USA) and dissolved in saline solution (NaCl 0.9%, Eurospital, Trieste, Italy); human plasma was acquired from Siemens (control Plasma N; Munich, Germany); i-SBF, a buffer fluid (pH=7.4 ± 0.1) with the same concentrations of dissociated ions of human plasma was prepared according to literature.[15]

NMRD Profiles: NMRD profiles of (Gd-DTPA)2-Chol were acquired in different media (saline, human plasma, saline added with 35 g/L of HSA) at 37°C using a Stelar Spinmaster–FFC field-cycling relaxometer (Mede, Italy) over a continuum of magnetic field strengths from 0.00024 to 0.47 T (corresponding to a proton Larmor frequency range of 0.01-20 MHz) and on a Stelar SpinMaster spectrometer ranging from 0.47 to 1.65 T (i.e. 20-70 MHz). The relaxometer switched the magnetic field strength in the millisecond time scale by working under complete computer control with an uncertainty in water proton relaxation rate ($R_1=1/T_1$) of ± 1%. The magnetic field strength of the spectrometer was manually varied by acting on the current flowing in the electromagnet. The temperature was controlled by a Stelar VTC-91 airflow heater, equipped with a copper-constantan thermocouple. Each sample was preheated at 37°C in an external dry block and then left 10 minutes inside the internal air flow to assure the temperature stabilization. Relaxation times at fields below 4 MHz were measured by means of a pre-polarized sequence, whereas points at higher fields were measured by means of a non-polarized sequence. Typical experimental settings included: acquisition field 9.5 MHz, 16 averaged transients, 16 data points for each T_1 measurement. Data points from 0.47 T (20 MHz) to 1.7 T (70 MHz) were collected on a Stelar Spinmaster spectrometer working at adjustable field. T_1 were measured by standard Inversion Recovery pulse sequence with 16 tau-delays and 2 averaged transients.

Relaxometric Characterization: T_1 was measured at a proton Larmor frequency of 20 MHz and 60 MHz and at fixed temperature (310 K) in different media and as a function of HSA concentration by using a spin analyser Minispec MQ-20 and MQ-60 (Bruker Biospin, Rheinstetten, Germany). A standard inversion recovery sequence, where the inversion time varied from 10 ms to at least 5 times T_1 in 15 points was used. The temperature was kept constant using a thermostatic bath connected to the sample holder of the spectrometer.

Interaction with Human Serum Albumin: The water proton relaxation rate (20 MHz and 37°C) of (Gd-DTPA)2-Chol was measured with the spin analyser Minispec MQ-20 as a function of HSA, with a concentration ranging between 0 and 2 mM at fixed gadolinium concentration (0.1 mM) and as a function of (Gd-DTPA)2-Chol concentration, ranging between 0 and 3 mM at fixed HSA concentration (0.5 mM).

Determination of Gd concentration: The gadolinium concentration of each sample was verified using a relaxometric procedure,[4e] consisting in diluting the samples 1:1 with HCl (37%) and left them overnight at 120°C in a sealed vial. The treatment led to a complete release of Gd(III) as free-aqua ion, thus allowing the determination of its concentration by measurements of r_1 at 25°C. The following equation was used to estimate Gd(III) concentration: $R_1=R_{1d}+r_{1Gd(III)}\cdot[Gd(III)]$, in which R_{1d} is the diamagnetic contribution.

^{17}O NMR measurements: aqueous solutions of $(Gd\text{-}DTPA)_2$-Chol containing 5% of ^{17}O (Yeda, Israel) were used to perform variable temperature ^{17}O NMR measurements at 14 T with a Bruker ADVANCE600 spectrometer, equipped with a 5 mm probe. A D_2O external lock was used. The observed transverse relaxation rate R^{obs}_{2p} was calculated from the signal full width at half height ($\Delta_{1/2}$): $R^{obs}_{2p}=\pi\cdot\Delta_{1/2}$ and R_{2p} (i.e. the paramagnetic contribution) was obtained by subtracting the diamagnetic contribution.

Transmetallation: Transmetallation by $ZnBr_2$ was evaluated by measuring the decrease of water longitudinal relaxation rate at 37°C and 20 MHz (Minispec MQ-20, Bruker Biospin, Rheinstetten, Germany) of buffered phosphate solutions (pH=7, $[KH_2PO_4]$=26 mM, $[Na_2HPO_4]$= 41 mM containing 2.5 mM of GBCA and 2.5 mM of Zn^{2+} according to the protocol reported in literature.[25]

In vivo characterization: All the procedures involving the animals were conducted according to the national and international laws on experimental animals (L.D. 26/2014; Directive 2010/63/EU). 4 weeks old adult male Wistar Rats (n=12) (Charles River Laboratories, Calco (LC), Italy) were housed in groups of 3. A 5 day acclimation period was given before the experiments. Animals were kept in limited access, air-conditioned facilities (20-24°C room temperature, 45-55% relative humidity, 15-20 air changes/h, 12-h light cycle). Food and water were available at libitum.

MRI in vivo bio distribution: MR experiments were performed using an Icon spectrometer (Bruker Biospin, Germany) operating at 1 T (i.e. at a proton Larmor frequency of 42 MHz). During MRI experiment, animals were anaesthetized with isoflurane gas (about 1%) in O_2. Anesthesia was maintained by adjustment of gas level in function of breath rate. Before injection of each test article, ^1H sequences (RARE T_2-weighted) were acquired on the animal in order to have a proper anatomical reference. A series of T_1-weighted 3D-FLASH (Repetition Time = 50 ms, Flip Angle = 50°, Echo Time = 5.4 ms, Number of averages = 2, Matrix Size (3D) = 192x192x8, Field of view = 5 x 5 x 1.6 cm; Acquisition time = 153 s) scans were then acquired before and after the intravenous administration of an aqueous solution of Gd-DTPA (50 mM, n=3), B22956/1 (25 mM, n=4) and (Gd-DTPA)2-Chol (25 mM, n=4) at an injection rate of about 2 mL/min through a catheter placed in the tail vein of the animal. Gd-DTPA was administered at a dose of 0.1 mmol/kg, while the remaining two agents were administered at a dose of 0.05 mmol/kg corresponding to an administration volume of 2 mL/kg. The kinetic of the Gd chelates was followed up to 60 minutes post injection.

Image analysis was performed by positioning the region of interest (ROIs) over liver, kidney, muscle and blood vessel. ROIs positioning and signal quantification was performed by using a home-developed plugin, running on ImageJ (imagej.nih.gov/ij/). Signal enhancement (Enh) was calculated as follows: Enh = 100 ($Signal_{postCA}$ - $Signal_{preCA}$) / $Signal_{preCA}$, where $Signal_{preCA}$ and $Signal_{postCA}$ indicate MR signal before and after contrast agents administration. Mean and standard deviation of the enhancement over the groups were calculated by using Excel (Microsoft, USA). Plots were performed with Mathematica (Wolfram, USA).

Pharmacokinetics Study: The pharmacokinetic study took place at least two weeks after the MRI experiments, on the same rats (n=4 per group). At least 24 hours before test article injection, all animals were put under gas anesthesia and a blood volume of 200 µL was sampled from the caudal vein. The pharmacokinetic study took place at least 24 hours after the pre-dosing sampling. After test article injection, a blood volume of 200 µL was sampled from the caudal vein of each rat at the following time points: 2, 10, 20, 40 and 120 minutes post injection. The animals were kept under gas anesthesia for all the duration of the experiments and breath rate was maintained at 45-50 breaths per minute. Gd-DTPA was administered at a dose of 0.1 mmol/kg, while $(Gd\text{-}DTPA)_2$-Chol and B22956/1 were administered at a dose of 0.05 mmol/kg corresponding to an administration volume of 2 mL/kg.

Relaxometric measurements: Collected blood samples were transferred in NMR tubes and T_1 was measured at 20 MHz and 37°C using the Minispec MQ-20 spectrometer. Gadolinium concentration ([Gd]) was evaluated according to the following formula: $[Gd] = (1/T_1\text{-}1/T_{10})/r_1$, where T_{10} and T_1 are the longitudinal relaxation time before and after CA administration, while r_1 is the relaxivity of the CA, according to literature data or internal

measurements. Interpolation of data of Gd concentration as a function of time post administration was performed with Mathematica (Wolfram, USA). Specifically, the terminal phase elimination rate constant was estimated by log-linear regression of those data points visually assessed to be in the terminal phase of the profile.

ICP-MS measurements and analytical conditions: A selection of blood samples already measured by NMR were analyzed by ICP-MS. For this latter analysis samples were prepared by mixing the collected 0.2 mL of blood in 0.4 mL of nitric acid (65% w/w). Sample digestion for the destruction of the organic matrix was performed by subjecting the samples to a wet ashing process with a microwave oven system (MARS-5 CEM Corporation). ICP-MS assay was carried out on an ELAN 6100 Perkin Elmer Spectrometer. The LOQ (Limit of Quantitation) for gadolinium in blood was 0.010 µg (value verified with recovery study on 0.2 mL of blood sample). Data from the two assays were compared as internal check of data reliability.

Pathological Model of cerebral ischemia induction: All the procedures involving the animals were conducted according to the national and international laws on experimental animals (L.D. 26/2014; Directive 2010/63/EU). 5 weeks old adult male Sprague Dawley Rats (n=12, Charles River Laboratories, Calco (LC), Italy) were housed in groups of 3. A 7 day acclimation period was waited before the ischemic induction. Animals were kept in limited access, air-conditioned facilities (20-24°C room temperature, 45-55% relative humidity, 15-20 air changes/h, 12-h light cycle). Food and water were available ad libitum. Animals were socially housed for psychological/environmental enrichment and were provided with items such as a device for hiding in and an object for chewing, except when interrupted by study procedures/activities. 5mg/mL of Rose Bengal was dissolved in 2 mL of sterile saline and used for the photochemical induction of cerebral permanent ischemia. The animal was positioned on the stereotaxic device and its scalp was exposed to better identify the Bregma. The following coordinates were used AP=1mm, L=3mm, to position a green light beam (wavelength= 550nm) to cover a cortical zone of around 20 mm^2. Irradiation was performed continuously for 20 mins while Rose Bengal was injected via the tail vein as subsequent boli of 0.1 mL each minute. Animals that showed only limited or none clinical sign were imaged by MRI starting from 7 to 14 days after ischemia induction to check lesion development. $(Gd\text{-}DTPA)_2$-Chol and a commercial macrocyclic agent were administered once to each animal, when the ischemic lesion was judged suitable on the basis of acquired anatomical MR images.

MRI Ischemia Study: MR experiments were performed on a 3 T scanner (Bruker Biospin, Germany). During the MRI experiments, animals were anaesthetized with sevoflurane gas (about 1%) in O_2. Anesthesia was maintained by adjustment of gas level in function of breath rate. Before *i.v.* injection of test and reference articles, ^1H sequences (RARE T_2-weighted) were acquired on the animal in order to have a proper anatomical

reference. A series of T_1-weighted MSME scans were then acquired at the magnetic field of 3 T before and after the intravenous administration of saline solutions of $(Gd\text{-}DTPA)_2$-Chol (*i.e.* 25 mM of Gd) and of the selected macrocyclic agent (*i.e.* 50 nM of Gd) at an injection rate of about 2 mL/min through a catheter placed in the tail vein of the animal and at a dose of 0.05 mmol Gd/kg for the former and 0.1 mmol Gd/kg for the latter. The kinetic of the $(Gd\text{-}DTPA)_2$-Chol was followed up to 90 minutes in continuous, whereas the kinetic of the macrocyclic CA was followed for 60 minutes in continuous. At 24 hours from the injection one further T_1-weighted MSME scan was acquired on animals administered with $(Gd\text{-}DTPA)_2$-Chol to conclude the planned MRI experiment. Animals were sacrificed right after by overdose of anesthesia.

Ex vivo Studies: At the end of each successful MRI section, 24 hours after CA administration, animals were sacrificed by overdose of anesthesia. Post mortem: (i) blood was collected from the heart and stored at 2-8°C in tubes containing lithium heparin; (ii) liver was collected, weighted, placed in disposable tubes and then stored at -80°C. Samples were maintained at the Imaging Facility up to the end of the study and then they were processed for ICP-MS determination of gadolinium content.

Evans Blue dye staining: Evans Blue dye (1%) was injected into the rat tail vein after CA administration, to see whether there was a leakage of albumin into the lesion after 12-14 days. After the injection, the rat was kept awake into a cage for 1 hour before being sacrificed by overdose of anesthesia. Brain was collected and frozen at -4°C. Brain was then visualized on the optical microscope (AxioZoom V16, ZEISS) for a colored qualitative test of the nature of the lesion.

Results and Discussion

$(Gd\text{-}DTPA)_2$-Chol is comprised of a dimeric structure of two DTPA molecules and a deoxycholic-like moiety that permits binding to serum Albumin. Synthesis is reported in the paper F. La Cava *et al.,* 2018[94].

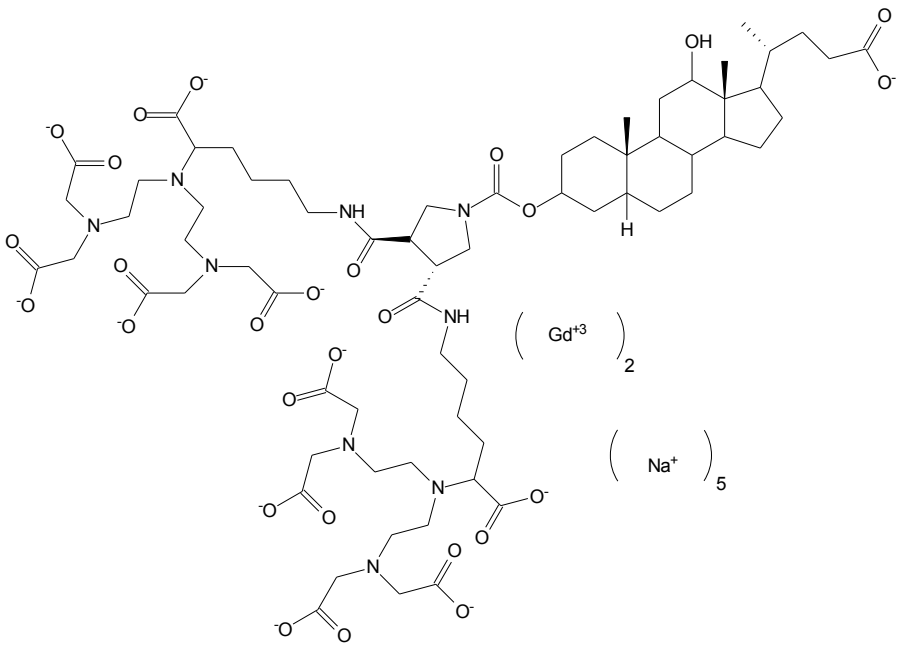

The complex was first investigated by acquiring Nuclear Magnetic Resonance Dispersion Profiles (NMRD) at 310 K and at magnetic field strengths ranging from 0.24 mT to 1.65 T in different media (Figure 1). The profiles acquired in physiological solution and i-SBF[105] (a solution that mimics the ionic content of plasma) were superimposable, at least at a physiological pH, meaning that there is no contribution from the prototropic exchange[106]. However, an addition of 35 g/L of Human Serum Albumin (HSA) to the saline solution, or the use of human plasma medium, strongly affected the NMRD profile obtained. In particular, it is possible to observe a peak centered at approx. 30-40 MHz, which is the typical behavior that originates from a specific binding of a paramagnetic complex to serum proteins. It is observed a gain in relaxivity of a factor of three, as typical for albumin binder complexes as reported in literature.[107]

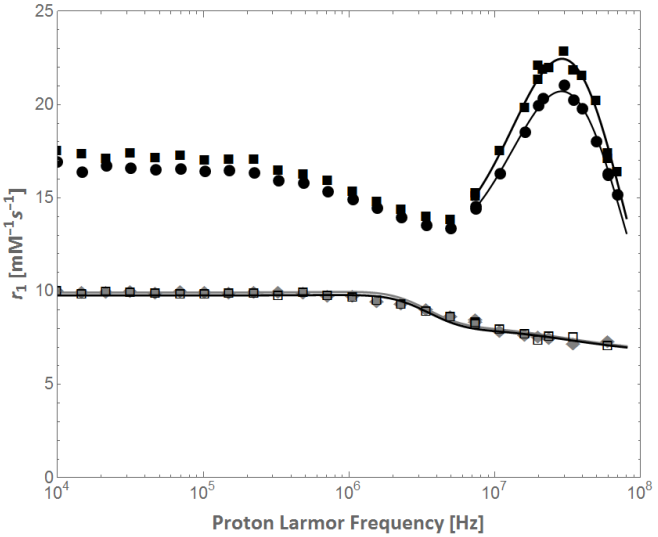

Figure 1 *Proton NMRD profiles of (GdDTPA)2-Chol at 310 K in saline (grey diamonds), in i-SBF (empty squares), in saline added with 35 g/L of HSA (filled squares) and in human plasma (filled circles). Solid lines represent the best fittings of each dataset according to a Solomon-Bloemberger inner sphere and outer sphere model (saline and i-SBF) or to Lipari-Szabo model (saline added with HSA and human plasma).*

Relaxivity values measured at 20 MHz, the most common frequency used in analytical characterization, and at 60 MHz, corresponding to approx. 1.5 T, the typical magnetic field strength used in clinic, are reported in the table below:

Table 1. Relaxivity values ($mM^{-1}s^{-1}$) of (GdDTPA)2-Chol at 20 and 60 MHx, 310 K in different media.

Medium	20 MHz	60 MHz
Saline	7.66 ± 0.53	7.61 ± 0.44
i-SBF	7.25 ± 0.25	7.15 ± 0.17
HSA	21.27 ± 0.89	17.01 ± 0.83
Human plasma	19.88 ± 0.27	16.37 ± 0.25

While saline and i-SBF values are quite constant, as the magnetic field strength increases, data in the presence of HSA or in plasma shows a remarkable reduction from 20 to 60 MHz, being in the proximity of the aforementioned peak.

In addition, relaxivity values were compared with other Gd-complexes in saline or water and in plasma or serum at 20 MHz, in Table 2.

Table 2. Relaxivity values ($mM^{-1}s^{-1}$) of $(GdDTPA)_2$-Chol, B22956/1, MS-325 and Gd-DTPA at 20 MHz, 310 K, in different media.

Medium	$(GdDTPA)_2$-Chol	B22956/1	MS325	Gd-DTPA
saline/water	7.7	6.4	5.8	3.4
plasma/serum	19.9	27	28	3.8

Relaxivity in water is mainly affected by the molecular weight (MW), decreasing as the size of the molecule diminishes. Gd-$DTPA_2$-Chol exhibits a relaxivity of about 7.7 $mM^{-1}s^{-1}$ having a MW of 1774 Da, B22956/1 of 6.4 $mM^{-1}s^{-1}$ with a MW of 1059 Da, Ms-235 of 5.8 $Mm^{-1}s^{-1}$ with a MW of 976 Da, and Gd-DTPA of 3.4 $mM^{-1}s^{-1}$ with a MW of 547 Da.

The gain in relaxivity for dimers and polymers is less than expected by the increase in MW. Actually, despite an increase of about 70% in MW with respect to B22956/1 only a 20% of increase in relaxivity is observed. When moving to serum or plasma, the increment of albumin binder complexes (all but Gd-DTPA) is marked (3 to four times) with Gd-$DTPA_2$-Chol having a r_1 of 19.9 $mM^{-1}s^{-1}$, slightly inferior than the two albumin binder monomers B22956/1 and MS325. Relaxivity values for albumin binder dimer complexes vary in literature. Pushparaj et al.,[108] [109] proposed a dinuclear complex decorated with isovaleric acid with a relavity of 15.25 $mM^{-1}s^{-1}$ in HSA at 37°C and a complex called [Gd2{VA-acamido-pn(DO3VA)2}(H2O)2] with a relaxivity of 27.8 $mM^{-1}s^{-1}$. Parac-Vogt et al.[110], proposed a dinuclear complex linked to a bisindole derivative of trimethoxybenzaldeyde with a

relaxivity of 15.2 $mM^{-1}s^{-1}$ at the same experimental conditions. Gambino et al., [111]proposed instead Gd2L1, with a relaxivity of 41.4 $mM^{-1}s^{-1}$. However, this data did not refer to physiological conditions (where r_1 could be largely inferior), but to the presence of large excess of protein (*i.e.* the concentration of HSA is 1 mM, while that of the complex is 0.07 mM).

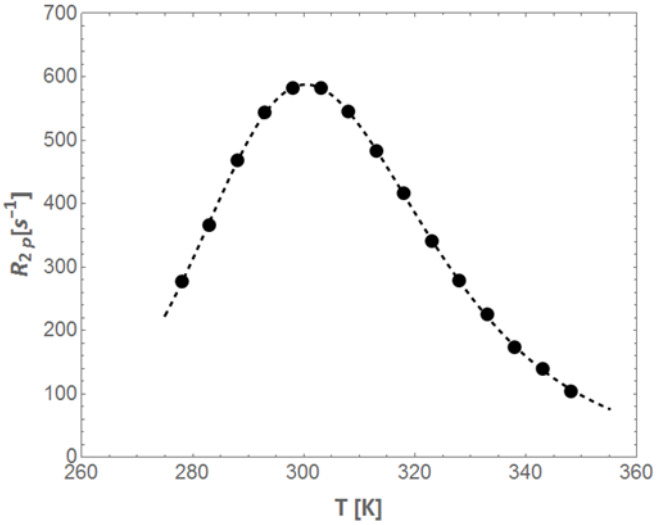

Figure 2. *Temperature dependence of water ^{17}O R2p at 14.1 T in the presence of about 15 mM of $(GdDTPA)_2$-Chol.*

Additional and more technical information about $(GdDTPA)_2$-Chol have been obtained by fitting the NMRD profiles as well as by acquiring and analyzing the temperature dependence of ^{17}O R_{2p} values in the 280-350 K range (Figure 2). This latter experiment allowed the estimation of the exchange lifetime (τ_M) of the water molecule coordinated to the paramagnetic ion, which resulted to be 68 ± 3 ns. This value is just shorter with respect to B22956/1, that displays a τ_M of 122 ns[112] and similar to that of MS-325 (τ_M^{310K} = 83 ns[113]). A τ_M in the order of 100 ns is in the optimal range for the attainment of high relaxivity in the presence of long τ_R, as occurs in the presence of a binding to serum protein. The knowledge of τ_M is useful in the interpolation procedure of NMRD experimental data points. Data acquired in saline or i-SBF were fitted according to the classical inner sphere[114] and outer sphere[115] model, based on the Solomon-Bloembergen theory.[116] A summary of the best fitting parameters, in terms of τ_R, zero-field-splitting (ZFS) energy (Δ^2), electronic correlation time for the modulation of the ZFS interaction (τ_v) and electronic relaxation time (τ_{S0}, calculated from the two latter parameters) is reported in Table 3.

Table 3. Best-Fitting Parameters of NMRD Profiles in saline and i-SBF for (GdDTPA)2-Chol

Medium	τ_v [ps]	Δ^2 [10^{19} s^{-2}]	τ_{S0} [ps]	τ_R [ps]
saline	52.1 ± 0.2	1.55 ± 0.03	106 ± 5	180 ± 2
i-SBF	48.8 ± 0.5	1.67 ± 0.05	102 ± 3	178 ± 2

Data obtained in the presence of HSA and in plasma were interpolated only in the range 10^7-10^8 MHz (as commonly reported in literature,[117,118] using a Lipari-Szabo[119] model (that takes into account the presence of motion due to internal rotation) and keeping fixed the electronic parameters estimated above. A summary of the best fitting parameters, in terms of local and global rotational time (τ_l and τ_g) and the order factor (K, indicated also as S^2, which describes the degree of spatial restriction of local motion, K = 0 no restriction, K = 1 fully restriction), is reported in Table 4. A K value of 0.7/0.8 indicates a moderate dominance of the global motion.

Table 4. Best-Fitting Parameters of NMRD Profiles in HSA (35 g/L) and in human plasma for (GdDTPA)2-Chol

Medium	τ_l[ps]	τ_g[ns]	K
HSA	176 ± 3	2.4 ± 0.2	0.745 ± 0.001
plasma	179 ± 5	2.4 ± 0.7	0.666 ± 0.003

The fitting procedure was performed by keeping fixed some parameters of the relaxation model, such as: the hydration number (set to 1), the distance between protons of the coordinated water and Gd ion (0.31 nm), the distance of closest approach of the outer sphere water protons (0.36 nm), the water diffusion constant in saline (2.2×10^{-5} cm^2 s^{-1}), saline with 35 g/L HSA (2.9×10^{-5} cm^2 s^{-1})24, and in human plasma (2.28×10^{-5} cm^2 s^{-1}, as estimated according to the Einstein-Smoluchowski law under the assumption of spherical particle in a medium of viscosity η equal to 1.2 mPa s). All the other parameters obtained from the data fitting were in the normal range observed for similar gadolinium chelates[6c]. A marked increase of the global rotational time (approx. two orders of magnitude) was observed in the presence of plasma proteins, thus fully supporting the occurrence of protein binding.

The affinity of a gadolinium complex to serum albumin is usually expressed in terms of number of equivalent binding sites (n) with an association constant K_A. These binding parameters, as well as the relaxivity of the supramolecular adduct, were determined using the proton relaxivity enhancement method,[120] which is based on the execution of two titrations. The first one, called M-titration, consists of measuring the relaxation enhancement at fixed HSA concentration when varying complex concentration, whereas in the second one, called E-titration, the amount of HSA is varied and the gadolinium concentration is kept fixed. Measured data points together with their best fitting interpolations are shown in Figure 3.

The change of slope observed in the M-titration (Figure 3, top) at a $(GdDTPA)_2$-Chol/HSA ratio of about 3 may indicate the presence of three equivalent (*i.e.,* with a similar K_A value) binding sites, while best fitting parameters obtained by fitting E-titration data (Figure 3, bottom) led to an affinity constant K_A of $(8.0 \pm 1.3) \times 10^3$ M^{-1} (*i.e.* n $K_A = 2.4 \times 10^4$ M^{-1}) and a

relaxivity of the bound fraction r_{1b} of 22.9 ± 0.3 $mM^{-1}s^{-1}$. Since nK_A, rather than K_A alone, better expresses the affinity, the obtained value is similar to other products reported in literature: B22956/1 has a K_A of 4.5×10^4 M^{-1},[16] B25716/1 of 2×10^4 M^{-1},[16] MS-325 of 1.1×10^4 M^{-1} [11] and the dimer described by Parac-Vogt et al. [14] of 1×10^4 M^{-1}. All of them showed less affinity than the complex Gd-AAZTA-MADEC proposed by Longo et al.,[121] for which a K_A = 8.9×10^5 M^{-1} was reported. As far as the r_{1b} value is concerned, the value obtained for $(GdDTPA)_2$-Chol is very similar to the relaxivity values observed in human plasma, suggesting a bound fraction close to 100%. Therefore, in the absence of leaky vasculature, it is expected that the amount of free agent that can extravasate from the blood pool is very limited, allowing a selective enhancement of the vascular compartment and a marked reduction of the renal excretion.

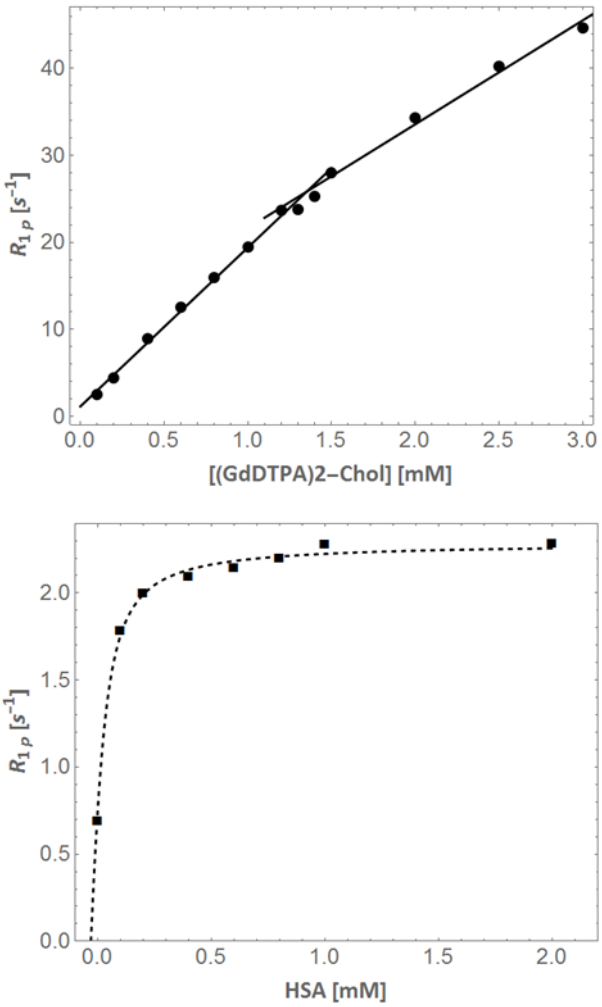

Figure 3. *Top panel: Relaxation rate difference (R1p=R1 – R1d,where R1d is the diamagnetic term) as a function of (GdDTPA)2-Chol concentration ranging between 0 and 3 mM for a 0.5 mM solution of HSA. Bottom panel: ⍰R1 as a function of HSA concentration ranging between 0 and 2 mM for a 0.1 mM solution of (GdDTPA)2-Chol.*

In vitro transmetallation process of the $(GdDTPA)_2$-Chol was carried out to have an indication about the relative stability of the complex. This assay was

performed according to the method described by Laurent et al.,[122] resulting in the curve showed in Figure 4. This easy protocol requires very small amounts of product and a simple low-resolution NMR system. As clearly observable in Figure 4, $(GdDTPA)_2$-Chol displayed a stability just inferior to the parent Gd-DTPA, and appears to be much more stable than Gd-DTPA-BMA, another well-known commercial agent.

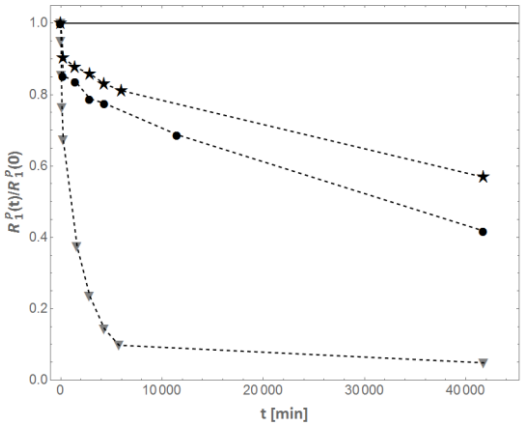

Figure 4 *Time evolution of the normalized R^{1P} (paramagnetic relaxation rate) at 310 K, 20 MHz for Gd-DTPA-BMA (grey triangles), Gd-DTPA (black stars) and GdDTPA)2-Chol (black dots).*

MRI bio-distribution study

The *in vivo* T_{1w} contrast enhancing properties of $(GdDTPA)_2$-Chol were determined on healthy rats at a dosage of 0.05 mmol/kg. The results obtained were compared with B22956/1 (at the same dosage) and Gd-DTPA (at the standard dose of 0.1 mmol/kg). Axial abdominal sections were acquired and signal from liver, cortical kidney, muscle and vessels was evaluated. Figure 5 shows the time course of the percentage signal enhancement in different anatomical districts for the three products up to 60 minutes.

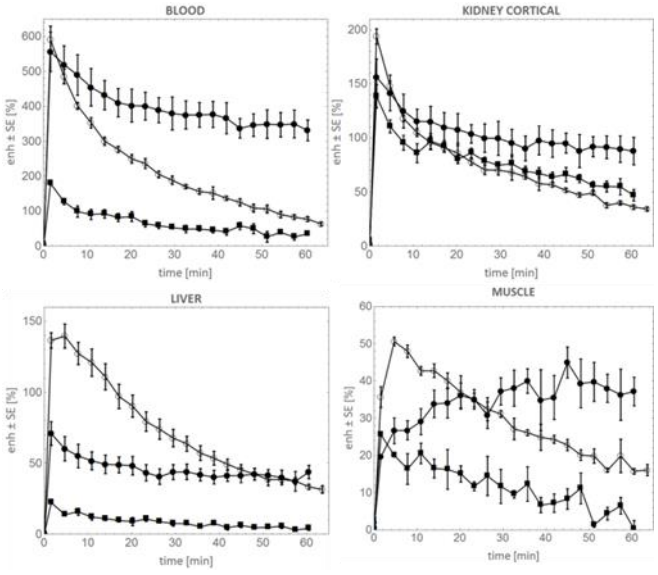

Figure 5. *Time evolution of the MRI signal enhancement after administration of $(GdDTPA)_2$-Chol (filled circles), B22956/1 (empty circles) and Gd-DTPA (filled squares) in different anatomical regions.*

$(GdDTPA)_2$-Chol and B22956/1 showed comparable maximum enhancement in blood (approx. 600%), while Gd-DTPA reached an about three times lower value, despite the double injected dose. An overall difference factor of six is thus observed, which is well in agreement with the difference in relaxivity (3.8 $mM^{-1}s^{-1}$ for Gd-DTPA vs 20 $mM^{-1}s^{-1}$ for $(GdDTPA)_2$-Chol and 27 $mM^{-1}s^{-1}$ for B22956/1). Conversely, the roughly 20% higher r_1 of B22956/1 vs $(GdDTPA)_2$-Chol did not translate in a higher enhancement.

As it is possible to observe into Figure 5, $(GdDTPA)_2$-Chol blood kinetic is much slower than the remaining CAs. Further insight about this behavior will be discussed in the next section, in light of the blood pharmacokinetic results.

Signal enhancement in kidney is similar for the three CAs, but having in mind the differences in relaxivity, this experimental evidence indicates that the gadolinium concentration in the renal compartment after Gd-DTPA administration is much higher than for the other CAs, indicating the renal route as the main excretion pathway for such agent.

The liver compartment shows a difference in the maximum signal enhancement for the three CAs, approaching 150 % for B22956/1, 70% for $(GdDTPA)_2$-Chol and 25% for Gd-DTPA. Once more, a slower kinetic is observed for $(GdDTPA)_2$-Chol. It is well known that biliary excretion is the favorite route for B22956/1. The average cumulative amounts of Gd that were recovered in feces and in urine after 8 hours following *i.v.* administration of 0.1 mmol/kg to anesthetized rats corresponded to 85.6% ± 4.3% of the injected dose and 18.2% ± 4.4%, respectively.[8] The completely reverse situation occurs after administration of Gd-DTPA, which is primarily excreted in the urine (90% in rats, as reported in the leaflet). Again, a different behavior was observed for $(GdDTPA)_2$-Chol, with both renal and hepatic excretion much slower than the other CAs and the latter playing a more limited role with respect to what observed after B22956/1 administration.

Maximum signal enhancement in muscle reached 50% for B22956/1, 40% for $(GdDTPA)_2$-Chol and 25% for Gd-DTPA. The kinetic of Gd-DTPA and B22956/1 was characterized by a very rapid wash-in and a wash-out comparable with blood compartment. Conversely, for $(GdDTPA)_2$-Chol a very slow wash-in is observed: the signal continuously increases reaching a plateau at the end of the observation window and no wash-out is detected up to 60 minutes.

The slower kinetic of $(GdDTPA)_2$-Chol in all the investigated anatomical districts, and especially the markedly tardy wash-in in muscle, can be accounted for in terms of a higher average (over time and/or over the number of molecules) molecular weight of that complex with respect to the other CAs. This means that a larger fraction of $(GdDTPA)_2$-Chol is bound to albumin, or that such bond has a longer residence time. While this is obvious when considering Gd-DTPA, since it does not bind albumin and it

has the typical features of an extracellular fluid complex, the explanation is trickier in the case for B22956/1, which is a known albumin binder. The experimental evidences suggest that a larger fraction of $(GdDTPA)_2$-Chol is bound to albumin or that the supra-molecular adduct has a longer residence time. The nK_A values of the two Gd chelates is very similar (4 x 10^4 M^{-1} and 2.4 x 10^4 M^{-1} respectively), but a non-identical bound fraction could be a consequence of the different relative abundance of Gd-complex and plasma protein, due to the dimeric structure of $(GdDTPA)_2$-Chol, translating in half the number of Gd-carrying molecules. Moreover, the binding kinetic and the binding strength can differ in principle between the two complexes. A reversible protein binding is in fact always associated with a small, but significant, concentration of free chelate, which continuously undergoes excretion (not only renal but also hepatic in the case of B22956/1, that is known to have a rapid liver uptake) diminishing the plasma half-life.

Pharmacokinetic profile of $(GdDTPA)_2$-Chol

Blood samples were collected at different times after *i.v.* administration through the tail vein of $(GdDTPA)_2$-Chol, B22956/1 (both at a dosage of 0.05 mmol/kg) and Gd-DTPA (at a dosage of 0.1 mmol/kg) on healthy rats (n=4 animals for each group). Measurement of blood Gd concentration from the collected samples were obtained by relaxometric method for all rats and confirmed for n=1 representative animal by ICP-MS (see Experimental Section for details). Data acquired with the two techniques resulted to be very similar, with at worst a factor of two (observed for very small concentration values).

Mean data from relaxometry, shown in Figure 6, were interpolated as described in the dedicated section in order to estimate the half elimination time ($t_{1/2\beta}$.), then summarized in Table 5, in comparison to literature data.

Table 5. Elimination half time in plasma for different Gd-complexes.

CA	This work $t_{1/2\beta}$ [min]	Literature $t_{1/2\beta}$ [min]
$(GdDTPA)_2$-Chol	128 ± 29	not available
B22956/1	17.5 ± 0.9	23.7(mice)[121],21(rat males), 26 (rat females)[121]
Gd-DTPA	17.7 ± 0.6	14.94±1.95[123], 19.6[124]
MS-325	not measured	23[125]

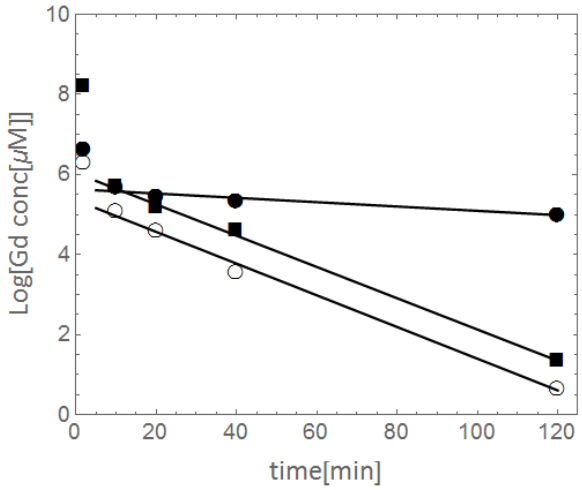

Figure 6 *Time evolution of Gd-complex concentration after single intravenous injection of $(GdDTPA)_2$-Chol (filled circles), B22956/1 (empty circles) and Gd-DTPA (filled squares).*

As a confirmation of MRI results, elimination half time of $(GdDTPA)_2$-Chol was much longer (approx. 7 times) than the other CAs. It is worth to notice that B22956/1 and MS-325, known as a blood pool agent, have a $t1/_{2\beta}$. similar to Gd-DTPA. As well described in literature for MS-325,[125] plasma pharmacokinetics in rats is indistinguishable from that of extracellular agents, because of a rapid liver uptake that decreases the plasma concentration. On the other hand, long plasma half-life (2-3 hours) is observed in rabbits and monkeys, evidence attributable not only to the low free concentration available for renal excretion but also, to the lack of hepatocellular uptake. The same explanation applies to B22956/1, which is known to have a high degree of liver uptake and biliary excretion. Conversely, the less efficient hepatic elimination observed by MRI for (GdDTPA)2-Chol is at least a partial explanation for the longer $t_1/_{2\beta}$.

DCE-MRI Efficacy study on permanent cerebral ischemia

Permanent cerebral ischemia[126] was successfully induced on 10 out of 12 Sprague Dawley Rats. Only one animal was humanely sacrificed one day after the ischemic induction. The remaining one animal was discarded from data analysis due to the absence of a detectable ischemic lesion even after the successful single *i.v.* administration of the CA. All the survived/not humanely sacrificed animals showed a well-identifiable ischemic lesion in MRI between 11-13 days after the ischemic induction. Furthermore, observed ischemic lesions were considered sufficiently homogenous in terms of volumetric dimensions and perfusion.

A total of n = 5 successful MRI experiments were performed after a single *i.v.* administration of $(GdDTPA)_2$-Chol at the dose of 0.05 mmol Gd/kg and n = 5 after *i.v.* administration of macrocyclic CA at the dose of 0.01 mmol Gd/kg in ischemic lesion bearing rats. Representative images before and after administration of each CA and at the respective dose are reported in Figure 7.

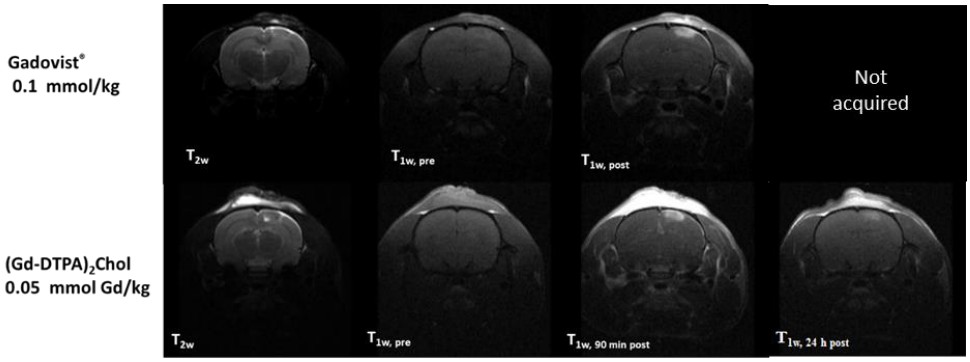

Figure 7 *Representative T_{2w} and T_{1w} images pre and post contrast administration of (Gd-DTPA)$_2$-Chol*

MRI results are reported as a function of averaged signal enhancement (over each group) ± standard error as a function of time post injection in Figure 8.

As it is possible to notice in Figure 8, (Gd-DTPA)$_2$-Chol exhibits a really different kinetic from the one of the macrocyclic, this latter being characterized by an immediate increase in signal just after injection, and a progressive decrease right after up to an almost complete washout in 60 minutes. Conversely, in accordance to its pharmacokinetic profile, (Gd-DTPA)$_2$-Chol slowly accumulates into the ischemic lesion, as a result of the increase in molecular weight given by the complex capability to bind strongly with serum albumin due to its affinity in 3 binding sites. This is not the case for the macrocyclic CA, which shows the typical behaviour of the extracellular fluid CAs with no specific interactions or bindings to plasma proteins.

Right after the injection (at half the dose), the enhancement observed after (Gd-DTPA)$_2$-Chol is statistically lower than the selected macrocyclic CA. Then, since (Gd-DTPA)$_2$-Chol continues to accumulate, the enhancement becomes comparable and starting from 40 minutes it becomes significantly higher than that obtained with the commercial Gd-complex. After 40 minutes, there is no further increase in signal enhancement, which reaches a plateau for all the 90 minutes of observation window.

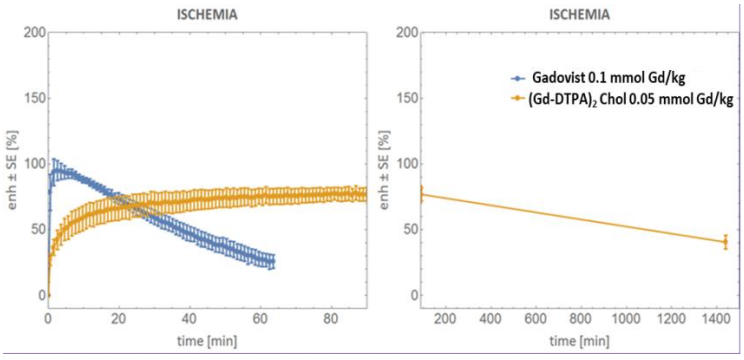

Figure 8 *Signal enhancement (averaged over group) ± standard error as a function of time. Up panel represents the ischemic lesion and bottom panel the healthy contralateral brain after the administration of (Gd-DTPA)$_2$-Chol 0.05 mmol Gd/kg(n=5).*

$(Gd\text{-}DTPA)_2$-Chol washout is confirmed by acquisition at 24 hours post injection, where signal enhancement is characterized by a 50% decrease compared to the initial signal observed in the 90 minutes monitoring.

It is worth to notice that, even if the molecular rotational motion contribution to r_1 is valued at low-to-intermediate magnetic field strength (0.5-1.5 T), $(GdDTPA)_2$-Chol enhancement measured at 3 T was comparable to the macrocyclic commercial agent, injected at double the dose.

As already noticed, the kinetic profile of $(Gd\text{-}DTPA)_2$-Chol is in accordance on what was observed on healthy rats, both because of the binding properties with serum albumin and because of the specific biological characteristic of the ischemic lesion. Cerebral ischemia is in general characterized by three phases that were observed and further studied in the optimization protocol of this model in this PhD thesis. In particular, at 12 days post ischemia induction, the lesion is characterized by gliosis, fibrosis and inflammation, and since this phase is strongly characterized by cellular proliferation for tissue replacement, there is a leakage of the Blood Brain Barrier (BBB) in its lesion core during the period in which damaged blood vessels are being replaced[127]. During this phase, endogenous proteins diffuse into the parenchyma, especially serum albumin[128], thus explaining the accumulation of $(Gd\text{-}DTPA)_2$-Chol and its slow elimination rate into the lesion.

Albumin presence into the lesion was also confirmed by Evans Blue dye, commonly used to detect vascular protein leakage by direct visualization of tissue coloration[129]. Evans Blue is usually administered as an intravital dye as it binds to serum albumin via basophilic interactions, it is non-toxic, and can be directly visualized for qualitative considerations by the striking blue colour within tissue[130]. One animal with a 12 days old ischemic lesion was injected with the dye right after the MRI session of the macrocyclic CA. One hour after Evans Blue *i.v.* administration, the rat was sacrificed and the brain was excised and froze at 4 °C and visualized at the optic microscope (Figure 9).

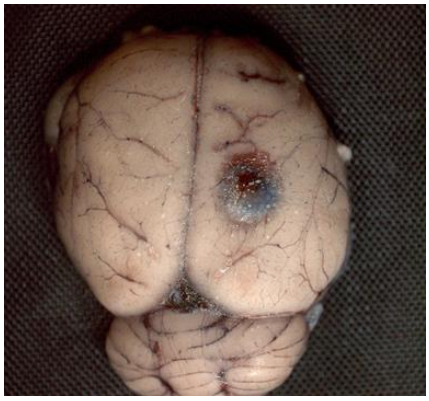

Figure 9 *Excised rat brain bearing a subacute chronic ischemic lesion (12 days post induction), previously administered with Evans Blue dye.*

Conclusions

A novel albumin-binding dinuclear gadolinium complex has been described in terms of full relaxometric characterization, in vivo preclinical behavior in an MRI biodistribution study, and in a blood pharmacokinetics analysis. These latter studies were carried out in comparison with two well-known GBCAs: Gd-DTPA and B22956/1.

Data from NMRD profiles proved that the relaxivity in water is slightly superior to analogous complexes, settling around 7.7 $mm^{-1} s^{-1}$ (water, 310 K, 20 MHz). A notable binding affinity toward albumin led to a significant increase in r_1, reaching a value of ~20 $mm^{-1} s^{-1}$ in the range of 20–40 MHz, not too far from the operating magnetic field strength of clinical MRI scanners.

A series of features of the presented compound, such as good affinity for albumin, high number of binding sites, properties of carrying two Gd ions per molecule, and limited hepatobiliary elimination, all contributed to an unexpected long blood elimination half-life (~130 minutes, in rats). This fact translates into an optimal confinement in the vascular space and thus into an extension of the available time window for MR angiography, suggesting this to be an optimized blood pool agent with respect to B22956/1 and MS-325, at least for preclinical applications. Moreover, as observed in healthy muscle, the extravasation inside tissues and especially tumors is expected to last for a prolonged period of time, as high-molecular-weight contrast agents (such as $(GdDTPA)_2$-Chol when bound to protein) slowly and preferentially accumulate in pathological tissues characterized by enhanced vascular permeability and retention (the well-known EPR effect).

The good *in vitro* results, coupled with the pharmacokinetic profile, paved the way to test the compound in an *in vivo* pathological model of permanent cerebral ischemia. The choice of the model was linked to $(GdDTPA)_2$-Chol features. It is well known that a stroke event leads to vessels disruption, usually followed by leakage of vascular proteins during the tissue remodeling phase happening especially into the brain, 2 to 10 days post infarction. Since $(GdDTPA)_2$-Chol main feature is its binding to Albumin, CA diagnostic capability was tested in a pathological model of cerebral stroke.

The kinetic profile observed during Dynamic Contrast Enhanced MRI experiments in ischemic rats is in accordance to what observed in the pharmacokinetic study on healthy rats. The compound exhibited a slow accumulation into the lesion, and its enhancement, with the exception of the first minutes after injection, was firstly comparable (around 30 minutes) and then superior (beyond 40 minutes) to the macrocyclic agent injected at double the dose, even if the molecular rotational motion contribution to r_1 is valued at low-to-intermediate magnetic field strength (0.5-1.5 T).

The strong binding to albumin, the slow accumulation into fibrotic tissue observed after administration of $(GdDTPA)_2$-Chol, and its high enhancement despite the low dose injected are valuable features and could be exploited for different applications into cerebral pathology staging and follow-up.

4. Lead Compound

Introduction

This chapter will focus on the *in vitro* and *in vivo* characterization of a novel dimeric macrocyclic gadolinium based contrast agent (GBCA), tested for its pharmacokinetics properties and efficacy in MRI studies of healthy animals and pathological models of mice and rats previously discussed in this thesis.

As stated before, a new GBCA with a better efficacy is needed to widen the current commercial portfolio in clinical Contrast Enhanced MRI. A new GBCA was previously designed and synthetized and tested *in vitro* for its relaxometric properties and, since it appeared to be a suitable candidate for clinical translation, it was tested for its efficacy *in vivo* on different pathological models.

The GBCA macrocyclic compound structure, namely Lead Compound, is confidential, and therefore it will not be disclosed.

To improve the characteristics of the Lead Compound a series of strategies were exploited. Since it is well known in literature that macrocyclic structures are characterized by high kinetic inertness and chemical stability[131], lead compound was designed with a macrocyclic structure to increase its stability and reduce the chance of transmetallation *in vivo* and thus, Gd release. In addition, a dimeric structure was chosen to improve its relaxometric properties, so that the same efficacy of the commercial products can be obtained reducing the recommended clinical dose (0.1 mmol/kg to 0.05 mmol/kg). In particular, the Lead Compound showed good results in terms of relaxivity with an r1 about twice the value of macrocyclic commercial products at the same experimental conditions.No significant binding to Human Serum Albumin was observed, and relaxivity was not significantly influenced by pH at physiological levels.

Lead Compound was characterized *in vitro* for its relaxometric properties (*i.e.* relaxivity in different media, pH profile, HSA titration, thermal stability) and its efficacy was proved *in vivo* in healthy mice and in pathological models, in regards with two reference articles (Gadovist®, Dotarem®). In this chapter, the results of the efficacy studies performed on healthy mice, rat glioma, mouse meningioma, rat ischemia and mouse breast tumor will be discussed.

Materials and Methods

In vivo Efficacy Studies: All the procedures involving animals were conducted according to the national and international laws on

experimental animal research (L.D. 26/2014; Directive 2010/63/EU). No validated non-animal alternatives are known to meet the objectives of the study. Animals were purchased from Charles River Laboratories, Calco (LC), Italy. Animals used were the following, divided per efficacy study:

- Healthy study: 5 weeks old female C57BL/6 mice (n=30)
- Glioma study: 5 weeks old male Wistar Rats (n=28)
- Meningioma study: 28 athymic female nude mice, between 4 and 5 weeks old
- Photoinduced cerebral ischemia study: 28 Sprague Dawley male rats, 5 weeks old
- Breast study: 28 BALB/C female mice, 6 weeks old.

Animals were kept, air-conditioned facilities (20-24°C room temperature, 45-55% relative humidity, 15-20 air changes/h, 12-h light cycle). Food and water were available at libitum.

Cell culture and preparation, together with the induction modalities of the different pathological models, are thoroughly described in the first chapter of this thesis.

MRI Experiments: During MRI experiments, animals were anaesthetized with isoflurane or sevoflurane gas (about 1%) in O2. Anesthesia was maintained by adjustment of gas level in function of breath rate. Before *i.v.* injection of test and reference articles, anatomical 1H sequences (T1-weighted and/or T2-weighted) were acquired on the animal in order to have a proper anatomical reference. A series of T_1-weighted 3D-FLASH or 2D-MSME scans were then acquired before and after the intravenous administration of GBCAs. (See the table below) The kinetic of the Gd chelates was followed up to 60 minutes post injection. After a successful *i.v.* injection and MRI experiment, animals were sacrificed by overdose of anesthesia; if not, animals could return to the Animal Facility rooms up to the next available MRI session. In this second case animals could be monitored daily to evaluate their general condition (spontaneous behavior, reaction to handling, body weight (weekly), etc.). In the case of clinical signs onset causing pain or distress, the Veterinary Officer could possibly administer analgesic, *i.e.* carprofen (2.5-5 mg/kg every 24 h), or in case of the pathological model of ischemia, buprenorphine (0.05 mmol/kg every 8 h). In case of moribund animals, or animals obviously in pain or showing signs of severe and enduring distress could be humanely sacrificed. Criteria for making the decision to kill moribund or severely suffering animals, and guidance on the recognition of predictable or impending death, are the subject of an OECD Guidance Document.[132]

Table A: Experimental MRI setup for all the studies performed.

Study	Magnetic Field (T)	Coil	MRI Sequence (^{1}H)	Time of treatment (after induction) (days post)	Doses (Gd mmol/kg)
Healthy	3	Volume	RARE T_2-weighted, 3D FLASH T_1-weighted	-	Dotarem® = 0.1 Gadovist® = 0.1 Lead= 0.05, 0.1, 0.3
Glioma	3	Brain Surface	RARE T_2-weighted, 2D MSME T_1-weighted	7-13	Dotarem® = 0.1 Gadovist® = 0.1 Lead= 0.05, 0.1
Meningioma	1	Brain Surface	RARE T_2-weighted, 2D MSME T_1-weighted	14-21	Dotarem® = 0.1 Gadovist® = 0.1 Lead= 0.05, 0.1
Ischemia	3	Brain Surface	RARE T_2-weighted, 2D MSME T_1-weighted	12	Dotarem® = 0.1 Gadovist® = 0.1 Lead= 0.05, 0.1
Breast	3	Circular Surface	3D MSME T_1-weighted	7-9	Dotarem® = 0.1 Gadovist® = 0.1 Lead= 0.05, 0.1

Data Analysis: Image analysis was performed by positioning the regions of interest (ROIs) over liver, kidney, muscle and main blood vessel (in the case of healthy mice) and over lesion and contralateral healthy region or muscle (in the case of pathological models). ROIs positioning and signal quantification will be performed by using a home-developed plugin, running on ImageJ (imagej.nih.gov/ij/). Signal enhancement (Enh) was calculated as follows:

$$Enh = 100 (Signal_{postCA} - Signal_{preCA}) / Signal_{preCA},$$

where $Signal_{preCA}$ and $Signal_{postCA}$ indicates MR signal before and after CA administration.

In the case of pathological model, Contrast-to-noise ratio was evaluated as additional parameter as follows:

$$CNR = (Signal_{lesion} – Signal_{Controlateral/muscle}) / SD_{Noise}$$

where $Signal_{lesion}$ and $Signal_{Controlateral/muscle}$ indicates MR signal coming from ROI placed respectively over lesion (tumor or ischemia) and on healthy contralateral tissue or muscle, SD_{Noise} indicates the standard deviation of the pure image noise.

Before formal analysis, box plots were used to detect anomalous data points within group. Any observation detected as significantly different was considered anomalous and, after further evaluation, if necessary, deleted. Different types of analysis were carried out on the basis of data distribution and homogeneity of variance among groups, as follows:

- the Levene's test was used to test the homogeneity of variance among groups. In case of homogeneity of variance, the ANalysis Of VAriance (ANOVA) was applied in order to test the null hypothesis, i.e., that treatment groups originate from the same distribution. If significant differences between groups are detected, pairwise multiple comparisons were performed with the method proposed by Tukey[133,134];

- when necessary the linear correlation was tested using the Pearson correlation test and the relative correlation coefficient, i.e. ρ, was calculated.

Mean, standard deviation and standard error of the enhancement over the groups were calculated by using Excel (Microsoft, USA). Plots and statistical analysis were performed with Mathematica (Wolfram, USA).

Lead compound DCE-MRI Efficacy study on healthy mice: Comparison with Dotarem and Gadovist. Results

Animals were divided according to administration conditions (dose and tested contrast agent) into five different groups. A summary of the performed experiments is reported in Table A.

Table A: Summary of Experiments

Group	Animal ID	Compound	Injected dose (mmol/kg)	Treatment
1	01- 05 (n = 5)	Lead	0.3	Each animal of the group received a single successful *i.v.* treatment
2	06 - 12 (n = 7)	Lead	0.1	Each animal of the group received a single successful i.v. treatment
3	13-19 (n = 7)	Lead	0.05	Each animal of the group received a single successful *i.v.* treatment
4	20 - 24 (n = 5)	Gadovist®	0.1	Each animal of the group received a single successful *i.v.* treatment
5	25 - 29 (n = 5)	Dotarem®	0.1	Each animal of the group received a single successful *i.v.* treatment
n.a.	30	n.a.	n.a.	*i.v.* treatment not performed, catheterization failed

MRI experiments were successfully carried out on 29 out of 30 animals. One animal did not undergo the planned MRI experimental protocol because the catheterization procedure failed and consequently, it could

not be administered with one of the selected CAs. In summary, n = 5 successful MRI experiments were performed after a single *i.v.* administration of Dotarem®, Gadovist® both at the dose of 0.1 mmol/kg and Lead at 0.3 mmol/kg, while n = 7 after a single *i.v.* administration of Lead at 0.05 and 0.1 mmol/kg. Representative images before and after administration of each CA and at the respective dose are reported in Figure 1.

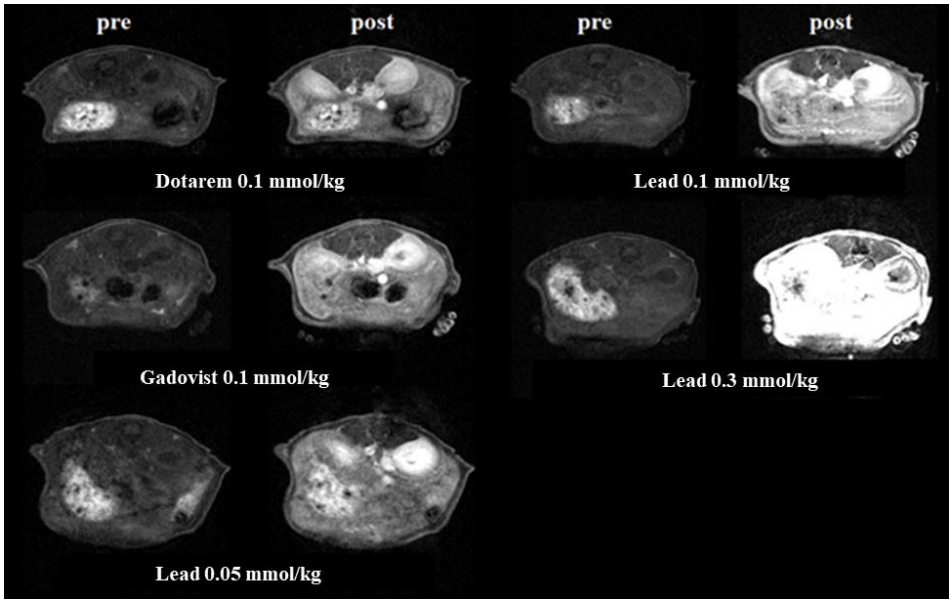

Figure 1 *Representative images pre and post contrast administration (1 minute) for each CA. All the images are reported with the same gray scale.*

MRI results are reported as a function of averaged signal enhancement (over each group) ± standard error as a function of time post injection in Figure 2 and in Figure 3.

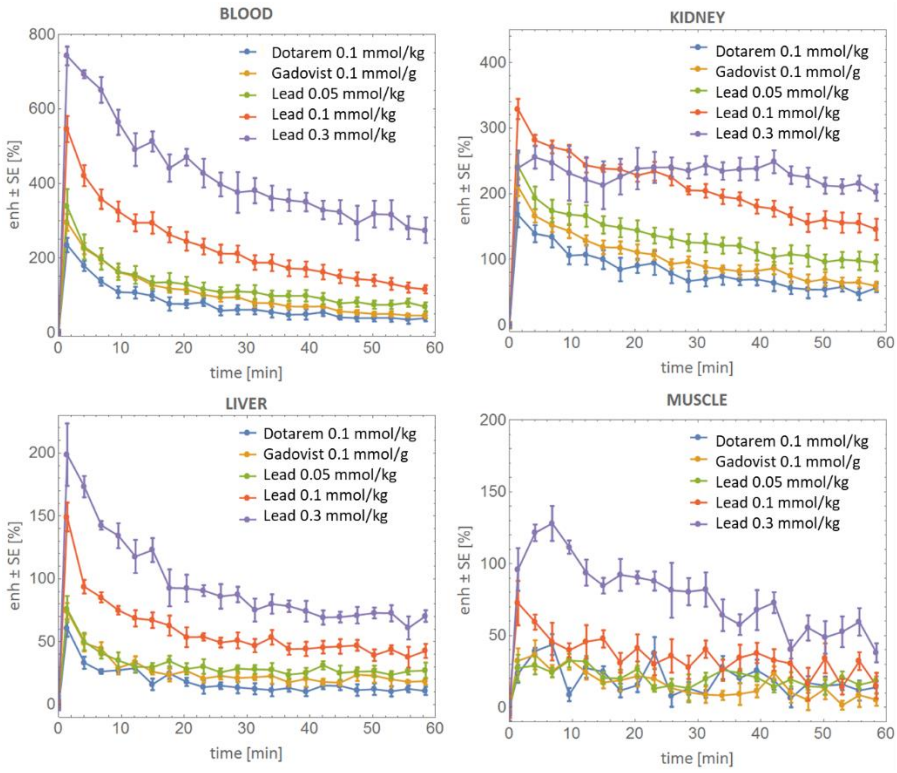

Figure 2 *Signal enhancement (averaged over groups) ± standard error as a function of time. Each panel represents a different anatomical region, while curves referring to different CAs are plotted in different colors (blue for Dotarem® at 0.1 mmol/kg(n=5), orange for Gadovist® at 0.1 mmol/kg(n=5), green, red and purple for Lead at 0.05(n=7), 0.1(n=7) and 0.3(n=5) mmol/kg), respectively.*

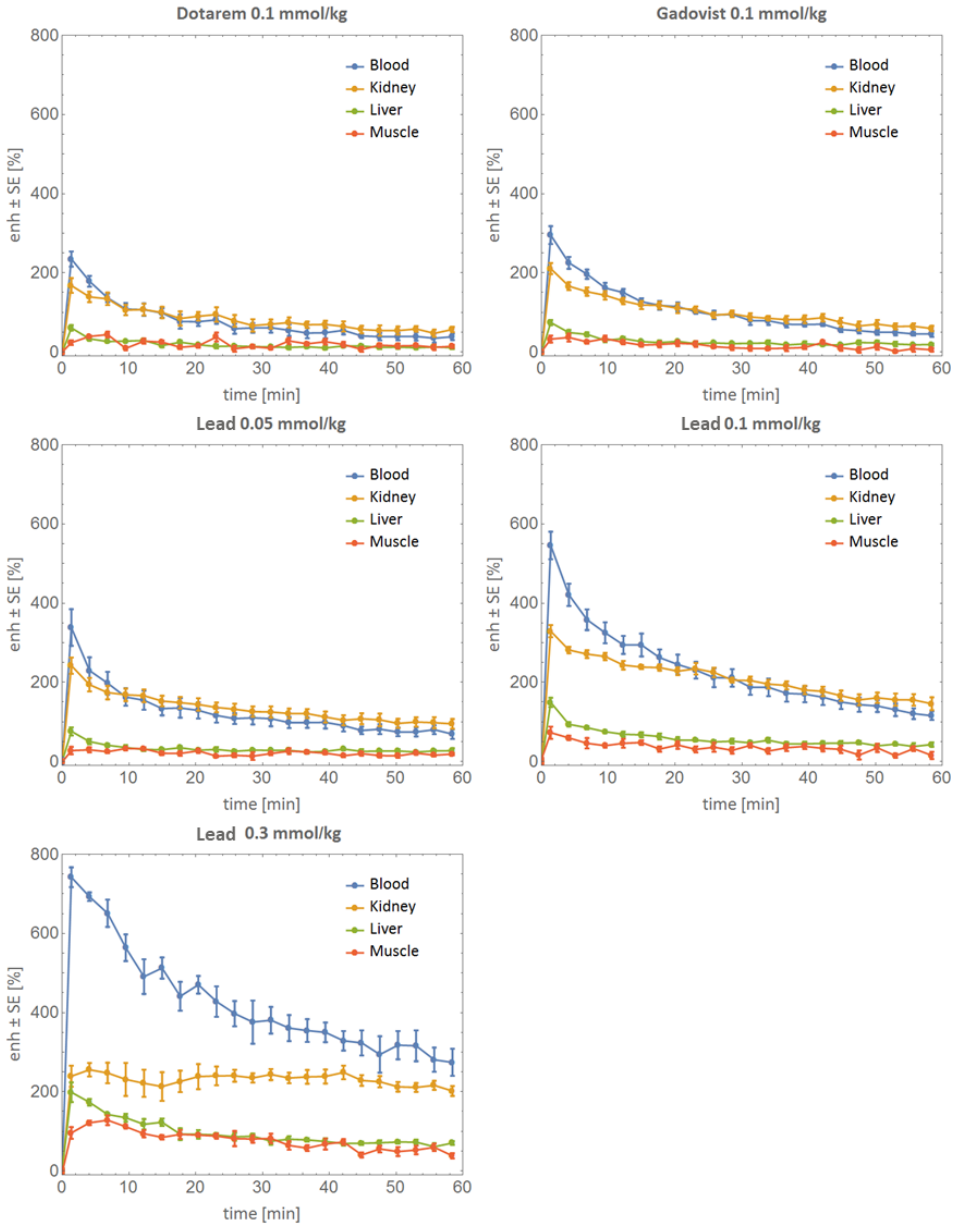

Figure 3 *Signal enhancement (averaged over groups) ± standard error as a function of time. Each panel represents a different treatment condition in terms of CA or dose (Dotarem® at 0.1 mmol/kg(n=5), Gadovist® at 0.1 mmol/kg(n=5), Lead at 0.05(n=7), 0.1(n=7) and 0.3(n=5) mmol/kg) with the same scale, while curves referring to different anatomical regions are plotted in different colors (blue for blood, orange for kidney, green for liver and red for muscle).*

Generally, the homogeneity of data was very good and it can be appreciated by the small standard errors in both figures, indicating that the adopted MRI experimental setup was robust and reliable. Figure 2 panels represent a different anatomical region, whereas each curve refers to different treatment condition (*i.e.* CA and/or dose). For simplicity, every treatment condition is plotted in different colors (blue for Dotarem® administered at 0.1 mmol/kg, orange for Gadovist® at 0.1 mmol/kg, green for Lead at 0.05 mmol/kg, red for Lead at 0.1 mmol/kg and purple for Lead at 0.3 mmol/kg). The same data is also represented in Figure 9 but in this case each panel represents a different treatment condition in term of CA and/or administered dose plotted with the same scale, while the curves referring to different anatomical regions are plotted in different colors (blue for blood, orange for kidney, green for liver and red for muscle).

A series of interesting features can be extracted by looking at the different compartments.

Blood compartment:

- Groups treated with Dotarem®, Gadovist® (both administrated at the dose of 0.1 mmol/kg) and Lead (at 0.05 mmol/kg) show comparable maximum signal enhancement despite the Lead group administered at half dose. The absence of statistical difference (with a confident level of 5%) between these groups is also maintained in time after the administration;

- The maximum signal enhancement of Lead administered at the same dose of Gadovist® and Dotarem®, *i.e*. 0.1 mmol/kg, is statistically different if compared to the same compound administered at the half dose (approx. 1.6 times higher) and to Gadovist® and Dotarem® at the same dose (approx. 2 times higher). Confidence levels are of 5%, 1% and 0.1% respectively.

- The signal enhancement of Lead group administered at the dose of 0.3 mmol/kg is statistically higher than all other experimental groups with a variable confidence level between 0.1, 5 % up to the end of MRI protocol, *i.e.* 1 hour after the administration. At this dosage, Lead shows a maximum signal enhancement approx. 3, 2, 1.4 times higher than that observed in groups treated with the two reference articles at the standard dose, Lead at 0.05 and 0.1 mmol/kg respectively.

- All the investigated compounds seem to have a comparable kinetic. The percentage decrease of signal enhancement in blood compartment (evaluated after 30 and 60 minutes after the administration of the CA, see Table B) are similar regardless the dosage, with the only exception for Lead at 0.3 mmol/kg. This difference can be reasonable explained as due to a T_2 /T_{2*} decrease of the MRI signal intensity due to a higher local concentration of gadolinium just after the administration of the CA.

Table B: Percentage blood enhancement decrease calculated at 30 and 60 minutes after injection.

CA	Dose [mmol/kg]	Blood Enh. Decrease [%]	
		30 min	60 min
Dotarem	**0.1**	74 ± 6	84 ± 4
Gadovist	**0.1**	73 ± 4	85 ± 3
Lead	**0.05**	68 ± 7	80 ± 5
	0.1	66 ± 4	79 ± 2
	0.3	49 ± 5 *	63 ± 5

Kidneys:

- Signal enhancement in kidneys is similar for Dotarem®, Gadovist® and for Lead administered at the dose of 0.05 mmol/kg. When the Lead is

administered at 0.1 and 0.3 mmol/kg, it shows a higher signal enhancement, which is statistically different with respect to the previous ones (with a confidence level ranging between 0.1 and 5%).

- When administered at a higher dosage, *i.e.* 0.3 mmol/kg, Lead shows a signal enhancement lower than that observed at 0.1 mmol/kg in the first part of the observation window. After 20 minutes however, signal enhancement becomes higher than that of the other CAs and it seems to reach a plateau close to the end of the observation window (*i.e.* 60 minutes). The initial decrease observed at short times can be explained as due to a T_2 /T_{2*} decrease of the MRI signal intensity, probably due to a higher local concentration of gadolinium during the first minutes of kidney's filtration.

- The kinetic of Lead, Dotarem® and Gadovist® administered at 0.1 mmol/kg is characterized by a rapid wash-in and wash-out reasonably comparable with blood compartment. This is true also when lead is administered at 0.05 mmol/kg. However, when Lead is administered at 0.3 mmol/kg, the kinetic changes. It exhibits the same wash-in but a longer wash-out with respect to the other CAs or doses. This consideration can be biased by the initial decrease of the signal enhancement probably provoked by a higher local gadolinium concentration.

Liver:

- Maximum signal enhancement is quite the same (*i.e.* on average close to 65%) for Lead administered at 0.05 mmol/kg, Dotarem® and Gadovist® both at 0.1 mmol/kg. A higher maximum signal enhancement is observed for Lead when administered at 0.1 and 0.3 mmol/kg, approx. 150 % and 200 % respectively (with a confidence level ranging between 0.1 and 5%).

- The kinetic of all the administered CAs, regardless of the administered dose, is very rapid. Wash-in and wash-out is comparable with blood compartment for all the CAs. Signal enhancement continuously decreases up to the end of the observation window (*i.e.* 60 minutes).

Muscle:

- Maximum signal enhancement reaches approximately 130 % for Lead administered at 0.3 mmol/kg, 72% for Lead at 0.1 mmol/kg. Lead at 0.05 mmol/kg and Dotarem® and Gadovist® at 0.1 mmol/kg have a maximum enhancement lower than 50 %.

- All the administered CAs, *i.e*. Lead, Dotarem® and Gadovist®, regardless of the administered dose, show a kinetic characterized by a very rapid wash-in and wash-out. The signal enhancement continuously decreases up to the end of the observation window (*i.e.* 60 minutes).

It is worth to notice that the MRI signal enhancement is not in absolute directly proportional to the gadolinium concentration. Relaxivity plays a fundamental role in influencing the signal enhancement observed, and is

difficult to know the exact gadolinium concentration in different tissues. In order to keep in to account both these two main contributions, *i.e.* relaxivity and gadolinium concentration (reasonably assumed to be directly proportional to the administered dose), the blood enhancement obtained just after injection for each CA and administration dose was plotted *versus* the respective paramagnetic longitudinal rate, *i.e.* $1/T_{1p}$, in Figure 4.

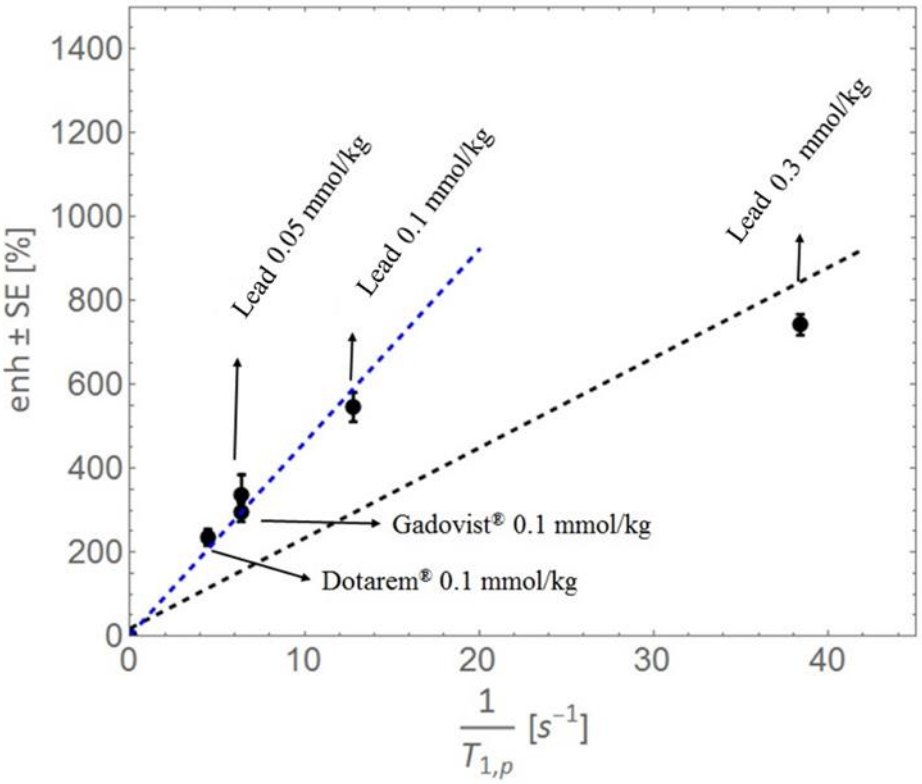

Figure 4 *Blood signal enhancement measured after injection versus the respective paramagnetic longitudinal rate, i.e. 1/T1p. Dashed lines represent error weighted trend lines calculated excluding (blue dashed line, ρ = 0.99, significance level of 1%) or including (black dashed line, ρ = 0.90, significance level of 5%) the enhancement referred to Lead at 0.3 mmol/kg*

The latter term, *i.e.* $1/T_{1p}$, was calculated for each administration condition simply multiplying the relaxivity value of each CA (i.e. Dotarem® = 3.5 ± 0.2[135] $mM^{-1}s^{-1}$, Gadovist® = 5.0 ± 0.3[6] $mM^{-1}s^{-1}$ and Lead = 10.05 ± 0.13 $mM^{-1}s^{-1}$, according to literature data and measurement in human plasma at 37°C and at 3 T) by the gadolinium concentration. This concentration was estimated under the assumption of a homogenous distribution of each CA in the blood compartment, reached 1.4 minutes after injection, and simply using the following data: the administrated dose (*i.e.* 0.05, 0.1 and 0.3 mmol/kg), the mean mouse body weight (*i.e.* 0.020 kg) and finally the total mouse blood volume (*i.e.* 1.57 mL). On data plotted in Figure 4, a Pearson correlation test was performed under the null hypothesis that these data are linearly independent and the alternative hypothesis of linear correlation. The statistical test confirmed that the populations tested are not linearly independent, with a 5% confident level (p-Value approx. equal to 0.02, Pearson Correlation coefficient ρ = 0.93). The same test, performed excluding data obtained from Lead at the dose of 0.3 mmol/kg (gadolinium dose higher than those commonly used in clinical practice, *i.e.*

0.05, 0.1 mmol/kg), gives the same result but with a stronger evidence (see Figure 4).

The blood enhancement after the injection of the lead at 0.3 mmol/kg seems to deviate more from a linear trend than other data. However, the blood enhancement shown in Figure 4 linearly correlates with the $1/T_{1p}$. This deviation is only observed at the higher dose of Lead, probably because of the transverse relaxation contribution to the signal enhancement. The contribution can decrease the enhancement significantly at high gadolinium concentration, even if it was minimized in the MRI acquisition protocol adopted in this study (*i.e.* short echo time).

In summary, keeping the blood enhancement observed immediately after the administration of Gadovist® (*i.e.* the test article with the higher relaxivity) at the standard dose as reference among data reported in Figure 4, the enhancement ratio for Dotarem® at 0.1 mmol/kg and Lead at 0.05, 0.1 and 0.3 mmol/kg is equal to 0.8, 1.2, 1.9 and 2.5 respectively. Taking into account the different relaxivity values, these ratios highlight the equivalence, in terms of efficacy, between Gadovist® administrated at the standard dose of 0.1 mmol/kg and the test article at the half dose. Equivalent consideration can be done qualitatively by observing the MRI images pre- and post-administration of Lead, see Figure 7.

Finally, the kinetic of the test article in all the investigated regions and at all the administrated doses is similar to that observed for the reference articles. As reported in Table B, after approximately 30 and 60 minutes of the injection, blood enhancement decreases of approximately 70 % and 80% respectively for all CAs. Lead at the dose of 0.3 mmol/kg shows a lower decrease at 30 minutes probably due to a T_2/T_{2*} contribution to the MRI signal that is expected to be higher just immediately after the administration.

Lead compound DCE-MRI Efficacy study on a Rat C6 Glioma model: Comparison with Dotarem and Gadovist. Results

Animals were divided in four different groups, one for each administration condition (*i.e.* dose and tested contrast agent). A summary of the performed experiments is reported in Table A.

Table A: Summary of the Experiments

Group	Sex	Animal Treatment ID	Compound	Injected dose (mmol/kg)	Treatment
1	M	01 - 07 (n = 7)	Lead	0.1	Each animal of the group received a single successful *i.v.* treatment
2	M	08 -14 (n = 7)	Lead	0.05	Each animal of the group received a single successful *i.v.* treatment
3	M	15 - 20 (n = 6)	Gadovist®	0.1	Each animal of the group received a single successful *i.v.* treatment
4	M	21 - 26 (n = 6)	Dotarem®	0.1	Each animal of the group received a single successful *i.v.* treatment
n.a.	M	27	n.a.	n.a.	died during the inoculation surgery
n.a.	M	28	n.a.	n.a.	not treated because of a small tumor volume

MRI experiments were successfully carried out on 26 out of 28 animals. Two animals did not undergo the planned MRI treatment, one animal died during surgery and another did not develop a tumor mass with a volume suitable for the study. All the 26 rats showed a well-identifiable tumor mass in MRI between 7-15 days from the inoculation day. Furthermore, all the observed tumors were homogenous in terms of the volumetric dimensions and perfusion.

No evident critical clinical signs, strictly imputable to the induced pathology, were observed by the Veterinary Officer in any animal before CAs administration. Therefore, all the 26 animals underwent to the planned MRI treatment. Only minor clinical signs were observed by the Veterinary Officer, but they were related to the condition of the wound caused by the surgery.

All the planned *i.v.* injections and MRI acquisition sessions were successfully performed and at the end of each experimental session, the treated rat was humanely sacrificed by overdose of anesthesia.

In summary, as reported in Table A, n = 6 successful MRI experiments were performed after a single *i.v.* administration of Dotarem® and Gadovist®, both at the dose of 0.1 mmol/kg, while n = 7 rats were imaged after a single *i.v.* administration of Lead at 0.05 and 0.1 mmol/kg. Representative images before and after administration of each CA and at the respective dose are reported in Figure 5.

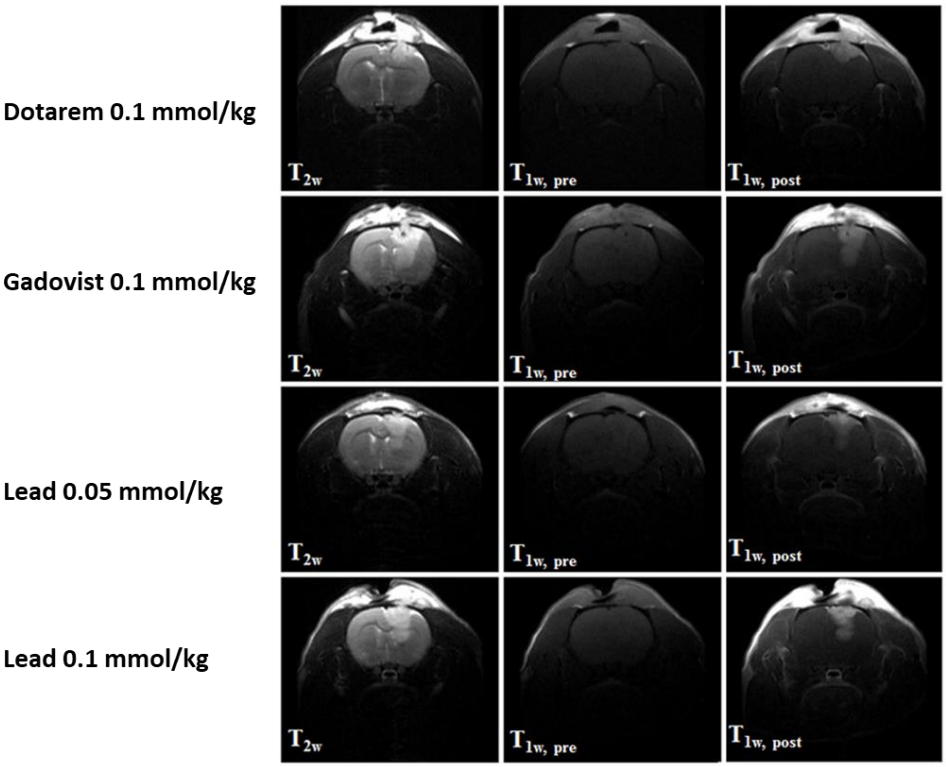

Figure 5 *Representative T_{2w} and T_{1w} images pre and post (5 minutes) contrast administration for each CA. All the T_{1w} images are reported with the same gray scale.*

As expected by the homogeneity of the tumor mass, no significant outliers were detected and the normal distribution of the experimental data was successfully verified.

MRI results are reported as a function of averaged signal enhancement (over each group) ± standard error as a function of time post injection in Figure 6.

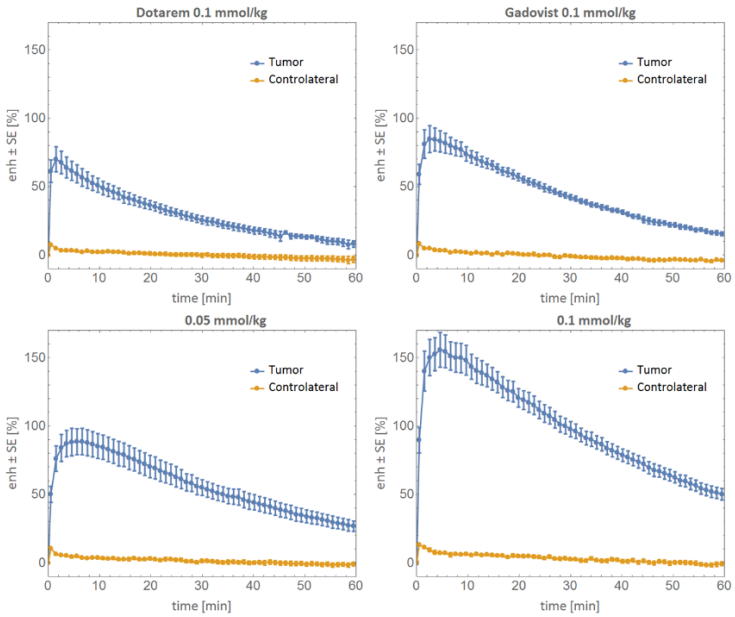

Figure 6 *Signal enhancement (averaged over groups) ± standard error as a function of time. Each panel represents a different treatment condition in terms of CA or dose (Dotarem® 0.1 mmol/kg(n=6), Gadovist® 0.1 mmol/kg(n=6), Lead 0.05(n=7) and 0.1(n=7) mmol/kg)*

For simplicity, distribution and other features of the analyzed compounds will be treated by looking separately at the two main compartments: Glioma Tumor, and Contralateral Healthy Brain.

Glioma tumor compartment:

- Groups treated with Dotarem®, Gadovist® (administrated at the dose of 0.1 mmol/kg) and Lead (at 0.05 mmol/kg) show a comparable maximum signal enhancement despite the Lead group being administrated at half the dose, with a significance level of 5%, as reported in Figure 6. The absence of statistical difference is maintained in time after administration only for Gadovist® and Lead at 0.05 mmol/kg. Dotarem® group remains compatible only with Gadovist® but not with Lead at half the dose (with a significance level of 1-5%).

- Lead maximum signal enhancement, when administrated at the same dose of Dotarem®, Gadovist®, *i.e.* 0.1 mmol/kg, is statistically different. The abovementioned feature remains true if we compare Lead maximum signal enhancement administered at 0.1 mmol/kg to itself administrated at half the dose (approx. 1.8 times higher). The statistical significance level ranges between 0.1 and 1% .

- The kinetic of Dotarem®, Gadovist® and Lead seems to be comparable. All the CAs, regardless the dosage, show a peak in enhancement at 5-6 minutes after the administration, followed by a monotonically decrease in time. As intuitively deducible from Figure 6, both Dotarem® and Gadovist® show approx. 90% decrease of the respective maximum enhancement at the end of the observation time window, *i.e.* 60 minutes, while Lead, regardless the dosage, shows lower decrease, *i.e.* approx. 70% at the same time.

Contralateral healthy compartment (i.e. healthy brain):

- Groups treated with Dotarem® and Gadovist® show a comparable maximum signal enhancement. This absence of statistical difference is maintained in time after administration with a significance level of 5%..

- Lead groups, *i.e.* treated at 0.05 and at 0.1 mmol/kg, show both a maximum signal enhancement statistically different with respect to the two control articles, with a significance level ranging between 0.1 and 5 % (see Figure 6). Furthermore, the maximum signal enhancement of Lead administrated at the standard dose, *i.e.* 0.1 mmol/kg, is not compatible to itself at half the dose with a significance level of 0.1 %.

- All the administrated CAs, *i.e.* Dotarem®, Gadovist® and Lead, regardless the administrated dose, show a kinetic characterized by a very rapid wash-in and wash-out. The signal enhancement continuously decreases up to the end of the observation time window (*i.e.* 60 minutes). Furthermore, regardless the CAs and the dosage, all the observed signal enhancements became mutually compatible already after 30 minutes from the injection up to the end of the MRI experimental session (significance level of 5%).

As it was already described in the Lead Compound efficacy studies in healthy mice, the MRI signal enhancement is not in absolute directly proportional to the gadolinium concentration, since the mathematical function describing it is much more complicated and, moreover, relaxivity plays a fundamental role. In order to keep in to account both these two main contributions, the tumor enhancement obtained in the firsts minutes (*i.e*. 5-6 minutes) after the injection for each CA and administration dose was plotted versus the respective paramagnetic longitudinal relaxation rate, *i.e.* $1/T_{1p}$, as reported in Figure 7. The paramagnetic longitudinal relaxation rate could not be estimated directly from the tumor tissue. For this reason, it was assumed to be proportional to the blood longitudinal relaxation rate, *i.e.* $1/T_{1p} = k \cdot 1/T_{1p,blood}$. The a-dimensional multiplicative constant k resumed the differences in terms of environment, *i.e.* tumor tissue *vs.* blood tissue, and of gadolinium concentration reached in the tumor tissue with respect to that reached in blood. The term $1/T_{1p,blood}$ was calculated for each administration condition simply multiplying the relaxivity value of each CA (*i.e.* Dotarem® = 3.5 ± 0.2[135] $mM^{-1}s^{-1}$, Gadovist® = 5.0 ± 0.3[7] $mM^{-1}s^{-1}$ and Lead = 10.05 ± 0.13 $mM^{-1}s^{-1}$, according to literature data and internal measurement in human plasma at 37°C and at 3 T) by the gadolinium concentration. This concentration was estimated under the assumption of a homogenous distribution of each CA in the blood compartment reached in the first minutes after injection, and simply using the following data: the administered dose (*i.e.* 0.05 and 0.1 mmol/kg), the mean rat body weight (*i.e.* 0.350 kg) and finally the total rat blood volume (*i.e.* 11 mL). On data plotted in Figure 7, a Pearson correlation test was performed under the null hypothesis that these data are linearly independent and the alternative hypothesis of linear correlation. This statistical test confirmed that the populations tested are not liner independent with a 1 % significance level (p-Value approx. equal to 0.001, Pearson Correlation coefficient $\rho = 0.99$).

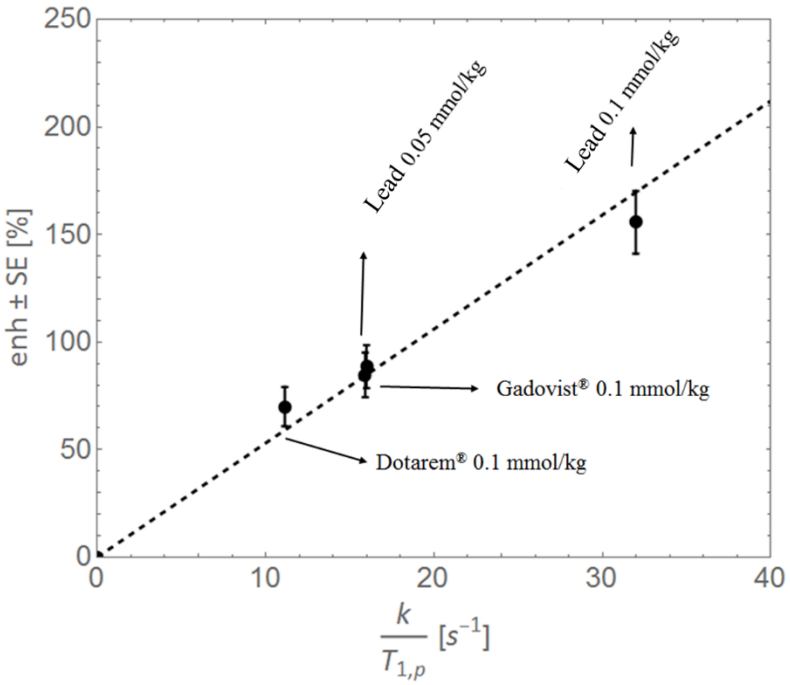

Figure 7 *Maximum glioma tumor signal enhancement measured (approx. reached 5-7 min after injection) versus the estimated paramagnetic longitudinal rate, i.e. k/T1p. Dashed line represents error weighted trend line (ρ = 0.99, significance level of 1%).*

The contrast between healthy and pathological tissue can be better evaluated by reporting data from the different groups in terms of CNR and visualize it as function of time in Figure 8. The maximum CNR for all the selected CAs, regardless the dosage, shows a maximum in the first 5-6 minutes after the injection. Specifically, the maximum CNR of Lead administrated at 0.05 and 0.1 mmol/kg is respectively approx. 1.2 and 2.1 times higher than the CNR calculated in the same condition for the two reference commercial articles. In analogy to what observed for the enhancements, the CNR monotonically decreases in time maintaining constant the statistical difference of Lead administrated at 0.1 mmol/kg with respect to the other treatment conditions.

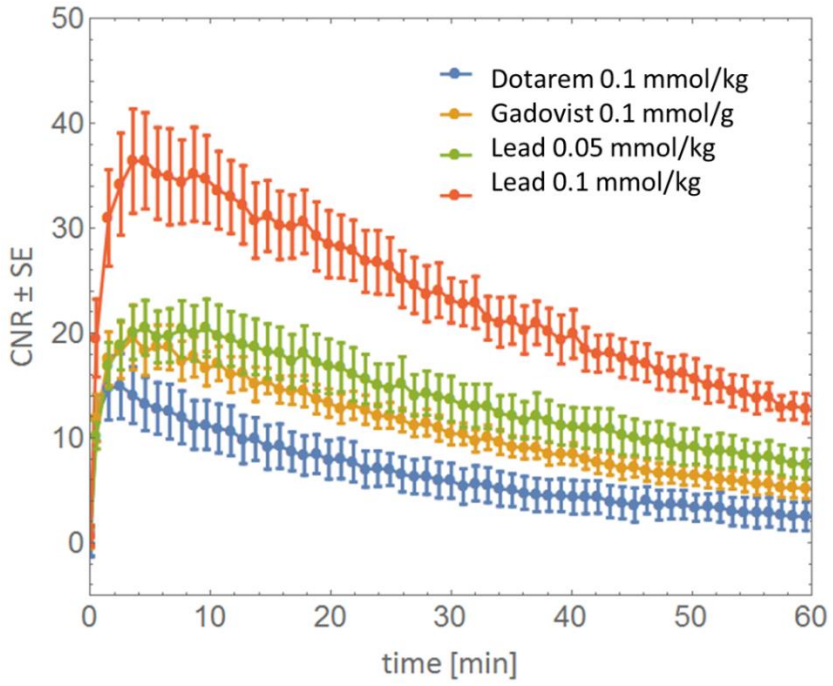

Figure 8 *CNR (averaged over groups) ± standard error as a function of time. Curves referring to a different administration condition (i.e. in terms of dose or GBCA) are plotted in different colors (blue for Dotarem® 0.1 mmol/kg$^{(n=6)}$, orange for Gadovist® 0.1 mmol/kg$^{(n=6)}$, green and red respectively for Lead 0.05$^{(n=7)}$ and 0.1$^{(n=7)}$ mmol/kg).*

Lead compound DCE-MRI Efficacy study on CH157MN Convexity Meningioma on nude mice: Comparison with Dotarem and Gadovist. Results

Animals successfully treated with a selected CA were divided in four different groups, one for each administration condition (*i.e.* dose and injected contrast agent). A summary of the performed experiments in reported in Table A.

Table A: Summary of the experiments

Group	Animal ID	Compound	Dose (mmol/kg)	Treatment
1	1 - 4 (n = 4)	Lead	0.1	Each animal of the group received a single successful *i.v.* treatment
2	5 - 8 (n = 4)	Lead	0.05	Each animal of the group received a single successful *i.v.* treatment
3	9 - 12 (n = 4)	Gadovist®	0.1	Each animal of the group received a single successful *i.v.* treatment
4	13 - 16 (n = 4)	Dotarem®	0.1	Each animal of the group received a single successful *i.v.* treatment
n.a.	17	Lead	0.05	Single *i.v.* treatment not successful
	18	n.a.	n.a.	Not treated: humanely sacrificed at the end of the inoculation surgery
	19	n.a.	n.a.	Not treated: died immediately before the planned MRI session.
	20 - 28	n.a.	n.a.	Not treated: MRI non-detectable tumor mass

MRI experiments were successfully carried out on 16 out of 28 animals. As reported in Table A, one tumor bearing mouse was not included after the planned treatment in its proper group due to a not successfully *i.v.* injection. Furthermore 11 out of 28 animals could not be treated for the following reasons:

- one mouse was humanely killed at the end of the inoculation procedure,
- one tumor bearing mouse, among those enrolled for the treatment, died under anesthesia before the planned *i.v.* treatment,
- 9 mice did not develop a MRI-detectable tumor mass within the declared time-point, *i.e.* 30 days after the tumor induction.

Only 64% of the remaining mice (*i.e.* 27 mice) developed a tumor. This event is not in accordance to the results reported in previous chapter, where the CH157MN meningioma tumor model was optimized. A reasonable explanation of this mismatch can be found in the microbiological check carried out on the CH157MN cell cultures used for the present study. The mycoplasma test confirmed a mycoplasma contamination on the cell cultures used in 4 out of 6 surgery sessions. As well reported in literature[136], the contamination of cell cultures by mycoplasma is still one of the major problem in cell culture. Mycoplasma is resistant to most antibiotics commonly employed in cell cultures and, among the myriad of different effects described in literature[136], they can

promote an alteration of cellular proliferation (*i.e.* growth, viability). This effect may have lead the unexpected lower tumor take rate (approx. 50%) observed for the mice inoculated using contaminated cellular cultures

All the mice that underwent to the planned treatment showed a well-identifiable tumor mass in MRI approx. between 14-21 days from the inoculation procedure. Furthermore, all the observed tumors were homogenous in terms of the volumetric dimensions and perfusion.

No evident critical clinical signs, strictly imputable to the induced pathology, were observed by the Veterinary Officer before CAs administration. Therefore, all the 18 animals (including also the two mice which did not undergo to a successful/complete treatment) underwent the planned MRI treatment. Only minor clinical signs were observed by the Veterinary Officer, but they were related to the suture of the wound. No additional analgesic administration was necessary.

16 *i.v.* injections and MRI acquisition sessions were successfully performed and at the end of each experimental session, the treated mouse was humanely sacrificed by overdose of anesthesia.

In summary, as reported in Table A, n= 4 successful MRI experiments were performed after a single *i.v.* injection of each selected CA at dose of 0.05 (only for Lead) and 0.1 mmol/kg (for Gadovist®, Dotarem® and Lead).

Representative images before and after administration of each CA and at the respective dose are reported in Figure 9.

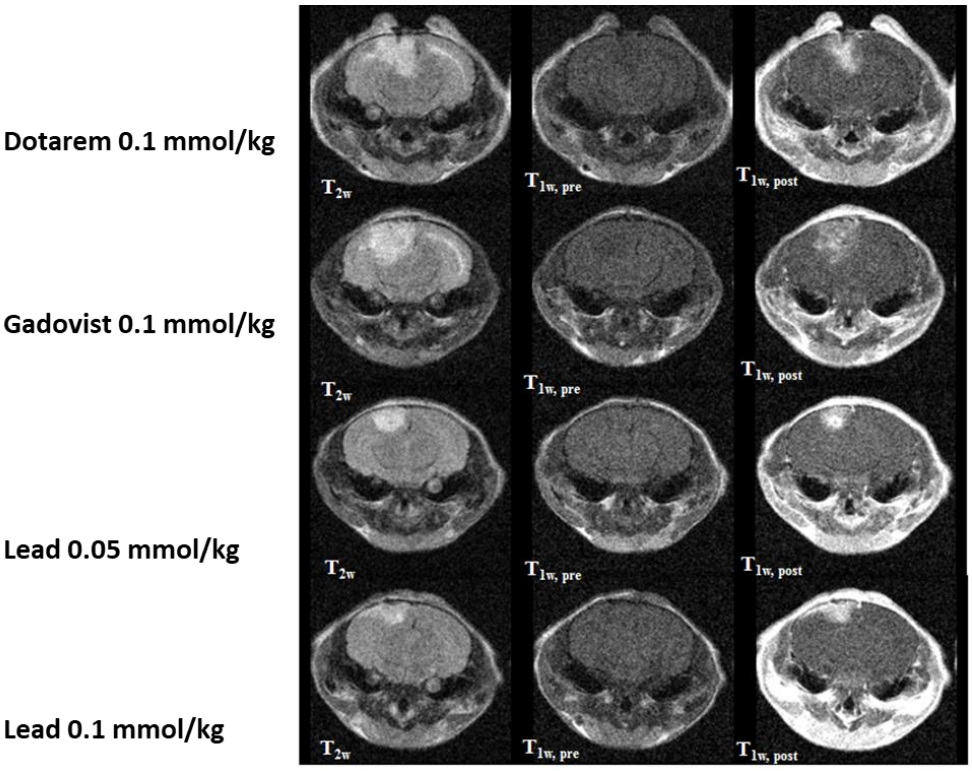

Figure 9 *Representative $T_{2weighted}$ and $T_{1weighted}$ images pre and post (5 minutes) contrast administration for each CA. All the T1w images are reported with the same gray scale.*

MRI results are reported as a function of averaged signal enhancement (over each group) ± standard error as a function of time post injection in Figure 10. As general note, the homogeneity of experimental data was very good, as it can be appreciated by the small standard errors, indicating that the adopted\optimized MRI experimental setup was robust and reliable and the tumor mass was homogeneous. In Figure 16 each panel represents a different anatomical region (*i.e.* meningioma tumor and healthy controlateral brain tissue), while each curve referring to different treatment condition (*i.e.* CA and/or dose) is plotted in different colors (blue for Dotarem® 0.1 mmol/kg, orange for Gadovist® 0.1 mmol/kg, green for Lead 0.05 mmol/kg, red for Lead 0.1 mmol/kg).

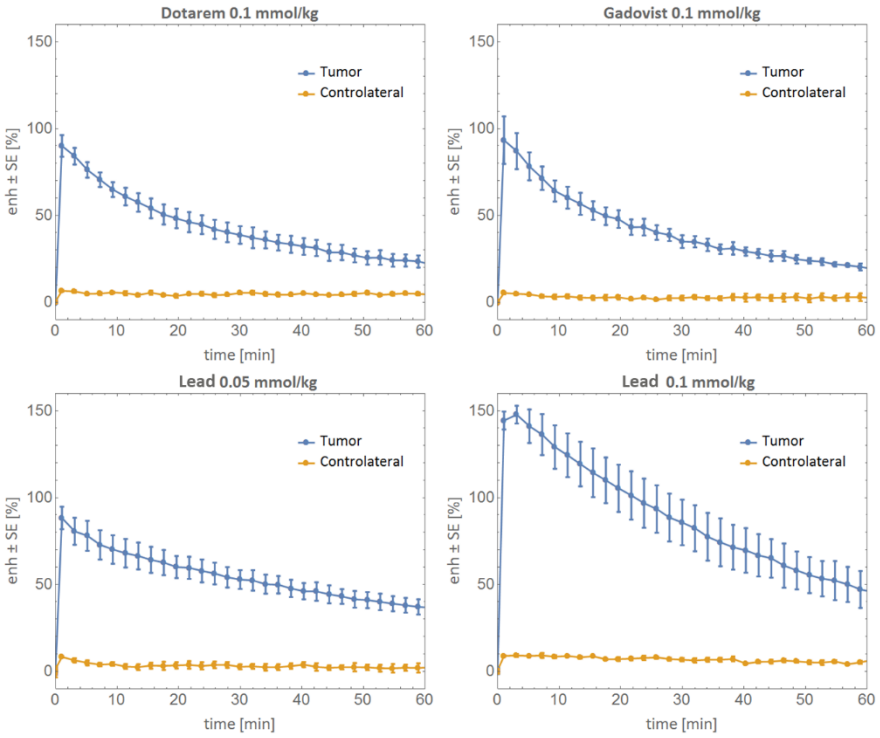

Figure 10 *Signal enhancement (averaged over groups) ± standard error as a function of time. Each panel represents a different treatment condition in terms of CA or dose (Dotarem® 0.1 mmol/kg$^{(n=4)}$, Gadovist® 0.1 mmol/kg$^{(n=4)}$, Lead 0.05$^{(n=4)}$ and 0.1$^{(n=4)}$ mmol/kg) with the same scale, while curves referring to different anatomical regions are plotted in different colors (blue for meningioma tumor and orange for healthy contralateral brain).*

As for the previous study, for simplicity results are going to be discussed by looking and the Tumor Compartment and the Contralateral Healthy Brain separately.

Meningioma tumor compartment:

- Groups treated with Dotarem®, Gadovist® (both administered at the dose of 0.1 mmol/kg) and Lead (at 0.05 mmol/kg) show a comparable maximum signal enhancement despite the Lead group administered at half the dose with a significance level of 5. Furthermore, this absence of statistical difference is maintained in time with the same significance.
- The maximum signal enhancement of Lead administrated at the same dose of Dotarem®, Gadovist®, *i.e.* 0.1 mmol/kg, is statistically different if compared to itself administrated at half the dose (approx. 1.7 times

higher) and to the two reference articles (*i.e.* Dotarem® and Gadovist®) at the same does (approx. 1.6 times higher), with a statistical significance level of 0.1 %.

- The kinetic of Dotarem®, Gadovist® and Lead seems to be comparable. All the CAs, regardless of the dosage, show a peak in enhancement at 1-3 minutes after the administration, followed by a monotonically decrease in time. As intuitively deducible from Figure 16, Dotarem®, Gadovist® both show approx. 80% decrease of the respective maximum enhancement at the end of the observation time window, *i.e.* 60 minutes, while Lead, regardless the dosage, shows a lower decrease, *i.e.* approx. 65% at the same time.

Contralateral healthy compartment (i.e. healthy brain):

- Groups treated with Dotarem®, Gadovist® (both administration at the dose of 0.1 mmol/kg) and Lead (at 0.05 mmol/kg) show a comparable maximum signal enhancement. This absence of statistical difference is maintained in time after administration, with a significance level of 5%.

- Lead group treated at 0.1 mmol/kg shows a maximum signal enhancement statistically different with respect to the two control articles, with a significance level ranging between 0.1 and 1 % and statistically compatible to itself at half the dose with a significance level of 5 %.

- All the administrated CAs, regardless of the administrated dose, show a kinetic characterized by a very rapid wash-in and wash-out. The signal enhancement continuously decreases up to the end of the observation time window (*i.e.* 60 minutes). Furthermore, regardless the CAs and the dosage, all the observed signal enhancements became mutually compatible already after 30 minutes from the injection up to the end of the MRI experimental session significance level of 5%.

As for the previous studies, to take into account the role of relaxivity and the gadolinium concentration into the determination of the MRI signal enhancement, the signal enhancement acquired in the first minutes after the administration dose was plotted versus the respective paramagnetic longitudinal relaxation rate, *i.e.* $1/T_{1p}$, as reported in Figure 11.

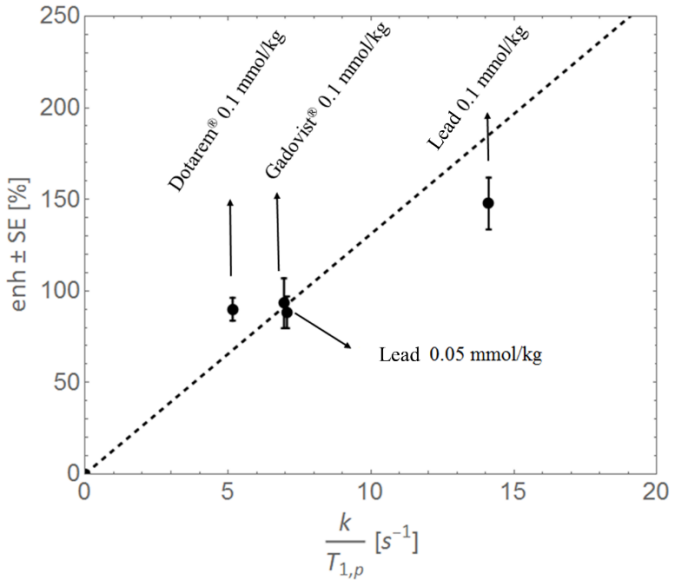

Figure 11 *Maximum meningioma tumor signal enhancement measured (approx. reached 1-3 min after injection) versus the estimated paramagnetic longitudinal rate, i.e. k/T1p. Dashed line represents error weighted trend line (ρ = 0.96, significance level of 1%)*

$1/T_{1p}$, as already stated before, could not be estimated directly from the tumor tissue. For this reason, it was assumed to be proportional to the blood longitudinal relaxation rate, *i.e.* $1/T_{1p} = k \cdot 1/T_{1p,blood}$. The a-dimensional multiplicative constant *k* resumed the differences in terms of environment, *i.e.* tumor tissue *vs.* blood tissue, and of gadolinium concentration reached in the tumor tissue with respect to that reached in blood. The term $1/T_{1p,blood}$ was calculated for each administration condition simply multiplying the relaxivity value of each CA CA (*i.e.* Dotarem® = 4.05 ± 0.06 $mM^{-1}s^{-1}$, Gadovist® = 5.46 ± 0.06 $mM^{-1}s^{-1}$ and Lead = 11.08 ± 0.33 $mM^{-1}s^{-1}$, according to measurement in human plasma at 37°C and at 1 T or close) by the gadolinium concentration. This concentration was estimated under the assumption of a homogenous distribution of each CA in the blood compartment reached in the first minutes after injection, and simply using the following data: the administered dose (*i.e.* 0.05 and 0.1 mmol/kg), the mean mouse body weight (*i.e.* 0.020 kg) and finally the total mouse blood volume (*i.e.* 1.57 mL). On data plotted in Figure 11, a Pearson correlation test was performed under the null hypothesis that these data are linearly independent and the alternative hypothesis of linear correlation. This statistical test confirmed that the populations tested are not liner independent with a 1 % significance level (p-Value approx. equal to 0.0098, Pearson Correlation coefficient ρ = 0.96).

To better evaluate the contrast between healthy and pathological tissue, data from the different groups are also reported in terms of CNR (and visualized as function of time in Figure 12. The maximum CNR for all the selected CAs, regardless the dosage, show a maximum in the first 1-3 minutes after the injection. Specifically the maximum CNR of Lead administrated at 0.05 and 0.1 mmol/kg is respectively approx. 1.0 and 1.7 times higher than the CNR calculated in the same condition for the two reference commercial articles. The CNR monotonically decreases in time,

maintaining constant the statistical difference of Lead administrated at 0.1 mmol/kg with respect to the other treatment conditions up to 30 minutes after the *i.v.* injection.

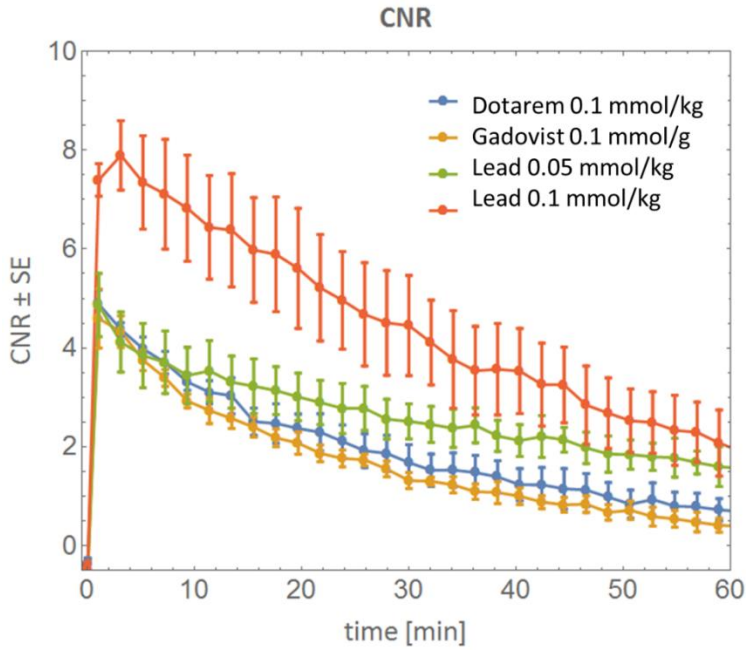

Figure 12 *CNR (averaged over groups) ± standard error as a function of time. Curves referring to a different administration condition (*i.e. *in terms of dose or GBCA) are plotted in different colors (blue for Dotarem® 0.1 mmol/kg$^{(n=4)}$, orange for Gadovist® 0.1 mmol/kg$^{(n=4)}$, green and red respectively for Lead 0.05$^{(n=5)}$ and 0.1$^{(n=4)}$ mmol/kg).*

Lead compound DCE-MRI Efficacy study on a photoinduced rat cerebral ischemia model: Comparison with Dotarem and Gadovist. Results

Animals were divided in four different groups, one for each administration condition (*i.e.* dose and injected contrast agent). A summary of the performed experiments is reported in Table A.

Table A: Summary of the experiments

Group	Animal ID	Compound	Dose (mmol Gd/kg)	Treatment
1	8, 9, 16, 20, 23, 24 (n = 6)	Lead	0.1	Each animal of the group received a single successful *i.v.* treatment
2	5, 12, 15, 19, 22, 26 (n = 6)	Lead	0.05	Each animal of the group received a single successful *i.v.* treatment
3	6, 11, 17, 25, 28 (n = 5)	Gadovist®	0.1	Each animal of the group received a single successful *i.v.* treatment
4	2, 10, 13, 18, 27 (n = 5)	Dotarem®	0.1	Each animal of the group received a single successful *i.v.* treatment

MRI experiments were successfully carried out on 22 out of 28 animals. Only one animal died during the ischemic induction procedure while other two animals were humanely sacrificed one day after the ischemic induction. The remaining three animals were discarded from data analysis because of an unsuccessful single *i.v.* administration. All the survived/not humanely sacrificed animals, *i.e.* 25 out of 28, showed a well-identifiable ischemic lesion in MRI between 11-13 days after the ischemic induction. Furthermore observed ischemic lesions were considered sufficiently homogenous in terms of volumetric dimensions and perfusion and also in good agreement with the results reported in the optimization study.

No critical clinical signs strictly imputable to the induced ischemic lesion were observed by the Veterinary Officer in any animal before CAs administration, therefore all the 25 animals underwent to the planned MRI treatment. Among the observed clinical signs, no neurological deficits or clinical signs closely linked to the induced pathology were observed, only cases of tail phlebitis were noted. However, the majority of the observed tail phlebitis were judged by the Veterinary Officer not serious enough to be incompatible with the animal care policy. Only two rats were humanely sacrificed for a serious tail phlebitis.

All the animals eligible for the planned *i.v.* injections and MRI acquisition sessions (*i.e.* 25 out of 28 rats) were humanely sacrificed by overdose of anesthesia at the end of each experimental session.

In summary, as reported in Table A, n = 5 successful MRI experiments were performed after a single *i.v.* administration of Dotarem® and Gadovist®, both at the dose of 0.1 mmol Gd/kg, while n = 6 rats were imaged after a single *i.v.* administration of Lead at 0.05 and 0.1 mmol Gd/kg. Representative images before and after administration of each CA and at the respective dose are reported in Figure 13.

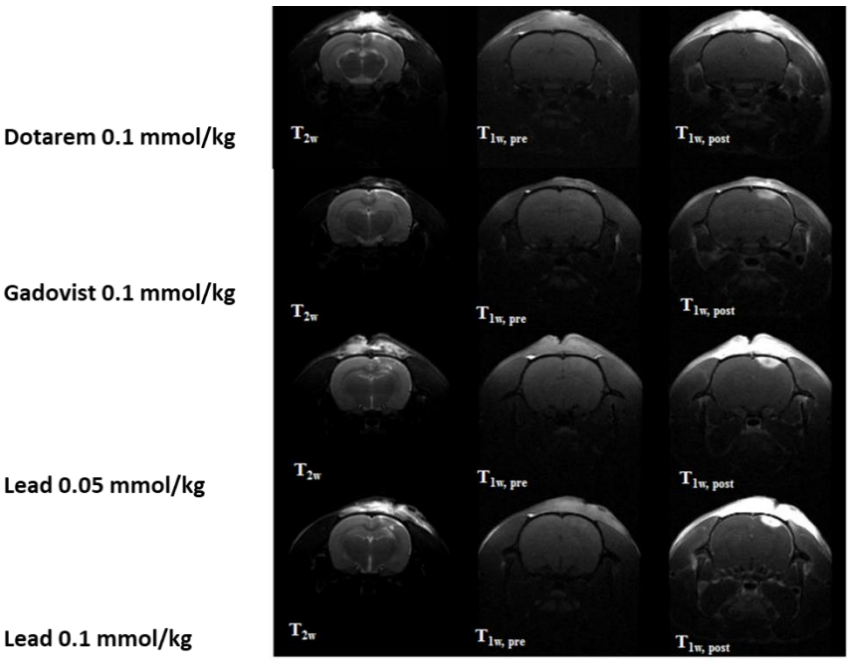

Figure 13 *Representative $T_{2weighted}$ and $T_{1weighted}$ images pre and post (5 minutes) contrast administration for each CA. All the T1w images are reported with the same gray scale.*

MRI results are reported as a function of averaged signal enhancement (over each group) ± standard error as a function of time post injection in Figure 14.

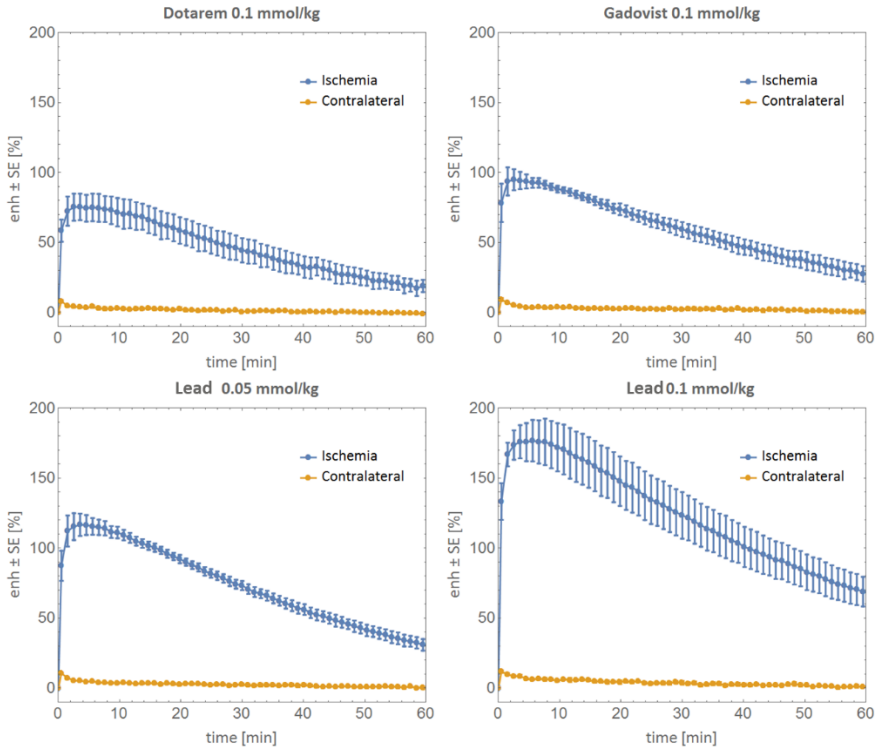

Figure 14 *Signal enhancement (averaged over groups) ± standard error as a function of time. Each panel represents a different treatment condition in terms of CA or dose (Dotarem® 0.1 mmol Gd/kg$^{(n=5)}$, Gadovist® 0.1 mmol Gd/kg$^{(n=5)}$, Lead 0.05$^{(n=6)}$ and 0.1$^{(n=6)}$ mmol Gd/kg) with the same scale, while curves referring to different anatomical regions are plotted in different colors (blue for ischemia and orange for healthy contralateral brain).*

In Figure 14 each panel represents a different treatment condition in terms of CA and/or administered dose plotted with the same scale, while the curves referring to the two different anatomical regions are plotted in different colors (blue for ischemic lesion and orange for healthy contralateral brain tissue).

CAs features are going to be extracted by looking at the two anatomical regions: Ischemic lesion compartment and contralateral healthy brain.

Ischemic lesion compartment:

- Group treated with Gadovist® (administered at the dose of 0.1 mmol Gd/kg) and Lead (at 0.05 mmol Gd/kg) show a comparable maximum signal enhancement despite the Lead group being administered at half the dose, with a significance level of 5%. This absence of statistical difference is also maintained in time after administration. Quite analogous considerations can be extended to the group treated with Dotarem®: actually, only the maximum enhancement turns out to be not compatible with respect to Lead at half the dose (with a significance level of 5%).

- Lead maximum signal enhancement, when administrated at the same dose of Dotarem®, Gadovist®, *i.e.* 0.1 mmol/kg, is statistically different if compared to itself administrated at half the dose (approx. 1.5 times higher) and to the two reference articles (*i.e.* Dotarem® and Gadovist®) at the same doses (approx. 2 times higher). The statistical significance is of 0.1 %.

- The kinetic of Dotarem®, Gadovist® and Lead seems to be comparable. All the CAs, regardless of the dosage, show a peak in enhancement at 5-6 minutes after the administration, followed by a decrease in time. As intuitively deducible from Figure 20 Dotarem®, Gadovist® and Lead at 0.05 mmol Gd/kg show approx. 75% decrease of the respective maximum enhancement at the end of the observation time window, *i.e.* 60 minutes, while Lead administered at the full standard dose, *i.e.* 0.1 mmol Gd/kg, shows a slightly lower decrease, *i.e.* approx. 64% at the same time.

Contralateral healthy compartment:

- Groups treated with Dotarem® and Gadovist® (both administration at the dose of 0.1 mmol Gd/kg) show a comparable maximum signal enhancement. This absence of statistical difference is maintained in time after administration with a significance level of 5%.

- Lead group treated at 0.1 mmol Gd/kg, shows a maximum signal enhancement statistically comparable with respect to itself at the half of the dose, *i.e.* 0.05 mmol Gd/kg, and to the two control articles with a significance level of 5 %.

- All the administrated CAs, *i.e.* Dotarem®, Gadovist® and Lead, regardless of the administrated dose, show a kinetic characterized by a very rapid wash-in and wash-out. The signal enhancement continuously decreases up to the

end of the observation time window (*i.e.* 60 minutes). Furthermore, all the observed signal enhancements became mutually compatible already after 30 minutes from the injection up to the end of the MRI experimental session (significance level of 5%).

The term $1/T_{1p,blood}$ was calculated for each administration condition simply multiplying the relaxivity value of each CA (*i.e.* Dotarem® = 3.5 ± 0.2 $mM^{-1}s^{-1}$, Gadovist® = 5.0 ± 0.3 $mM^{-1}s^{-1}$ and Lead = 10.05 ± 0.13 $mM^{-1}s^{-1}$, according to literature data and internal measurement in human plasma at 37°C and at 3 T) by the gadolinium concentration. The concentration was estimated under the assumption of a homogenous distribution of each CA in the blood compartment reached in the first minutes after injection, and simply using the following data: the administered dose (*i.e.* 0.05 and 0.1 mmol Gd/kg), the mean rat body weight (*i.e.* 0.350 kg) and finally the total rat blood volume (*i.e.* 22 mL). On data plotted in Figure 15, a Pearson correlation test was performed under the null hypothesis that these data are linearly independent and the alternative hypothesis was set of linear correlation. Pearson correlation test confirmed that the populations tested are not linearly independent, with a 1 % significance level (p-Value approx. equal to 0.003, Pearson Correlation coefficient ρ = 0.98).

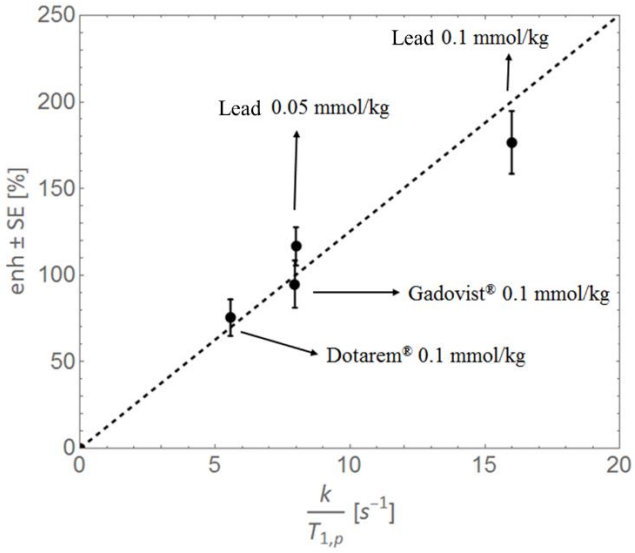

Figure 15 *Maximum ischemic lesion signal enhancement measured (approx. reached 4-6 min after injection) versus the estimated paramagnetic longitudinal rate, i.e. k/T1p. Dashed line represents error weighted trend line (ρ = 0.98, significance level of 1%).*

Data from different groups was also reported in terms of Contrast to Noise Ratio (CNR) and then visualized as a function of time. As it is possible to see from Figure 16, the CNR for all the selected CAs, regardless the dosage, shows a maximum in the first 5-6 minutes after the injection. Lead maximum CNR, administrated at 0.05 and 0.1 mmol/kg is respectively approx. 1.5 and 2.3 times higher than the CNR calculated in the same condition for the two reference commercial articles. Moreover, in analogy to what observed for the enhancements, the CNR monotonically decreases in time maintaining constant the statistical difference of Lead administrated at 0.1 mmol/kg with respect to the other treatment conditions.

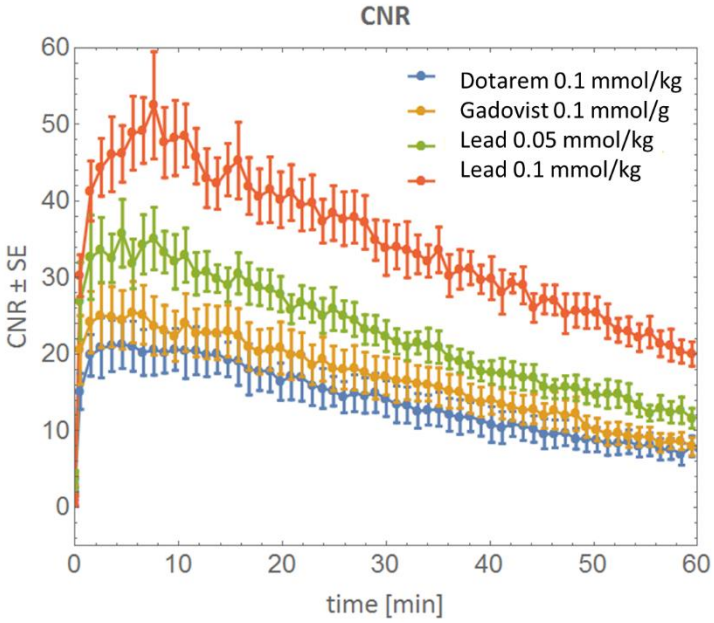

Figure 16 *CNR (averaged over groups) ± standard error as a function of time. Curves referring to a different administration condition (i.e. in terms of dose or GBCA) are plotted in different colors (blue for Dotarem® 0.1 mmol/kg(n=5), orange for Gadovist® 0.1 mmol/kg(n=5), green and red respectively for Lead 0.05(n=6) and 0.1(n=6) mmol/kg).*

Lead compound DCE-MRI Efficacy study on 4T1 breast tumor in mice: Comparison with Dotarem and Gadovist. Results

All animals underwent cells inoculation to induce the development of 4T1 breast tumor and developed a suitable tumor mass within 5-8 days as expected on the basis of the preliminary study. Animals were divided in 4 experimental groups, according to administered contrast agent and dose, as summarized in Table A. Since no critical clinical signs were observed by the Veterinary Officer in any animal before CAs administration, all animals were enrolled for the MRI session. MRI experiments were successfully carried out on 28 out of 28 animals (*i.e.* 7 animals for each experimental group). At the time of contrast enhanced MRI, two animals showed a tumor mass slightly beyond the set range of 20-60 mm^3 (*i.e.* dr01 with a mass of 62 mm^3 and da02 with a mass of 75 mm^3). Since the difference in volume was small and the average tumor volume was comparable among the groups, both animals were included, with the remaining 26, in the analysis. All animals were sacrificed at the end of the study, with no need of humanitarian sacrifice.

Table A: Summary of experiment. The symbol * indicates a tumor volume out of the range declared in methods (*i.e.* 20-60 mm^3), specifically, dr01 reached a volume of 62 mm^3 and da02 of 75 mm^3.

Group	Animal ID	Compound	Dose (mmol Gd/kg)	Tumor volume (mean ± SE) mm^3	Contrast Enhanced MRI
1	r01, n01, dr02, n02, a03, r03, dl04	Dotarem	0.1	37.4 ± 3.3	5-8 days after induction (tumor volume ranging between 21-75 mm^3)
2	a01, dr01*,da01, r02, l03, r04, dr04	Gadovist	0.1	37.7 ± 5.5	
3	l01, dl02, da02*, da03,dr03, da04, l04	Lead	0.05	36.6 ± 6.7	
4	l01, l02, a02, n03, dl03, n04, a04	Lead	0.1	37.6 ± 3.8	

Representative images before and after administration of each CA and at the respective dose are reported in Figure 17.

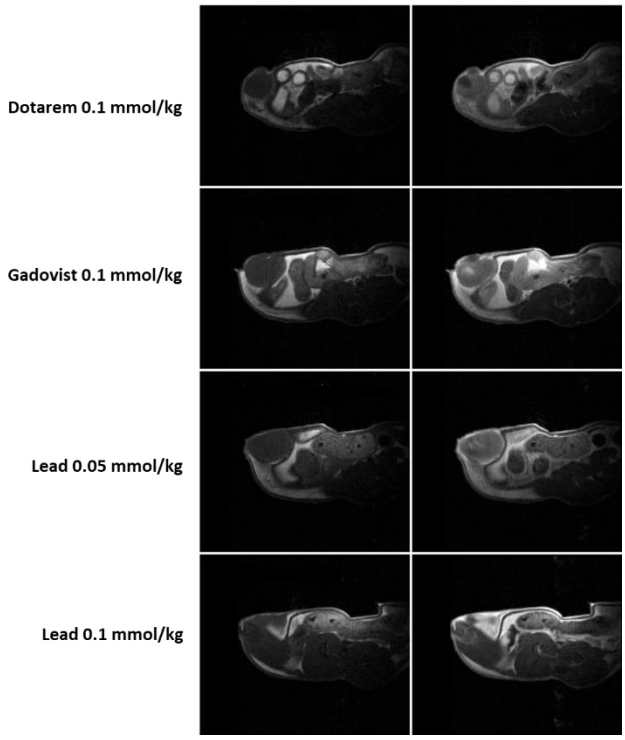

Figure 17 *Representative $T_{1weighted}$ images pre and post contrast administration for each CA.*

As expected by the homogeneity of the tumors, no significant outliers were detected and the normal distribution of the experimental data was successfully verified.

MRI results are reported as a function of averaged signal enhancement (over each group) ± standard error as a function of time post injection in Figure 18. Each panel represents a different treatment condition in terms of CA and/or administered dose, while the curves referring to the two different anatomical regions are plotted in different colors (blue for tumor and orange for muscle). Muscle was selected as the control region instead of the mammary fat pad. The reason beyond that is given by the fact that the mammary fat pad is already characterized by hyper-intensity in pre contrast images. Moreover, is the host of the tumor, and an inflammatory process could be present and create false results. In the case of n=1 animal for Dotarem® and n=2 animals for Lead at both doses, the paw was not observable in the MR images acquired and thus the ROI over the muscle was not selected.

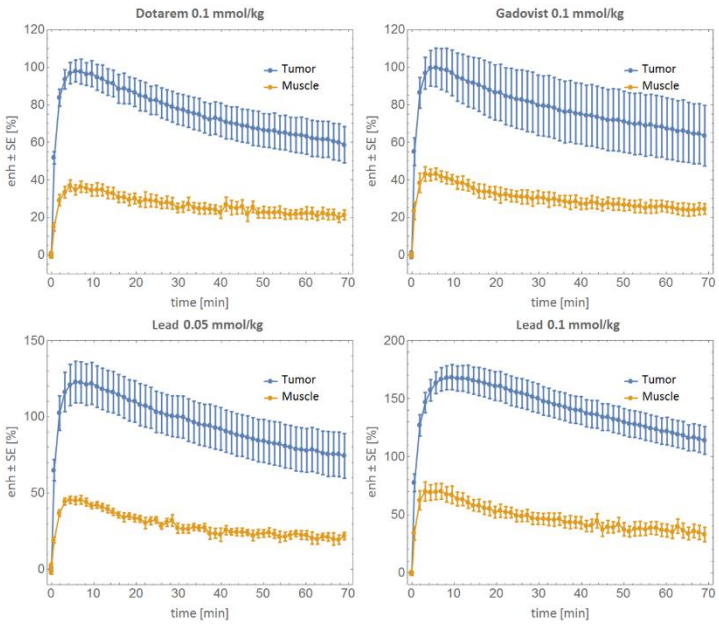

Figure 18 *Signal enhancement (averaged over groups) ± standard error as a function of time. Each panel represents a different treatment condition in terms of CA or dose (Dotarem® 0.1 mmol Gd/kg (n=7 for tumor, n=6 for muscle), Gadovist® 0.1 mmol Gd/kg (n=7 for tumor, n=7 for muscle), Lead 0.05 mmol Gd/kg (n=7 for tumor, n=5 for muscle and 0.1 mmol Gd/kg (n=7 for tumor, n=5 for muscle), while curves referring to different anatomical regions are plotted in different colors (blue for tumor and orange for muscle).*

CAs behavior was extracted by looking at the two different compartments: Tumor mass and Muscle.

Tumor mass:

- Group treated with Dotarem® and Gadovist® (administered at the dose of 0.1 mmol Gd/kg) and Lead (at 0.05 mmol Gd/kg) show a comparable maximum signal enhancement despite the Lead group being administered at half the dose. This absence of statistical difference is also maintained in time after administration.

- The maximum signal enhancement of Lead administrated at the same dose of Dotarem®, Gadovist®, *i.e.* 0.1 mmol/kg, is statistically different if compared to itself administrated at half the dose (approx. 1.4 times higher) and to the two reference articles (*i.e.* Dotarem® and Gadovist®) at the same does (approx. 1.65 times higher), with a statistical significance level of 5% (Lead at half dose), 1 % (Gadovist®), 0.1% (Dotarem®). This statistical difference is maintained in time after administration with respect to Dotarem® and Gadovist® (pValue ≤0.01 at 30 minutes, pValue≤0.05 at 60 minutes).

- All the CAs show a comparable kinetic. Moreover, regardless of the dosage, all the CAs show a peak in enhancement at 5-6 minutes after the administration, followed by a monotonically decrease in time. As intuitively deducible from Figure 24, Dotarem®, Gadovist® and Lead at 0.05 mmol Gd/kg show approx. 40% decrease of the respective maximum enhancement at the end of the observation time window, *i.e.* 60 minutes, while Lead administered at the full standard dose, *i.e.* 0.1 mmol Gd/kg, shows a slightly lower decrease, *i.e.* approx. 30% at the same time.

Muscle:

- Group treated with Dotarem® and Gadovist® (administered at the dose of 0.1 mmol Gd/kg) and Lead (at 0.05 mmol Gd/kg) show a comparable maximum signal enhancement. This absence of statistical difference is also maintained in time.

- When Lead is administrated at the same dose of Dotarem®, Gadovist®, *i.e.* 0.1 mmol/kg, it shows a maximum signal enhancement which is statistically different if compared to itself administrated at half the dose (approx. 1.5 times higher) and to the two reference articles (*i.e.* Dotarem® and Gadovist®) at the same does (approx. 1.8 and 1.5 times higher, respectively). The statistical significance level is of 1% (Lead at half dose and Gadovist®), and of 0.1% (Dotarem®). This statistical difference is maintained in time up to 30 minutes (1% of significance for Dotarem® and Lead, 5% for Gadovist®).

- All the administrated CAs, show a kinetic characterized by a very rapid wash-in and wash-out, regardless of the administrated dose. The signal enhancement continuously decreases up to the end of the observation time window (*i.e.* 60 minutes). Furthermore, all the observed signal enhancements showed approx. 50% decrease of the respective maximum at the end of the observation time window, *i.e.* 60 minutes.

The paramagnetic longitudinal relaxation rate, *i.e.* $1/T_{1p}$, was expressed in function of the signal enhancement and is reported in Figure 25. $1/T_{1p}$, could not be estimated directly from the tumor lesion (or generally a tissue); for this reason it was assumed to be proportional to the blood longitudinal relaxation rate, *i.e.* $1/T_{1p} = k \cdot 1/T_{1p,blood}$. The a-dimensional multiplicative constant *k* resumed the differences in terms of environment, *i.e.* tissue *vs.* blood, and of gadolinium concentration reached in the tissue

with respect to that reached in blood. The term $1/T_{1p,blood}$ was calculated for each administration condition simply multiplying the relaxivity value of each CA (*i.e.* Dotarem® = 3.5 ± 0.2 $mM^{-1}s^{-1}$, Gadovist® = 5.0 ± 0.3 $mM^{-1}s^{-1}$ and Lead = 10.05 ± 0.13 $mM^{-1}s^{-1}$, according to literature data and internal measurement in human plasma at 37°C and at 3 T) by the gadolinium concentration. This concentration was estimated under the assumption of a homogenous distribution of each CA in the blood compartment reached in the first minutes after injection, and simply using the following data: the administered dose (*i.e.* 0.05 and 0.1 mmol Gd/kg), the mean mouse body weight (*i.e.* 0.020 kg) and finally the total mouse blood volume (*i.e.* 1.57 mL). On data plotted in Figure 19, a Pearson correlation test was performed under the null hypothesis that these data are linearly independent and the alternative hypothesis of linear correlation. This statistical test confirmed that the populations tested are not linearly independent with a 1 % significance level (p-Value approx. equal to 0.01, Pearson Correlation coefficient ρ = 0.95 for tumor and p-Value approx. equal to 0.007, Pearson Correlation coefficient ρ = 0.97 for muscle).

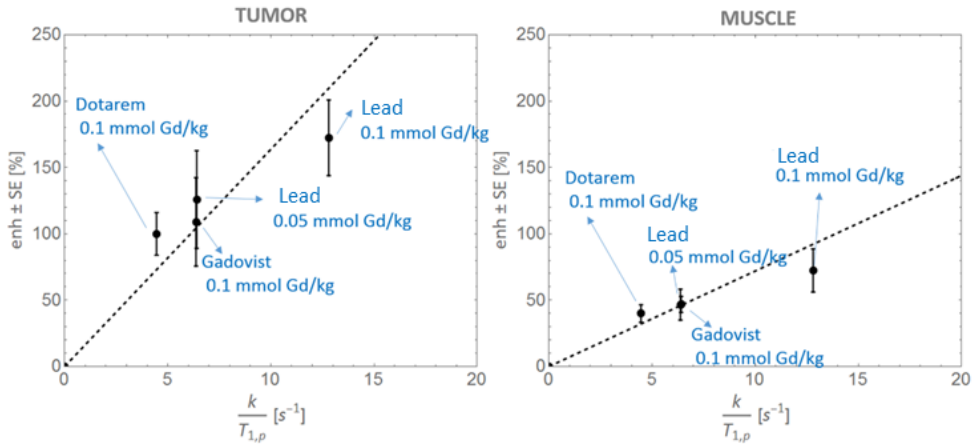

Figure 19 *Maximum tumor and muscle signal enhancement measured (approx. reached 4-6 min after injection) versus the estimated paramagnetic longitudinal rate,* i.e. k/T_{1p}. *Dashed line represents error weighted trend line.*

Conclusions

A MRI Biodistribution study was properly performed on 29 healthy mice before the pathological studies. This study confirmed that the observed MRI enhancement strongly correlates (*i.e.* Pearson correlation coefficient ρ > 0.9) with both gadolinium administration dose and relaxivity values for all the selected CAs. As consequence of the low molecular weight and the absence of an albumin binding affinity of the Lead, the renal elimination is still the primary way and the hepatic route plays a not significant role. Same goes for the reference articles, *i.e.* Dotarem® and Gadovist®.

Since the MRI biodistribution study on healthy mice showed positive results, the efficacy studies of Lead compound were performed on the pathological models previously optimized and validated in pilot studies mentioned before.

C6 glioma tumor was induced on 26 out of 28 Wister rats. All tumor bearing rats underwent a successful MRI session after one single *i.v.*

injection of CA. CH157MN meningioma tumor was successfully induced on 18 out of 28 Athymic nude mice. Among the tumor bearing mice, 16 underwent to a successful MRI session after one single *i.v.* injection of CA. Cerebral ischemia was successfully photochemically induced on 25 out of 28 Sprague Dawley rats. 22 rats underwent successful MRI session after one single *i.v.* injection of CA according to the treatment plan. 4T1 breast tumor was successfully induced on 28 out of 28 BALB/c mice. All animals underwent a successful MRI session after one single *i.v.* injection of CA according to the treatment plan.

As a general result, all the studies confirmed that the observed MRI enhancement in the pathological tissue (Tumor, Ischemia) strongly correlates (*i.e.* Pearson correlation coefficient > 0.9) with both gadolinium administered dose and relaxivity values, for all the selected CAs. In line with the superior relaxivity of the Lead compound, it has been demonstrated that Lead has the same efficacy with respect to the reference article with the highest relaxivity, *i.e.* Gadovist®, when injected at half the dose of 0.05 mmol/kg and an efficacy approx. two times higher when injected at the same dose, *i.e.* 0.1 mmol/kg.

Finally, since Lead efficacy at 0.05 mmol/kg is comparable to the efficacy of commercial CAs administrated at the standard clinical dose (*i.e.* 0.1 mmol/kg), this study demonstrated that gadolinium dosage could be effectively reduced in clinic, without harming the diagnostic efficiency or follow up in different pathologies. Moreover, this new CA could lead the way into a reduction of the standard clinical dose of gadolinium, and therefore decreasing the chance of a retention of this metal ion into tissues.

5. Discussion and Future Perspectives

In this thesis, two novel gadolinium based contrast agents were tested and characterized *in vitro* and *in vivo*. In particular, $(Gd\text{-}DTPA)_2$-Chol, a linear, dimeric, albumin binder GBCA was fully characterized *in vitro* in terms of relaxometric properties and then its bio-distribution was evaluated on healthy animals and a pathological model of ischemia. In addition, Lead, a dimeric macrocyclic GBCA, selected as possible candidate for clinical translation, was tested for its pharmacokinetics and its efficacy on a series of pathological models, properly selected: glioma, meningioma, cerebral ischemia and breast cancer.
Before starting the preclinical development, all the pathological models were selected to guarantee a suitable preclinical development and to reduce the attrition rate[137]. Moreover, the induction procedure was optimized to obtain a feasible and reproducible protocol, associated to a reduced pain and stress of the animal, in accordance to the 3Rs guidelines.[138] Every pathological model discussed in the thesis was correctly induced, characterized and refined. By looking at the animal welfare, animal models were correctly optimized in order to reduce severe suffering and, when a setup caused less clinical signs, it was preferred over others (*i.e.,* Convexity over Skull Base Meningioma). In all cases, MRI was used as a non-invasive method in order to help identify a specific time window of treatment and to assess tissue permeability. Additionally, histology was used to validate the diseased tissue that was observed in MRI, confirm it, and stage it according to WHO guidelines. The establishment of different pathological models and their setup and optimization is of vital importance in the preclinical development of new imaging probes. Often, there is a lack of a consensus animal model in preclinical research: pathology induction procedures are not fully reported in literature, animal welfare is usually left aside, and unfortunately, experiments are not entirely reproducible. This thesis aim is also an attempt to give researchers a know-how on inductions of pathologies in rodents, not only for the development of new MRI probes, but for different applications in the preclinical research.

$(Gd\text{-}DTPA)_2$-Chol presented a series of interesting features, such as good affinity for albumin, high number of binding sites, properties of carrying two Gd ions per molecule, and limited hepatobiliary elimination. These properties contributed to an unexpected long blood elimination half-life, resulting into an optimal confinement in the vascular space and thus into an extension of the available time window for MR angiography. $(Gd\text{-}DTPA)_2$-Chol presents similar relaxivity to other contrast agents previously

reported in literature, such as MS-325 and B22956/1 [104,113]. However it displayed a longer blood elimination half-life (7 times longer than that of B22956/1 in rats): this characteristic may be opening new insights into the time availability window needed for angiography. Further studies should be performed in rats with a MRI coronary angiography protocol.
Moreover, $(Gd\text{-}DTPA)_2$-Chol slow accumulation into fibrotic tissue observed after its administration into the pathological model of cerebral ischemia, and its high enhancement despite the low dose injected are valuable features that could be exploited for different applications into cerebral pathology staging and follow-up.

Lead compound does not have an affinity to Albumin, thus has a renal elimination. Like $(Gd\text{-}DTPA)_2$-Chol, it carries two Gd ions per molecule, and thus has an improved relaxivity. Moreover, being Lead a macrocycle, it also has an improved stability *in vitro* and *in vivo*, and thus less chance to be retained into tissues. Preclinical studies demonstrated that Lead has the same efficacy of commercial compounds, *i.e.* Gadovist® and Dotarem®, when injected at the half dose 0.05 mmol Gd/kg and an efficacy approximately two times higher when injected at the same dose, *i.e.* 0.1 mmol Gd/kg, which is the clinical dose currently used for GBCAs. In essence, Lead preclinical trials demonstrated that gadolinium dosage could be effectively reduced in clinic, without harming the diagnostic efficiency or follow up in different pathologies with MRI.
Finally, these features, together with the excellent behavior and enhancement in all the preclinical studies, make Lead Compound a suitable candidate to the start of phase I clinical trials.

Overall, this work demonstrated that is possible to reduce clinical Gadolinium injected dose with the use of dimeric compounds. Even if the design of a contrast agent which shares high relaxivity, low toxicity and good stability is a difficult challenge, it is feasible. The use of dimeric contrast agents instead of macromolecular complexes as dendrimers, nanoparticles or liposomes may be the way to go. Often, macromolecular agents exhibit slow leakage from the blood vessels to the interstitial space. This phenomenon provides long imaging windows but limits their applicability. Moreover, their pharmacokinetic profiles are also a concern; as these molecules may also be important “targets” for enzymatic systems, undesired metabolism may occur. Finally, it has been demonstrated that problems with the excretion of these macromolecular agents are recurrent, as the glomerular filtration can decrease drastically.[139] For this reason, dimerization can be a straightforward way to obtain CAs with improved relaxivity without drastically increasing the molecular weight and size.[140] Of course, this approach may present some drawbacks, such as aggregation of complexes and formation of potentially toxic diastereomers.

Overall, the improvement of stability and efficiency of contrast agents is a good start for the development of next-generation agents for improved lesion enhancement, characterization, diagnosis, and, thus, clinical efficacy.

6. Published Papers and Conference Abstracts.

Part of the work reported in this thesis was published on two refereed papers, which are attached at the end. Two papers are still being prepared and will be submitted in the upcoming year.

1. Speaker at WMIC 2018, Seattle (USA)

An improved blood pool MRI agent with dinuclear structure: characterization and *in vivo* bio-distribution.

Francesca La Cava[a], Alberto Fringuello Mingo[b], Luigi Miragoli[b], Enzo Terreno[a] , Enrico Cappelletti[b], Luciano Lattuada[b] , Sonia Colombo Serra[b], Luisa Poggi[b], Fabio Tedoldi[b]

Gadolinium-based contrast agents (GBCAs) are widely used in clinical Magnetic Resonance Imaging (MRI). More than 40 million doses are given worldwide each year and search for new candidates is still active. The crucial properties of a GBCA in terms of efficacy is the relaxivity (r_1), *i.e.* the ability to reduce the relaxation time of surrounding protons. It is possible to increase r_1 by reducing the molecular rotational motion, either by increasing the size of the contrast agent or by promoting noncovalent binding with plasma protein. In this work both strategies are used. A dinuclear gadolinium chelate containing two moieties of diethylenetriaminepentaacetic acid, covalently conjugated to an analogue of deoxycholic acid is proposed (GdDTPA)2-Chol). The increment of molecular size also assigns to the molecule useful pharmacokinetic properties, lengthening elimination half time and promoting a macromolecular behavior.

A full *in vitro* relaxometric characterization was performed: *i.e* (*1*) acquisition of nuclear magnetic resonance dispersion (NMRD) in different media; (*2*) the study of binding affinity to HSA; (*3*) transmetallation assay. In addition, *in vivo* MRI bio-distribution and blood pharmacokinetic were compared with Gd-DTPA (Magnevist®, Bayer) and gadocoletic acid trisodium salt (B22956/1, Bracco Imaging Spa), two complexes that respectively share the same chelating cage and the same deoxycholic residue. MRI study consisted in the acquisition of T_1-weighted gradient echo images at 1T post GBCA administration in rats, while pharmacokinetic analysis was performed by collecting blood samples at different times post injection, measuring the gadolinium concentration by relaxometric assay and coupled plasma mass spectroscopy (ICP-MS).

(GdDTPA)2-Chol relaxivity at 20 MHz and 37°C in saline is 7.7 $mM^{-1}s^{-1}$; the presence of physiological ions or medium viscosity did not affect significantly r_1. Conversely, the addition of HSA to saline or the use of plasma medium increased r_1 up to approx. 20 $mM^{-1}s^{-1}$. NMRD profiles showed the typical peak observed in presence of binding; dedicated titration experiments allowed to estimate the affinity constant and the number of binding sites. $(GdDTPA)_2$-Chol demonstrated a *in vivo* much slower kinetic in blood than the remaining CAs, also confirmed by the pharmacokinetic study (approx. 7 times longer elimination half time).

The good binding affinity with HSA, the relatively high number of binding sites and the dinuclear structure lead to a bound fraction of $(GdDTPA)_2$-Chol next to 100%. This feature, together with a reduced hepatic elimination with respect to B22956/1, translates in an extremely long elimination half time. The *in vivo* behavior is very similar to a macromolecule, opening the field of application of the complex beyond angiography, since macromolecular CAs are known to preferentially accumulate in tumor tissue.

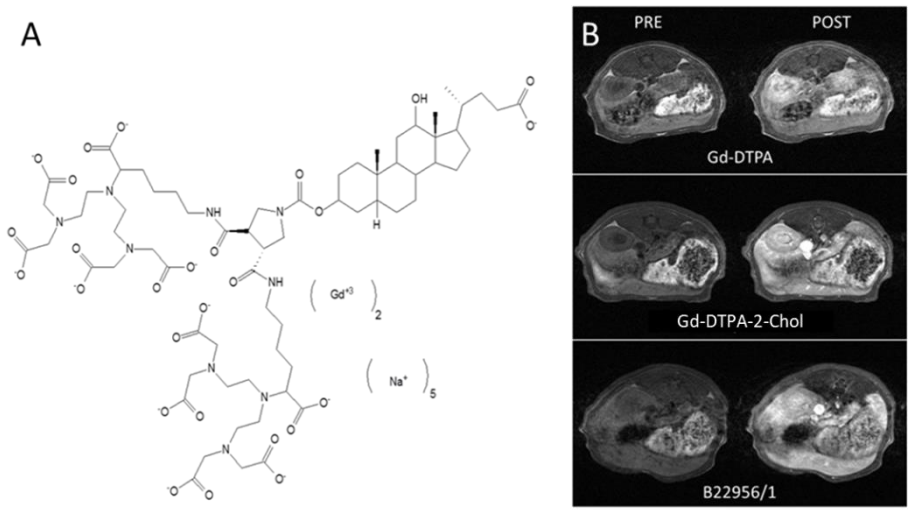

Figure 1: A) Chemical structure of (GdDTPA)2-Chol. B) Representative gradient echo images (axial abdominal section) acquired at 1T pre and post GBCA administration.

2. Poster presented at WMIC 2018, Seattle (USA).

CNS pathological models in rodents for MRI applications: induction and optimization methods

Francesca La Cava[a], Alberto Fringuello Mingo[b], Luigi Miragoli[b], Claudia Cabella[b], Pietro Irrera[b], Enzo Terreno[a], and Sonia Colombo Serra[b]

Magnetic Resonance Imaging (MRI) is a powerful technique providing information to distinguish different tissue properties and disorders[1]. Gadolinium Based Contrast Agents (GBCAs) are widely used in clinic and have been indispensable for monitoring treatment and investigating pathology[1], such as the identification of Cerebral Nervous System (CNS) areas with a disrupted blood–brain barrier corresponding to tumors and inflammatory disorders[2]. The number of Contrast Enhanced (CE)-MRI procedures performed globally has largely grown and is likely to rise in the future, as this modality becomes available to more patients, and as the information obtained from a single contrast injection increases[3].

In the preclinical development phase, the use of animal models is essential for the evaluation of new molecules and to properly test GBCAs efficacy. The aim of this work is to optimize current CNS pathological models for *in vivo* GBCA validation studies. Stereotaxic surgery was used to investigate three different CNS pathological models in rodents. Glioblastoma Multiforme[4] was induced in Wistar rats after inoculation of C6 glioma cells, Convexity and Skull base Human Meningioma[5] in nude mice after local injection of CH157MN cells And lastly, a

cerebral ischemia[6] model in Sprague-Dawley rats using a photoactivated dye, Bengal Rose.

The pathological models were followed by MRI acquisition of T_{2w} sequences to monitor onset and development of the pathology. Assessment of vascularity and permeability by CE-MRI confirmed the models to be suitable for *in vivo* GBCAs validation.

18 rats were used to induce C6 glioma. Mortality was limited and tumor take rate high. A tumor mass was generally visible starting from 2-3 weeks from induction. 24 nude mice were used for induction of Convexity Meningioma, and 24 for the induction of the Skull Base Model. No mortality was observed for the Convexity, while the Skull Base proved to have a higher mortality.

Rose Bengal (dose 40 mg/kg) was used to induce cerebral ischemia in 24 Sprague Dawley Rats. A higher enhancement in CE-MRI matched to an higher permeability of the hematoencephalic barrier, as confirmed by Blue Evans test.

In these studies, non-invasive MRI was introduced as a way to characterize in real time the evolution of cerebral pathologies even from early stages. The feasibility and high reproducibility of the three pathological models proved them to be effective for GBCA validation MRI studies. Moreover, the *in vivo* models showed a marked perfusion by small size CA, probably due to enhanced vascularization and permeability.

Onset of the pathologies was controlled in a precise time window, allowing the operator to control the growth and appearance of the disease, as well as the permeability properties, by injecting CA at different time points to maximize the observed enhancement. The precise locations as seen on MRI of the Glioma, Meningioma tumors and the penumbra lesion of the Ischemia proved to mimic the complex situations in human beings[7-8-9] thus demonstrating that orthotopic diseases could be used as a "bridge" to fill the gap between clinical and preclinical efficacy studies.

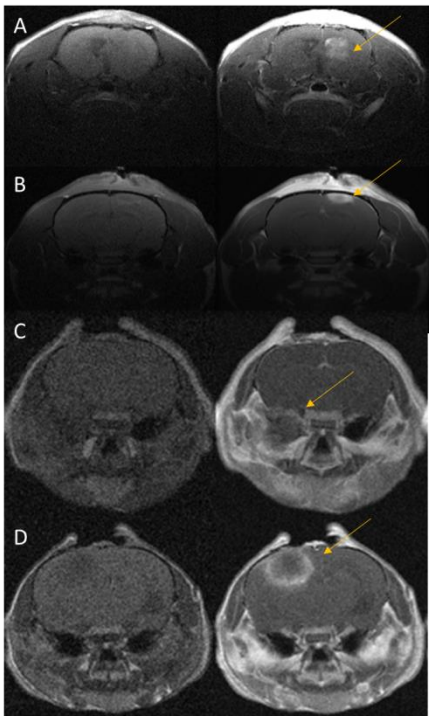

Figure 1: representative pre post GBCA administration axial sections from all the four pathological models. (**A**:Glioma Rat model; **B**:Ischemia Rat Model; **C**: Skull Base Meningioma; **D**: Convexity Meningioma)

[1] Gong E. , et al. J. Magn. Reson. Imaging 2018; DOI 10.1002/jmri.25970
[2] Schoerner W, et al. Neurosurg Rev. 1984;7(4):303–312
[3] Lohrke J. et al. Adv Ther. 2016; 33: 1–28.
[4] Grobben B., et al. Cell Tissue Res 2002; 310:257–270
[5] Ragel BT., et al, J Neurosurg 108:304–310, 2008
[6] Fluri F., et al, Drug Design, Development and Therapy 2015; 9: 3445-3454
[7] Koutcher J. et al, Neoplasia. 2002 Nov; 4(6): 480–485
[8] Campbell et al, American Journal of Clinical Oncology. 2009;32
[9] Canazza A. et al, Frontiers on Neurology doi: 10.3389/fneur.2014.00019.

3. Poster presented at EMIM 2019, Glasgow (UK).

An easy to go method for Breast Tumor Induction into mice: US-Guided Injection and MRI characterization.

La Cava F., Fringuello Mingo A., Colmbo Serra S., Di Vito A., Cabella C., Oliva P., Cordaro A., Brioschi C., Terreno E., and Miragoli L.

Introduction

Breast cancer is the most common cancer for US women.[1] MRI with the use of Contrast Agents (CAs) is a recommended screening, especially for high-risk women. [2]

The use of animal models is essential to test contrast efficacy of CAs under development. Breast cancer orthotopic models can be achieved with orthotopic implantation under direct vision of the mammary fat pad or percutaneous blind injection (OP) in the nipple area.[3-4] To overcome the invasiveness of surgery and the limited accuracy of OP, ultrasound was introduced as a guide for precise localization. The model was then characterized by MRI.

Methods

BT20 cells (10^6 to 10^7 in 100 µl) were injected into the fourth mfp of nu/nu mice via classic surgery (n=6), and ultrasound (US) guided injection (n=16) by using a Vevo Lazr 2100 Ultrasound System with a MS700 Transducer (55 MHz). 4T1 ($5x10^5$ to 10^6 in 50 µl) and TS/A ($5x10^4$ to $5x10^5$ in 50 µl) cells were injected into the mammary fat pad of 26 BALB/C female mice by using US guided injection.

All the animals survived to the tumor induction procedure. Tumor growth was monitored by caliper measurement and/or US imaging weekly or closer. Mice developing noticeable masses were recruited for contrast enhanced (CE) MRI studies, performed by a Bruker Biospec 3T equipped with a 20mm diameter surface coil. At the end of the study, tumor identity was confirmed by histology.

Results/Discussion

Both surgery and US-guided injection were successful in locating the BT20 tumor mass into the mfp, as confirmed by MR imaging and histology. Despite no intraoperative death occurred, the invasiveness of surgery was not negligible. US-guided injection better preserving the animal welfare was selected as the method of choice.

The growth of BT20 tumor was limited, reaching a maximum volume of 10 mm^3. When detectable the diseased mass showed a 50-80% signal enhancement after CA administration at 0.1 mmol/kg.

4T1 and TS/A cells were injected into the mfp to confirm the validity of the US-guided injection. The growth of 4T1 tumor was noticeably fast, leading to observable masses (10 mm^3) already 3-4 days after inoculation and progressively increasing to the endpoint of 300 mm^3 in 2 weeks or earlier. After administration of CA, a 100% enhancement was observed with spin and echo gradient sequences.

The growth curve of TS/A tumor is under monitoring and the characterization by CE MRI is ongoing.

Conclusion

Breast cancer drug development is ineffective without a reliable preclinical model, which is hard to identify. In this study, a novel “easy to go” method to induce breast cancer was developed and three different cell lines were tested. The use of CE MRI served as a way to fully characterize the tumor and study its vascularization, rendering this model useful for efficacy studies, thus bridging the gap between clinical and preclinical research.

References

1. Centers for Disease Control and Prevention. Breast Cancer Statistics. Available at: https://www.cdc.gov/cancer/breast/statistics/. Accessed January 16, 2019

2. Mainiero MB, Lourenco A, Mahoney MC, et al. ACR Appropriateness Criteria breast cancer screening. JAmCollRadiol 2016; 13(11S): R45–R49.

3. Talmadge JE, Singh RK, Fidler IJ, et al. Murine models to evaluate novel and conventional therapeutic strategies for cancer. Am J Pathol. 2007; 170(3):793–804. [PubMed: 17322365]

4. Rashid OM. Et al. Breast Cancer Res Treat. 2014 Oct;147(3):501-12. doi: 10.1007/s10549-014-3118-0

4. Poster Presented at WMIC 2019, Montreal (Canada).

On the diagnostic capability of a dinuclear blood pool GBCA in a pathological model of rat cerebral ischemia.

La Cava F., Fringuello Mingo A., Colombo Serra S., Irrera P., Di Vito A., Cabella C., Miragoli L., Terreno E., and Poggi L.

Gadolinium based contrast agents (GBCAs) have been widely used in clinic to boost the visibility of pathology and delineation of lesions in Magnetic Resonance Imaging acquisitions. Approximately, 40 million administrations are made worldwide every year and search for new candidates is still active.

$(GdDTPA)_2$-Chol, a dinuclear gadolinium(III) chelate containing two moieties of diethylenetriaminepentaacetic acid (DTPA), covalently conjugated to an analogue of deoxycholic acid was synthesized and characterized *in vitro*. Relaxivity (r_1) resulted improved by an increment of the size of the contrast agent; moreover, r_1 further increased by the occurrence of a noncovalent binding with plasma proteins, resulting in a fairly high relaxivity in plasma (approx. 20 $mM^{-1}s^{-1}$, 20 MHz, 310 K. $(GdDTPA)_2$-Chol was tested for its *in vivo* bio-distribution and pharmacokinetic on healthy rats[4] and showed unexpectedly long elimination half-life. In this work, the diagnostic capability of $(GdDTPA)_2$-Chol was tested in a pathological model of permanent cerebral ischemia in rats with a 3 T scanner equipped with a dedicated brain surface coil.

Ischemia was successfully induced after *i.v.* perfusion of Rose Bengal and cortical irradiation by green light in n=11 Sprague Dawley rats. The onset of the pathology was assessed by T_2-weighted images 1 week later and administration of $(GdDTPA)_2$-Chol (0.05 mmol/kg, n=5) and of a commercial macrocyclic GBCA (0.1 mmol/kg, n=6) was performed 12 days after induction, when the lesion reached the chronic stage of the disease, corresponding to an increase in blood brain barrier permeability. $(GdDTPA)_2$-Chol T_1-contrast enhancement was monitored for 90 min in continuous and evaluated 24 h post *i.v.* administration, while commercial GBCA enhancement was followed for 60 min in continuous

Even if the molecular rotational motion contribution to r_1 is valued at low-to-intermediate magnetic field strength (0.5-1.5 T), $(GdDTPA)_2$-Chol enhancement was comparable to the macrocyclic commercial agent, injected at double the dose. Moreover, a difference in distribution and accumulation of the compound into the lesion can be observed: $(GdDTPA)_2$-Chol accumulated slowly into the lesion as a result of the increased molecular size after binding with serum albumin, and reached a plateau after about 20 min, according to the durable availability of the compound characterized by a long elimination rate.

Blue Evans administration into ischemic rats confirmed $(GdDTPA)_2$-Chol behavior: at the chronic stage the lesion is resolved and is replaced by gliosis and fibrosis, the lesion appears more permeable, thus resulting albumin extravasation , as confirmed by both $(GdDTPA)_2$-Chol and Blue Evans distribution.

The strong binding to albumin and the slow accumulation into fibrotic tissue observed after administration of $(GdDTPA)_2$-Chol are valuable features and could be exploited for different applications into cerebral pathology staging and follow-up.

5. Poster Presented at WMIC 2019, Montreal (Canada).

An Ultrasound-Guided Injection method for a refinement and efficient Breast Tumor Induction into mice.

La Cava F., Fringuello Mingo A., Colombo Serra S., Di Vito A., Cabella C., Oliva P., Cordaro A., Brioschi C., Poggi L., Terreno E., and Miragoli L.

Breast cancer is the most common cancer for US women.[1] Although there are many factors that may increase an individual woman's breast cancer risk, women are generally considered high-risk if their lifetime risk of breast cancer is greater than or equal to 20%. For those high-risk women, a supplemental screening such as MRI with the use of Contrast Agents (CAs) is recommended together with the mammography.[2]

The use of animal models is essential to test contrast efficacy of CAs under development. Breast cancer orthotopic models can be achieved by implantation under direct vision of the mammary fat pad or orthotopic percutaneous blind injection (OP) in the nipple area.[3-4] To overcome the invasiveness of surgery and the limited accuracy of OP, ultrasound was introduced as a guide for precise localization. The model was then characterized by MRI, after CA administration.

BT20 cells (10^6 to 10^7 in 100 µL) were injected into the fourth mammary fat pad (mfp) of female nu/nu mice via classic surgery (n=6), and ultrasound (US) guided injection (n=16) by using a Vevo Lazr 2100 US System with a MS700 Transducer (55 MHz). 4T1 ($5x10^5$ to 10^6 in 50 µL, n=7 and n=6 respectively) and TS/A ($5x10^4$ to $5x10^5$ in 50 µL, n=5 and n=8 respectively) cells were injected into the mfp of Balb/C female mice by using US guided injection.

All the animals survived the tumor induction procedure and did not show suffering signs. Tumor growth was monitored by MRI imaging weekly or closer. Mice developing noticeable masses were recruited for Contrast Enhanced (CE) MRI studies, performed by a Bruker Biospec 3 T equipped with a 20 mm diameter surface coil. At the end of the study, tumor identity was confirmed by histology.

Both surgery and US-guided injection were successful in locating the BT20 tumor mass into the mfp, as confirmed by MRI and histology. Despite no intraoperative death occurred, the invasiveness of surgery was not negligible. US-guided injection, reducing the animal post-operative suffering, resulted an optimized refinement procedure, being in line with 3Rs principle.

The growth of BT20 tumor was limited, reaching a maximum volume of 10 mm^3 in 6 weeks. When detectable, the diseased mass showed a 50-80% signal enhancement after CA administration at 0.1 mmol/kg.

4T1 and TS/A cells were injected into the mfp to confirm the validity of the US-guided injection. 4T1 tumor growth was noticeably fast, leading to observable masses (10 mm^3) already 4 days after inoculation and progressively increasing to the endpoint (300 mm^3) in two weeks or earlier. After CA administration, a 100% enhancement was observed with spin and gradient echo sequences.

TS/A tumor was clearly visible starting from 6-10 days after cell inoculation and reaching the endpoint (300 mm^3) after 3 weeks when $5x10^5$ cells were inoculated, while keeping below 150 mm^3 after 25 days when the lower cell numerosity was used. Immediately after CA injection, the boundary of the tumor mass and shortly later the core became bright, reaching an overall maximum enhancement around 70-80%.

Breast cancer drug development is ineffective without a reliable preclinical model, which is hard to identify. In this study, a refinement method to induce breast cancer was developed and three different cell lines were tested. The use of CE MRI served as a way to fully characterize the tumor and study its vascularization, rendering this model useful for efficacy studies, thus bridging the gap between clinical and preclinical research.

References

1. Centers for Disease Control and Prevention. Breast Cancer Statistics. Available at: https://www.cdc.gov/cancer/breast/statistics/. Accessed January 16, 2019

2. Mainiero MB, Lourenco A, Mahoney MC, et al. ACR Appropriateness Criteria breast cancer screening. JAmCollRadiol 2016; 13(11S): R45–R49.

3. Talmadge JE, Singh RK, Fidler IJ, et al. Murine models to evaluate novel and conventional therapeutic strategies for cancer. Am J Pathol. 2007; 170(3):793–804. [PubMed: 17322365]

4. Rashid OM. Et al. Breast Cancer Res Treat. 2014 Oct; 147(3):501-12. doi: 10.1007/s10549-014-3118-0

7. Acknowledgments

This work would have not been possible without the help and guidance of my colleagues, who supported me in every step of the way during my PhD.

Therefore, my sincere thanks go to Sonia Colombo Serra and Alberto Fringuello Mingo that were with me from the beginning of the PhD. Thank you for the patience demonstrated while I was learning everything, for the support and the cheerful times.

Thanks to Luigi Miragoli, which was my mentor and guidance during the surgeries and all the procedures involving animals. I could not have done without you.

Thanks to all the Preclinical Imaging Laboratory at Bracco Imaging SpA, for always being there when I needed help, and for being such an amazing lab.

Thanks to Enzo Terreno, which was my academic supervisor and first gave me the opportunity to embark in this journey.

Thanks to Goran Angelovski, for accepting me as a visiting student at Max Planck Institute for Biological Cybernetics and to Tanja Gambino, who became immediately a friend, more than a co-worker.

Nothing would have been possible without the support given me by my family and my love, Jeremy. Thank you for believing in me every day, even when I did not.

Finally, thanks to my best friends, Gilda and Ludovica, who shared with me every moment, even from afar; and thanks to Serena and Valeria, who are there for me every day, sharing the joys and pains of life.

8. References

[1] Runge, V. M. Invest. Radiol. 2017, 52, 317−323.

[2] Wahsner J., Gale E.M., Rodríguez-Rodríguez A., Caravan P. Chem Rev.2019;119,2;957-1057

[3] Morkos SK., Eur J Radiol 2008; 66: 175-9

[4] Rooney WD, Johnson G, Li X, Cohen ER, Kim SG, Ugurbil K, Springer CS Jr. Magn. Reson. Med. 2007; 57: 308–318.

[5] Rudin M., Molecular Imaging 2nd Edtion, Imperial College Press, 2013

[6] Murphy KJ, Brunberg JA, Cohan RH., AJR Am J Roentgenol. 1996;167:847–9.

[7] Prince MR, Arnoldus C, Frisoli JK. J Magn Reson Imaging.1996;6:162–6.

[8] Grobner T. Nephrol Dial Transplant 2006; 21: 1104–8.

[9] Todd DJ, Kagan A, Chibnik LB, Kay J. Arthritis Rheum 2007; 56: 3433–41.

[10] Available from: www.esur.org/fileadmin/content/NSF/NSF-ESUR_Guideline_Final.pdf

[11] Kanda, T.; Kawaguchi, H., Neuroradiology 2013, 55, 1268−1269.

[12] Kanda, T.; ishii, K.; Kawaguchi, H.; Kitajima, K.; Takenaka, D.,Radiology 2014, 270, 834−841

[13] McDonald RJ, McDonald JS, Kallmes DF, Jentoft ME, Murray DL, Thielen KR, Williamson E.E, Eckel LJ., Radiology 2015; 275: 772–82.

[14] Stojanov DA, Aracki-Trenkic A, Vojinovic S, Benedeto-Stojanov D, Ljubisavljevic S. Eur Radiol 2016; 26: 807–15.

[15] Tibussek D, Rademacher C, Caspers J, Turowski B, Schaper J, Antoch G, Klee D. Radiology 2017; 285: 223–30.

[16] Conte G, Preda L, Cocorocchio E, Raimondi S, Giannitto C, Minotti M., De Piano F., Petralia G., Ferrucci PF., Bellomi M. Eur Radiol 2017; 27: 4372–8.

[17] Frenzel T, Apte C, Jost G, Schockel L, Lohrke J, Pietsch H.. Invest Radiol 2017; 52: 396–404.

[18] Frenzel T, Lengsfeld P, Schirmer H, Hutter J, Weinmann HJ. C. Invest Radiol 2008; 43: 817–28.

[19] Hershberg RD, Reed GH, Slotboom AJ, deHaas GH. Biochemistry 1976; 15: 2268–74.

[20] Frenzel, T.; Apte, C.; Jost, G.; Schockel, L.; Lohrke, J.; Pietsch, H. Invest. Radiol. 2017, 52, 396−404.

[21] Gianolio, E.; Bardini, P.; Arena, F.; Stefania, R.; Di Gregorio, E.; Iani, R.; Aime, S. Radiology 2017, 285, 839−849.

[22] PRAC confirms restrictions on the use of linear gadolinium agents EMA/424715/2017

[23]FDA Medical Imaging Drugs Advisory Committee Meeting Gadolinium Retention after Gadolinium Based Contrast Magnetic Resonance Imaging in Patients with Normal Renal Function, Briefing Document September 8, 2017

[24] Wahsner J., Gale E.M., Rodríguez-Rodríguez A., Caravan P. Chem Rev.2019;119,2;957-1057

[25] Werner, E. J.; Datta, A.; Jocher, C. J.; Raymond, K. N. Angew. Chem., Int. Ed. 2008, 47, 8568−8580.

[26] Shen Y, Goerner FL, Snyder C, et al. Invest Radiol.2015;50:330–338

[27] Robic C, Port M et al. Invest Radiol 2019;54: 475–484

[28] Vagner A., Gianolio E., Aime S. et al. Chem. Commun., 2016,52, 11235-11238

[29] Leygue N, Enel M, Diallo A, et al. European Journal of Organic Chemistry, 2019, 18, (2899-2913).

[30] Granato L., Longo D., et al. Chemistry & Biodiversity, 16, 11, (2019).

[31] Pellico J, Ellis CM, Davis JJ, Contrast Media & Molecular Imaging,(1-13), (2019).

[32] Denayer, T.; Stohr, T.; Van Roy, M. New Horizons in Translational Medicine 2 (2014) 5-11

[33] Russell, W.M.S. and Burch, R.L.; The Principles of Humane Experimental Technique, Methuen, London (1959).

[34] Louis DN, Perry A, Reifenberger G, von Deimling A, Figarella-Branger D, Cavenee WK, Ohgaki H, Wiestler OD, Kleihues P, Ellison DW.; Acta Neuropathol. 2016;131:803–20.

[35] Ostrom QT, Gittleman H, Farah P, Ondracek A, Chen Y, Wolinsky Y, Stroup NE, Kruchko C, Barnholtz-Sloan JS.; Neuro Oncol. 2014 May;16(5):760.
[36] https://seer.cancer.gov/statfacts/html/brain.html#risk last accessed 15 May 2019
[37] Ahmed R, Oborski MJ, Hwang M, Lieberman FS, Mountz JM. Cancer Manage Res. 2014 ;6:149–70.
[38] Upadyay, N.;Waldman A.D.; The British Journal of Radiology, 84 (2011), S107–S111
[39] Benda P, Lightbody J, Sato G, Levine L, Sweet W; Science(1968) 161:370–371
[40] Auer R, Del Maestro RF, Anderson R Can J Neurol Sci (1981) 8:325–331
[41] Vajkoczy P, Schilling L, Ullrich A, Schmiedek P, Menger M D, J Cereb Blood Flow Metab (1998), 18(5)
[42] Louis DN, Ohgaki H, Wiestler OD, Cavenee WK WHO Classification of Tumours of the Central Nervous System,Who Press (2016)
[43] Tu TW, Turtzo LC, Williams RA, Lescher JD, Dean DD, Frank JA, J Neuropathol Exp Neurol. 2014 December ; 73(12): 1152–1165
[44] Kao HW, Chiang SW, Chung HW, Tsai FY, Chen CY, BioMed Research International 2013
[45] Wiemels J, Wrensch M, Claus EB, J Neurooncol. 2010;99(3):307. Epub 2010.
[46] Louis DN, Perry A, Reifenberger G, von Deimling A, Figarella-Branger D, Cavenee WK, Ohgaki H, Wiestler OD, Kleihues P, Ellison DW, Acta Neuropathol. 2016 Jun;131(6):803-20
[47] Marosi C, Hassler M, Roessler K, Reni M, Sant M, Mazza E, Vecht C, Crit Rev Oncol Hematol. 2008;67(2):153.
[48] Carroll RS, Zhang J, Dashner K, Sar M, Wilson EM, Black PM, J Neurosurg. 1995;82(3):453.
[49] Blankenstein MA, Verheijen FM, Jacobs JM, Donker TH, van Duijnhoven MW, Thijssen JH, Steroids. 2000;65(10-11):795.
[50] Nakasu S, Hirano A, Shimura T, Llena JF. Surg Neurol. 1987 Apr;27(4):319-22.
[51] M Nakamura, F Roser, J Michel, C Jacobs, M Samii, Neurosurgery, 53 (2003), pp. 62-71
[52] Morris Z, Whiteley WN, Longstreth WT Jr, Weber F, Lee YC, Tsushima Y, Alphs H, Ladd SC, Warlow C, Wardlaw JM, Al-Shahi Salman R, BMJ. 2009 339:b3016.
[53] Wilms G, Lammens M, Marchal G et-al. J Comput Assist Tomogr. 1989;13 (5): 763-8.
[54] Hsu CC, Pai CY, Kao HW, Hsueh CJ, Hsu WL, Lo CP J Clin Neurosci. 2010;17(5):584.
[55] Zhang H, Rödiger LA, Shen T, Miao J, Oudkerk M, Neuroradiology. 2008 Jun;50(6):525-30.
[56] Nagar VA, Ye JR, Ng WH, Chan YH, Hui F, Lee CK, Lim CC., AJNR Am J Neuroradiol. 2008 Jun;29(6):1147-52.
[57] Jensen RL, Origitano TC, Lee YS, Weber M, Wurster RD, Neurosurgery. 1995 Feb;36(2):365-73.
[58] Lee WH, Neurosurgery 1990;27:389-95
[59] Greene H. S. N., Hildegarde A, Journal of Neurosurgery, 1945; 315-331
[60] McCutcheon IE, Friend KE, Gerdes TM, Zhang BM, Wildrick DM, Fuller GN., J Neurosurg 92:306-314,2000
[61] Ragel BT, Jensen RL, Gillespie DL, Prescott SM, Couldwell WT. Cancer. 2007;109:588-597.
[62] Ragel BT, Elam IL, Gillespie DL. J Neurosurg. 2008;108:304-310.
[63] Akat , Mennel HD, Kremer P, Gassler N, Bleck CK, Kartenbeck J, Acta Neuropathol (Berl) 106:337-347, 2003
[64]Tsai JC, Goldman CK, Gillespie GY.J Neurosurg. 1995;82:864-873
[65] La Cava F, Fringuello Mingo A, Irrera P, Di Vito A, Cordaro A, Brioschi C,Colombo Serra S, Cabella C, Terreno E, Miragoli L., AMEM 2019 (2) 58-63
[66] Louis DN, Ohgaki H, Wiestler OD, Cavenee WK WHO Classification of Tumours of the Central Nervous System,Who Press (2016)
[67] Campbell BA, Jhamb A, Maguire JA, Toyota B, Ma R. Am J Clin Oncol. 2009;32:73-85.
[68] Roth GA, Forouzanfar MH, Moran AE, Barber R, Nguyen G, Feigin VL, Naghavi M, Mensah GA, Murray CJ.N Engl J Med 2015; 372: 1333–1341.

[69] Feigin VL, Krishnamurthi RV, Parmar P,Norrving B, Mensah GA, Bennet DA, Barker-Collo S, Moran AE, Sacco RL, Truelsen T,Davis S, Pandian JD, Naghavi M,Forouzanfar MH, Nguyen G, Johnson CO, Vos T, Meretoja A, Murray CJL, Roth GA, Neuroepidemiology 2015;45:161–176
[70] Amarenco P., Bogousslavsky J, Caplan L.R., Donnan G.A., Wolf M.E.,Hennerici M.G., Cerebrovasc. Dis. 36 (2013) 1–5
[71] Lipton P. Physiol Rev. 1999;79(4):1431–1568.
[72] El Khoury R, Jung R, Nanda A, Sila C, Abraham MG, Castonguay AC, Zaidat OO Neurology. 2012 Sep 25;79(13 Suppl 1):S26-34.
[73] Srinivasan A, Goyal M, Al Azri F, Lum C, Radiographics. 2006 Oct;26 Suppl 1:S75-95.
[74] Yamori Y, Horie R, Handa H, Sato M, Fukase M. Stroke. 1976;7(1):46–53.
[75] Fluri F, Schuhmahnn MK, Kleinschnitz C, Drug Design, Development and Therapy 2015:9 3445–3454
[76] Watson BD,Dietrich WD, Busto R, Watchel MS, Ginsberg MD, Ann Neurol 1985;17:497-504
[77] Macrae IM, Br J Pharmacol 2011, 164:1062-1078
[78] Noce A, Frigeni V, Demicheli F, Miragoli L, Tirone P., Investigative Radiology. 34(4):262, April 1999
[79] Tuor UI, Deng Q, Rushforth D,Foniok T, Qiao M, Journal of Neuroscience Methods 268, 2016; 56-65
[80] Lee MC, Jin CY, Kim HS, Kim JH, Kim MK, Kim HI, Lee YJ, Son YJ, Kim YO, Woo YJ, Chonnam Med J 2011; 47:90-98
[81] Dahan A, Yassen A, Romberg R, Sarton E, Teppema L, Olofsen E, Danhof M BJA: British Journal of Anaesthesia, 2006,Volume 96,(05), 627–632.
[82] Lefkov, Sharon H; Müssig, Dirk, Journal of the American Association for Laboratory Animal Science, 2007,46 (6). 63-64(2).
[83] Centers for Disease Control and Prevention. Breast Cancer Statistics. Available at: https://www.cdc.gov/cancer/breast/statistics/. Accessed January 16, 2019.
[84] Mainiero MB, Lourenco A, Mahoney MC, et al. JAmCollRadiol 2016; 13(11S): R45–R49.
[85] Saslow D, Boetes C, Burke W, et al. CA Cancer J Clin 2007;57:75–89.
[86] Swain S. 2008 ASCO Clinical Science Symposium, 2008.
[87] Zaky SS, Lund M, May KA,et al. Ann Surg Oncol2011;18:2858–65.
[88] Gluz O, Liedtke C, Gottschalk N, Pusztai L, Nitz U, Harbeck, Ann Oncol 2009;20:1913–27.
[89] Sung JSS, Jochelson MS, Brennan S, Joo S, Wen YH, Moskowitz C, Zheng J, Dershaw D, Morris EA, The Breast Journal, Volume 19 Number 6, 2013 643–649
[90] Choi JJ, Kim SH, Cha ES, Kang BJ, Lee JH, Lee SY, Jeong SH, Yim HW, Song BJ, JKSMRM 14:95-102(2010)
[91] Costantini M,Belli P,Distefano D, Bufi E, Di Matteo M, Rinaldi P, Giuliani M, Petrone G, Magno S, Bonomo L, Clinical Breast Cancer, Vol. 12, No. 5, 331-9
[92] Ozzello L, Sordat B, Merenda C, Carrel S, Hurlimann J and Mach JP. Journal of The National Cancer Institute 1974; 52(5).
[93] Lasfargues EY, Ozzello L. J Natl Cancer Inst. 1958;21(6):1131-47.
[94] Dexter D.L., Kowalski H.M., Blazar B.A., Fligiel Z., Vogel R., Heppner G.H. Cancer Res, 1978,. 38, 3174–3181.
[95] P. Nanni, C. De Giovanni, P.-L. Lollini, G. Nicoletti & G. Prodi. Clin. Expl. Metastasis, 1: 373-380, 1983.
[96] Nicoletti G., Brambilla P., De Giovanni C., Lollini PL, Del Re B, Marocchi A, Mocarelli P, Prodi G, Nanni P Br J Cancer. 1985 Aug; 52(2): 215–222.
[97] a) A. Accardo, D. Tesauro, L. Aloj, C. Pedone, G. Morelli, Coord. Chem. Rev. 2009, 253, 2193-2213; b) E. Terreno, D Delli Castelli, A. Viale, S. Aime S. Chem Rev. 2010, 110, 3019-3042.
[98] a) J. Tang, Y. Sheng, H. Hu, Y. Shen, Prog. Polymer Sci. 2013, 38, 462-502; b) M. Botta, L. Tei, Eur. J. Inorg. Chem. 2012, 1945-1960; c) A. J. L. Villaraza, A. Bumb, M. W. Brechbiel, Chem. Rev. 2010, 110, 2921-2959.
[99] P. Caravan, Acc. Chem. Res. 2009, 42, 851-862.

[100] A. Gossmann, Y. Okuhata, D. M. Shames, T. H. Helbich, T. P. L. Roberts, M. F. Wendland, S. Huber, R. C. Brasch, Radiology 1999, 213, 265-272.
[101] La Cava F, Fringuello Mingo A, Miragoli L, Terreno E, Cappelletti E, Lattuada L, Poggi L, Colombo Serra S. ChemMedChem 2018, 13,824 –834
[102] a) T. L. Pushparaj, V. Alexander, Int. J. Appl. Bioeng. 2016, 10, 11-17; b) T. L. Pushparaj, V. Alexander, Int. J. Sci. Eng. Res. 2016, 7(12), 1600-1605. c) T. N. Parac-Vogt, K. Kimpe, S. Laurent, L. Vander Elst, C. Burtea, F. Chen, R. B. Muller, Y. Ni, A. Verbruggen, K. Binnemans, Chem. Eur. J. 2005, 11, 3077-3086; d) V. V. Martin, W. H. Ralston, M. R. Hynes, J. F. W. Keana, Bioconjugate Chem. 1995, 6, 616 –623; e) G. Gambino, S. De Pinto, L. Tei, C. Cassino, F. Arena, E. Gianolio, M. Botta. J. Biol. Inorg. Chem. 2014, 19, 133–143.
[103] R. Felix, A. Heshiki, N. Hosten, H. Hricak, Magnevist Monograph, Blackwell Science, Oxford, 3rd edn, 1998
[104] C. de Haën, P. L. Anelli, V. Lorusso, A. Morisetti, F. Maggioni, J. Zheng, F. Uggeri, F. M. Cavagna, Invest. Radiol. 2006, 41, 279-291.
[105] A. Oyane, K. Onuma, A. Ito, H. M. Kim, T. Kokubo, T. Nakamura, *J. Biomed. Mater. Res.* 2003, *64A*, 339-348.
[106] a) S Aime, M Botta, M Fasano, E Terreno, *Acc. Chem. Res*. 1999, *32*, 941-949; b) A. Fringuello Mingo, S. Colombo Serra, S. Baroni, C. Cabella, R. Napolitano, I. Hawala, L. Lattuada, F. Tedoldi, I. M. Carnovale S. Aime, *Magn Reson Med.* 2017;*78*, 1523-1532.
[107] M. Rohrer, H. Bauer, J. Mintorovitch, M. Requardt, H-J. Weinmann, Invest. Radiol. 2005, 40, 715–724.
[108] T. L. Pushparaj, V. Alexander, Int. J. Appl. Bioeng. 2016, 10, 11-17;
[109] T. L. Pushparaj, V. Alexander, Int. J. Sci. Eng. Res. 2016, 7(12), 1600-1605.
[110] T. N. Parac-Vogt, K. Kimpe, S. Laurent, L. Vander Elst, C. Burtea, F. Chen, R. B. Muller, Y. Ni, A. Verbruggen, K. Binnemans, *Chem. Eur. J*. 2005, *11*, 3077-3086;
[111] Gambino, S. De Pinto, L. Tei, C. Cassino, F. Arena, E. Gianolio, M. Botta. J. Biol. Inorg. Chem. 2014, 19, 133–143.
[112] E. Gianolio, C. Cabella, S. Colombo Serra, G. Valbusa, F. Arena, A. Maiocchi, L. Miragoli, F. Tedoldi, F. Uggeri, M. Visigalli, P. Bardini, S. Aime, J. Biol. Inorg. Chem. 2014, 19, 715–726.
[113] P. Caravan, N. J. Cloutier, M. T. Greenfield, S. A. McDermid, S. U. Dunham, J. W. M. Bulte, J. C. Amedio Jr., R. J. Looby, R. M. Supkowski, W. DeW. Horrocks Jr., T. J. McMurry, R. B. Lauffer, J. Am. Chem. Soc. 2002, 124, 3152 –3162
[114] a) N. Blombergen, J. Chem. Phys. 1957, 27, 572–573; b) Solomon, Phys. Rev. 1955, 99, 559–565.
[115]J. Freed, J. Chem. Phys. 1978, 68, 4034–4037.
[116] S. Aime, M. Botta, E. Terreno. Adv. Inorg. Chem. 2005, 57, 173–237.
[117] S. Baroni, S. Colombo Serra, A. Fringuello Mingo, G. Lux, G. B. Giovenzana, L. Lattuada, *Chemistry Select* 2016, 1, 1607-1612.
[118] G. A. Rolla, M. Botta, L. Tei, C. Cabella, S. Ghiani, C. Brioschi, A. Maiocchi. Chem. Eur. J. 2013, 19, 11189-11193.
[119] a) G. Lipari, A. Szabo, J. Am. Chem. Soc. 1982, 104, 4546–4559; b) G. Lipari, A. Szabo, J. Am. Chem. Soc. 1982, 104, 4559–4570.
[120] S. Aime, M. Fasano, E. Terreno, M. Botta in The Chemistry of Contrast Agents in Medical Magnetic Resonance Imaging, (Eds.: A. E. Merbach, É. Tóth), Wiley VCH, Weinheim, 1st edn, 2001, pp. 193-242.
[121] D. L. Longo, F. Arena, L. Consolino, P. Minazzi, S. Geninatti-Crich, G. B. Giovenzana, S. Aime, Biomaterials 2016, 75, 47-57.
[122] S. Laurent, L. Vander Elst, F. Copoix, R. N. Muller, Invest. Radiol. 2001, 36, 115-122.
[123] V. V. Martin, W. H. Ralston, M. R. Hynes, J. F. W. Keana, Bioconjugate Chem. 1995, 6, 616–623;
[124] H. J. Weinmann, R. C. Brasch, W. R. Press, G. E. Wesbey, Am. J. Roentgenol. 1984, 142, 619–624.
[125] D. J. Parmelee, R. C. Walovitch, H. S. Ouellet, R. B. Lauffer, Invest. Radiol. 1997, 32, 741–747.
[126] Watson BD, Dietrich WD, Busto R, Wachtel MS, Ginsberg MD.. Ann Neurol. 1985;17:497–504.
[127] J. E. Burda, M. V. Sofroniew, Neuron, 2014, 81.

[128] T.G. Bush, N. Puvanachandra, C.H. Horner, A. Polito, T. Ostenfeld, C.N. Svendsen, L. Mucke, M.H. Johnson, M.V. Sofroniew, Neuron, 1999,23.

[129] Matsuda R, Nishikawa A, Tanaka H. J. Biochem. 1995; 118: 959-964.

[130] Nidavani R. B., Mahalakshmi AM , Shalawadi M. Journal of Applied Pharmaceutical Science 4 (11); 2014: 106-113

[131] Robert P, Violas X, Grand S, Lehericy S, Idée JM, Ballet S, Corot C.,Investigative Radiology (2016) 51: 2.

[132] Guidance document on the recognition, assessment, and use of clinical signs as humane endpoints for experimental animals used in safety evaluation. OECD. December 21, 2001.

[133] Gerald Van Belle, Lloyd D. Fisher, Patrick J. Heagerty, Thomas Lumley. Biostatistics (Second Edition). John Wiley & Sons, Inc. 2004.

[134] Michael R. Stoline. The American Statistician, 35, 134-141.

[135] Rohrer M, Bauer H, Mintorovitch J, Requardt M, Weinmann HJ. Investigative Radiology 2005; 40(11):715-724.

[136] Drexler HG, Uphoff CC Cytotechnology (2002) 39: 75-90.

[137] Hutchinson L., Kirk R., Nature Reviews Clinical Oncology volume 8, pages189–190 (2011)

[138] https://www.ema.europa.eu/en/documents/scientific-guideline/guideline-principles-regulatory-acceptance-3rs-replacement-reduction-refinement-testing-approaches_en.pdf

[139] Q. Dong, D. R. Hurst, H. J. Weinmann, T. L. Chenevert, F. J. Londy, M. R. Prince, Invest. Radiol. 1998, 33, 699–708.

[140] Fontès A, Karimi S., et al. Eur. J. Inorg. Chem. 2015, 1579–1591

CHEMMEDCHEM

CHEMISTRY ENABLING DRUG DISCOVERY

Accepted Article

Title: Synthesis, characterization and biodistribution of a novel dinuclear gadolinium complex with improved properties as blood pool MRI agent

Authors: Francesca La Cava, Alberto Fringuello Mingo, Luigi Miragoli, Enzo Terreno, Enrico Cappelletti, Luciano Lattuada, Luisa Poggi, and Sonia Colombo Serra

To be cited as: *ChemMedChem* 10.1002/cmdc.201800052

Link to VoR: http://dx.doi.org/10.1002/cmdc.201800052

A Journal of

ChemPubSoc Europe

WILEY-VCH

www.chemmedchem.org

WILEY-VCH

FULL PAPER

Synthesis, characterization and biodistribution of a novel dinuclear gadolinium complex with improved properties as blood pool MRI agent

Francesca La Cava[a], Alberto Fringuello Mingo[b], Luigi Miragoli[b], Enzo Terreno[a], Enrico Cappelletti[b], Luciano Lattuada[b], Luisa Poggi[b] and Sonia Colombo Serra*[b]

Abstract: A dinuclear gadolinium(III) chelate containing two moieties of diethylenetriaminepentaacetic acid (DTPA), covalently conjugated to an analogue of deoxycholic acid has been synthesized and widely characterized. A full relaxometric analysis was carried out, consisting of (i) the acquisition of nuclear magnetic resonance dispersion (NMRD) profiles in different media; (ii) the study of binding affinity to serum albumin; (iii) the measurement of ^{17}O transverse relaxation rate *vs* temperature and (iv) a transmetallation assay. Biodistribution MRI in vivo studies at 1 T and blood pharmacokinetic were carried out in comparison with Gd-DTPA (Magnevist®) and gadocoletic acid trisodium salt (B22956/1), two well-known Gd-complexes both sharing the same chelating cage and the same deoxycholic residue of the herein investigated Gd-complex ((GdDTPA)2-Chol). A good affinity to the plasma protein and, in particular, the availability of more than one binding site, allows the complex to reach a fairly high relaxivity value in plasma (approx. 20 $mM^{-1}s^{-1}$, 20 MHz, 310 K) as well as to show unexpectedly strongly enhanced properties of blood pooling, with an elimination half time in rats about 7 times longer than B22956/1.

Introduction

Magnetic Resonance Imaging (MRI) is a well-known imaging technique that provides proton signal intensity maps of *in vivo* water molecules.[1] The intrinsic contrast between tissues which mostly arises from variation of relaxation times among water protons, is often not sufficient for a reliable diagnosis of inflammation, lesions and in general pathology onset. For this reason, exogenous contrast enhancing agents, such as in particular gadolinium based contrast agents (GBCAs) are widely used in clinical practice.[2] Currently, more than 30 million doses are given worldwide each year, corresponding to about 30% of total MRI examinations.[3] Despite first GBCAs were introduced in the market more than 25 years ago, the research in this field is still active and it aims at discovering new candidates with superior or different properties with respect to the commercial portfolio.[4]

[a] F. La Cava, Prof. E. Terreno
Center of Excellence for Preclinical Imaging (CEIP)
Department of Molecular Biotechnologies and Health Sciences
University of Torino
Via Ribes 5, 10010 Colleretto Giacosa (TO)

[b] Dr. A. Fringuello Mingo, L. Miragoli, E. Cappelletti, Dr. L. Lattuada, Dr. L. Poggi and Dr. S. Colombo Serra
Bracco Research Centre,
Bracco Imaging SpA
Via Ribes 5, 10010 Colleretto Giacosa (TO)
E-mail:sonia.colombo@bracco.com

The crucial property of a GBCA in terms of efficacy is the longitudinal relaxivity (r_1), that is the concentration-normalized ability to reduce the longitudinal relaxation time (T_1) of surrounding protons. One of the most successful strategy to increase r_1 is the reduction of the molecular rotational motion (τ_R), attainable through various routes, such as the incorporation of the contrast agent into micelles, liposomes or nanoparticles,[5] the synthesis of polymers or dendrimers functionalized with gadolinium complexes,[6] or the promotion of non-covalent binding with plasma proteins.[7]

The establishment of a supramolecular adduct between the gadolinium complex and the serum proteins not only induces a marked relaxivity enhancement, but it also influences the *in vivo* distribution properties. The fraction of paramagnetic complex bound to protein can hardly extravasate from the healthy vascular compartment, providing selective enhancement of vessels and leading to a preferential accumulation in tumor tissues, thanks to the hyper-permeability of cancer vasculature.[8]

In the present study, two strategies have been exploited at the same time to increase τ_R, *i.e.* the presence of multiple paramagnetic centers and the non-covalent binding to albumin. Specifically, the new dinuclear gadolinium (GdDTPA)2-Chol, containing two moieties of diethylenetriaminepentaacetic acid (DTPA) covalently conjugated to deoxycholic acid, was designed and synthesized. Indeed, similar dinuclear products have been already reported in literature,[9] but they were characterized by lower relaxivity and/or inferior (or not explored) blood pool properties. To demonstrate the good interaction with Human Serum Albumin (HSA) and the enhanced properties of retention in the vascular compartment, the novel dinuclear gadolinium (GdDTPA)2-Chol was fully characterized by relaxometric analysis (NMRD profiles, ^{17}O paramagnetic transverse relaxation rate (R_{2p}) *vs* temperature curve, HSA binding study) and preclinically evaluated by a MRI bio-distribution study and a blood pharmacokinetic analysis. The *in vivo* behavior was compared with the clinically approved GBCA gadopentetate dimeglumine (Gd-DTPA, Magnevist®, Bayer)[10] and with a blood pool agent tested in Phase I trials, *i.e.* gadocoletic acid trisodium salt (B22956/1, Bracco Imaging).[11]

Results and Discussion

Synthesis: The synthesis of (GdDTPA)2-Chol (complex **8**) is shown in Scheme 1. The *trans*-1-(benzyl)-3,4-pyrrolidinedicarboxylic acid **2** was chosen as short, symmetrical linker and synthesized as reported in literature.[12] It was activated with pivaloyl chloride and coupled to the bifunctional chelating agent **1**, , which can be easily synthesized from commercially available *N*-ε-Z-lysine methyl ester following the Rapoport's procedure.[13] The bisamide **3** was debenzylated by catalytic

hydrogenolysis and the corresponding amine **4** was reacted with chloroformate **5**, easily obtained by reaction of methyl deoxycholate with a solution of phosgene in toluene.[14] The methyl and t-butyl esters of **6** were fully and simultaneously hydrolyzed with an excess of lithium hydroxide in 1,4-dioxane and the corresponding ligand **7** was then treated with gadolinium trichloride to give the complex **8** as penta sodium salt.

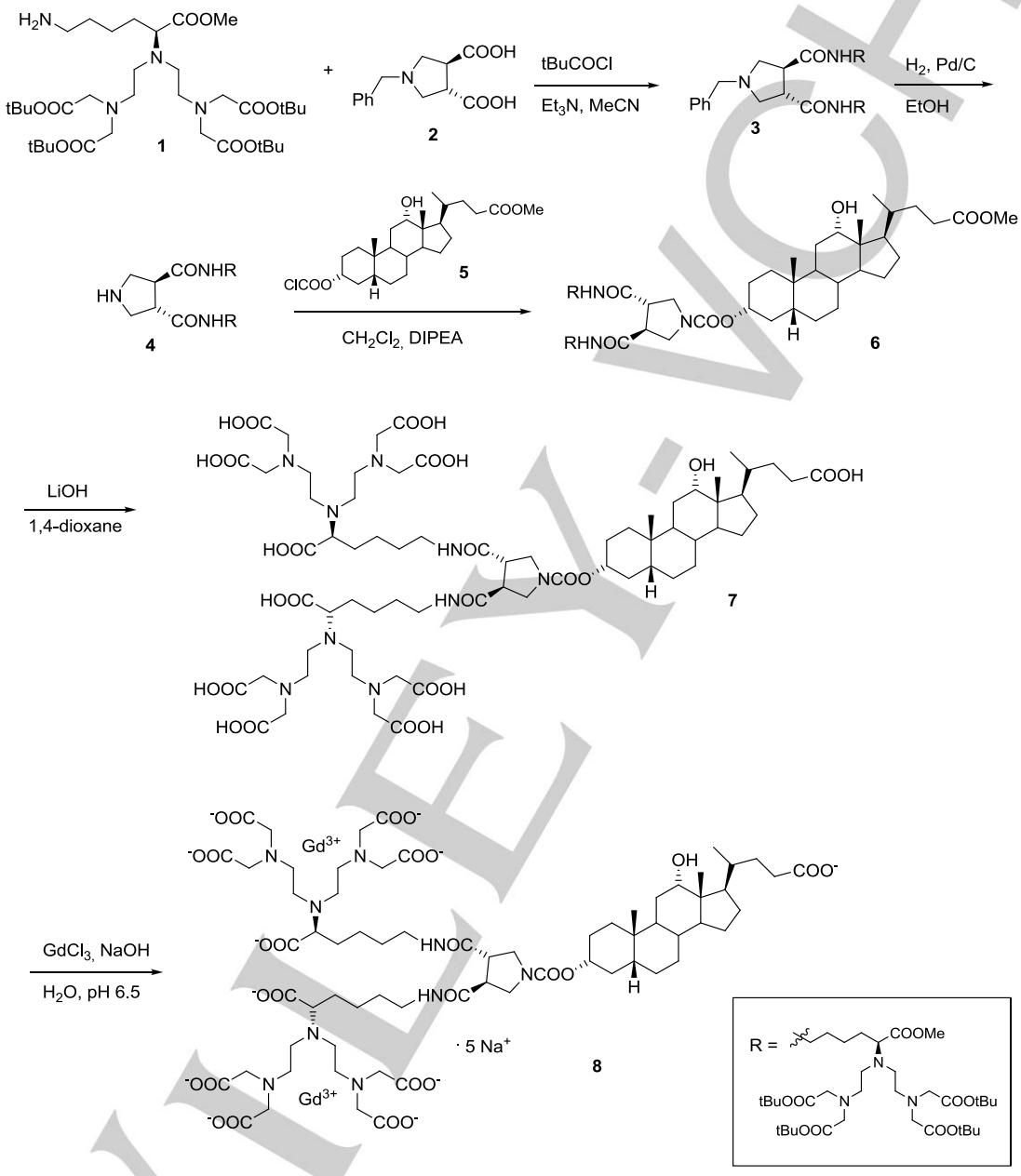

Scheme 1. Synthesis of (GdDTPA)2-Chol.

Relaxometric characterization: (GdDTPA)2-Chol was investigated by recording nuclear magnetic resonance dispersion (NMRD) profiles at 310 K and at magnetic field strengths ranging from 0.24 mT to 1.65 T in different media. The profiles acquired in physiologic solution and in i-SBF (a medium mimicking the ionic content of plasma)[15] were superimposable (Figure 1), indicating the absence of a contribute from prototropic exchange[16] at least at physiological pH. Conversely, the addition of 35 g/L of HSA to saline or the use of plasma medium strongly affected the performance of (GdDTPA)2-Chol. In particular, the appearance of the relaxivity peak centered around 30-40 MHz is a clear indication of the binding of the paramagnetic complex to the

serum protein. The gain in relaxivity was about a factor of three, approaching the typical values reported for albumin binder Gd-complexes.[4e,4f,17]

To facilitate the reader in the comparison of relaxivity values in different media, Table 1 reports data obtained at 20 MHz, the most common frequency used in the analytical characterization of Gd-complexes, and at 60 MHz, the most common magnetic field strength used in clinic. While saline and i-SBF values are quite constant as the magnetic field strength increases, data in the presence of HSA or in plasma showed a remarkable reduction from 20 to 60 MHz, according to the NMRD data.

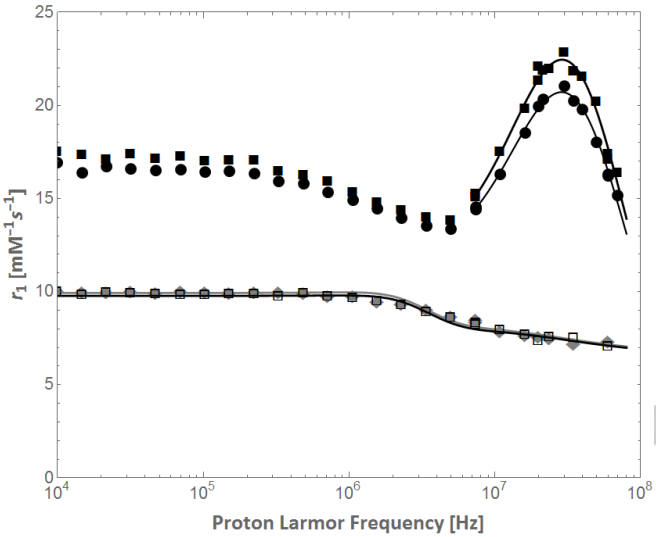

Figure 1. Proton NMRD profiles of (GdDTPA)2-Chol at 310 K in saline (grey diamonds), in i-SBF (empty squares), in saline added with 35 g/L of HSA (filled squares) and in human plasma (filled circles). Solid lines represent the best fittings of each dataset according to a Solomon-Bloemberger inner sphere and outer sphere model (saline and i-SBF) or to Lipari-Szabo model (saline added with HSA and human plasma).

Table 1. Relaxivity values (mM^{-1}s^{-1}) of (GdDTPA)2-Chol at 20 and 60 MHx, 310 K in different media.

Medium	20 MHz	60 MHz
Saline	7.66 ± 0.53	7.61 ± 0.44
i-SBF	7.25 ± 0.25	7.15 ± 0.17
HSA	21.27 ± 0.89	17.01 ± 0.83
Human plasma	19.88 ± 0.27	16.37 ± 0.25

Table 2. Relaxivity values (mM^{-1}s^{-1}) of complex **8**, B22956/1, MS-325 and Gd-DTPA at 20 MHz, 310 K, in different media.

Medium	(GdDTPA)2-Chol	B22956/1[a]	MS325[b]	Gd-DTPA[b]
saline/water	7.7	6.4	5.8	3.4
plasma/serum	19.9	27	28	3.8

[a] Investigator Brochure[11], human serum [b] Rohrer et al., bovine plasma[17]

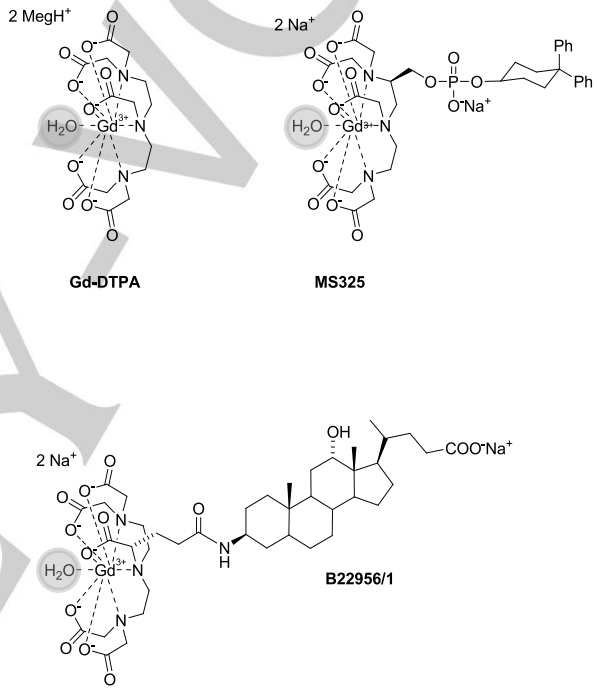

Figure 2. Structure of the complexes selected as reference products. The grey circles highlight the coordinated water molecule, responsible for the inner sphere contribution. The T_1 of the proton of the coordinated water is strongly reduced thanks to the proximity to the Gd ion; moreover, as a consequence of the exchange process between such a molecule and the bulk water, the effect of the paramagnetic ion is transferred to all the surrounding protons.

In addition, Table 2 reports the comparison with the relaxivity values of other Gd-complexes (whose structures are reported in Figure 2) measured in saline (or water) and in plasma (or serum) at 20 MHz. The relaxivity in water is mainly affected by the molecular weight (MW) of the complex, decreasing as the weight of the molecule diminishes. (GdDTPA)2-Chol exhibited a relaxivity of 7.7 mM^{-1}s^{-1} having a MW of 1774 Da, B22956/1 of 6.4 mM^{-1}s^{-1} with a MW of 1059 Da, MS-235 of 5.8 mM^{-1}s^{-1} with a MW of 976 Da and Gd-DTPA of 3.4 mM^{-1}s^{-1} with a MW of 547 Da. However, as observed for dimers and polymers[9c] the gain in relaxivity is often less than expected by the increase of molecular weight, here, despite an increase of about 70% in MW with

respect to B22956/1, the relaxivity of (GdDTPA)2-Chol was only 20% larger. When moving to serum (or plasma), the increment of albumin binder complexes (all but Gd-DTPA) is remarkable (3 to 4 times), with (GdDTPA)2-Chol having a r_1 of 19.9 $mM^{-1}s^{-1}$, slightly inferior than the two albumin binder monomers B22956/1 and MS325. Comparing to albumin binder dimers proposed in literature, one finds the following relaxivity values: 15.25 $mM^{-1}s^{-1}$ in HSA at 37°C for the dinuclear complex decorated with isovaleric acid;[9a] 27.8 $mM^{-1}s^{-1}$ for the complex [Gd2{VA-acamido-pn(DO3VA)2}(H2O)2] proposed by the same authors;[9b] 15.2 $mM^{-1}s^{-1}$ at the same experimental conditions for the dinuclear complex linked to a bisindole derivative of trimethoxybenzaldehyde;[9c] 41.4 $mM^{-1}s^{-1}$ for Gd2L1 presented by Gambino et al.[9e] This latter data did not refer to physiological conditions (where r_1 could be largely inferior), but to the presence of large excess of protein (*i.e.* the concentration of HSA is 1 mM, while that of the complex is 0.07 mM).

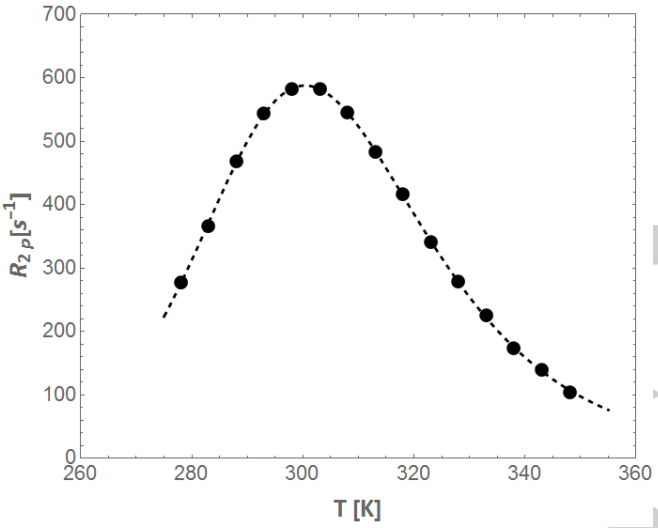

Figure 3. Temperature dependence of water ^{17}O R_{2p} at 14.1 T in the presence of about 15 mM of (GdDTPA)2-Chol.

Additional and more technical information about (GdDTPA)2-Chol have been obtained by fitting the NMRD profiles as well as by acquiring and analyzing the temperature dependence of ^{17}O R_{2p} values in the 280-350 K range (Figure 3). This latter experiment allowed the estimation of the exchange lifetime (τ_M) of the water molecule coordinated to the paramagnetic ion, that resulted to be 68 ± 3 ns. This value is just shorter with respect to B22956/1, that displays a τ_M of 122 ns[4e] and similar to that of MS-325 (τ_M^{310K} = 83 ns[18]). A τ_M in the order of 100 ns is in the optimal range for the attainment of high relaxivity in the presence of long τ_R, as occurs in the presence of a binding to serum protein. The knowledge of τ_M is useful in the interpolation procedure of NMRD experimental data points. Data acquired in saline or i-SBF were fitted according to the classical inner sphere[19] and outer sphere[20] model, based on the Solomon-Bloembergen theory.[21] A summary of the best fitting parameters, in terms of τ_R, zero-field-splitting (ZFS) energy (Δ^2), electronic correlation time for the modulation of the ZFS interaction (τ_v) and electronic relaxation time (τ_{S0}, calculated from the two latter parameters) is reported in Table 3.

Table 3. Best-Fitting Parameters of NMRD Profiles in saline and i-SBF for (GdDTPA)2-Chol

Medium	τ_v [ps]	Δ^2 [10^{19} s^{-2}]	τ_{S0} [ps]	τ_R [ps]
saline	52.1 ± 0.2	1.55 ± 0.03	106 ± 5	180 ± 2
i-SBF	48.8 ± 0.5	1.67 ± 0.05	102 ± 3	178 ± 2

Data obtained in the presence of HSA and in plasma were interpolated only in the range 10^7-10^8 MHz (as commonly reported in literature,[14,22] using a Lipari-Szabo[23] model (that takes into account the presence of motion due to internal rotation) and keeping fixed the electronic parameters estimated above. A summary of the best fitting parameters, in terms of local and global rotational time (τ_l and τ_g) and the order factor (K, indicated also as S^2, which describes the degree of spatial restriction of local motion, K = 0 no restriction, K = 1 fully restriction), is reported in Table 4. A K value of 0.7/0.8 indicates a moderate dominance of the global motion.

Table 4. Best-Fitting Parameters of NMRD Profiles in HSA (35 g/L) and in human plasma for (GdDTPA)2-Chol

Medium	τ_l[ps]	τ_g[ns]	K
HSA	176 ± 3	2.4 ± 0.2	0.745 ± 0.001
plasma	179 ± 5	2.4 ± 0.7	0.666 ± 0.003

Some parameters of the relaxation model were kept fixed during the fitting procedure such as: the hydration number (set to 1), the distance between protons of the coordinated water and Gd ion (0.31 nm), the distance of closest approach of the outer sphere water protons (0.36 nm), the water diffusion constant in saline (2.2 × 10^{-5} cm^2 s^{-1}), saline with 35 g/L HSA (2.9 × 10^{-5} cm^2 s^{-1})[24], and in human plasma (2.28 × 10^{-5} cm^2 s^{-1}, as estimated according to the Einstein-Smoluchowski law under the assumption of spherical particle in a medium of viscosity η equal to 1.2 mPa s). All the other parameters obtained from the data fitting were in the normal range observed for similar gadolinium chelates[4e,9c]. A marked increase of the global rotational time (approx. two orders of magnitude) was observed in the presence of plasma proteins, thus fully supporting the occurrence of protein binding.

Binding of (GdDTPA)2-Chol to serum albumin: The affinity of a gadolinium complex to serum albumin is usually expressed in terms of number of equivalent binding sites (n) with an association constant K_A. These binding parameters, as well as the relaxivity of the supramolecular adduct, were determined using the proton relaxivity enhancement method,[25] which is based on the execution of two titrations. The first one, called M-titration, consists of measuring the relaxation enhancement at fixed HSA

concentration when varying complex concentration, whereas in the second one, called E-titration, the amount of HSA is varied and the gadolinium concentration is kept fixed. Measured data points together with their best fitting interpolations are shown in Figure 4.

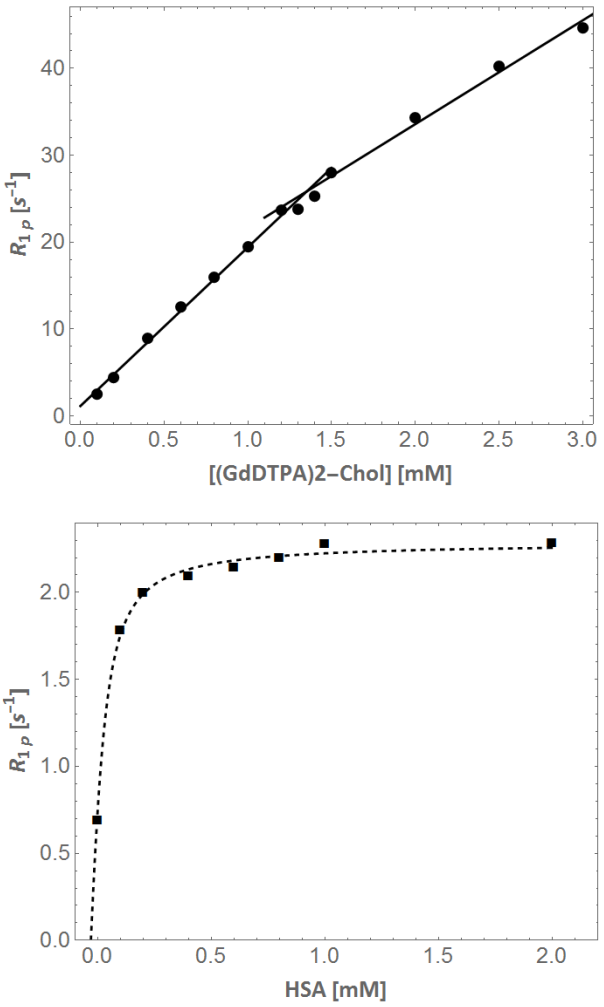

Figure 4. Top panel: Relaxation rate difference ($R_{1p}=R_1 - R_{1d}$,where R_{1d} is the diamagnetic term) as a function of (GdDTPA)2-Chol concentration ranging between 0 and 3 mM for a 0.5 mM solution of HSA. Bottom panel: ΔR_1 as a function of HSA concentration ranging between 0 and 2 mM for a 0.1 mM solution of complex **8**.

The change of slope observed in the M-titration (Figure 4, top) at a (GdDTPA)2-Chol/HSA ratio of about 3 may indicate the presence of three equivalent (*i.e.,* with a similar K_A value) binding sites, while best fitting parameters obtained by fitting E-titration data (Figure 4, bottom) led to an affinity constant K_A of (8.0 ± 1.3) × 10^3 M^{-1} (*i.e.* n K_A = 2.4 × 10^4 M^{-1}) and a relaxivity of the bound fraction r_{1b} of 22.9 ± 0.3 $mM^{-1}s^{-1}$. Since nK_A, rather than K_A alone, better expresses the affinity, the obtained value is similar to other products reported in literature: B22956/1 has a K_A of 4.5×10^4 M^{-1}, [4e] B25716/1 of 2×10^4 M^{-1},[4e] MS-325 of 1.1×10^4 M^{-1} [17] and the dimer described by Parac-Vogt et al.[9c] of 1×10^4 M^{-1}. All of them showed less affinity than the complex Gd-AAZTA-MADEC proposed by Longo et al.,[4f] for which a K_A = 8.9×10^5 M^{-1} was reported. The nature and detailed features of the three binding sites have not been further investigated being out of the scope of the present work. It is worth to notice that even if B22956/1 and (GdDTPA)2-Chol share the same deoxycholic acid residue, they could share one binding site, as well as have completely different mechanism of binding. Dedicated competition studies would be required to collect experimental evidences and knowledge on this topic. As far as the r_{1b} value is concerned, the value obtained for (GdDTPA)2-Chol is very similar to the relaxivity values observed in human plasma, suggesting a bound fraction close to 100%. Therefore, in the absence of leaky vasculature, it is expected that the amount of free agent that can extravasate from the blood pool is very limited, allowing a selective enhancement of the vascular compartment and a marked reduction of the renal excretion. The protein binding characterization was repeated for rat serum albumin, obtaining a comparable affinity to HSA, even if just slightly superior. In the case of B22956/1, the affinity to human and rat serum albumin was evaluated by De Haen et al.[11] in terms of fraction of bound complex and it resulted similar between the two species, despite slightly inferior for rats (86% in rats versus 95% in human). These two observations together suggest that the difference between the fraction of (GdDTPA)2-Chol and B22956/1 bound to albumin can be slightly larger in rats than in human.

Transmetallation of (GdDTPA)2-Chol by zinc(III): Transmetallation assay carried out according to the method described by Laurent et al[26] afforded the curve showed in Figure 5. This easy protocol, which requires very small amounts of product and a simple low-resolution NMR system, allows the study of the *in vitro* transmetallation process of Gd complexes, giving an indication about the relative stability. As clearly observable in Figure 5, (GdDTPA)2-Chol displayed a stability just inferior to the parent Gd-DTPA, and appears to be much more stable than Gd-DTPA-BMA, another well-known commercial agent.

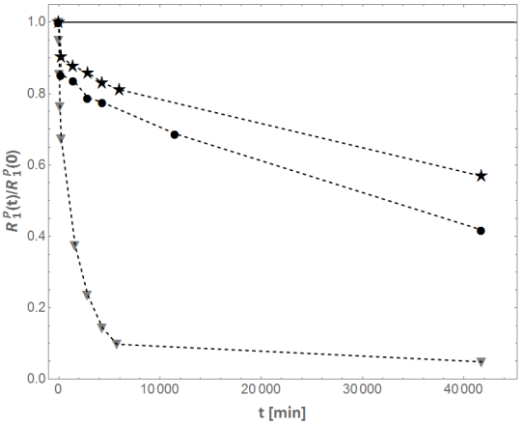

Figure 5. Time evolution of the normalized R_1^P (paramagnetic relaxation rate) at 310 K, 20 MHz for Gd-DTPA-BMA (grey triangles), Gd-DTPA (black stars) and GdDTPA)2-Chol (black dots).

MRI bio-distribution study: The *in vivo* T_{1w} contrast enhancing properties of (GdDTPA)2-Chol were determined on healthy rats at a dosage of 0.05 mmol/kg. The results obtained were compared with B22956/1 (at the same dosage) and Gd-DTPA (at the standard dose of 0.1 mmol/kg). Axial abdominal sections were acquired and signal from liver, cortical kidney, muscle and vessels was evaluated. Figure 6 shows the time course of the percentage signal enhancement in different anatomical districts for the three products up to 60 minutes.

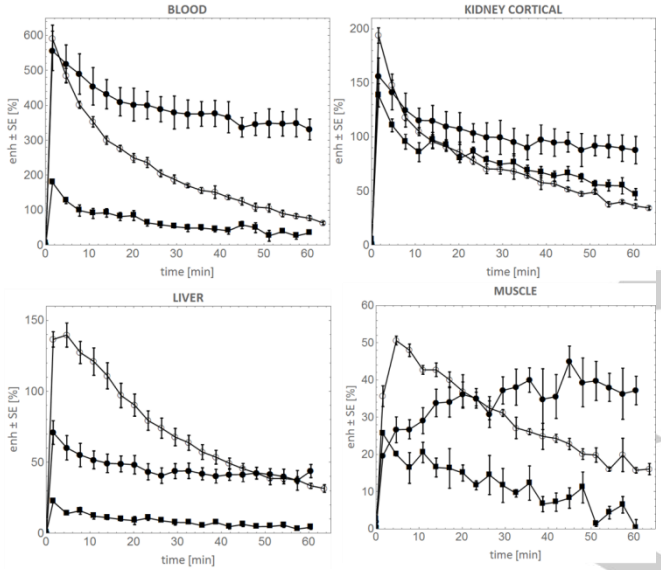

Figure 6. Time evolution of the MRI signal enhancement after administration of (GdDTPA)2-Chol (filled circles), B22956/1 (empty circles) and Gd-DTPA (filled squares) in different anatomical regions.

(GdDTPA)2-Chol and B22956/1 showed comparable maximum enhancement in blood (approx. 600%), while Gd-DTPA reached an about three times lower value, despite the double injected dose. An overall difference factor of six is thus observed, which is well in agreement with the difference in relaxivity (3.8 $mM^{-1}s^{-1}$ for Gd-DTPA vs 20 $mM^{-1}s^{-1}$ for (GdDTPA)2-Chol and 27 $mM^{-1}s^{-1}$ for B22956). Conversely, the roughly 20% higher r_1 of B22956/1 vs (GdDTPA)2-Chol did not translate in a higher enhancement.

(GdDTPA)2-Chol is characterized by a blood kinetic much slower than the remaining CAs. Further insight about this behavior will be discussed in the next section, in the light of blood pharmacokinetic results.

Signal enhancement in kidney is similar for the three CAs, but having in mind the differences in relaxivity, this experimental evidence indicates that the gadolinium concentration in the renal compartment after Gd-DTPA administration is much higher than for the other CAs, indicating the renal route as the main excretion pathway for such agent.

Focusing on the liver compartment, the maximum signal enhancement is different for the three CAs, approaching 150 % for B22956/1, 70% for (GdDTPA)2-Chol and 25% for Gd-DTPA. Once more, a slower kinetic is observed for complex **8**. It is well known that biliary excretion is the favorite route for B22956/1. The average cumulative amounts of Gd that were recovered in feces and in urine after 8 hours following i.v. administration of 0.1 mmol/kg to anesthetized rats corresponded to 85.6% ± 4.3% of the injected dose and 18.2% ± 4.4%, respectively.[11] The completely reverse situation occurs after administration of Gd-DTPA, which is primarily excreted in the urine (90% in rats, as reported in the leaflet). Again, a different behavior was observed for (GdDTPA)2-Chol, with both renal and hepatic excretion much slower than the other CAs and the latter playing a more limited role with respect to what observed after B22956/1 administration. Maximum signal enhancement in muscle reached 50% for B22956/1, 40% for (GdDTPA)2-Chol and 25% for Gd-DTPA. The kinetic of Gd-DTPA and B22956/1 was characterized by a very rapid wash-in and a wash-out comparable with blood compartment. Conversely, for (GdDTPA)2-Chol a very slow wash-in is observed: the signal continuously increases reaching a plateau at the end of the observation window and no wash-out is detected up to 60 minutes.

The slower kinetic of (GdDTPA)2-Chol in all the investigated anatomical districts, and especially the markedly tardy wash-in in muscle, can be accounted for in terms of a higher average (over time and/or over the number of molecules) molecular weight of that complex with respect to the other CAs, meaning that a larger fraction of (GdDTPA)2-Chol is bound to albumin, or that such a bound has a longer residence time. While this is obvious when considering Gd-DTPA, since it does not bind albumin and it has the typical features of an extracellular fluid complex, the explanation is trickier in the case for B22956/1, which is a known albumin binder. The experimental evidences suggest that a larger fraction of (GdDTPA)2-Chol is bound to albumin or that the supra-molecular adduct has a longer residence time. The nK_A values of the two Gd chelates is very similar (4×10^4 M^{-1} and 2.4×10^4 M^{-1} respectively), but a non-identical bound fraction could be a consequence of the different relative abundance of Gd-complex and plasma protein, due to the dimeric structure of (GdDTPA)2-Chol, translating in half the number of Gd-carrying molecules. Moreover, the binding kinetic and the binding strength can differ in principle between the two complexes. A reversible protein binding is in fact always associated with a small, but significant, concentration of free chelate, which continuously undergoes excretion (not only renal but also hepatic in the case of B22956/1, that is known to have a rapid liver uptake) diminishing the plasma half-life.

Pharmacokinetic profile of (GdDTPA)2-Chol: Blood samples were collected at different times after i.v. administration through the tail vein of (GdDTPA)2-Chol, B22956/1 (both at a dosage of 0.05 mmol/kg) and Gd-DTPA (at a dosage of 0.1 mmol/kg) on healthy rats (n=4 animals for each group). Measurement of blood Gd concentration from the collected samples were obtained by

relaxometric method for all rats and confirmed for n=1 representative animal by ICP-MS (see Experimental Section for details). Data acquired with the two techniques resulted to be very similar, with at worst a factor of two (observed for very small concentration values).

Mean data from relaxometry, shown in Figure 7, were interpolated as described in the dedicated section in order to estimate the half elimination time ($t_{1/2\beta}$), then summarized in Table 5, in comparison to literature data.

Table 5. Elimination half time in plasma for different Gd-complexes.

CA	This work $t_{1/2\beta}$ [min]	Literature $t_{1/2\beta}$ [min]
(GdDTPA)2-Chol	128 ± 29	not available
B22956/1	17.5 ± 0.9	23.7(mice)[4f],21(rat males)[11], 26 (rat females)[11]
Gd-DTPA	17.7 ± 0.6	14.94±1.95[9c], 19.6[27]
MS-325	not measured	23[28]

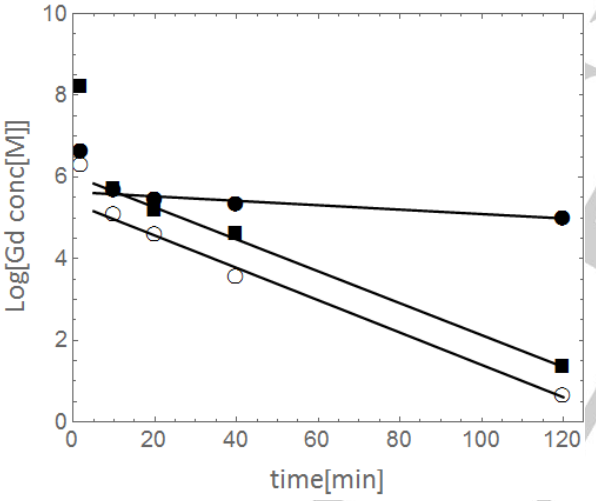

Figure 7. Time evolution of Gd-complex concentration after single intravenous injection of (GdDTPA)2-Chol (filled circles), B22956/1 (empty circles) and Gd-DTPA (filled squares).

As a confirmation of MRI results, elimination half time of (GdDTPA)2-Chol was much longer (approx. 7 times) than the other CAs. It is worth to notice that B22956/1 and MS-325, known as blood pool agent, have a $t_{1/2\beta}$ similar to Gd-DTPA. As well described in literature for MS-325,[28] plasma pharmacokinetics in rats is indistinguishable from that of extracellular agents, because of a rapid liver uptake that decreases the plasma concentration. On the other hand, long plasma half-life (2-3 hours) are observed in rabbits and monkeys, evidence attributable not only to the low free concentration available for renal excretion but also to the lack of hepatocellular uptake. The same explanation applies to B22956/1, which is known to have a high degree of liver uptake and biliary excretion. Conversely, the less efficient hepatic elimination observed by MRI for (GdDTPA)2-Chol is at least a partial explanation for the longer $t_{1/2\beta}$.

Conclusions

A novel albumin-binding dinuclear gadolinium complex has been described in terms of synthetic procedure, full relaxometric characterization, *in vivo* preclinical behavior in an MRI bio-distribution study, and in a blood pharmacokinetic analysis. These latter studies were carried out in comparison with two well-known GBCAs: Gd-DTPA and B22956/1.

Data from NMRD profiles proved that the relaxivity in water is slightly superior to analogue complexes, settling around 7.7 $mM^{-1}s^{-1}$ (water, 310 K, 20 MHz). A noticeable binding affinity toward albumin led to a significant increase of r_1, reaching a value of about 20 $mM^{-1}s^{-1}$ in the range 20-40 MHz, not too far from the operating magnetic field strength of clinical MRI scanners.

A series of features of the presented compound, such as the good affinity to albumin, the high number of binding sites, the properties of carrying two Gd ions for molecules, the limited hepatobiliary elimination, contributed together to an unexpected long blood elimination half time (approx. 130 min, in rats). This fact translates into an optimal confinement in the vascular space and thus into an extension of the available time window for MR angiography, suggesting this agent to be an optimized blood pool with respect to B22956/1 and MS-325, at least for preclinical applications. Moreover, as observed in the healthy muscle, the extravasation inside tissues and especially tumors is expected to last a prolonged period of time, since high molecular weight contrast agents (such as (GdDTPA)2-Chol when bound to protein) slowly and preferentially accumulate in pathological tissues characterized by enhanced vascular permeability and retention (the well-known EPR effect).

The improved MRI properties of (GdDTPA)2-Chol are thus expected to be very useful for MR angiography and dynamic contrast enhanced MRI in preclinical models and potentially translatable in clinic.

Experimental Section

*General information***.** Chemicals and solvents were obtained from commercial sources and used without further purification. Compounds **2**[12] and **5**[14] were synthesized as reported in literature. TLC was performed on Merck silica gel 60 TLC plates F254 and visualized by using UV, 1% $KMnO_4$ in 1M NaOH or ceric ammonium molybdate. Flash chromatography was carried out on silica gel 60 (230-400 mesh). Melting points were determined on a Büchi 540 apparatus and are uncorrected. The ^1H and ^{13}C spectra were recorded on a Bruker AC 200 instrument operating at 4.7 Tesla. Mass spectra were recorded with a ThermoFinnigan TSQ700 triple-quadrupole instrument equipped with an electrospray ionization source. Analytical HPLC was performed on a

Merck-Hitachi L6200 and L6000 system equipped with a L4500 UV detector with the following methods: *Method 1)* stationary phase: Lichrosorb RP-SelectB 5 µm; column 250x4 mm; mobile phase: eluent A=0.01M KH_2PO_4 and 0.017M H_3PO_4 in water, eluent B=acetonitrile; gradient elution: t=0 min (5%B), t=25 min (80%B), t=30 min (80%B); flow rate: 1 mL min^{-1}; detection 210 nm; *Method 2)* Lichrosorb RP-SelectB 5 µm; column 250x4 mm; mobile phase: eluent A=0.017M H_3PO_4 in water, eluent B= acetonitrile; gradient elution: t=0 min (35%B), t=25 min (85%B), t=30 min (85%B); flow rate: 1 mL min^{-1}; detection 210 nm; *Method 3)* stationary phase: Eclipse XDB-C8 3.5 µm; column 150x4.6 mm; mobile phase: eluent A=0.01M KH_2PO_4, 0.01M K_2HPO_4, 0.3mM EDTA in water, eluent B=acetonitrile; gradient elution: t=0 min (7%B), t=5 min (7%B), t=50 min (40%B); flow rate: 1 mL min^{-1}; detection 200 nm. Elemental analyses were performed by Redox laboratories, Monza, Italy.

*Synthesis of **1**.* *N*-ε-Z-Lysine methyl ester hydrochloride (Bachem) (10.6 g; 32.2 mmol) and *N*-(2-bromoethyl)-*N*-[2-(1,1-dimethylethoxy)-2-oxoethyl]glycine 1,1-dimethylethyl ester[13] (27.2 g; 77.1 mmol) were dissolved in acetonitrile (160 mL). To this solution, 2 M phosphate buffer (pH 8, 160 mL) was added and the mixture was vigorously stirred for 2 h. The aqueous phase was replaced with fresh 2 M phosphate buffer (160 mL) and the mixture stirred for more 70 h. The mixture was separated and the organic phase evaporated to give a residue which was dissolved in CH_2Cl_2 (150 mL), washed with water (2 x 100 mL), dried (Na_2SO_4) and evaporated. The crude was purified by flash chromatography (*n*-hexane/EtOAc=7:3) to give a yellow oil (18.1 g) which was dissolved in MeOH (300 mL). To this solution, 5% Pd on carbon (2 g) was added and the mixture was hydrogenated for 4 h. The mixture was filtered through a Millipore® FH 0.5 µm filter, the catalyst was washed with MeOH (50 mL) and the filtrates were evaporated to give **1** as a yellow oil (14.8 g; 21 mmol). Yield 65%. **TLC** R_f 0.13 (*n*-hexane/EtOAc=1:1). **HPLC** 99.0% (area %, method 1). **^{1}H NMR** ($CDCl_3$): δ 1.35 (s, 36H), 1.40-1.66 (bm, 6H), 2.45-2.73 (bm, 13H), 3.31 (s, 8H), 3.55 (s, 3H). **^{13}C NMR** ($CDCl_3$): δ 23.52, 28.06, 29.67, 33.07, 41.70, 50.32, 50.93, 53.65, 55.99, 63.81, 80.73, 170.56, 173.85. **MS** (ESI^+) m/z calcd for $[C_{35}H_{66}N_4O_{10}]$ 702.5, found 352.1 ($M+2H^+$, 48%), 703.6 ($M+H^+$, 100%). **Elemental analysis** calcd (%) for $C_{35}H_{66}N_4O_{10}$: C 59.80, H 9.46, N 7.97; found: C 59.46, H 9.42, N 7.46.

*Synthesis of **3**.* Pivaloyl chloride (4.4 mL; 35.3 mmol) was added dropwise to a solution kept under nitrogen of *trans*-1-(benzyl)-3,4-pyrrolidinedicarboxylic acid **2** (4.0 g; 16.0 mmol) and triethylamine (4.9 mL; 35.3 mmol) in acetonitrile (110 mL) cooled at 0°C. After 20 min at 0°C a solution of N^2,N^2-bis[2-[bis[2-(1,1-dimethylethoxy)-2-oxoethyl]amino]ethyl]-L-lysine methyl ester **1** (24.8 g; 35.3 mmol) in acetonitrile (90 mL) was added dropwise in 10 min. The mixture was allowed to rise to room temperature and after 1 h was evaporated. The residue was dissolved in EtOAc (300 mL), the solution was washed with water (2 x 100 mL), dried (Na_2SO_4) and evaporated. The crude was purified by flash chromatography (*n*-hexane/EtOAc=1:2) to give **3** as a yellow oil (17.5 g; 10.9 mmol). Yield 68%. **TLC** R_f 0.24 (*n*-hexane/EtOAc=1:1). **HPLC** 98.4% (area %, method 1). **^{1}H NMR** ($CDCl_3$): δ 1.38 (s, 72H), 2.5-3.3 (bm, 40H), 3.35 (s, 16H), 3.58 (s, 6H), 3.60 (s, 2H), 6.67 (bm, 2H), 7.23-7.26 (m, 5H).**^{13}C NMR** ($CDCl_3$): δ 23.72, 28.12, 29.18, 29.54, 39.36, 48.07, 50.36, 50.99, 53.67, 56.00, 59.44, 63.70, 80.76, 127.27, 128.38, 128.66, 138.22, 170.57, 173.40, 173.76. **MS** (ESI^+) m/z calcd for $[C_{83}H_{143}N_9O_{22}]$ 1618; found 810 ($M+2H^+$, 100%), 821 ($M+H^++Na^+$, 50%), 1619 ($M+H^+$, 22%). **Elemental analysis** calcd (%) for $C_{83}H_{143}N_9O_{22}$: C 61.57, H 8.90, N 7.79; found: C 61.58, H 8.99, N 7.48.

*Synthesis of **4**.* A mixture of compound **3** (21.6 g; 13.4 mmol), 5% Pd/C (2.2 g) and EtOH (250 mL) was stirred at room temperature for 4 h under hydrogen atmosphere. The mixture was filtered through a Millipore® FH 0.5 µm filter, the catalyst washed with EtOH (80 mL) and the combined solutions were evaporated to give **4** as a yellow oil (18.2 g; 11.9 mmol). Yield 90%. **HPLC** 99.0% (area %, method 1). **^{1}H NMR** ($CDCl_3$): δ 1.38 (s, 72H), 2.5-3.3 (bm, 41H), 3.35 (s, 16H), 3.58 (s, 6H), 6.53 (bm, 2H). **^{13}C NMR** ($CDCl_3$): δ 23.61, 28.12, 29.04, 29.43, 39.37, 49.93, 50.26, 51.02, 51.83, 53.63, 55.99, 63.57, 80.82, 170.61, 173.51, 173.82. **MS** (ESI^+) m/z calcd for $[C_{76}H_{137}N_9O_{22}]$ 1528, found 765 ($M+2H^+$, 78%), 776 ($M+H^++Na^+$, 100%), 1529 ($M+H^+$, 18%). **Elemental analysis** calcd (%) for $C_{76}H_{137}N_9O_{22}$: C 59.70, H 9.03, N 8.24; found: C 59.12, H 9.38, N 7.72.

*Synthesis of **6**.* Compound **4** (17.8 g; 11.7 mmol) was dissolved in dichloromethane (50 mL) and the resulting solution was added dropwise to a solution containing chloroformate **5** (5.5 g; 11.7 mmol), *N*,*N*-diisopropylethylamine (4.5 mL; 25.6 mmol) and dichloromethane (150 mL), kept at 0°C. After the addition the solution was stirred at room temperature for 3 h then was washed with water (2 x 100 mL), dried (Na_2SO_4) and evaporated. The crude was purified by flash chromatography (*n*-hexane/EtOAc=1:2) to give **6** as a yellow oil (17 g; 8.7 mmol). Yield 74%. **TLC** R_f 0.29 (*n*-hexane/EtOAc=1:1). **HPLC** 94.4% (area %, method 2). **^{1}H NMR** spectral data are not reported, being useless for the assignment of the structure due to the broadness and extreme overlapping of the signals. **^{13}C NMR** ($CDCl_3$): δ 12.69, 17.27, 23.09, 23.58, 26.02, 26.99, 27.39, 28.15, 28.76, 29.05, 29.37, 30.89, 31.03, 32.77, 33.63, 34.06, 34.92, 35.06, 35.97, 39.40, 41.86, 46.44, 46.67, 47.25, 48.22, 50.23, 51.03, 51.41, 53.59, 56.01, 63.45, 72.99, 74.91, 80.80, 154.29, 170.63, 173.78, 174.60. **MS** (ESI^+) m/z calcd for $[C_{102}H_{177}N_9O_{27}]$ 1960, found 981 ($M+2H^+$, 100%), 1961 ($M+H^+$, 54%). **Elemental analysis** calcd (%) for $C_{102}H_{177}N_9O_{27}$: C 62.46, H 9.10, N 6.43; found: C 62.15, H 9.16, N 6.32.

*Synthesis of ligand **7**.* A 2 M aqueous solution of LiOH (190 mL) was added dropwise to a solution of compound **6** (14.0 g; 7.1 mmol) in 1,4-dioxane (190 mL) at room temperature. After 26 h the solution was concentrated (150 mL) and 2 M HCl (175 mL) was added dropwise. The precipitate was filtered, washed with water (5 x 50 mL) and vacuum dried. The crude was purified by flash chromatography ($CHCl_3$/MeOH/NH_4OH=6:3:1). The solid obtained was dissolved in water (50 mL) and 1 M HCl (15 mL) was added dropwise until final pH was 1.8. The precipitate was filtered, washed with water (2 x 25 mL) and vacuum dried to give ligand **7** as a white solid (8.7 g; 5.9 mmol). Yield 83%. **m.p.** 210-215°C. **TLC** R_f 0.38 ($CHCl_3$/MeOH/NH_4OH=5:4:2). **HPLC** 98.9% (area %, method 3). **^{1}H NMR** spectral data are not reported, being useless for the assignment of the structure due to the broadness and extreme overlapping of the signals. **^{13}C NMR** (D_2O+KOD): δ 15.39, 19.51, 25.57, 26.25, 28.77, 29.77, 30.28, 31.17, 31.71, 35.11, 36.17, 36.63, 37.35, 38.50, 42.27, 44.57, 48.97, 49.42, 49.97, 50.37, 50.66, 51.60, 54.33, 60.87, 70.36, 76.12, 79.56, 158.73, 175.31, 180.44, 187.08. **MS** (ESI^+) m/z calcd for $[C_{67}H_{107}N_9O_{27}]$ 1469.7, found 736 ($M+2H^+$, 100%), 1470.8 ($M+H^+$, 19%). **Elemental analysis** calcd (%) for $C_{67}H_{107}N_9O_{27}$: C 54.72, H 7.33, N 8.57; found: C 54.84, H 7.38, N 8.77.

*Synthesis of (Gd-DTPA)2-Chol (complex **8**).* Ligand **7** (7.1 g; 4.8 mmol) was suspended in water (200 mL) and dissolved by addition of 1 M NaOH (32 mL) until pH was 6.5. A solution of $GdCl_3$ (3.5 g; 9.6 mmol) in water (20 mL) was added dropwise while keeping pH 6.5 by continuous addition of 1 M NaOH (17.5 mL). After 1 h at room temperature, the solution was loaded onto an Amberlite® XAD 16.00 resin column (400 mL) which was eluted with a H_2O/MeCN gradient (MeCN=0→5%). The fractions containing the product were evaporated to give (Gd-DTPA)2-Chol as a white solid (8.3 g; 4.4 mmol). Yield 92%. **m.p.** >300°C. **HPLC** 100% (area %, method 3). **MS** (ESI^-) m/z calcd for $[C_{67}H_{96}Gd_2N_9Na_5O_{27}]$ 1889, found 443.5 ($M-5Na^++H^+$, 100%), 591.8 ($M-5Na^++2H^+$, 86%), 910.1 ($M-3Na^++H^+$, 27%). **Elemental analysis** calcd (%) for $C_{67}H_{96}Gd_2N_9Na_5O_{27}$: C 42.60, H 5.12, N 6.67, Gd 16.65, Na 6.09; found: C 41.82, H 5.33, N 6.55, Gd 16.28, Na 6.18.

Sample Preparation: In vitro experiments were carried out using (Gd-DTPA)2-Chol diluted properly in the medium of interest to reach the

desired gadolinium concentration. HSA was obtained by Sigma Aldrich (St. Louis, Missouri, USA) and dissolved in saline solution (NaCl 0.9%, Eurospital, Trieste, Italy); human plasma was acquired from Siemens (control Plasma N; Munich, Germany); i-SBF, a buffer fluid (pH=7.4 ± 0.1) with the same concentrations of dissociated ions of human plasma was prepared according to literature.[15]

NMRD Profiles: NMRD profiles of (Gd-DTPA)2-Chol were acquired in different media (saline, human plasma, saline added with 35 g/L of HSA) at 37°C using a Stelar Spinmaster–FFC field-cycling relaxometer (Mede, Italy) over a continuum of magnetic field strengths from 0.00024 to 0.47 T (corresponding to a proton Larmor frequency range of 0.01-20 MHz) and on a Stelar SpinMaster spectrometer ranging from 0.47 to 1.65 T (i.e. 20-70 MHz). The relaxometer switched the magnetic field strength in the millisecond time scale by working under complete computer control with an uncertainty in water proton relaxation rate ($R_1=1/T_1$) of ± 1%. The magnetic field strength of the spectrometer was manually varied by acting on the current flowing in the electromagnet. The temperature was controlled by a Stelar VTC-91 airflow heater, equipped with a copper-constantan thermocouple. Each sample was preheated at 37°C in an external dry block and then left 10 minutes inside the internal air flow to assure the temperature stabilization. Relaxation times at fields below 4 MHz were measured by means of a pre-polarized sequence, whereas points at higher fields were measured by means of a non-polarized sequence. Typical experimental settings included: acquisition field 9.5 MHz, 16 averaged transients, 16 data points for each T_1 measurement. Data points from 0.47 T (20 MHz) to 1.7 T (70 MHz) were collected on a Stelar Spinmaster spectrometer working at adjustable field. T_1 were measured by standard Inversion Recovery pulse sequence with 16 tau-delays and 2 averaged transients.

Relaxometric Characterization: T_1 was measured at a proton Larmor frequency of 20 MHz and 60 MHz and at fixed temperature (310 K) in different media and as a function of HSA concentration by using a spin analyser Minispec MQ-20 and MQ-60 (Bruker Biospin, Rheinstetten, Germany). A standard inversion recovery sequence, where the inversion time varied from 10 ms to at least 5 times T_1 in 15 points was used. The temperature was kept constant using a thermostatic bath connected to the sample holder of the spectrometer.

Interaction with Human Serum Albumin:
The water proton relaxation rate (20 MHz and 37°C) of (Gd-DTPA)2-Chol was measured with the spin analyser Minispec MQ-20 as a function of HSA, with a concentration ranging between 0 and 2 mM at fixed gadolinium concentration (0.1 mM) and as a function of (Gd-DTPA)2-Chol concentration, ranging between 0 and 3 mM at fixed HSA concentration (0.5 mM).

Determination of Gd concentration: The gadolinium concentration of each sample was verified using a relaxometric procedure,[4e] consisting in diluting the samples 1:1 with HCl (37%) and left them overnight at 120°C in a sealed vial. The treatment led to a complete release of Gd(III) as free-aqua ion, thus allowing the determination of its concentration by measurements of r_1 at 25°C. The following equation was used to estimate Gd(III) concentration: $R_1=R_{1d}+r_{1Gd(III)}\cdot[Gd(III)]$, in which R_{1d} is the diamagnetic contribution.

^{17}O NMR measurements: aqueous solutions of (Gd-DTPA)2-Chol containing 5% of ^{17}O (Yeda, Israel) were used to perform variable temperature ^{17}O NMR measurements at 14 T with a Bruker ADVANCE600 spectrometer, equipped with a 5 mm probe. A D_2O external lock was used. The observed transverse relaxation rate R^{obs}_{2p} was calculated from the signal full width at half height ($\Delta_{1/2}$): $R^{obs}_{2p} = \pi \cdot \Delta_{1/2}$ and R_{2p} (i.e. the paramagnetic contribution) was obtained by subtracting the diamagnetic contribution.

Transmetallation: Transmetallation by $ZnBr_2$ was evaluated by measuring the decrease of water longitudinal relaxation rate at 37°C and 20 MHz (Minispec MQ-20, Bruker Biospin, Rheinstetten, Germany) of buffered phosphate solutions (pH=7, $[KH_2PO_4]$=26 mM, $[Na_2HPO_4]$= 41 mM containing 2.5 mM of GBCA and 2.5 mM of Zn^{2+} according to the protocol reported in literature.[25]

In vivo characterization: All the procedures involving the animals were conducted according to the national and international laws on experimental animals (L.D. 26/2014; Directive 2010/63/EU). 4 weeks old adult male Wistar Rats (n=12) (Charles River Laboratories, Calco (LC), Italy) were housed in groups of 3. A 5 day acclimation period was given before the experiments. Animals were kept in limited access, air-conditioned facilities (20-24°C room temperature, 45-55% relative humidity, 15-20 air changes/h, 12-h light cycle). Food and water were available at libitum.

MRI in vivo bio distribution: MR experiments were performed using an Icon spectrometer (Bruker Biospin, Germany) operating at 1 T (i.e. at a proton Larmor frequency of 42 MHz). During MRI experiment, animals were anaesthetized with isoflurane gas (about 1%) in O_2. Anesthesia was maintained by adjustment of gas level in function of breath rate. Before injection of each test article, ^1H sequences (RARE T_2-weighted) were acquired on the animal in order to have a proper anatomical reference. A series of T_1-weighted 3D-FLASH (Repetition Time = 50 ms, Flip Angle = 50°, Echo Time = 5.4 ms, Number of averages = 2, Matrix Size (3D) = 192x192x8, Field of view = 5 x 5 x 1.6 cm; Acquisition time = 153 s) scans were then acquired before and after the intravenous administration of an aqueous solution of Gd-DTPA (50 mM, n=3), B22956/1 (25 mM, n=4) and (Gd-DTPA)2-Chol (25 mM, n=4) at an injection rate of about 2 mL/min through a catheter placed in the tail vein of the animal. Gd-DTPA was administered at a dose of 0.1 mmol/kg, while the remaining two agents were administered at a dose of 0.05 mmol/kg corresponding to an administration volume of 2 mL/kg. The kinetic of the Gd chelates was followed up to 60 minutes post injection.
Image analysis was performed by positioning the region of interest (ROIs) over liver, kidney, muscle and blood vessel. ROIs positioning and signal quantification was performed by using a home-developed plugin, running on ImageJ (imagej.nih.gov/ij/). Signal enhancement (Enh) was calculated as follows: Enh = 100 ($Signal_{postCA}$ - $Signal_{preCA}$) / $Signal_{preCA}$, where $Signal_{preCA}$ and $Signal_{postCA}$ indicate MR signal before and after contrast agents administration.
Mean and standard deviation of the enhancement over the groups were calculated by using Excel (Microsoft, USA). Plots were performed with Mathematica (Wolfram, USA).

Pharmacokinetics Study: The pharmacokinetic study took place at least two weeks after the MRI experiments, on the same rats (n=4 per group). At least 24 hours before test article injection, all animals were put under gas anesthesia and a blood volume of 200 µL was sampled from the caudal vein. The pharmacokinetic study took place at least 24 hours after the pre-dosing sampling. The animals were kept under gas anesthesia for all the duration of the experiments and breath rate was maintained at 45-50 breaths per minute. Gd-DTPA was administered at a dose of 0.1 mmol/kg, while (Gd-DTPA)2-Chol and B22956/1 were administered at a dose of 0.05 mmol/kg corresponding to an administration volume of 2 mL/kg.

Relaxometric measurements: Collected blood samples were transferred in NMR tubes and T_1 was measured at 20 MHz and 37°C using the Minispec MQ-20 spectrometer. Gadolinium concentration ([Gd]) was evaluated

according to the following formula: $[Gd] = (1/T_1-1/T_{10})/r_1$, where T_{10} and T_1 are the longitudinal relaxation time before and after CA administration, while r_1 is the relaxivity of the CA, according to literature data or internal measurements. Interpolation of data of Gd concentration as a function of time post administration was performed with Mathematica (Wolfram, USA). Specifically, the terminal phase elimination rate constant was estimated by log-linear regression of those data points visually assessed to be in the terminal phase of the profile.

ICP-MS measurements and analytical conditions: A selection of blood samples already measured by NMR were analyzed by ICP-MS. For this latter analysis samples were prepared by mixing the collected 0.2 mL of blood in 0.4 mL of nitric acid (65% w/w). Sample digestion for the destruction of the organic matrix was performed by subjecting the samples to a wet ashing process with a microwave oven system (MARS-5 CEM Corporation). ICP-MS assay was carried out on an ELAN 6100 Perkin Elmer Spectrometer. The LOQ (Limit of Quantitation) for gadolinium in blood was 0.010 µg (value verified with recovery study on 0.2 mL of blood sample). Data from the two assays were compared as internal check of data reliability.

Acknowledgements

The authors acknowledge Simona Baroni, Elisa De Laurentis, Roberto Celeste, Luca Biondi and Pietro Irrera for their important technical contribution in the acquisition of NMRD profiles, ICP data, sample mineralization, ^{17}O-R_{2p} profiles and pharmacokinetic study, respectively.

Keywords: GBCA • dinuclear • HSA • blood pool • MRI

[1] a) D. B. Plewes, W. Kucharczyk, *J. Magn. Reson. Imaging.* **2012**, *35*, 1038-1054; b) C. Westbrook, C. Kaut Roth, J. Talbot, *MRI in Practice*, Wiley-Blackwell, Chichester, 4th edn, **2011**.

[2] a) A. Merbach, L. Helm, É. Tóth, *The Chemistry of Contrast Agents in Medical Magnetic Resonance Imaging*, Wiley VCH, Weinheim, 2nd edn, **2013**; b) C. F. G. C. Geraldes, S. Laurent, *Contrast Media Mol. Imaging* **2009**, *4*, 1-23; c) P. Hermann, J. Kotek, V. Kubíček, I. Lukeš, *Dalton Trans.***2008**, 3027-3047.

[3] J. Lohrke, T. Frenzel, J. Endrikat, F. C. Alves, T. M. Grist, M. Law, J. M. Lee, T. Leiner, K-C. Li, K. Nikolaou, M. R. Prince, H. H. Schild, J. C. Weinreb, K. Yoshikawa, H. Pietsch, *Adv. Ther.* **2016**, *33*, 1-28.

[4] a) M. Salerno, D. S. D. Porqueras, *Coord. Chem. Rev.* **2016**, *327-328*, 27-34; b) G-L. Davies, I. Kramberger, J. J. Davies, *Chem. Commun.* **2013**, *49*, 9704-9721; c) Z. Zhou, Z-R. Lu, *WIREs Nanomed. Nanobiotechnol.* **2013**, *5*, 1–18; P. d) Fries, A. Müller, R. Seidel, P. Robert, G Denda., M. D. Menger, G. Schneider, A. Buecker, *Invest Radiol*. **2015**, *50*, 835-842; e) E. Gianolio, C. Cabella, S. Colombo Serra, G. Valbusa, F. Arena, A. Maiocchi, L. Miragoli, F. Tedoldi, F. Uggeri, M. Visigalli, P. Bardini, S. Aime, *J. Biol. Inorg. Chem.* **2014**, *19*, 715–726. f) D. L. Longo, F. Arena, L. Consolino, P. Minazzi, S. Geninatti-Crich, G. B. Giovenzana, S. Aime, *Biomaterials* **2016**, *75*, 47-57.

[5] a) A. Accardo, D. Tesauro, L. Aloj, C. Pedone, G. Morelli, *Coord. Chem. Rev.* **2009**, *253*, 2193-2213; b) E. Terreno, D Delli Castelli, A. Viale, S. Aime S. *Chem Rev.* **2010**, 110, 3019-3042.

[6] a) J. Tang, Y. Sheng, H. Hu, Y. Shen, *Prog. Polymer Sci.* **2013**, *38*, 462-502; b) M. Botta, L. Tei, *Eur. J. Inorg. Chem.* **2012**, 1945-1960; c) A. J. L. Villaraza, A. Bumb, M. W. Brechbiel, *Chem. Rev.* **2010**, *110*, 2921-2959.

[7] P. Caravan, *Acc. Chem. Res.* **2009**, *42*, 851-862.

[8] A. Gossmann, Y. Okuhata, D. M. Shames, T. H. Helbich, T. P. L. Roberts, M. F. Wendland, S. Huber, R. C. Brasch, *Radiology* **1999**, *213*, 265-272.

[9] a) T. L. Pushparaj, V. Alexander, *Int. J. Appl. Bioeng.* **2016**, *10*, 11-17; b) T. L. Pushparaj, V. Alexander, *Int. J. Sci. Eng. Res.* **2016**, *7(12)*, 1600-1605. c) T. N. Parac-Vogt, K. Kimpe, S. Laurent, L. Vander Elst, C. Burtea, F. Chen, R. B. Muller, Y. Ni, A. Verbruggen, K. Binnemans, *Chem. Eur. J.* **2005**, *11*, 3077-3086; d) V. V. Martin, W. H. Ralston, M. R. Hynes, J. F. W. Keana, *Bioconjugate Chem.* **1995,** *6*, 616 –623; e) G. Gambino, S. De Pinto, L. Tei, C. Cassino, F. Arena, E. Gianolio, M. Botta. *J. Biol. Inorg. Chem.* **2014**, *19*, 133–143.

[10] R. Felix, A. Heshiki, N. Hosten, H. Hricak, *Magnevist Monograph*, Blackwell Science, Oxford, 3rd edn, 1998.

[11] C. de Haën, P. L. Anelli, V. Lorusso, A. Morisetti, F. Maggioni, J. Zheng, F. Uggeri, F. M. Cavagna, *Invest. Radiol.* **2006**, *41*, 279-291.

[12] M. Joucla, J. Mortier, *Bull. Soc. Chim. Fr.* **1988**, 579-583.

[13] M. A. Williams, H. Rapoport, *J. Org. Chem.* **1993**, *58*, 1151-1158

[14] S. Baroni, S. Colombo Serra, A. Fringuello Mingo, G. Lux, G. B. Giovenzana, L. Lattuada, *Chemistry Select* **2016**, 1, 1607-1612.

[15] A. Oyane, K. Onuma, A. Ito, H. M. Kim, T. Kokubo, T. Nakamura, *J. Biomed. Mater. Res.* **2003**, *64A*, 339-348.

[16] a) S Aime, M Botta, M Fasano, E Terreno, *Acc. Chem. Res*. **1999**, *32*, 941-949; b) A. Fringuello Mingo, S. Colombo Serra, S. Baroni, C. Cabella, R. Napolitano, I. Hawala, L. Lattuada, F. Tedoldi, I. M. Carnovale S. Aime, *Magn Reson Med.* **2017**;*78*, 1523-1532.

[17] M. Rohrer, H. Bauer, J. Mintorovitch, M. Requardt, H-J. Weinmann, *Invest. Radiol.* **2005**, *40*, 715–724.

[18] P. Caravan, N. J. Cloutier, M. T. Greenfield, S. A. McDermid, S. U. Dunham, J. W. M. Bulte, J. C. Amedio Jr., R. J. Looby, R. M. Supkowski, W. DeW. Horrocks Jr., T. J. McMurry, R. B. Lauffer, *J. Am. Chem. Soc.* **2002**, *124*, 3152 –3162.

[19] a) N. Blombergen, *J. Chem. Phys.* **1957**, *27*, 572–573; b) Solomon, *Phys. Rev.* **1955**, *99*, 559–565.

[20] J. Freed, *J. Chem. Phys.* **1978**, *68*, 4034–4037.

[21] S. Aime, M. Botta, E. Terreno. *Adv. Inorg. Chem.* **2005**, *57*, 173–237.

[22] G. A. Rolla, M. Botta, L. Tei, C. Cabella, S. Ghiani, C. Brioschi, A. Maiocchi. *Chem. Eur. J.* **2013**, *19*, 11189-11193.

[23] a) G. Lipari, A. Szabo, *J. Am. Chem. Soc.* **1982**, *104*, 4546–4559; b) G. Lipari, A. Szabo*, J. Am. Chem. Soc***. 1982**, *104*, 4559–4570.

[24] L. Vander Elst, A. Sessoye, S. Laurent, R. N. Muller., *Helv. Chim. Acta*, **2005**, *88*, 574-587.

[25] S. Aime, M. Fasano, E. Terreno, M. Botta in *The Chemistry of Contrast Agents in Medical Magnetic Resonance Imaging*, (Eds.: A. E. Merbach, É. Tóth), Wiley VCH, Weinheim, 1st edn, **2001**, pp. 193-242.

[26] S. Laurent, L. Vander Elst, F. Copoix, R. N. Muller, *Invest. Radiol.* **2001**, *36*, 115-122.

[27] H. J. Weinmann, R. C. Brasch W. R., Press, G. E. Wesbey, *Am. J. Roentgenol.* **1984**, *142*, 619-624.

[28] D. J. Parmelee, R. C. Walovitch, H. S. Ouellet, R. B. Lauffer, *Invest Radiol.* **1997**, *32*, 741-747.

10.1002/cmdc.201800052

WILEY-VCH

Entry for the Table of Contents

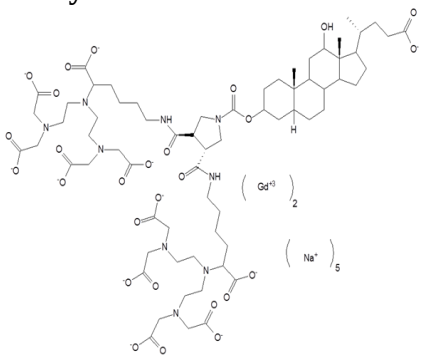

A novel dinuclear gadolinium(III) chelate, covalently conjugated to an analogue of deoxycholic acid is presented. The complex showed a fairly high relaxivity ($20mM^{-1}s^{-1}$) and a strong interaction with human serum albumin in three binding sites. This property translate in long blood elimination half time and in a macromolecule-like behavior, revealing the product as an optimal blood-pool agent.

Received: 24 September 2018 | Revised: 6 December 2018 | Accepted: 7 December 2018

DOI: 10.1002/ame2.12050

TECHNICAL NOTE

Orthotopic induction of CH157MN convexity and skull base meningiomas into nude mice using stereotactic surgery and MRI characterization

Francesca La Cava[1] | Alberto Fringuello Mingo[2] | Pietro Irrera[1] | Aldo Di Vito[2] | Alessia Cordaro[2] | Chiara Brioschi[2] | Sonia Colombo Serra[2] | Claudia Cabella[2] | Enzo Terreno[1] | Luigi Miragoli[2]

[1]Department of Molecular Biotechnologies and Health Sciences, Center of Excellence for Preclinical Imaging (CEIP), University of Torino, Colleretto Giacosa, TO, Italy

[2]Bracco Research Centre, Bracco Imaging SpA, Colleretto Giacosa, TO, Italy

Correspondence
Francesca La Cava, Department of Molecular Biotechnologies and Health Sciences, Center of Excellence for Preclinical Imaging (CEIP), University of Torino, Colleretto Giacosa, TO, Italy.
Email: flacava@unito.it

Abstract

Meningioma in vivo research is hampered by the difficulty of establishing an easy and reproducible orthotopic model able to mimic the characteristics of a human meningioma. Moreover, leptomeningeal dissemination and high mortality are often associated with such orthotopical models, making them useless for clinical translation studies. An optimized method for inducing meningiomas in nude mice at two different sites is described in this paper and the high reproducibility and low mortality of the models are demonstrated. Skull base meningiomas were induced in the auditory meatus and convexity meningiomas were induced on the brain surface of 23 and 24 nude mice, respectively. Both models led to the development of a mass easily observable by imaging methods. Dynamic contrast enhanced MRI was used as a tool to monitor and characterize the pathology onset and progression. At the end of the study, histology was performed to confirm the neoplastic origin of the diseased mass.

KEYWORDS

animal models, neuroscience, pharmaceutical development, preclinical imaging, solid tumors

1 | INTRODUCTION

This study focuses on the induction of two orthotopic meningioma models: a skull base meningioma of the auditory meatus, and a convexity meningioma. The models were selected as examples of meningioma tumors in mice, to be used in preclinical studies for translational research, being examples of brain tumors with the highest incidence. Despite the relatively low mortality characterizing these human meningiomas, the development of early diagnostic tools and/or effective therapies is extremely important to improve the outcome of the medical treatment of this pathology.[1,2]

Both models were induced using the CH157MN cell line, isolated in 1977 from a 41-year-old woman.[3] This line was selected because of its ability to reproduce histological, immunohistochemical and structural features of human meningioma. A CH157MN model has been described by Ragel et al[4,5] in 2007 and 2008, but these papers focused on characterization of the model via luciferase rather than on a description of the induction or characterization by MRI (tumors

were imaged post mortem by MRI, but only to calculate tumor volume, rather than to give a precise localization and description of the model in real time). Similarly, Giogigeni et al[6] and Karsy et al[7] adopted the model, but they used bioluminescence imaging to monitor tumor growth and response to treatment. Using this methodology, it was possible to approximate the effectiveness of treatment by observing a reduction in tumor mass. However, since bioluminescence imaging lacks resolution, it was not possible to determine the precise location and characteristics of the tumors because their burden, depth, and localization could not be accurately measured. In our study, 47 athymic female nude mice (5-6 weeks old) were inoculated with CH157MN cells and imaged weekly on a 1 T scanner, before and after administration of a commercial gadolinium based contrast agent (GBCA). MRI provided a non-invasive method of accurately evaluating of tumor growth, vascularization and GBCA perfusion/permeability.

2 | PROTOCOL

All the procedures involving animals were conducted according to national and international laws for the care and use of laboratory animals (L.D. 26/2014; Directive 2010/63/EU). This experimental protocol was approved by the Italian Ministry of Health with Authorization 724/2017 PR.

CH157MN cells were cultured in DMEM F12 with 7% FBS. For tumor induction, they were resuspended in 3-8 μL of serum-free DMEM F12.

2.1 | Tumor induction

Mice were subcutaneously injected with carprofen (5 mg/kg) 1 hour before the surgery. Anesthesia was induced with sevoflurane gas and then maintained systemically with Rompun® (5 mg/kg) and Zoletil® (40 mg/kg). Each mouse was then mounted on the stereotaxic apparatus and its temperature was continuously monitored and maintained in the range 36.5-38.5°C. After cleaning the skin with a disinfectant (iodopovidone), a local anesthesia was administered (lidocaine) at a dose of 3 mg/kg. Bregma was then exposed and the induction sites identified using the following coordinates: 3 mm anterior, 2 mm lateral to bregma and 2 mm under the frontal bone for the convexity meningioma, and at the skull base (13-14 mm) for Skull Base Meningioma. At each site, a small hole was drilled manually, and 3-8 μL of cell suspension, containing 5×10^4-5×10^5 CH157MN cells for the skull base site and 10^5-10^6 cells for the convexity site, was injected manually at a rate of approximately 1 μL/3 min using a Hamilton syringe with 25G needle. The hole was closed using either bone wax or surgical glue after removing the needle, and the mouse was removed from the stereotaxic apparatus. The wound was sutured with surgical glue or silk thread. Carprofen (5 mg/kg) was subcutaneously administered for 3 days after surgery. For more information, see Supporting Information.

2.2 | Imaging protocol

Mice were imaged once or twice a week using a 1 T Icon (Bruker Biospin, Ettlingen, Germany) scanner. After preliminary anatomical scans, MSME sequences were acquired before and after the intravenous administration of the GBCA. The following parameters were set: matrix size = 128 × 128, field of view = 1.6 × 1.6 cm, slice thickness 1.2 mm, TE (echo time) = 9.2 milliseconds, TR (repetition time) = 350 milliseconds, acquisition time = 90 seconds, NA = 2.

3 | RESULTS

CH157MN meningiomas were induced in 47 nude mice, according to the experimental protocols summarized in Table 1. The induction was successful in 35/47 animals. Specifically:

- 15/24 mice developed skull base meningiomas (four mice did not survive the systemic anesthesia and one showed clinical signs immediately after the surgery; four mice did not develop any tumors).
- 20/23 mice developed convexity meningiomas (one mouse did not survive the systemic anesthesia; two mice did not develop any tumors).

As detailed in Table 1, once the inoculation site had been set, different experimental conditions were tested (ie the cell number and the method adopted to suture the surgical wound) to optimize the protocol.

The convexity meningioma model was generally more successful than the skull base model, in terms of both surgical procedure and animal welfare. Specifically, the intra-operative mortality was lower for three out of four groups inoculated superficially, indicating, as expected, a minor surgery risk, since the needle stops at the surface rather than passing through the brain to reach the auditory meatus. Even after surgery, the occurrence of clinical signs was more severe in the skull base model, with the appearance of unsteady gait, domed head and loss of equilibrium. Loss of equilibrium was probably due to the specific location of the tumor in the auditory meatus. A further advantage of the convexity model was that the tumor take rate was superior. Tumor volume, growth rate and maximum enhancement after GBCA administration were comparable between the two sites. All the different procedures to close the skull hole adopted for both the skull base and convexity meningioma models were effective at avoiding the appearance of any extra-cranial mass. Surgical glue is preferred to silk thread for suturing the wound, to prevent the animal from opening the wound by over-grooming.

A standard needle was used during cell inoculation in only three animals. For all the other experimental groups the tip of the needle was cut, since only one animal out of the three inoculated using a standard needle developed an observable tumor mass; most likely the standard tip prevented release of tumor cells.

TABLE 1 Experimental scheme and results

Group	Total animals	Cell number/suture procedure	Site	Stereotaxic coordinates	Intraoperatory mortality	Tumor take rate	Average tumor volume (mm^3)	Average maximum enhancement (%)	Clinical signs
1	6	5×10^4 suspended in 3 μL, surgical glue to seal/suture both the skull hole and the wound	Skull base	Ant. 3 mm, Lat. 2 mm, Vent. 12-13 mm and needle with tip; Ant. 3 mm, Lat. 2 mm, Vent. at skull and needle without tip	1/6	4/5	55	80	Neurological damage, unsteady gait, tumbling, apathy
2	6	5×10^5 suspended in 3 μL, surgical glue to seal/suture the skull hole and the wound	Skull base	Ant. 3 mm, Lat. 2 mm, Vent. at skull and needle without tip	1/6	3/5	85	70	No observations
3	6	5×10^4 suspended in 3 μL, silk thread (5.0) to suture the wound	Skull base	Ant. 3 mm, Lat. 2 mm, Vent. at skull and needle without tip	1/6	2/5	45	70	Loss body weight <8%, dyspnea, isolation from the group, dehydration, closed eye lids, unsteady gait
4	6	5×10^5 suspended in 5 μL, silk thread (5.0) to suture the wound	Skull base	Ant. 3 mm, Lat. 2 mm, Vent. at skull and needle without tip	2/6	4/4	50	55	Tachipnea, isolation from the group, immobility, closed lid eye, loss of coordination and equilibrium
5	6	10^5 suspended in 3 μL, surgical glue to seal/suture the skull hole and the wound	Convexity	Ant. 3 mm, Lat. 2 mm, Vent. 2 mm and needle without tip	1/6	5/5	62	70	Domed head
6	5	10^6 suspended in 8 μL, surgical glue to seal/suture the skull hole and the wound	Convexity	Ant. 3 mm, Lat. 2 mm, Vent. 2 mm and needle without tip	0/5	4/5	50	70	No observations
7	6	10^5 suspended in 3 μL, bone wax to seal the skull hole and silk thread (5.0) to suture the wound	Convexity	Ant. 3 mm, Lat. 2 mm, Vent. 2 mm and needle without tip	0/6	5/6	40	80	Domed head and retracted eyes
8	6	10^6 suspended in a 6 μL, bone wax to seal the skull hole and silk thread (5.0) to suture the wound	Convexity	Ant. 3 mm, Lat. 2 mm, Vent. 2 mm and needle without tip	0/6	5/6	50	60	Domed head and retracted eyes

From 1 week after tumor induction to the end of the observation period (ie, 30 days after tumor induction) or the occurrence of one of the end-points (ie, tumor mass larger than 0.15 cm^3, weight loss ≥20%), animals without significant or prolonged clinical signs were imaged weekly (or more frequently) using MRI and administered with GBCA in the presence of a clearly visible tumor mass. In the case of skull base meningiomas, euthanasia after the occurrence of severe or prolonged clinical signs was required for 10 animals: two animals just after the surgical procedure, one animal 1 week post tumor induction and seven animals 2 weeks post tumor induction. In the case of the convexity meningiomas, euthanasia was required for four animals: two animals 1 week post tumor induction and two animals 2 weeks post tumor induction.

A tumor mass was generally visible 1 week-10 days after induction at both inoculation sites, as shown for representative animals in all geometrical sections of T_2-weighted images (Figure 1A and 1B). T_1-weighted images (pre- and post-contrast) together with signal enhancement vs time quantification are shown in panels A and B of Figure 2 for skull base and convexity meningiomas, respectively. In pre-contrast images, brain tissue and tumor mass gave the same signal, but after GBCA administration the diseased tissue gave an enhanced signal and was clearly distinguishable from the contralateral region, ie auditory meatus for skull base meningioma and healthy brain for convexity meningioma. The tumor mass was enhanced by between 50% and 120% in all images with two exceptions, immediately after induction and when the tumor mass was not yet well developed. Finally, meningioma identity and tissue vascularization were assessed by histological analysis. Both CH157MN orthotopic tumors exhibited histological analogies with human grade III meningioma tumor, such as nuclear polymorphism, large cells with eccentric nuclei and abundant cytoplasm and mitosis (Figure 3). The tumors displayed infiltrative growth, widespread vascularization and, often, the presence of hemorrhages.

4 | DISCUSSION

Meningiomas have a 30% of incidence rate in humans. Even though they are mostly benign tumors, their intracranial location makes it difficult to remove them surgically, often leading to serious and potentially lethal outcomes. There is a need in preclinical brain tumor research for a reliable model of preclinical meningioma that is reproducible and well characterized. Here we describe and characterize two models of meningioma: skull base and convexity meningiomas in nude mice. Skull base meningiomas were successfully induced in the auditory meatus of female nude mice. There are some critical steps in the induction of this model that should be performed for the correct induction of the tumor. In particular, an optimal ventral coordinate of 14 mm from the dura mater to the skull base site was identified based on the fact that the needle encountered resistance when moved further. This value is correct if the mouse used is the same strain, sex and age as we describe. Another important step for a correct induction is the rate of cellular release into the auditory meatus. A large volume of medium is needed to keep cells in suspension, so it is important that the release happens slowly and carefully. An accumulation of fluid in the auditory meatus could cause

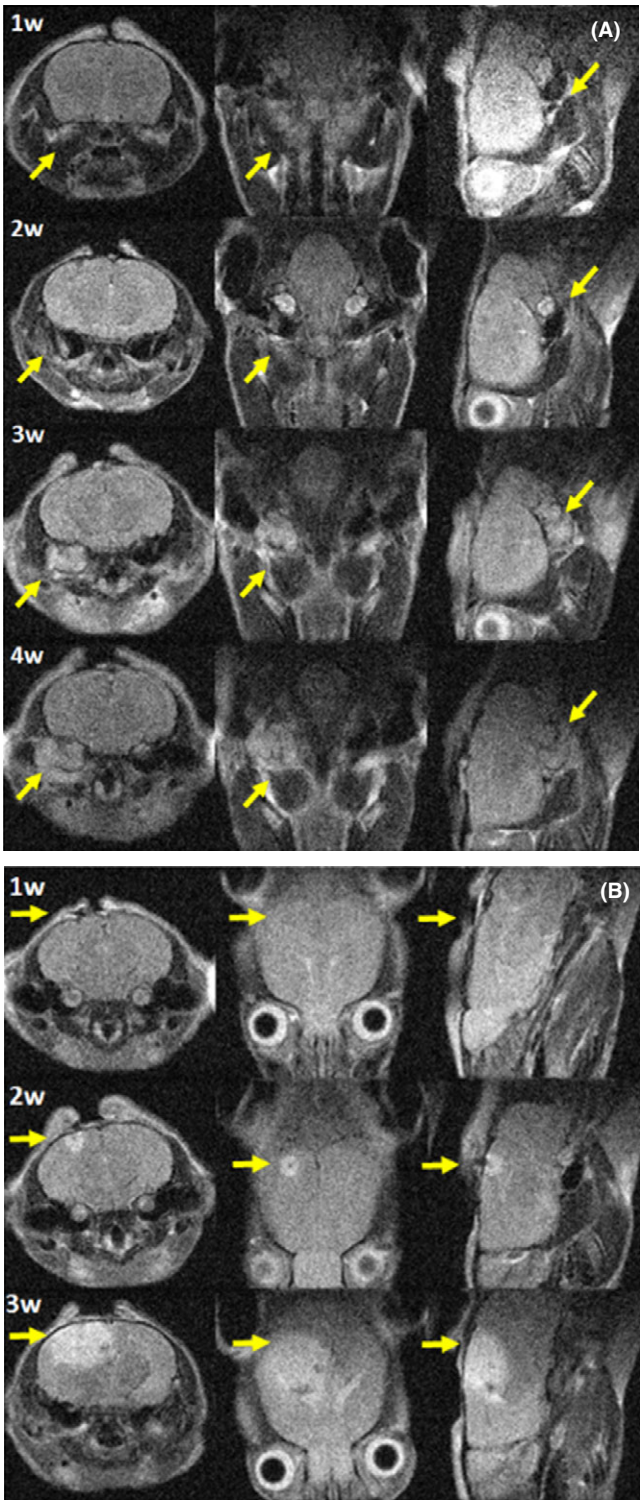

FIGURE 1 Representative anatomical T2-weighted images at different weeks post tumor induction in all geometrical sections (from left to right axial, coronal and sagittal). A, skull base meningioma and B, convexity meningioma

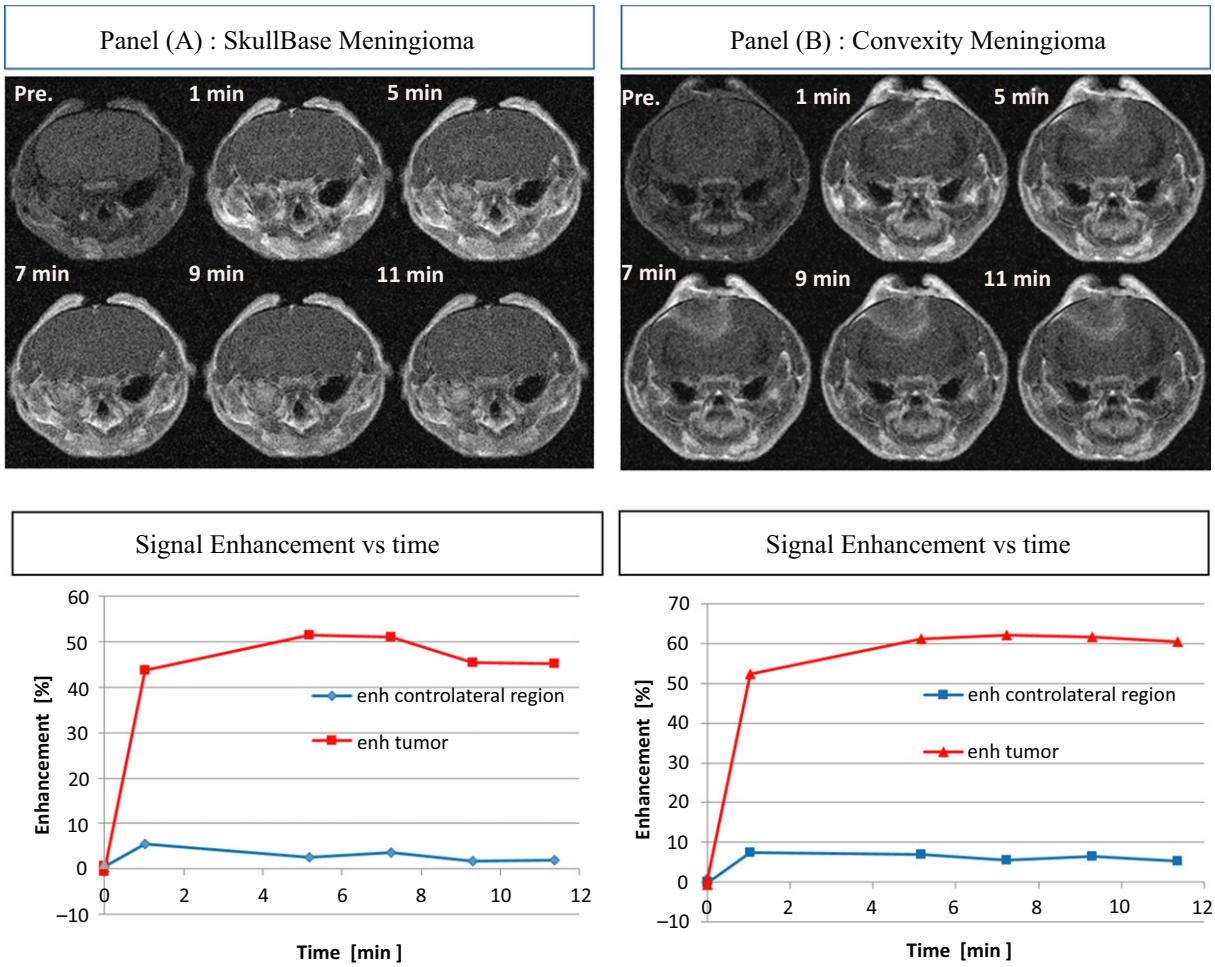

FIGURE 2 A, Skull Base and B, Convexity Meningioma Representative contrast enhanced T1-weighted images and MSME signal enhancement as a function of time for healthy contralateral tissue (blue) and tumor mass (red)

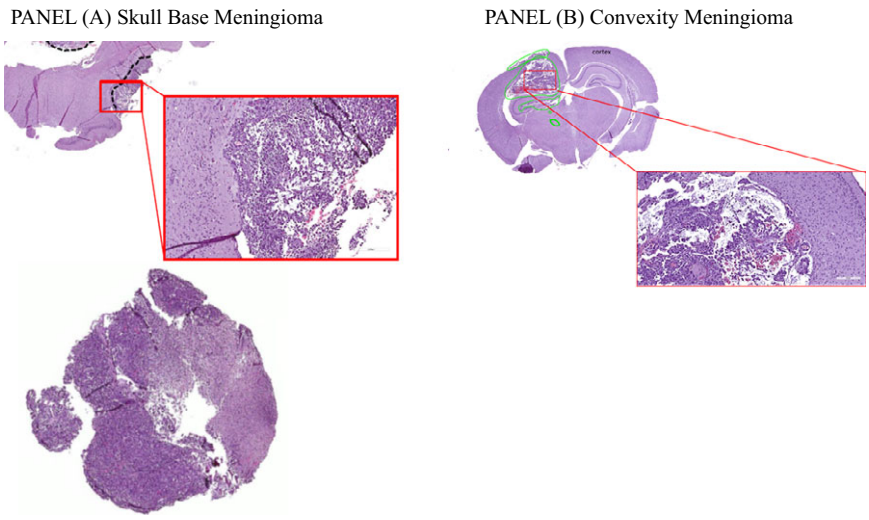

FIGURE 3 Representative examples of histological images of A, skull base meningioma, and B, convexity

severe clinical symptoms such as loss of equilibrium at the end of the procedure. Convexity meningiomas were easier to induce and overall caused fewer clinical symptoms and required less troubleshooting. However, the dura mater should be preserved for a successful induction. In particular, it should not be damaged when drilling through the skull: the hole should be drilled manually and the operator should use magnifying glasses. Drilling should stop when the drill encounters less resistance.

Non-invasive MRI was used from early in the development of the tumors to characterize in real time the evolution of the cerebral pathologies. The onset of the pathologies was monitored at different time points, allowing the operator to monitor the appearance and growth of the disease, as well as the permeability properties, by injection of GBCA.

The feasibility and high reproducibility of these pathological models indicates their suitability for GBCA validation MRI studies. The precise location of the meningioma tumors, as seen with MRI, has been shown to mimic the complex situations in human patients.[8] The enhanced signals for tumor masses obtained after GBCA administration in the investigated orthotopic meningiomas shows that these models could be used to "bridge" the gap between clinical and preclinical efficacy studies.

ACKNOWLEDGEMENTS

Human meningioma cells (CH157MN) were a kind gift from Dr Yancey Gillespie, University of Alabama.

CONFLICT OF INTEREST

None.

AUTHOR CONTRIBUTIONS

FLC, LM, AFM, PI, SCS, CC, ADV conceived and designed the study. FLC, LM, PI and ADV focused on surgery setup and cellular culture; AFM and SCS optimized the MRI experimental protocol and carried out data analysis; CB and AC performed histologies. All authors contributed to revising the manuscript and gave their final approval for manuscript publication.

ORCID

Francesca La Cava https://orcid.org/0000-0002-7722-557X

REFERENCES

1. McCutcheon IE, Friend KE, Gerdes TM, Zhang BM, Wildrick DM, Fuller GN. Intracranial injection of human meningioma cells in athymic mice: an orthotopic model for meningioma growth. *J Neurosurg*. 2000;92:306-314.
2. van Furth WR, Laughlin S, Taylor MD, et al. Imaging of murine brain tumors using a 1.5 Tesla clinical MRI system. *Can J Neurol Sci*. 2003;30:326-332.
3. Tsai JC, Goldman CK, Gillespie GY. Vascular endothelial growth factor in human glioma cell lines: induced secretion by EGF, PDGF-BB, and bFGF. *J Neurosurg*. 1995;82:864-873.
4. Ragel BT, Jensen RL, Gillespie DL, Prescott SM, Couldwell WT. Celecoxib inhibits meningioma tumor growth in a mouse xenograft model. *Cancer*. 2007;109:588-597.
5. Ragel BT, Elam IL, Gillespie DL, et al. A novel model of intracranial meningioma in mice using luciferase-expressing meningioma cells. *J Neurosurg*. 2008;108:304-310.
6. Gogigeni VR, Nalla AK, Gupta R, Dinh DH, Klopfenstein JD, Rao JS. Chk2-mediated G2/M cell cycle arrest maintains radiation resistance in malignant meningioma cells. *Cancer Lett*. 2011;313:64-75.
7. Karsy M, Hoang N, Barth T, et al. Combined hydroxyurea and verapamil in the clinical treatment of refractory meningioma: human and orthotopic xenograft studies. *World Neurosurg*. 2016;86:210-219.
8. Campbell BA, Jhamb A, Maguire JA, Toyota B, Ma R. Meningiomas in 2009: controversies and future challenges. *Am J Clin Oncol*. 2009;32:73-85.

SUPPORTING INFORMATION

Additional supporting information may be found online in the Supporting Information section at the end of the article.

How to cite this article: La Cava F, Fringuello Mingo A, Irrera P, et al. Orthotopic induction of CH157MN convexity and skull base meningiomas into nude mice using stereotactic surgery and MRI characterization. *Animal Model Exp Med*. 2019;2:58–63. https://doi.org/10.1002/ame2.12050